Université de Paris VI Pierre et Marie Curie
ED 386: Sciences mathématiques de Paris Centre

Modélisation mathématique du rôle et de la dynamique temporelle de la protéine p53 après dommages à l'ADN induits par les médicaments anticancéreux

THÈSE

présentée et soutenue publiquement le 1 Septembre 2015

pour l'obtention du diplôme de

Doctorat en mathématiques appliquées

par

Ján Eliaš

après avis des rapporteurs

Mark Chaplain
Roberto Natalini

devant le jury composé de

Luis Almeida	Examinateur
Mark Chaplain	Rapporteur
Jean Clairambault	Directeur de thèse
Marie Doumic-Jauffret	Examinatrice
Robin Fåhraeus	Examinateur
Marek Kimmel	Examinateur
Benoît Perthame	Directeur de thèse
Jack Tuszyński	Examinateur

Laboratoire Jacques-Louis Lions **INRIA (Mamba)**

Pierre and Marie Curie University
DS 386: Mathematical Sciences of central Paris

Mathematical model of the role and temporal dynamics of protein p53 after drug-induced DNA damage

THESIS

presented and defended publicly on the 1st of September 2015

to obtain

PhD in Applied Mathematics

by

Ján Eliaš

after the review by

Mark Chaplain
Roberto Natalini

in front of the jury composed of

Luis Almeida	Examinator
Mark Chaplain	Reviewer
Jean Clairambault	Thesis Advisor
Marie Doumic-Jauffret	Examinator
Robin Fåhraeus	Examinator
Marek Kimmel	Examinator
Benoît Perthame	Thesis Advisor
Jack Tuszyński	Examinator

Jacques-Louis Lions Laboratory **INRIA (Mamba)**

To my parents.
To Eva who hung the moon.

Acknowledgement

First and foremost, I thank sincerely to Jean Clairambault and Benoît Perthame for the great opportunity to study at the UPMC, for their indispensable guidance and assistance on what could otherwise have been an arduous road to finish this thesis. They are truly ideal mentors, both of them demanding and generous: setting a high bar for performance, but also encouraging me to find my own way in terms of both topic and methods. I am indebted to them for their advice and support over the past three years.

Thanks are due to the staff of the Laboratory J.-L. Lions as well as to Mme Nathalie Bonte for her kindness and help on a wide range of travel and other issues.

Special thanks are due to Silvia and Olivier for making our time in Paris more easier.

Along the way I would like to acknowledge at least few people I have met in France, namely Luna, Rebecca, Nastasia, Faouzia, Sarah, Aurora, Andrada, Sarra, Rahma, Noémie, Wafaa, Carola, Tommaso, Alexander, Daisuke, Pierre J., Pierre L., Maxime, Thibault L., Thibault B., Malik, Mamadou, Benjamin, Casimir, Xavier, Ange, Camille, Romain and those from abroad, particularly Katharina, Romica, Sasha, Luyu, Bao and Gleb.

My thanks go to Antoine Le Hyaric for his assistance with FreeFem++.

Thanks go as well to Ayna and Mathias, Ramesh, Gopal and Mme Isabelle Bullier for sometimes hilarious French classes.

I would like to thank my family, especially my mum, to all other family members and friends for their trust and encouragement over the past years.

I must conclude by thanking the person who helped me the most toward the completion of this thesis: Eva, a source of humour and good cheer, unconditional love and support.

Abstract

Various molecular pharmacokinetic–pharmacodynamic models have been proposed in the last decades to represent and predict drug effects in anticancer therapies. Most of these models are cell population based models since clearly measurable effects of drugs can be seen on populations of (healthy and tumour) cells much more easily than in individual cells. The actual targets of drugs are, however, cells themselves. The drugs in use either disrupt genome integrity by causing DNA strand breaks and consequently initiate programmed cell death or block cell proliferation mainly by inhibiting proteins (cdks) that enable cells to proceed from one cell cycle phase to another. DNA damage caused by cytotoxic drugs or γ-irradiation activates, among others, the p53 protein-modulated signalling pathways that directly or indirectly force the cell to make a decision between survival and death.

The thesis aims to explore closely intracellular pathways involving p53, "the guardian of the genome", initiated by DNA damage and thus to provide oncologists with a rationale to predict and optimise the effects of anticancer drugs in the clinic. It describes p53 activation and regulation in single cells following their exposure to DNA damaging agents. We show that dynamical patterns that have been observed in individual cells can be reconstructed and predicted by compartmentalisation of cellular events occurring either in the nucleus or in the cytoplasm, and by describing protein interactions, using both ordinary and partial differential equations, among several key antagonists including ATM, p53, Mdm2 and Wip1, in each compartment and in between them. Recently observed positive role of Mdm2 in the synthesis of p53 is explored and a novel mechanism triggering oscillations is proposed. For example, new model can explain experimental observations that previous (not only our) models could not, e.g., excitability of p53.

Using mathematical methods we look closely on how a stimulus (e.g., γ-radiation or drugs used in chemotherapy) is converted to a specific (spatio-temporal) pattern of p53 whereas such specific p53 dynamics as a transmitter of cellular information can modulate cellular outcomes, e.g., cell cycle arrest or apoptosis. Mathematical ODE and reaction-diffusion PDE models are thus used to see how the (spatio-temporal) behaviour of p53 is shaped and what possible applications in cancer treatment this behaviour might have.

Protein-protein interactions are considered as enzyme reactions. We present some mathematical results for enzyme reactions, among them the large-time behaviour of the reaction-diffusion system for the reversible enzyme reaction treated by an entropy approach. To our best knowledge this is published for the first time.

Résumé

Plusieurs modèles pharmacocinétiques-pharmacodynamiques moléculaires ont été proposés au cours des dernières décennies afin de représenter et de prédire les effets d'un médicament dans les chimiothérapies anticancéreuses. La plupart de ces modèles ont été développés au niveau de la population de cellules, puisque des effets mesurables peuvent y être observés beaucoup plus facilement que dans les cellules individuelles.

Cependant, les véritables cibles moléculaires des médicaments se trouvent au niveau de la cellule isolée. Les médicaments utilisés soit perturbent l'intégrité du génome en provoquant des ruptures de brins de l'ADN et par conséquent initialisent la mort cellulaire programmée (apoptose), soit bloquent la prolifération cellulaire, par inhibition des protéines (cdks) qui permettent aux cellules de procéder d'une phase du cycle cellulaire à la suivante en passant par des points de contrôle (principalement en G_1/S et G_2/M). Les dommages à l'ADN causés par les médicaments cytotoxiques ou la γ-irradiation activent, entre autres, les voies de signalisation contrôlées par la protéine p53 qui forcent directement ou indirectement la cellule à choisir entre la survie et la mort.

Cette thèse vise à explorer en détail les voies intracellulaires impliquant la protéine p53, "le gardien du génome", qui sont initiées par des lésions de l'ADN, et donc de fournir un rationnel aux cancérologues pour prédire et optimiser les effets des médicaments anticancéreux en clinique. Elle décrit l'activation et la régulation de la protéine p53 dans les cellules individuelles après leur exposition à des agents causant des dommages à l'ADN. On montre que les comportements dynamiques qui ont été observés dans les cellules individuelles peuvent être reconstruits et prédits par fragmentation des événements cellulaires survenant après lésion de l'ADN, soit dans le noyau, soit dans le cytoplasme. Ceci est mis en œuvre par la description du réseau des protéines à l'aide d'équations différentielles ordinaires (EDO) et partielles (EDP) impliquant plusieurs agents dont les protéines ATM, p53, Mdm2 et Wip1, dans le noyau aussi bien que dans le cytoplasme, et entre les deux compartiments. Un rôle positif de Mdm2 dans la synthèse de p53, qui a été récemment observé, est exploré et un nouveau mécanisme provoquant les oscillations de p53 est proposé. On pourra noter en particulier que le nouveau modèle rend compte d'observations expérimentales qui n'ont pas pu être entièrement expliquées par les modèles précédents, par exemple, l'excitabilité de p53.

En utilisant des méthodes mathématiques, on observe de près la façon dont un stimulus (par exemple, une γ-irradiation ou des médicaments utilisés en chimiothérapie) est converti en un comportement dynamique spécifiques (spatio-temporel) de p53, en particulier que ces dynamiques spécifiques de p53, comme messager de l'information cellulaire, peuvent moduler le cycle de division cellulaire, par exemple provoquant l'arrêt du cycle ou l'apoptose. Des modèles mathématiques EDO et EDP de réaction-diffusion sont utilisés pour examiner comment le comportement (spatio-temporel) de p53 émerge, et nous discutons des conséquences de ce comportement sur les réseaux moléculaires, avec des applications possibles dans le traitement du cancer.

Les interactions protéine–protéine sont considérées comme des réactions enzymatiques. On présente quelques résultats mathématiques pour les réactions enzymatiques, en particulier on étudie le comportement en temps grand du système de réaction-diffusion pour la réaction enzymatique réversible à l'aide d'une approche entropique. À notre connaissance, c'est la première fois qu'une telle étude est publiée sur ce sujet.

Contents

Abbreviations

$[\,\cdot\,]$, molar concentration
ATM, Ataxia Telangiectasia Mutated protein
doxo, doxorubicin
BC, boundary condition(s)
BL, Burkitt lymphoma cells
DA-1, murine lymphoma cells
DDE, Delayed Differential Equations
DDR, DNA damage response
DNA, Deoxyribonucleic acid
DSB, double strand breaks
ER, endoplasmic reticulum
EnR, enzyme reaction
FRQ, Frequency protein
GNR, gene regulatory network
IR, irradiation (γ-irradiation)
LMA, Law of Mass Action
Lys, lysine residue
Mdm2, Mouse double minute 2 (Hdm2 in human cells, hereafter Mdm2 only)
MdmX, Mouse double minute 4 homolog (HdmX in human cells, hereafter MdmX only)
ML-1 myeloid leukaemia cells
NCS, neocarzinostatin
NES, nuclear export signal
NLS, nuclear localisation signals
ODE, Ordinary Differential Equations
OsA-CL, osteosarcoma cell line
p53, tumour protein p53
p53-P, phosphorylated p53 protein (this notation is applied for other proteins)
PDE, Partial Differential Equations
PK–PD, pharmacokinetic–pharmacodynamic
PTEN, Phosphatase and TENsin homolog
QSSA, quasi-steady-state approximation
RD, reaction-diffusion
RKO, colorectal carcinoma cells
Ser, serine residue
SSB, single strand breaks
$t_{1/2}$, half-life of a protein/mRNA
TF, transcription factor
Thr, threonine residue
Wip1, Wild-type p53-induced phosphatase 1
wm, wortmannin
wt, wild type

List of Figures

List of Tables

Introduction

"Beauty is the first test. There is no permanent place in the world for ugly mathematics."

– G. H. Hardy (1877–1947)

Shortly after disruption of the integrity of the genome of a cell by various pharmacological agents or ionising radiation, the cell responds dynamically by activating a variety of recognition and repair proteins recruited to DNA damage sites, by initiating various signalling pathways leading either to cell cycle arrest and parallel DNA repair, permanent cell cycle arrest or cell death. Among these pathways, the most important ones involve the tumour suppressor protein p53, the so-called guardian of the genome, that initiates expression of those genes that ultimately govern cell cycle arrest, DNA damage repair and apoptosis, Figure 1, involving the production of proteins of concentrations proportionally related to the concentrations of p53. At the cell population level (i.e., tissues, organs, whole human body) pharmacokinetics–pharmacodynamics (PK–PD) modelling has been broadly used to fully describe absorption, distribution, metabolism, excretion and toxicity of anticancer drugs. Much less, however, has been done at the single cell (molecular) level to describe drug effects, considering that individual cells are the actual targets of drug administration [29]. Some drugs (e.g., radiomimetic drugs including doxorubicin, bleomycin or etoposide, alkylating agents or oxaliplatin) directly cause DNA double strand breaks (DSB), others target essential cell cycle enzymes (such as topoisomerases or thymidylate synthase), leading to the production of abnormal DNA and forcing the cell to start the process of apoptosis, at least when DNA cannot be repaired [30].

Thus, to reproduce more realistically drug effects in cancer treatments, as described by PK–PD models with DNA damage as output, it may be helpful to include in existing models processes that appear in individual cells after DNA insult, beginning with a proper understanding of p53 activation and activity in single cells, with the perspective of subsequent integration of such activity into a cell fate decision process, Figure 2. Bearing in mind that p53 is inactive due to its gene mutations in around 50% of tumour cells, with the rate varying from 10–12% in leukaemia, 38–70% in lung cancers to 43–60% in colon cancers, *etc.* [111], the approaches involving processes occurring in individual cells with the dominant role of p53 can contribute to establishing new cancer therapies that could either restore p53's lost functionality or substitute for it in the activation of subsequent proteins in various p53-initiated pathways.

In this modelling enterprise, the main object of interest at the single cell level is thus the protein p53, its activation and its activity on proarrest and proapoptotic genes that enable the cell to make a decision between cell cycle arrest and DNA repair, permanent arrest of cell growth (so-called senescence) and cell death (apoptosis), Figure 1. Interestingly, the first p53-transcription independent wave of cells committing apoptosis in response to γ-irradiation is observed 30 minutes after DNA damage by rapid accumulation of p53 in the mitochondria. The second wave comes after a longer time phase and the decision of the cell to undergo

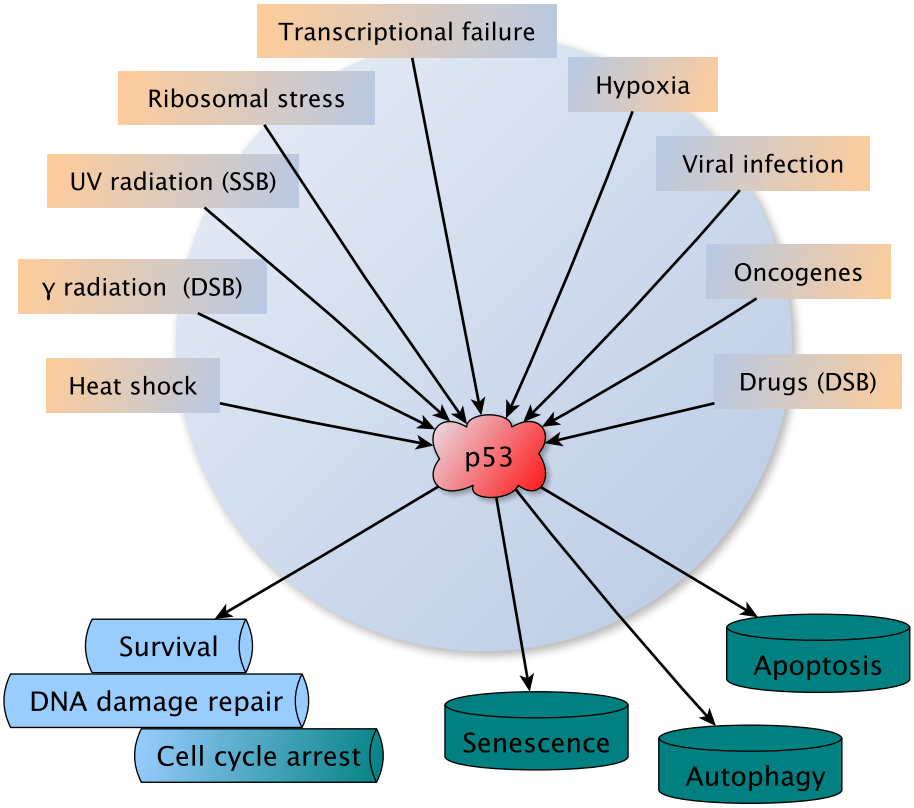

Figure 1. p53, the guardian of the genome: p53 responds to a variety of stress stimuli initiating cell cycle arrest, DNA damage repair, apoptosis or senescence [79, 147, 149].

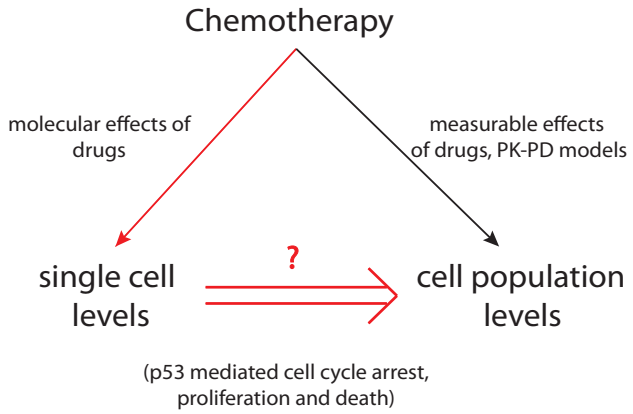

Figure 2. Action of chemotherapeutic agents is exploited in individual cells. Whilst there exist several PK–PD models for effects of a chemotherapy at the cell population level, much less is known about how specific drugs act in single cells.

apoptosis in this wave is determined by the concentrations of both proapoptotic and proarrest proteins, the expression of which is modulated by p53 [73, 111]. However, different sorts of such apoptotic proteins are produced, in a cell-stress, cell-type and tissue-type dependent manner. Various post-translational modifications, interactions of p53 with over 100 cellular cofactors and p53 cellular location have effects on determining what kind of proteins and when these proteins are produced [111].

The signalling of p53 in response to a variety of stimuli is complex, involving hundreds of

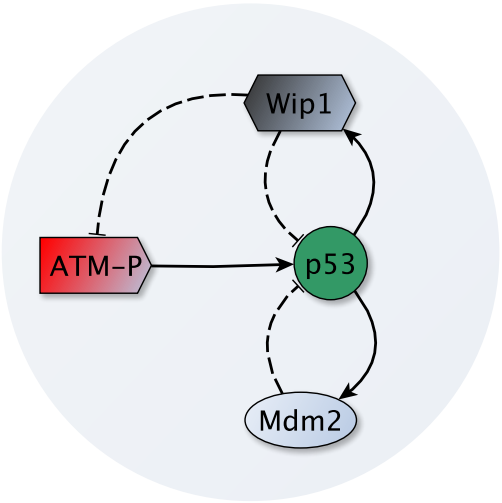

Figure 3. The ATM-p53-Mdm2-Wip1 dynamics: sensors of the DNA damage, phosphorylated ATM-P molecules target p53 for phosphorylation which prevents its interaction with Mdm2 and thus leads to inhibition of the ubiquitin dependent degradation of p53. Stabilised p53 acts as a transcription factor for a variety of genes, the $Mdm2$ and $Wip1$ genes among them. Wip1 dephosphorylates both ATM-P and p53, and thus allows Mdm2 to bind p53 and promote its ubiquitination.

elements and processes with some aspects not yet resolved or even explored. We are therefore forced to restrict ourself to signalling pathways involved in the response to a specific stimulus, where the gained knowledge creates a framework generally accepted among biologists. A solid basis in this direction comes from the experiments studying p53 dynamics across various (cancer) cell lines in response to γ-radiation or drugs causing DNA DSB.

Attention should be, however, paid to interpretation of experimental data. For instance, dynamical responses of individual cells can be very different even when they are exposed to the same stimulus. This can consequently lead to misinterpretations of the measurements of the dynamical behaviour over a population of cells. In some cases the observed dynamical behaviour obtained from cell populations can differ significantly from the patterns observed in individual cells [124]. This is also the case of p53 dynamics[1] which was originally described as damped oscillations when measured by immunoblots [86], later it was revealed that these oscillations are actually sustained with fixed amplitude and duration [77, 56]. Even if we realise that the specific dynamical behaviour can be assigned to a specific cellular outcome [124], this gives another argument for exploring dynamics of proteins at the single cell level and thus possibly give more accurate descriptions of the reality. Indeed, recent observations suggest that transient cell cycle arrest is accompanied with the oscillating p53 protein while cells expressing sustained p53 signalling frequently undergo senescence [108, 123].

In a simplified framework, the regulation of p53 in cells exposed to γ-IR or drugs is mainly achieved through its interactions with the Mdm2 ligase, which is itself a transcription target for p53. Mdm2 regulates p53 through (multiple-)ubiquitination process, followed by nuclear export and subsequent degradation of tagged p53 molecules. Phosphorylation of p53 serine 15 (Ser15) residue, which is located very close to the p53 kinase domain, the target of Mdm2, can mask it from Mdm2 ubiquitination and hence stabilise it at its highest concentrations

[1]The *dynamics* of a molecule is understood as the function describing how the concentration, activity, modification state, or localisation of the molecule changes over time. The dynamics encodes information in the frequency, amplitude, duration, or other features of the temporal signal, [124].

[42, 43, 147]. In response to DSB, p53 can be phosphorylated on Ser15 in three independent ways, one of which is phosphorylation by the ATM kinase [147]. The Wip1 phosphatase is another p53 target which acts in the pathway as a regulator; particularly, it dephosphorylates both ATM and p53, rendering them inactive, whence Wip1 closes negative feedback loops between these proteins as it is schematically shown on Figure 3. Recently, these four proteins have been shown to represent sufficient and necessary elements in the p53 (minimal) network which can produce p53 oscillations following DNA damage [15].

The ligase Mdm2 primarily acts as a negative regulator of p53 establishing homeostasis in DNA damage response (DDR). Recently published studies show that following ATM-dependent phosphorylation of Mdm2, the phosphorylated Mdm2 was observed not to target p53 for degradation but rather, and somehow surprisingly, to enhance p53 synthesis. Thus it can function as a positive regulator by undergoing certain post-translational modifications [54, 96].

The simplified p53 network relying on the p53-Mdm2 and ATM-p53-Wip1 negative feedbacks became basis for three articles where we continuously embedded a physiological and compartmental ODE model from [47] into a spatio-temporal PDE model [46, 45][2]. Both ODE and PDE models were aimed to reproduce basic biological observations as described in more details below. The third article [45] serves as an introduction into modelling protein (namely, p53 and FRQ) networks by reaction-diffusion equations which are largely overlooked by mathematicians and system biologists. In the reaction-diffusion PDE models, reaction terms describe protein-protein interactions and gene regulatory networks and diffusions naturally stand for migration of the species across and in between the two main cellular compartments: nucleus and cytoplasm.

[45] *J. Eliaš and J. Clairambault. Reaction-diffusion systems for spatio-temporal intracellular protein networks: A beginners guide with two examples. Computational and Structural Biotechnology Journal, 10(16):12–22, 2014.*

[46] *J. Eliaš, L. Dimitrio, J. Clairambault, and R. Natalini. The dynamics of p53 in single cells: physiologically based ODE and reaction–diffusion PDE models. Physical Biology, 11(4):045001, 2014.*

[47] *J. Eliaš, L. Dimitrio, J. Clairambault, and R. Natalini. The p53 protein and its molecular network: Modelling a missing link between DNA damage and cell fate. Biochimica et Biophysica Acta (BBA) - Proteins and Proteomics, 1844(1, Part B):232–247, 2014.*

Aims of the thesis

With the perspective of future (biological and pharmacological) applications, we consider *in silico* the p53 protein and its signalling in response to DNA damage, particularly to DSB caused by agents such as γ-radiation or drugs, at the single cell level. The principal aim of the thesis lies in a study of spatio-temporal dynamics of p53 in an individual cell and close examination of its dynamical patterns depending on a physical structure of the cell as well as other factors such as DNA damage dose.

[2]The articles are ordered from the most recent to the earliest.

Several aims are followed in the thesis. Among them,

- first and foremost, we aim to model p53 response to DNA damage more plausibly with respect to the relevant biological observations (discussed in the biological overview) including
  - a DNA damage-transmitting-signal (i.e., ATM) which is able to sense the presence of DSB and transmit the signal to p53, and regulators of p53 enabling to maintain homeostasis in the DDR (i.e., Mdm2 and Wip1), in their dynamical states rather than being constant substrates,
  - spatial representation of cells and thus differentiation of processes in the p53 pathway taking place either in the nucleus or in the cytoplasm; this gives a rise to physiologically more relevant cellular framework for the modelling; then
- we aim to provide an analysis of the models with respect to the extent of DNA damage and examine thus p53 dynamical responses to different doses of stimulus,
- we aim to provide an analysis of the models with respect to spatial variables and examine thus roles of the spatial structure of a cell in maintaining specific patterns in the p53 response,

since once we are successful in achieving of these goals, the model simulating realistic behaviour of p53 could become attractive for biologists (which is another "hidden" aim of this work).

We try to answer several other questions that can further contribute to a more detailed understanding of the complex p53 dynamics in cancer cells, which are exposed to damaging agents. Some of these questions are:

- What is the role of the sole p53-Mdm2 negative feedback in the p53 response? Can it be the only "force" triggering oscillations?
- Can a positive role of Mdm2 towards synthesis of p53 provide an independent mechanism for the oscillatory behaviour of p53?
- Based on the models, could we propose a molecular mechanism (which is unknown so far) underlying phenomena of the excitability of p53 in response to DSB?
- By assuming biological hypotheses giving into relation p53 patterns with a specific (irreversible) fate outcome, can the models be used to predict molecular targets in cancer treatment which, after being hit by a known or hypothetical pharmacological agent, could establish the phenotype in question? This brings us to:
- Could the proposed models be used to exploit dynamics of pharmacological agents (currently used in clinical trials) or possibly to direct biochemists in the investigation for new chemicals; to extend current PK–PD models with a molecular module which would describe the action of these agents more properly?

Except for all these mathbio aspects which rely on modelling, we consider some mathematical problems related to ODE and PDE systems for enzyme reactions. Although the enzyme reactions represent fundamental basis for our modelling, the particular results stay independent of the mathbio part.

Organisation of the thesis

The thesis consists of two autonomous parts: the first and most extensive part is devoted to the modelling p53 network, its activation and regulation in response to DNA damage. This part spreads over the first seven chapters which describe a "genealogy" of our mathematical modelling starting with biological and mathematical foundations, passing through a compartmental ODE model, two reaction-diffusion PDE models for p53 and finishing with general conclusions about p53 dynamics and its applications to cell fate decisions. Both PDE models exploit different mechanisms for triggering p53 oscillations. The second part consisting of one chapter only is dedicated to some issues related to enzyme reactions. Rather than being a compact text, this chapter is a collection of two independent results: one for an ODE system modelling irreversible enzyme reaction, the other one for a reaction-diffusion PDE system for the reversible enzyme reaction. What follows are short descriptions of the chapters.

Part I.

- **Chapter 1** highlights general biological knowledge about the p53 protein and other proteins regulating response of p53 to DNA damage including ATM, Mdm2 and Wip1. Dynamics of the proteins in cancers cells following genotoxic insult as well as p53-Mdm2 auto-regulatory feedback and observations from single cell experiments are briefly overviewed.
- **Chapter 2** introduces basic mathematical concepts used in modelling. The focus is on the Law of Mass Action applied to enzyme reaction as a prototypic reaction representing protein-protein interactions. Simple gene regulatory networks for Mdm2 and Wip1 proteins as well as induction and degradation of ATM and p53 are discussed. Further, transmission of the species throughout the membranes and issues around intracellular movement of the species are studied. The chapter is concluded with a review of other existing models simulating p53 dynamics.
- **Chapter 3** presents a physiological and compartmental ODE model for p53 dynamics following DNA damage. The model is based on the p53-Mdm2 negative feedback complemented with another negative feedback between ATM and Wip1. Analysis with respect to the DNA damage signal is provided.
- **Chapter 4** gives a general introduction into modelling protein networks by spatio-temporal reaction-diffusion equations. As an example, the dynamics of the Frequency (FRQ) protein from the well known Leloup–Goldbeter circadian clock ODE model is examined in new spatial settings.
- **Chapter 5** focuses on a reaction-diffusion model for the p53 protein and its signalling in an individual cell after DNA damage. This physiologically more plausible model considers the two negative feedback loops from the ODE model. The reaction-diffusion PDE model is examined with respect to several biological observations. Its analysis with respect to the DNA damage signal and spatial parameters is given.
- **Chapter 6** presents a novel mechanism for p53 oscillations relying on a positive role of Mdm2 towards p53. It is shown that this dual (positive vs. negative) function of Mdm2 depending on Mdm2's phosphorylation status can create a molecular framework generating p53 oscillations as well as it can explain the excitability of p53 in response to DSB.

- **Chapter 7** summarises all the work done in the previous chapters. It attempts to relate the developed models with the possible applications in cell fate decisions as well as PK–PD models.

Part II.

- **Chapter 8** considers two autonomous problems related to the enzyme reaction. In particular, the validity of the quasi-steady state approximation is given and the large time behaviour of a reaction-diffusion system for the reversible enzyme reaction is studied.

Part I

Modelling p53 network

1

Biological background

Our main object, the tumour suppressor p53, is found at low levels in normal cells under normal conditions. In response to a stimulus, it is activated and acts primarily as a transcription factor for many other genes which, if possible, silence fluctuations caused by the stimulus, if not possible, initiate processes forcing cells to trigger an irreversible state such as apoptosis or senescence to prevent the development of cancer. The biological knowledge about the p53 protein has became very broad since its discovery, thus in the following sections we give a summary of the basic properties of p53, its functional activity towards upstream and downstream substrates, its activation in response to genotoxic stress and other biological features which we think are important to mention. Other key players in the p53 network, in particular, ATM, Mdm2 and Wip1 are also reviewed in this chapter.
Dynamics of the p53 protein in cancers cells is of special interest for us with respect to possible future applications of our models. In this chapter we thus depict several observations of the dynamics of p53 and other proteins following DNA damage (such as DSB) caused by irradiation or drugs.

Organisation of the chapter is as follows: Sections 1.1-1.6 present short descriptions of the main antagonists, namely, p53, ATM, Mdm2 and Wip1. The p53-Mdm2 auto-regulatory feedback is described in Section 1.5. The dynamics of the proteins including single cells experiments are reviewed in Section 1.7.

1.1 The protein p53 in general

The protein p53 as a tumour suppressor controls transitions from G1 to S and from G2 to mitosis cell cycle phases during a tissue development and subsequent tissue regeneration relying on the divisions of cells at mitosis [27]. The p53 protein can respond to abnormal developmental pathways triggered by oncogene or tumour suppressor gene mutations, thus preventing the cell from turning it into a malignant cell [88]. It is also activated whenever the DNA is exposed to various stress conditions such as ionising γ-radiation, UV or various drugs in chemotherapies causing DNA damage and also by agents which do not cause DNA damage, for example, hypoxia, starvation, heat and cold, see e.g. [79, 147, 149] and Figure 1. In the response to these stresses, p53 transcriptionally activates a bench of proarrest and proapoptotic proteins leading either to cell cycle arrest (and thus it enables repair processes to fix the DNA damage), senescence or apoptosis [111], apparently, with no ability of p53 to preferentially activate proarrest target genes rather than proapoptotic genes and *vice-versa* due to the (higher/lower) affinity of p53 for these genes [73].

Although mutations of the *p*53 gene primarily do not cause cancer, inactivation of its transcriptional activity, mostly due to missense mutations located in the DNA-binding domain, can lead to failures in the prevention of unnatural growth whenever some other mutations of genes causing uncontrolled growth occur [66]. p53 mutations are common in human cancers (they occur in about 50% of mammalian cancer cells) and are frequently associated with aggressive disease courses and drug resistance, for example, patients with AML at diagnosis (with mutations in the *p*53 gene of 10%-15% initially) [162]. Patients with rare *p*53 gene germ line mutations known as Li-Fraumeni syndrome have an approximately 90% lifetime risk of developing cancer (50% before the age of 40 years) [90]. Interestingly, even when transcriptionally inactivated by a point mutation at the DNA-binding domain, about 70–80% of human carcinomas express such p53 mutants at high levels [154, 80]. Accumulation of high level mutant p53 expression during tumour development thus suggests that it may positively affect proliferation of cancer cells, [118] and citations therein.

In many other human tumours with wild-type and thus transcriptionally active p53, p53 activity is suppressed by its regulators Mdm2 and Wip1 which are over-expressed in these cancer cell lines. The *p*53 gene remains in its wild-type configuration, likely because the over-expression of the negative regulators decreases the selective pressure for direct mutational inactivation of the *p*53 gene, [92, 106] and citations therein.

The p53 protein is extensively studied protein and there can be found thousands of articles describing p53 signalling or reviewing it and its functions in more details (for reviews see, for instance, Vogelstein, Lane & Levine [147], Murray-Zmijewski, Slee & Lu [111] and Vousden & Lane [149]). In the following sections we point out only the most important facts that are further recalled in the modelling.

1.2 p53, a transcription factor

The *p*53 gene product functions as a transcription factor. The wild-type p53 protein can bind to specific nucleotide sequences, also called p53-responsive elements. When these elements are close to a promoter they stimulate expression in a p53-dependent manner both *in vivo* and *in vitro*. Mutations in the *p*53 gene can still produce p53 proteins that however fail to bind to DNA and fail to transcriptionally activate p53-responsive genes, [154] and citation therein.

Functional activity of p53 follows its nuclear stabilisation which means that for a certain amount of time p53 is able to retain its structural conformation preventing it from degradation or aggregation and to retain its activity when it is exposed to manipulations [147, 42]. The structural conformation relies on a series of post-translational modification (e.g., phosphorylation at Ser15) as discussed in Section 1.2.2 and formation of higher order homodimers as described firstly in Section 1.2.1.

1.2.1 p53 forms tetramers for effective gene transcription

The p53 protein forms tetramers and the tetramer formation is essential for its function [53, 66]. Indeed, tetrameric p53 cooperatively binds to DNA [152] and tetramerisation mediated by the tetramerisation domain regulates the DNA binding activity of p53 [139]. However, at low levels or when p53 moves across the nucleus, p53 is likely in the dimeric form [64, 152].

Using three-dimensional structural analysis it was found that the residues containing the putative nuclear export signal (NES) are suitable substrates for the export receptors whenever p53 is in the monomeric or dimeric state. Tetrameric p53 cannot be exported from the nucleus since the NES lies within the tetramerisation domain and is thus hidden from the

export receptors [139]. Notably, the domain of p53, which is required for oligomerisation, is also crucial for Mdm2 binding and Mdm2-dependent ubiquitination of p53 [106].

Thus, the tetramerisation of p53 molecules contributes to the nuclear accumulation and stabilisation of p53.

1.2.2 p53 activation and regulation following genotoxic stress

The tumour suppressor protein p53 can be activated in at least three independent ways: DNA damage caused, for example, by ionising radiation or electromagnetic γ-radiation, with initial activation of ATM and Chk2 proteins; aberrant growth signals; and various chemotherapeutic drugs, UV radiation and protein–kinase inhibitors. All three ways inhibit p53 degradation, lead to p53 accumulation and stabilisation in the nucleus, and thus enable the protein to accomplish its main transcriptional function [147].

The concentration of p53 in cells is believed to be determined mainly through its degradation [147][1]. In normal cells, p53 is kept at a low level mainly through Mdm2-dependent degradation (p53 is very short-lived with the half-life $20 - 30\,min$ [116]). Therefore, in order for p53 to accumulate in the nucleus and become active in response to stress, the p53-Mdm2 complexes must be interrupted so that p53 can escape from the degradation-promoting effects of Mdm2 [106, 135]. An accepted model for this disruption involves the kinase ATM (with possible action of Chk1, Chk2 and DNA-dependent protein kinases) which phosphorylates p53 on Ser15 localised at the amino-terminal site (*in vitro* and *in vivo*) very close to the binding site of its main regulator Mdm2. Phosphorylation of Ser15 masks p53 from Mdm2 (it blocks binding Mdm2 to p53); it stabilises p53 at high concentrations and thus it initiates p53 transcriptional activity [74, 147, 54, 43]. However, phosphorylation of Ser15 may not be exclusive for inability of p53 and Mdm2 to form complexes. There is evidence that the point mutation of another phosphorylation sites 22/23 resulted in the inability of p53 to interact with Mdm2 [74].

The phosphatase Wip1, a transcription target of p53, is then observed to act in the reverse way, compared with the action of ATM. It dephosphorylates both ATM and p53, making them inactive and unable to phosphorylate their substrates; in particular, inactive ATM cannot phosphorylate p53 on Ser15 and dephosphorylated p53 is then detectable by Mdm2, as represented on Figure 3, [15, 136, 137].

The E3 ligase Mdm2 is another transcription target for p53. Its p53-inhibiting activity consists either in single ubiquitination of p53 followed by the nuclear export of such labeled p53 or Mdm2 promotes multiple ubiquitination with the subsequent p53 degradation by the protein-degradation machinery [147]. Other proteins such as HAUSP can contribute to p53 stability by deubiquitination of p53, i.e. by opposing Mdm2 [111]. More details about the Mdm2 protein and its activity towards p53 are left to Section 1.4.

Among other things, full p53 transcriptional activation and stabilisation in highly specific situations require other post-translational modifications (phosphorylation, acetylation, methylation, sumoylation, ubiquitination, *etc.*) of one or more p53 residues. The situation become even more complicated considering that different modifications of the same p53 residue, e.g. methylation and ubiquitination of Lys370, result in different p53 effects [111].

[1] This means that the level of p53 expression and the actual concentration of p53 mRNA do not change significantly during the p53 signalling. These assumptions are also used in our model. Recent observations in [54, 96], however, suggest that the synthesis of p53 can be also regulated through a positive action of Mdm2. Further details are left to Chapter 6.

1.2.3 p53 transcriptional activity towards proarrest and proapoptotic proteins

The protein p53 as a transcription factor can activate hundreds of genes in response to a variety of stress signals, thus transforming such signals into various cellular responses. In addition, the p53 transcriptional activity is heterogeneous, depending not only on the incoming signal (its type and amplitude) but also on many other factors — the environment of the cell, type of cells, tissues, presence and abundance of cellular cofactors and enzymes causing modifications of over thirty residues of p53. All this can induce alterations in p53 stability, expression of substrate genes and cellular location [111].

Experiments on p53 activity on its substrates initially suggested that p53 activates genes likely with respect to its affinity for a specific promoter. Such conception assumed, for example, that low concentrations of p53 predominantly lead to the activation of genes of high binding affinity, mostly the genes coding for proarrest proteins. When the concentration of p53 is high, then it activates also genes of low binding affinity (i.e. proapoptotic genes). However, this model has been partially disproved by observations evidencing that post-translational modifications contribute to the activation of both proarrest and proapoptotic proteins without any preference being due to p53 affinity towards promoters [111]. Recent experiments in [73] support these ideas and contradict models based on a differential p53 affinity by showing that even low levels of p53 can activate both proarrest and proapoptotic genes, and that concentrations and durations of expression of p53 substrates are determined only by concentration and duration of expression of p53 itself.

Importantly, a stressed cell evaluates the presence of both proarrest and proapoptotic proteins produced in a p53-dependent manner at any time during its response to DNA damage. The cell determines a so-called "apoptotic ratio" with respect to protein concentrations, duration of their expression and other factors. Irreversible apoptosis is initiated whenever this ratio crosses a certain threshold [73]. Expression of those apoptosis-launching proteins is a rather complex process that depends on many factors (post-translational modifications, interactions with other cellular substrates, location), but from an intracellular PK–PD modelling point of view, the most interesting part, i.e. apoptotic response to therapeutic drugs, must certainly involve p53, [47].

1.3 Ataxia Telangiectasia Mutated protein, ATM

Although p53 activation by ATM in response to DNA damage is well documented, the precise molecular mechanisms of this activation are less well known and up to these days there are still unresolved differences between *in vivo* and *in vitro* observations. Roughly speaking, the kinase ATM mediates phosphorylation, directly or indirectly through Chk2, on several p53's residues [135]. It is generally accepted that these phosphorylation events suppress Mdm2-dependent inhibition of p53 activity via the prevention of p53-Mdm2 protein-protein interaction [147, 135].

In the following sections we review briefly how ATM is activated and regulated in response to DNA DSB.

1.3.1 ATM, a sensor of DSB

In unstressed human cells ATM exists in inactive form as a compound formed (dominantly) from two ATM molecules, which makes it stable in cells, retaining it in a constant concentration, and inaccessible to cellular substrates [7, 67]. In this oligomeric form, the kinase domain of ATM is bound to a region surrounding the residue Ser1981, Figure 1.1.

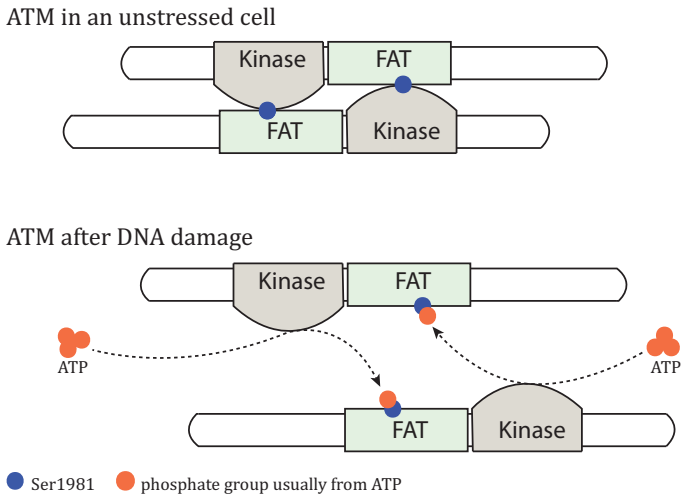

Figure 1.1. ATM molecules form dimers in an unstressed cell (above) which dissociate into active monomers through autophosphorylation of Ser1981 after DNA damage (below).

A cell exposure to stress agents (causing DSB such as γ-radiation or cytotoxic drugs[2]) induces rapid autophosphorylation of ATM on Ser1981 and this phosphorylation results in dimer dissociation and initiation of cellular ATM kinase activity *in vivo*. In ATM dissociation and activation, the active site of one ATM kinase (one out of two bound in the dimer) catalyses the phosphorylation reaction within which a phosphate group, commonly coming from ATP, is added to Ser1981 of the another ATM kinase (resulting in the so-called trans-autophosphorylation) [7], Figure 1.1.

Occasional DSB arising, for instance, from DNA replication are normally promptly corrected by the DNA repair machinery, with either no need to activate ATM or such activation being only moderate and temporary [13]. After DNA damage caused by other agents (at even as low doses as 0.1 Gy of ionising radiation), ATM activation occurs very promptly likely through sensing the changes in heterochromatin [7, 70]. ATM forms clearly detectable foci adjacent to DNA DSB, and even relatively low levels of nuclear ATM may be sufficient to elicit proper responses to DNA damage [159].

Experiments *in vitro* reveal a different mechanism for the ATM dimer dissociation and kinase activation. In particular, a complex of three proteins Mre11-Rad50-Nbs1 localises at the sites of DNA DSB [82, 117] and attracts ATM dimers to the unwinding DNA break ends [50] where it is further modified (mostly phosphorylated) by the members of the complex. This results in ATM dissociation followed by ATM activation and release of a fraction of the activated ATM from the DNA sites to the nucleus where it phosphorylates its substrates [82, 117].

1.3.2 Activity and regulation of ATM

In vivo, ATM activation following ionising radiation occurs very rapidly at distance from DNA DSB by means of Ser1981 autophosphorylation. When measured by immunoblots, the dynamics of p53 (measured through phosphorylation on Ser15) corresponds to the dynamics of ATM activation. Indeed, phosphorylation of p53 is similarly maximal at doses of 1–3 Gy

[2]In addition to exposure of cells to ionising radiation, cytotoxic drugs and restriction enzymes causing DNA DSB, phosphorylation of Ser1981 and ATM activation is also detectable by introducing chromatin-modifying treatments such as chloroquine or histone deacetylase inhibitors, which do not induce DSB [7].

of γ-radiation with little or no further increase up to doses of 30 Gy in fifteen minutes [7, 70]. In contrast, phosphorylation of other ATM substrates, e.g., Nbs1 (on Ser343) and H2AX[3] (on Ser139) occurs at the sites of DNA DSB and increases continuously in a dose-dependent manner up to 30 Gy [7, 70].

Similarly to the complex mechanisms of post-translational modifications of p53, ATM contains residues undergoing various modifications, e.g. phosphorylation of the ATM sites Ser367, Ser1893, Ser2996 and Thr1885, that influence various ATM roles in the ATM signalling pathway, mainly at the intra-S phase checkpoint [72, 71]. Acetylation of some residues has been observed in parallel to Ser1981 phosphorylation as a crucial event in ATM kinase activation and monomerisation [145]. Inactive ATM due to, e.g., a point mutation of the phosphorylation sites, fails to bind to DNA DSB *in vivo* [18].

Unlike for p53, the stability of the $370\,kDa$ large ATM protein is not determined through its degradation, but rather by reverse association of monomers to dimers (or multimers), i.e. dephosphorylation of active ATM monomers by some phosphatases and backward dimerisation (multimerisation) of such dephosphorylated monomers. Phosphatase Wip1 is likely the dominant player able to dephosphorylate ATM Ser1981 [136, 92]. It has been shown that inefficient Wip1 results in ATM kinase malfunction, and over-expression of Wip1 significantly reduces protein activation in the ATM-dependent signalling cascade after DNA damage. The ATM Ser1981 site is the main target of Wip1 *in vivo* and *in vitro*, however, Wip1 can dephosphorylate ATM on other sites [137].

1.4 Mouse double minute 2 protein, Mdm2

The *Mdm2* gene was originally identified as a gene amplified in a spontaneously transformed BALB/c 3T3 (3T3DM) cell line [49], and the Mdm2 protein was subsequently shown to bind to p53 in rat cells transfected with *p*53 genes [109]. Levine and his colleagues [109, 154] characterised, purified, and identified a cellular phosphoprotein with a molecular mass of 90 kDa that formed a complex with both mutant and wt p53 protein. The human *Mdm2* gene (*Hdm2* was cloned in human sarcomas in [114] (hereafter Hmd2 is always referred to as *Mdm2*). With an apparent $90\,kDa$ molecular weight of the full-length Mdm2, there are identified other isoforms (p85, p76, p74, p58-p57) which may arise from different spliced mRNA forms of the *Mdm2* gene or post-translational modifications of the Mdm2 protein. The full-length Mdm2 and p58 are able to form complexes with p53 only, [116].

Mdm2 regulates p53 levels negatively through a post-transcriptional mechanism [74], later on specified as a ubiquitin dependent degradation of p53 [61]. Thus the principal function of Mdm2, as an E3 ubiquitin ligase, together with the p300 transcriptional co-activator protein (in its capacity as an E4 ligase), is to mediate the ubiquitination and proteasome-dependent degradation of p53 (but also other growth regulatory proteins). Mdm2 mediates multiple mono-ubiquitin attachment to multiple p53 residues while p300 mediates subsequent polyubiquitination, [61, 106]. Notably, Mdm2 does not reduce p53 mRNA which levels remained fairly unchanged during protein signalling in some cancer cell lines with or without DNA damage [74, 61].

Overproduction of Mdm2 is therefore thought to suppress normal p53 levels and prevents the p53 response to cellular stress, [103] and citations therein. Note that Mdm2 was amplified in over 30% (in a third of 47 considered sarcomas) of human sarcomas, [114]. At least 5–10% of all human tumours possess Mdm2 over-expression, due to either gene amplification or transcriptional and post-transcriptional mechanisms. As expected, in many of those cases the

[3]Histone H2AX, one of the first targets of ATM, associates with irradiation-induced DNA DSB with a detectable loci signalising the presence of the DSB [7, 159].

*p*53 gene remains in its wild-type configuration, presumably because Mdm2 over-expression decreases the selective pressure for direct mutational inactivation of the *p*53 gene, [106] and citations therein. Thus Mdm2 is an oncogene, which may, however, help to activate apoptosis under conditions of genotoxic stress (doxorubicin) [54].

1.4.1 Activity and regulation of Mdm2

Mdm2 is a phosphoprotein that contains several conserved functional regions which can be phosphorylated in response to different cellular context including the residues Ser166 and Ser186 phosphorylated by Akt [100, 163, 113] and Ser395 targeted by ATM [98].

Phosphorylation of Mdm2 by ATM at Ser395 in response to γ-radiation and drugs results in increased autoubiquitination and degradation of Mdm2 at the beginning of DDR [139]. Recently, the ATM-dependent phosphorylation of Ser395 was observed to reverse the action of Mdm2 from being a negative regulator of p53 to a positive by stimulating p53 expression [54] (details are left to Chapter 6).

Akt (or protein kinase B) is a kinase appearing in the prosurvival PIK3 pathway. Following Akt activation by PIP3, Akt phosphorylates Mdm2 which is a necessary step for Mdm2 to be translocated from the cytoplasm to the nucleus. Another p53's downstream protein and tumour suppressor PTEN acts as a positive regulator for p53 through hydrolysation of PIP3 to PIP2 which is then unable to activate Akt, with the outcome of Mdm2 sequestered in the cytoplasm, [99, 101]. The p53-PTEN-PIP3-Akt positive feedback is often used in mathematical models, see BOX-1 and an overview of models in Section 2.5.

Mdm2 can be also regulated through its interaction with other proteins, e.g., ARF and p300 [103]. Following its binding to Mdm2, ARF significantly stimulates sumoylation of Mdm2, a post-translational modification, which results in less sufficient p53 ubiquitination [103]. ARF, at least when present in high amounts, can sequester Mdm2 in the cell nucleolus [106]. On the other site, phosphorylation of Mdm2 on Ser166/186 by Akt inhibits its interaction with ARF [100, 113]. Another substrate 14-3-3σ can also bind Mdm2 which leads to destabilisation of Mdm2 through enhancing Mdm2 autoubiquitination and accelerating turnover rate, 14-3-3σ can also affect translocation of Mdm2 from the nucleus to the cytoplasm [156].

BOX-1: PI3K/Akt pathway and Mdm2 nuclear translocation

PIP3 recruits several protein kinases including Akt and its upstream activators PDK1 and PDK2 to the cellular membrane. Phosphorylation of Akt at Ser308/473 is followed by its release from the membrane whereupon it can interact with and phosphorylate a range of substrates including proarrest protein p21 (which is then unable to function in favour of the cell cycle arrest) and Mdm2. Thus Akt promotes cell survival [101]. According to several works, Mdm2 is phosphorylated by Akt at the serine residue 166 and 186 [100, 163, 113] although phosphorylation of the latter site was not observed in [5, 58]. These phosphorylation events then stimulate nuclear entry of Mdm2 from the cytoplasm [100, 163].
While two reports [100, 163] show a clear cytoplasmic localisation of Mdm2 when not phosphorylated by Akt, other groups have shown that Mdm2 is localised in the nucleus irrespective of the Akt-dependent phosphorylation [5, 113]—a surprising discrepancy given that similar cell lines and procedures were performed in these experiments.

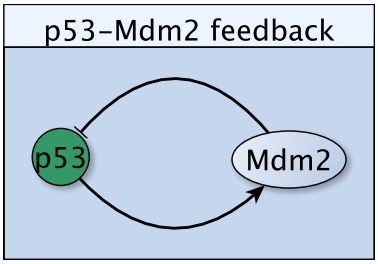

Figure 1.2. p53 regulates levels of Mdm2 through its transcription whilst Mdm2 negatively regulates levels of p53 through the ubiquitin-dependent degradation. Thus p53 and Mdm2 form a negative feedback (shortly written as $p53 \rightarrow Mdm2 \dashv p53$).

Mdm2 can also drive effectively its own ubiquitination [26]. Mdm2 is typically a very short-lived protein with the half-life $t_{1/2} = 30\,min$, [116, 80, 118].

1.5 The p53-Mdm2 auto-regulatory feedback loop

The *Mdm2* gene has two promoters, an internal promoter (Mdm2-P2), which responds strongly to wt p53[4] activation in several cell lines [11, 10, 154], and an upstream constitutive promoter (Mdm2-P1), which is not directly affected by p53 [10][5]. Activation of the Mdm2-P2 promoter follows either the introduction of over-expressed wild-type p53 into cells or the induction of endogenous wt p53 by γ-radiation. The Mdm2-P1 promoter is only mildly affected by excess of wt p53, [10].

The p53 protein regulates the *Mdm2* gene at the level of transcription and thus stimulates increased steady-state levels of Mdm2 mRNA. On the other hand, the Mdm2 protein regulates the p53 protein at the level of its transcriptional activity by the p53-Mdm2 complex formation, BOX-2. Mdm2 interacts with the amino-terminus of p53 in a region that is important for p53 transcriptional activity and thus inhibits its ability to bind DNA, [109, 115, 154]. Mdm2 also promotes either p53 monoubiquitination with a subsequent nuclear export of such labelled p53 to the cytoplasm or p53 polyubiquitination and degradation by the 26S proteasomal pathway [89, 106, 54] (see also Section 1.4). Thus Mdm2 can further regulate p53 by removing it from its site of action.

This creates an auto-regulatory feedback loop, Figure 1.2 and BOX-2, that regulates both the level and activity of the p53 protein and the expression of the *Mdm2* gene [154]. This negative feedback loop results in a low level of p53 expression in normal cells under normal conditions. In response to diverse stress stimuli, post-translational modifications increase the steady-state levels of p53, and alter its subcellular localisation with the outcome of cell cycle arrest and inducing pro-senescence/proapoptotic genes [147]. Thus, factors that disturb this loop and act to increase Mdm2 levels (either via amplification of this gene or increased Mdm2 activity, e.g. PI3K/Akt pathway) will promote cell proliferation, whereas factors that alter the ability of p53 protein to stimulate Mdm2 or inactivate Mdm2 activity (e.g., ARF) should lead to growth arrest [154]

[4] In p53-deficient MEFs, the Mdm2-P2 promoter was also regulated by the Ras-driven Raf/MEK/MAP kinase pathway, in a p53-independent manner [128].

[5] It has been however recently shown an indirect negative regulation of the Mdm2-P1 promoter by p53 through its upstream protein PTEN. Indeed, in Pten-null cell lines and prostate cancer tissues, Mdm2-P1 promoter activity is up-regulated, resulting in increased Mdm2 expression and enhanced production of the full-length (p90)Mdm2 isoform. PTEN controls Mdm2-P1 promoter activity through its lipid phosphatase activity and independently of p53 binding to the promoter [25]. This represents another mechanism for PTEN in controlling Mdm2 oncoprotein functions [25], see BOX-1.

Note that except for Mdm2-mediated degradation of p53, p53 may be targeted for degradation by other E3 ligases as well as by non-proteasomal mechanisms. However, Mdm2 is believed to be the major physiological antagonist of p53 [106]. In addition, no molar excess of Mdm2 over p53 is necessary for efficient p53 degradation: one molecule of Mdm2 may promote degradation of several p53 molecules [61]. Interestingly, whilst Mdm2 binding to p53 represents one inhibitory mechanism of p53 activity, stable p53-Mdm2 complexes were barely detectable in several cell lines including DA-1 murine lymphoma, ML-1 myeloid leukaemia and BALB/c-3T3 fibroblasts [61].

In addition to the p53-Mdm2 negative feedback, there are several other players which can (positively or negatively) contribute to the p53-Mdm2 loop. Currently there exist at least 7 negative feedbacks regulating p53, most of them between p53 and Mdm2 (and other proteins) and several positive feedbacks (between p53 and PTEN, p14/19 ARF, Rb, Dapk1, c-Ha-Ras, DDR1, Rorα), [60, 69].

BOX-2: p53-Mdm2 auto-regulatory loop

Auto-regulatory feedback loop between p53 and Mdm2 consists in regulation:

- of Mdm2 by p53 at the transcriptional level (p53 is a transcription factor for $Mdm2$ gene),
- of p53 by Mdm2 through either
  - p53-Mdm2 complex formation and inhibition of p53 activity,
  - promoting mono-ubiquitination and nuclear export of p53, or
  - promoting poly-ubiquitination and degradation of p53 by the 26S proteasomal pathway.

1.6 Wild-type p53-induced phosphatase 1, Wip1

The $Wip1$ gene was identified as a novel transcript whose expression was induced in response to γ-IR in a p53-dependent manner in the Burkitt lymphoma (BL) cells. The BL cells carry a wt $p53$ gene, they can arrest a cell in the G1 checkpoint and induce apoptosis following IR, [52] and citations therein.

The Wip1 protein with the apparent molecular mass of 61 kDa is a member of the serine/threonine protein phosphatase 2C (PP2C) family and was found exclusively in the nuclei of BL cells[6]. The levels of nuclear Wip1 increased with an apparent peak of its mRNA at 2 hr in a p53-dependent manner [52].

The $Wip1$ gene is amplified in several human cancers such as breast cancer, neuroblastoma, and ovarian carcinomas, predominantly those that still retain wt p53 [92, 95]. Patients with cancers which over-express Wip1 exhibited poorer prognosis than their counterparts with normal Wip1 [92]. This indicates that Wip1 can function as an oncogene in these (and other) tumours. Inactivation of Wip1 resulted in the activation of p53 and/or ATM pathways with a clear suppression of tumorigenesis in several murine models, [155] and citations therein.

The protein Wip1 targets p53 as well as other proteins including ATM, Mdm2, Chk1, Nbs1 and HA2X for dephosphorylation, [136, 137, 155]. Thus it is considered as a major

[6] Wip1 is even found to be tightly bound to chromatin throughout the cell cycle and it was shown to interact with H2AX (a marker of DSB) following γ-IR [95].

homeostatic regulator of the DDR, mainly because of dephosphorylating proteins that are substrates ATM [92].

1.7 Dynamics of the proteins in cancer cells following DNA damage

1.7.1 p53 dynamics measured over populations of cells

The levels of p53 in normal cells are regulated by the rapid turnover of the protein. Activation of the p53 pathway following DNA damage results in increased level of p53 mainly through the disruption of p53-Mdm2 interactions[7].

Several cancer cell lines tolerate wt p53 (which would be normally growth-suppressive) if they over-express the $Mdm2$ (and/or $Wip1$) gene [27, 92]. For instance, the osteosarcoma cell line (OsA-CL) and the myeloid leukaemia cells (ML-1) both have wt $p53$ gene and amplified $Mdm2$ gene. Exposure of these cells to γ-irradiation was associated with high levels of p53, which was active as a transcription factor for Mdm2. Figure 1.3 shows a time course of changes of p53 and Mdm2 in ML-1 cells after exposure to $2\,Gy$ of γ-irradiation. After DNA damage, p53 increases rapidly and peaks at about $3\,hrs$ post-irradiation. Then the p53 levels decrease by $5\,hrs$ after damage. In contrast, Mdm2 protein levels are not detectably changed at $1\,hr$ post-irradiation (suggesting that Mdm2 induction is transcriptionally dependent on p53), noticeably increase at the $3\,hrs$ time point, peaks at $5\,hrs$, and is decreasing by $9\,hrs$ post-irradiation. Notably, the level of Mdm2 peaks about 2 hours later than the level of p53 following γ-IR, [27].

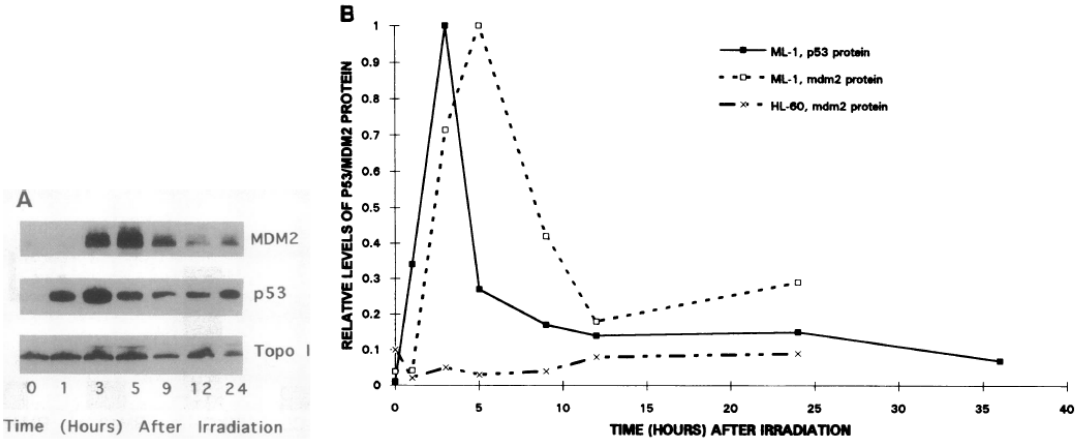

Figure 1.3. Induction of p53 and Mdm2 in ML-1 cells in response to IR of $2\,Gy$. (A) Immunoblot for p53 and Mdm2 proteins in ML-1 cells (expressing wt p53). Topoisomerase I (Topo I) protein levels are shown as a control. (B) Densitometric quantitation of the relative changes in the levels of p53 and Mdm2 proteins in ML-1 cells at various times after IR. For optimal display of changes over time, the levels were normalised so that the peaks of p53 and Mdm2 expression were equal to 1. Relative changes of Mdm2 protein levels in HL-60 cells (which do not have $p53$ gene) at various times after IR are also shown. The figure taken from [27], copyright by the National Academy of Sciences.

[7]Nuclear accumulation of p53 may be partly achieved through its increased half-life. p53 is a short-lived protein with $t_{1/2} = 20 - 30\,min$ [116]; the half-life of wt p53 in human Saos-2 cells without any Mdm2 was determined to 7.3 hours whilst the half-life of wt p53 in these cells with exogenous Mdm2 to 2.5 hours [74].

Another and similar time course of p53 and Mdm2 levels from the murine lymphoma cells (DA-1), ML-1 cells, and BALB/c-3T3 fibroblasts when exposed to the dose of $2\,Gy$ of γ-IR was observed in [61]. In case of DA-1 cells, p53 peaked at the $1\,hr$ and Mdm2 at $1.5-2\,hrs$ time point post-irradiation. In ML-1, p53 peaked at $1\,hr$ at remained at the peak for 2 hours than it started to decay; Mdm2 peaked at $3-4\,hrs$ in ML-1, Figure 1.4. Similarly to the previous case, maximal Mdm2 induction coincided with rapid p53 loss during recovery from DNA damage. The levels of p53 mRNA remained fairly unchanged [61].

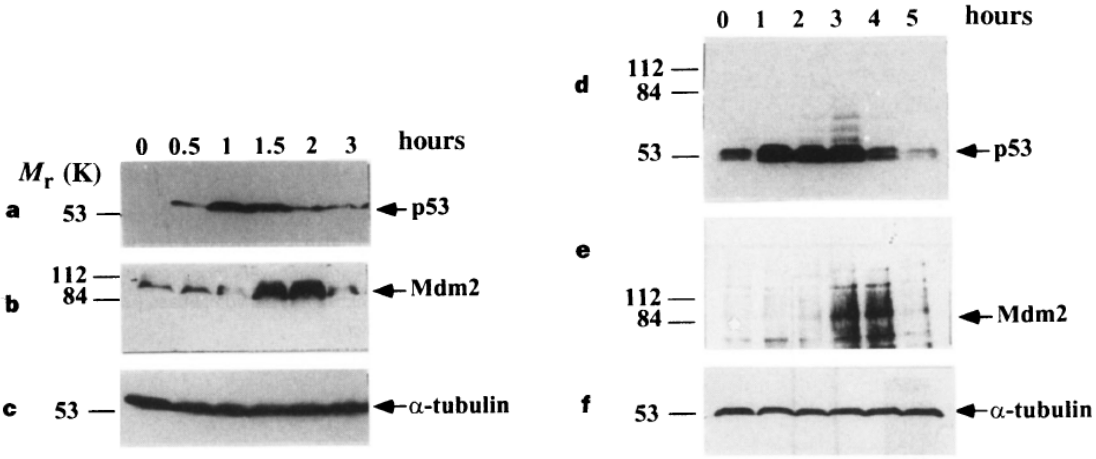

Figure 1.4. Immunoblots for p53 and Mdm2 induction in DA-1 (left panel) and ML-1 (right panel) cells in response to IR of $2\,Gy$. α-tubulin levels are shown as a control. The figures taken from [61]. Reprinted by permission from Macmillan Publishers Ltd: Letters to Nature [61], copyright 1997.

1.7.2 p53 oscillations in single cells

Experiments in individual living breast cancer cells showed that population-averaged analysis could lead to misinterpretation of actual dynamical responses of proteins. Indeed, using measurements across a population of cells (in immunoblots) it was observed that p53 exhibits a series of damped oscillations following DNA damage [86], Figure 1.5. New methods allowing high-resolution time-lapse imaging in individual living cells improved the previously observed p53 dynamics from damped to sustained oscillations of fixed amplitude and periods of oscillations [77, 56], Figure 1.6. Previously it was also observed that the levels of the phosphorylated ATM (ATM-P), when measured at high frequency during the first hour of DDR, increase rapidly and reach maximal level within $5-15\,min$ after damage, then followed by a slow decrease [7]. However, when phosphorylated ATM was measured every hour for a certain period of time, a series of oscillations were identified after DNA damage, [15, 124].

The concentrations of p53 (and also Mdm2, Wip1, ATM) exhibit sustained oscillations with the fixed amplitude and period (duration) of p53 pulses[8] which may persist for several days. In the case of p53, periods of oscillations range from $4-7\,hrs$ in different cells. A number of pulses can be also different from cell to cell and it depends on the dose of γ-irradiation or drugs (e.g., NCS), meaning that the number of pulses increases with the increasing damage dose, [56]. On the other side, the amplitude and duration of p53 pulses in DDR (initiated by

[8]In fact, due to a stochasticity in the protein signalling, the amplitudes of oscillations vary widely from peak to peak whilst the variation in periods is less significant [56], however, in average, oscillations are of fixed amplitude and duration [77].

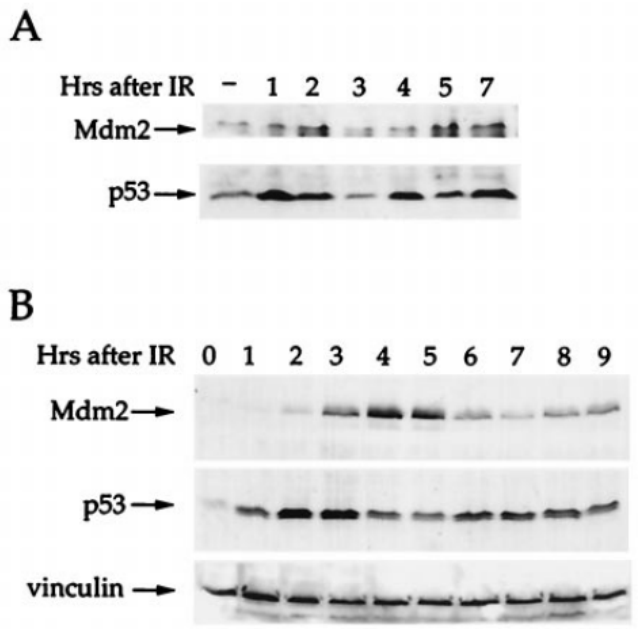

Figure 1.5. Protein levels of p53 and Mdm2 measured by western blot analysis giving oscillations after IR. (A) Mouse fibroblasts NIH 3T3 cells expressing wt p53 and wt Mdm2 were irradiated with 5 Gy of IR. (B) Human breast cancer epithelial MCF-7 cells, expressing wt p53 and wt Mdm2 were irradiated with 5 Gy of IR. Vinculin levels are shown as a control. The figure taken from [86], copyright by the National Academy of Sciences.

DSB) are independent of the damage dose [77, 56][9]. Originally observed damped oscillations are likely the consequence of the loss of synchronisation of p53 signalling in the cells and thus cancelling of pulses over a population of these cells, [124]. Note also that not all cells show oscillations of proteins after DNA damage; however, the fraction of oscillating cells increases with the irradiation dose [56].

Further single-cell experiments on the p53 and Mdm2 dynamics revealed that the p53-Mdm2 feedback loop itself is not sufficient to produce sustained oscillations [15]. Instead, the p53 pulses depend on oscillations of the proteins that sense and transmit the damage signal to p53, particularly ATM and Chk2 (Chk2 itself is a target for ATM), and on the second negative feedback loop between p53 and the phosphatase Wip1, which is schematically illustrated in Figure 3. Even the initial activation of p53 by ATM (and Chk2) is not sufficient to generate multiple p53 pulses and sustained p53 pulses are detectable in parallel to sustained ATM and Chk2 oscillations only; whenever ATM activity is inhibited, oscillatory behaviour of p53 also vanishes [15].

Hence, although Mdm2 is important for the regulation of p53, Mdm2 signalling without ATM and Wip1 does not lead to p53 oscillations in the experiments.

1.7.3 Intracellular localisation and compartmentalisation

Functional information may be encoded in the structural components of a cell (e.g., DNA or enzyme structures) but information in cells can be also transmitted through the spatio-temporal dynamics of signalling molecules [124].

[9] In contrast, p53 response to UV shows one sustained p53 pulse with the dose-dependent amplitude and duration [14], c.f., Figure 6.9.

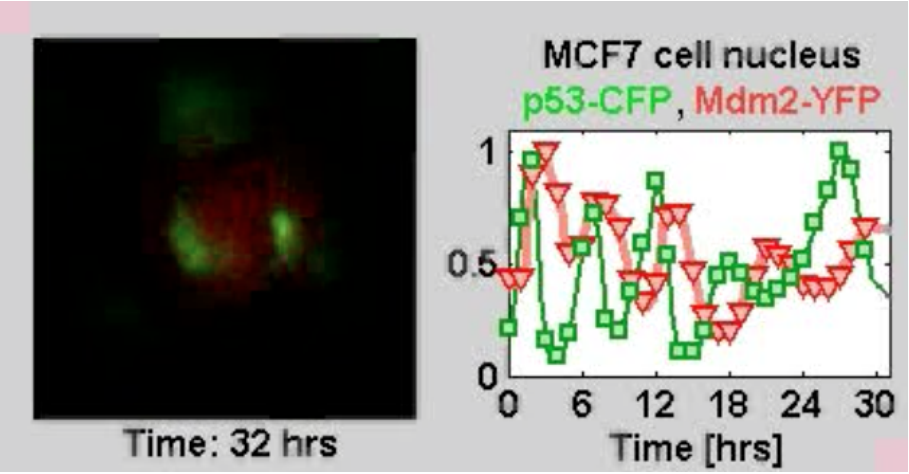

Figure 1.6. Oscillations of p53 and Mdm2 in a single cell: time-lapse imaging of the p53 and Mdm2 proteins fused with CFP (in green) and YFP (in red), respectively, in a single cell following DNA damage caused DSB. The levels of the proteins are normalised. Credits to the Uri Alon Lab [2].

The wt p53 protein, as a transcription factor, is largely nuclear when it is in the activated mode, but a certain fraction of p53 plays a part outside the nucleus [106], notably as a transcription-independent factor involved in the induction of apoptosis [59, 111]. The cytoplasmic clearance of p53 may lead to autophagy [59]. There are three nuclear localisation signals (NLS) at p53 and a couple of nuclear export signals (NES) and thus p53 is in principle able to shuttle between nucleus and cytoplasm through direct interaction with the nuclear import and nuclear export machineries [138]. Nonetheless, Mdm2 seems to be a dominant regulator of subcellular localisation of p53, likely because of the rapid clearance of p53 from the DNA sites [106, 42]. In addition, localisation of p53 is dependent on its oligomeric status [139] and except for Mdm2 there are other cellular substrates which can affect p53 location, see [111].

ATM is also predominantly concentrated in the nucleus with only 10-20% of its molecules found in the cytoplasm, particularly bound to peroxysomes and endosomes [81]. Fluorescent microscopy techniques have confirmed this spatial distribution of ATM between the nucleus and the cytoplasm. However, only the nuclear fraction of ATM is autophosphorylated in response to DNA damage induced by ionising radiation, and activated ATM proteins form detectable foci that are colocalised with the foci of γ-H2AX, a marker of DNA DSB. Cytoplasmic ATM can neither autophosphorylate itself nor phosphorylate its substrates [159].

The transcription and translation of the $Mdm2$ and $Wip1$ genes are localised to the nucleus and cytoplasm, respectively, [146]. Both their protein products Mdm2 and Wip1 are also observed to accumulate mainly in the nucleus in the DDR initiated by ionising radiation [5, 52, 116].

2

Conceptual and Mathematical Foundations

Bearing biological aspects in mind, we can proceed with modelling p53 protein network in a single cell. Motivated by the experiments, a model for p53 activation in response to DNA DSB should involve information-transmitting signal, ATM, which is able to sense the presence of DSB and deliver it to p53, and homeostatic regulators of the DNA damage response, Wip1 and Mdm2. The protein p53 is naturally involved in the modelling. This chapter presents basic concepts for modelling p53 protein network; mathematical principles and main hypotheses used in modelling are stated.

Organisation of the chapter is as follows: Section 2.1 introduces enzyme reactions although these reactions are studied more deeply in Chapter 8. Expression and regulation of Wip1 and Mdm2 through rather simple gene regulatory networks (GRN) as well as induction and regulation of ATM and p53 is discussed in Section 2.2. Sections 2.3 and 2.4 then focus on the intracellular movement of species in the nuclear and cytoplasmic compartments and their translocation between the compartments through the nuclear membrane. Obviously, these two section apply mainly to PDE models due to the spatial representation of the problem. A review of the existing mathematical models is given at the end of this chapter in Section 2.5.

2.1 Protein-protein interactions; post-translational modifications

Cellular responses are controlled either by one particular functionally active protein or by several proteins whose activation and activity towards other proteins in highly specific situations depend on other factors and conditions to which cells are exposed. On the molecular basis, roles of proteins in specific networks are influenced by protein-protein interactions either through post-translational modifications (by attaching a phosphate or acetyl group, ubiquitin to a protein, etc.) or by various compounds formation. For example, stabilisation of p53 through escape from proteasome degradation, which is the major mechanism for regulating p53 protein level, is achieved mainly via post-translational mechanism.

Post-translational modifications (e.g., protein-protein interactions) can be advantageously represented as enzyme reactions (EnR). The prototypic enzyme reaction is schematically

written as

$$S + E \underset{k_-}{\overset{k_+}{\rightleftharpoons}} C \xrightarrow{k_{p+}} E + P,$$

where the enzyme E converts the substrate S into the product P through a two-step process with the intermediate complex C. Using the Law of Mass Action (LMA) and the quasi-steady state approximation (QSSA), see [68, 133] or Section 8.1, we can write an equation for the concentration of substrate S. In particular,

$$\frac{\mathrm{d}[S]}{\mathrm{d}t} = -k_{p+}E_0\frac{s}{K_M + [S]} \quad \text{with} \quad K_M = \frac{k_- + k_{p+}}{k_+}$$

where k_{p+} is the kinetic (turnover) rate of the reaction and K_M is the affinity (Michaelis) constant. In the equation above, E_0 is the initial concentration of the enzyme E and the equation is thought to represent the total loss of the substrate S in the reaction and thus, by using conservation of mass, the total gain of the product P ($\mathrm{d}[P]/\mathrm{d}t = -\mathrm{d}[S]/\mathrm{d}t$). In practical simulations, E_0 is often replaced by the actual concentration $[E]$ at the time $t > 0$. The square brackets $[\cdot]$ denote concentration.

Thus, for instance, phosphorylation of p53 by ATM-P yielding p53-P can be written by

$$p53 + ATM\text{-}P \underset{k_-}{\overset{k_+}{\rightleftharpoons}} C \xrightarrow{k_{ph1}} ATM\text{-}P + p53\text{-}P,$$

which in turn gives terms for the loss of p53 and the gain p53-P, i.e.

$$\frac{\mathrm{d}[p53]}{\mathrm{d}t} = -\frac{\mathrm{d}[p53\text{-}P]}{\mathrm{d}t} = -k_{ph1}[ATM\text{-}P]\frac{[p53]}{K_{ph1} + [p53]}.$$

Similarly, ubiquitination of p53 by Mdm2, written as

$$p53 + Mdm2 \underset{k_-}{\overset{k_+}{\rightleftharpoons}} C \xrightarrow{k_{ub}} Mdm2 + p53_{ub},$$

which results to

$$\frac{\mathrm{d}[p53]}{\mathrm{d}t} = -\frac{\mathrm{d}[p53_{ub}]}{\mathrm{d}t} = -k_{ub}[Mdm2]\frac{[p53]}{K_{ub} + [p53]},$$

and so on.

Enzyme reactions used for post-translational modifications offer some benefits for further modelling since using advanced techniques (e.g., Ping-Pong method or Lineweaver-Burk plots), kinetic parameter k_{p+} and K_M can be estimated under specific experimental conditions. Thus for at least some reactions we can find these rates in the literature. In particular, rates for the Mdm2-dependent ubiquitination of p53 in [78], Wip1-dependent dephosphorylation of ATM-P and p53-P in [136, 137] and Wip1-dependent dephosphorylation of Mdm2-P in [155].

Further discussion on enzyme reactions is left to Chapter 8 where we show firstly validity for the QSSA in the ODE setting and then, after placing enzyme reactions to a spatio-temporal framework, we give some results on the large-time behaviour of a reaction-diffusion system corresponding to the reversible EnR.

2.2 GRN for Wip1 and Mdm2; production and degradation of ATM and p53

A gene regulatory network (GRN) for a specific gene may consist of two main subsequent events: transcription of the gene into the mRNA and its translation into gene's protein

product. From a modelling point of view, we can write two equations for the mRNA and the protein P,

$$\begin{aligned} \frac{\mathrm{d}[mRNA]}{\mathrm{d}t} &= I - \delta_{mRNA}[mRNA], \\ \frac{\mathrm{d}[P]}{\mathrm{d}t} &= k[mRNA] - \delta_P[P], \end{aligned} \tag{2.1}$$

where δ_{mRNA} and δ_P are degradation rates for mRNA and P, respectively; k is a translation rate; and I is a source term for the mRNA production, which usually depends on the specific properties of the protein network.

For example, in Goodwin's "protein-mRNA" model [57], the expression of a single gene is controlled by its protein product P (thus, closing the negative feedback loop). In this case

$$I = \frac{a_1}{A_1 + k_1[P]},$$

where a_1, A_1 and k_1 are some constants.

Another example of the source I, which is also applied here for the transcription of $Mdm2$ and $Wip1$ genes, involves Hill's kinetics (i.e. Hill function of coefficient n). In particular,

$$I = \underbrace{k_S \frac{[TF]^n}{K_S^n + [TF]^n}}_{\text{TF-dependent mRNA production}} + \underbrace{k_C}_{\text{TF-independent mRNA production}}$$

where the first term is the Hill function modelling transcription activity of a transcription factor TF. The protein p53 preferentially forms tetramers, binds DNA and transcriptionally acts as a tetramer [53, 66, 152]. Hence, p53-dependent transcription is modelled by choosing $n = 4$, since we adopt a generally accepted principle according to which n is equal to the number of binding sites of a transcription factor [152], see also [68] Chap. 1. In addition, at least Mdm2 has also a p53-independent promoter. Therefore, we consider a constant basal p53-independent production rate k_C for Mdm2 mRNA. It is not clear if Wip1 has another p53-independent promoter. Nevertheless, we consider a basal production rate for Wip1 mRNA as well. The parameters k_S and K_S are chosen so that p53 is the dominant TF for these genes and the levels of Mdm2 and Wip1 are proportional to the level of p53.

The mRNAs of Mdm2 and Wip1 (likely bound to another proteins acting as their "chaperones", mRNP) then move from the transcription sites in the nucleus to the cytoplasm where they are translated. We assume that translation of mRNAs into proteins occurs in the cytoplasm only and, following [1, 142], we adopt the hypothesis saying that the proteins synthesised outside of the endoplasmic reticulum (ER) move to the nucleus whereas the proteins produced in the ER associate likely with the structures in the cytoplasm. Translation is modelled as a linear contribution to the overall protein concentrations. The translation rate is usually independent of the coding sequence, and thus it is (more or less) similar for all proteins in a given cell type at given conditions [16]. Thus we assume that translation rates for Mdm2 and Wip1 are equal to each other (i.e., $k_{tm} = k_{tw}$).

The mRNA is degraded by a ribonuclease which competes with ribosomes to bind to mRNA. Roughly speaking, if a ribosome binds to mRNA, it will be translated, if a ribonuclease does, it will be degraded. Most eukaryotic mRNAs have half-lives less than 30 minutes and the most short-lived are those that encode proteins whose concentrations need to change rapidly based on the cellular context, such as transcription regulators [1]. Proteins are degraded by a complex cellular machinery, including the 26S proteasome which targets species tagged by ubiquitin (e.g., p53 but also Mdm2, Bax, p21 and other proteins [26]). Degradation

substrate	$t_{1/2}$ $[h]$	δ $[h^{-1}]$	source
p53 (with wt Mdm2)	1/3	2	[116]
p53 (without wt Mdm2)	7	0.1	[74]
p53 mRNA	1/3	2	[1]
Mdm2 mRNA	1	0.7	[104]
Wip1 mRNA*	–	0.7	–
Mdm2	0.5	1.38	[116, 118, 154]
Wip1*	–	1.38	–

Table 2.1. The half-lives $t_{1/2}$ and degradation terms δ of the species used in the models; *the half-lives of the Wip1 and its mRNA are not known, however, since it is short-lived protein as p53 and Mdm2 [26], we assume the same degradation terms as for Mdm2 and its mRNA.

depends on the oligomeric status (the monomer and multimers may be degraded at different rates).

The rate of degradation δ for species (proteins, mRNAs) as above can be deduced from a simple formula giving into relation the first-order (degradation) rate and the half-life $t_{1/2}$ of the species (usually a measurable quantity):

$$t_{1/2} = \frac{\log 2}{\delta}. \tag{2.2}$$

The half-life $t_{1/2}$ is the amount of time which is necessary for a species of a certain concentration to fall to half its value as measured at the beginning of the time period [105], p. 457. Table 2.1 summarises publicly available half-lives and the corresponding degradation rates for all the species[1].

Activation of ATM and its specific regulation following DNA damage as well as production and degradation of p53 are left to separate sections.

2.2.1 ATM activation in response to DSB

Specific regulation of ATM, explained in Section 1.3, allows us to exclude its synthesis from our considerations. The observed way of ATM regulation through its ability to switch between active monomeric and inactive dimeric states, keeping thus ATM in overall constant concentration, can be used rather than introducing another variable for ATM mRNA[2]. In response to DSB, ATM dimers dissociates into active monomers either by sensing changes in heterochromatin (as deduced from *in vivo* experiments) or through interaction with the MRN complex (as observed in *in vitro* experiments). Whether ATM is activated adjacent to or at a distance from the DNA, its activation is observed to be very fast, and we represent ATM monomerisation and activation as an enzymatic reaction initiated by an unknown signal E,

[1] Short half-lives of the species ($< 1\,hr$) strengthen the hypothesis that species that need to be changed promptly in their concentration, including regulators of the cell cycle and several transcription factors such as p53 are degraded rapidly mainly by ubiquitin-dependent proteolysis, [106, 26] and citations therein.

[2] Although we could not find any evidence in the literature, we assume that ATM is long-lived protein with the half-life of several hours; thus, we suppose that the degraded ATM molecules are continuously replaced by new ones so that the total concentration of ATM remains fairly constant. Since ATM is 370 kDa large protein we can speculate that its inactivation through the dimerisation instead of degradation is energetically more profitable.

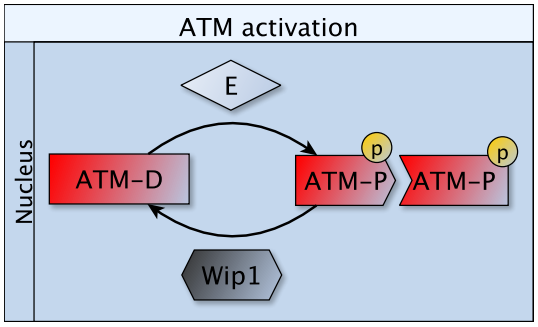

Figure 2.1. A schematic representation of ATM activation by a DNA-damage-transmitting substrate (although hypothetical) E and its deactivation by Wip1.

assumed to be a hypothetical molecule (E can be the MRN complex or any other protein; hereafter expressed in μM), Figure 2.1.

Taking all this together, we can represent ATM dimer dissociation and ATM activation (for simplicity these two events are assumed to occur simultaneously) by the reaction

$$ATM\text{-}D + E \rightleftharpoons Complex \xrightarrow{k_{ph2}} E + 2\,ATM\text{-}P,$$

c.f. (3.2) below, where ATM-D denotes dimeric ATM and ATM-P denotes phosphorylated active monomer. On the other site, ATM deactivation by Wip1 and subsequent dimerisation can be modelled (similarly as a simultaneous process) by

$$Wip1 + 2\,ATM\text{-}P \rightleftharpoons Complex \xrightarrow{k_{dph2}} ATM\text{-}D + Wip1,$$

c.f. (3.3) below. Application of the Law of Mass Action and QSSA[3], yields reaction terms for ATM-P and ATM-D losses and gains, respectively,

$$\begin{aligned}
\frac{d[ATM\text{-}D]}{dt} &= -k_{ph2}E\frac{[ATM\text{-}D]}{K_{ph2}+[ATM\text{-}D]} + k_{dph2}[Wip1]\frac{[ATM\text{-}P]^2}{K_{dph2}+[ATM\text{-}P]^2},\\
\frac{d[ATM\text{-}P]}{dt} &= \underbrace{2k_{ph2}E\frac{[ATM\text{-}D]}{K_{ph2}+[ATM\text{-}D]}}_{\text{ATM-P activation}} - \underbrace{2k_{dph2}[Wip1]\frac{[ATM\text{-}P]^2}{K_{dph2}+[ATM\text{-}P]^2}}_{\text{Wip1-depedent dephosphorylation of ATM-P}},
\end{aligned} \tag{2.3}$$

c.f. (3.4), which can be further merged, just by recalling the conservation of ATM molecules[4], into one equation for ATM-P,

$$\begin{aligned}
\frac{d[ATM\text{-}P]}{dt} =& 2k_{ph2}E\frac{\frac{1}{2}(ATM_{TOT}-[ATM\text{-}P])}{K_{ph2}+\frac{1}{2}(ATM_{TOT}-[ATM\text{-}P])}\\
&- 2k_{dph2}[Wip1]\frac{[ATM\text{-}P]^2}{K_{dph2}+[ATM\text{-}P]^2},
\end{aligned} \tag{2.4}$$

c.f. (3.12), which is the equation used in the ODE model. The single equation (2.4) for ATM-P above cannot be generally used in PDE models where the motion of ATM-P and

[3] Application of the LMA and QSSA and thus these equations are precisely derived in Section 3.2.1.

[4] ATM is conserved, i.e., $[ATM\text{-}P] + 2[ATM\text{-}D] = const$ over the time by our assumption on the constant concentration of ATM.

ATM-D is represented by diffusion, since both ATM conformations can diffuse with different rates. In addition, Hill function of the coefficient 2 rather than Michaelis function (as shown above in (2.3)) is used for the ATM activation by E in the PDE models. The rates k_{ph2}, K_{ph2}, k_{dph2} and K_{dph2} are free parameters, the first two of them chosen so that ATM is rapidly activated following DNA damage.

2.2.2 Modelling p53 production

Abundance of the p53 protein is mainly determined by its degradation rather than by its production [147], for this reason and for simplicity, we do not include p53 mRNA into our simulations[5]. Production of the cytoplasmic p53 is fully governed by a constant basal production rate k_S which is the only source for p53. In the case of PDE models we additionally assume that the total net production of p53 is the same as in the ODE case. This basically means that the production rate k_S gives a rise to the same amount of p53 molecules (measured in $\mu M/h$) in ODE and PDE when measured across the whole basal area in the cytoplasm (where this production is allowed). Similarly to [142], we assume that the basal production rate is active only in a ring-shaped region of the cytoplasm[6] (an annulus) separated from the nucleus by the ER, since proteins produced in the ER very likely do not enter the nucleus [1, 142], see Figure 2.2.

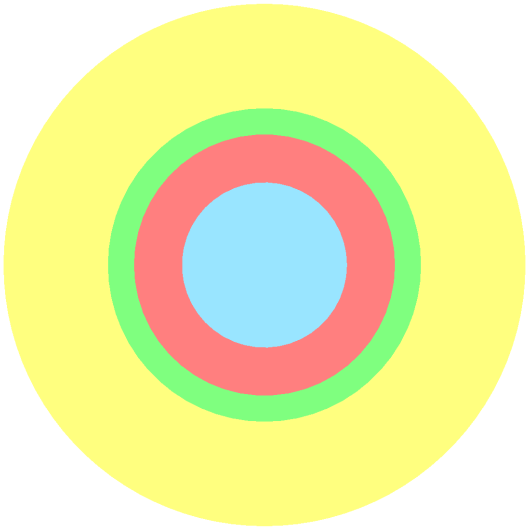

Figure 2.2. A schematic representation of a cell under consideration in 2D. The cell consists of the nucleus (central zone, blue) and the cytoplasm constituted of the endoplasmic reticulum (perinucleic annulus, red) where no translation is allowed and the translation zones (peripheral, green and yellow). The basal production of p53 is assumed to occur in the inner peripheral, i.e., not perinucleic, annulus (green).

2.2.3 Modelling p53 degradation

As already discussed in the biological overview, regulation of p53 by Mdm2 can be achieved through the three different mechanisms. One of them is the ubiquitin-dependent degradation.

[5] Except for Chapter 6 where p53 mRNA plays a prime role.

[6] Because of the above assumption on the total net production, this restriction of p53 production to an annulus in the cytoplasm is not relevant anymore; however, we have used it in [46] and thus we will consider it in the following.

Once p53 is sufficiently ubiquitinated, the p53 protein is exported to the cytoplasm and degraded by the 26S proteasome. Mdm2 plays a crucial role in the p53 ubiquitination as it attaches the first ubiquitin to p53. The effective p53 degradation however requires p53 to be polyubiquitinated. Nonetheless, we assume that the sole ubiquitination by Mdm2 is sufficient for p53 nuclear export and degradation for either degradation or nuclear export of p53. We do not include actions of any other proteins that can either cooperate with Mdm2 in the ubiquitination process (e.g., p300) or deubiquitinate p53 (e.g., Hausp). In addition, we do not assume any p53-Mdm2 complex formation since in some cancer cell lines (e.g., DA-1, ML-1 and BALB/c-3T3 cells) these complexes were barely detectable [61]. Thus the Mdm2-dependent degradation of p53, modelled as an enzyme reaction, yields

$$\frac{d[p53]}{dt} = - \underbrace{k_{ub}[Mdm2]\frac{[p53]}{K_{ub}+[p53]}}_{\text{ubiquitination of p53 by Mdm2}} - \underbrace{\delta_{p53}[p53].}_{\text{natural degradation}}$$

Note that, although Mdm2 is the main regulator of p53 (responsible for its nuclear clearance) we assume some natural Mdm2-independent degradation rates for the cytoplasmic p53 (with the half-life of $7\,hrs$ and the corresponding $\delta_{p53} = 0.1\,h^{-1}$, see Table 2.1). The rates for the Mdm2-dependent degradation $k_{ub} = 5\,min^{-1}$ and $K_{ub} = 1\,\mu M$ are taken from [78].

Stabilisation of p53 in the nucleus depends directly on its phosphorylation by ATM. Thus we assume that the phosphorylated p53-P cannot be degraded by Mdm2.

2.3 Diffusion of species in the cell

Recent photobleaching techniques enable to track the fusion of a protein with the green fluorescent protein (GFP) and thus measure diffusion of such fused proteins. Hinow *et al.* [64] estimate the nuclear diffusion of p53 fused with GFP in H1299 human large cell lung carcinoma cell to be $\sim$900 $\mu m^2/min$, slower than the diffusion of GFP itself ($\sim$2500 $\mu m^2/min$), likely due to multimer formation.

We can assume that an individual p53 monomer migrates faster with a higher diffusivity than the measured p53-GFP diffusivity. Hence, we will use the diffusion coefficient for p53 equal to 1000 $\mu m^2/min$ as an average whether it migrates as a monomer, or multimer (however, it cannot be exported through the nuclear membrane as a tetramer [138]). We are also aware of the fact that diffusion can be different in time and space due to many physical obstacles occurring in the cell or because of specific conditions to which the cell is exposed. For instance, the diffusion coefficient of p53-GFP reduced significantly after the drug treatment by cisplatin and etoposide in HeLa cells: both drugs induce p53 activation and accumulation in the nucleus with diffusion 900 $\mu m^2/min$ decreased up to 200 $\mu m^2/min$ measured 16 hours after anticancer drug activity, [65].

Due to the lack of experimentally measured data, we set the values of the diffusion coefficients for the other proteins by comparing their molecular weights. We will use diffusions of $1000\,\mu m^2/min$ for Mdm2 and Wip1 (90 and 61 kDa, respectively, comparing to $53\,kDa$ of monomeric p53) and $300\,\mu m^2/min$ for ATM ($370kDa$) (monomeric or dimeric).

An increasing number of studies indicate that eukaryotic mRNAs form large ribonucleoprotein particles (mRNP) that are transported from the sites of transcription to the nuclear pores by random Brownian motion [20, 146]. Diffusion of an average mRNA-protein complex vary in the range $1.2 - 2.4\,\mu m^2/min$ [20] and we will use the reference value for an average as well as Mdm2 and Wip1 mRNP complexes equal to $1.8\,\mu m^2/min$. When compared with the diffusion of proteins, the diffusivities for the mRNP are smaller of several orders in magnitude, however, note that mRNP complexes can be of weight as large as $1600\,kDa$ [34].

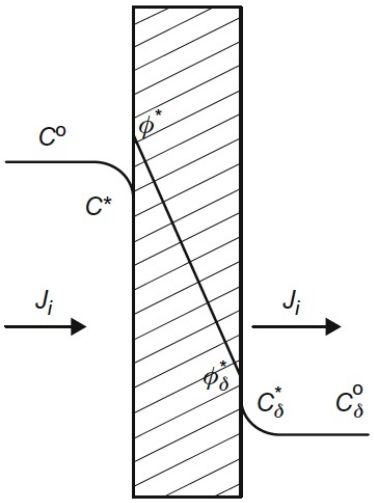

Figure 2.3. Passive transport throughout the nuclear membrane: initial concentrations C^0 and C^0_δ of a specie in two compartments divided by a membrane of the thickness δ. Due to interaction of the species with the membrane, the actual concentrations outside of the both sides of the membrane are $C^\star$ and $C^\star_\delta$ and inside of the membrane $\phi^\star$ and $\phi^\star_\delta$. These values are generally different and satisfy $\phi^\star = HC^\star$ and $\phi^\star_\delta = HC^\star_\delta$ where H is a characteristic parameter dependent on interaction of the species with the membrane. For the flux J, Fick's first law then implies $J = -D\dfrac{\mathrm{d}\phi}{\mathrm{d}y} \approx -D\dfrac{\phi^\star_\delta - \phi^\star}{\delta} = -\dfrac{DH}{\delta}(C^0_\delta - C^0)$, where D is a diffusion rate of a transported substrate through the membrane and the difference of concentrations $C^0_\delta - C^0$ is the driving force for the exchange of the substrate. The coefficient $p = DH/\delta$ is the permeability rate (measured in $\mu m/s$) and it is the property of membrane. For more details see [112], p. 8–9. Figure taken from [112], copyright by Elsevier.

Due to similar nuclear and cytoplasmic cytosol viscosity we will consider the same diffusion values for both compartments. Note that there are other possibilities how to approximate diffusion coefficients of proteins, for example, by using Einstein's formula [23] which, however, requires Stokes radii of the proteins, which are often not known.

2.4 Nucleocytoplasmic transmission, permeability

All the proteins under consideration have weights over 40 kDa (Table 5.2) so that they can use active transport only (and not passive transport) for their translocation between the two compartments. Similarly, mRNA–protein complexes (mRNPs), formed shortly after mRNA synthesis at the transcription site, released to the nucleoplasm and moving toward the nuclear membrane [146] usually have weights over 40 kDa[7]. However, comparing time scales of cargo translocations occurring within a period measured in seconds, a few minutes at most [127], and intracellular protein(mRNA)-dependent events which may hold over hours (e.g., accumulation of species in a compartment, regulation and degradation of the species in the compartments, [56, 77]), we will not involve active transport mechanism here and thus keep the model as simple as possible.

Instead, the transmission of a chemical is represented in our models by a diffusive flux through the boundary that is proportional to the difference between the nuclear and the

[7]The protein in the mRNP usually assists in the mRNA export to the cytoplasm [32], see [32] for the detailed description of mRNP translocation through the nuclear membrane.

cytoplasmic concentrations of the chemical, see Figure 2.3, i.e. we recall the so-called Kedem–Katchalsky boundary conditions (BC) as they have been suggested in [23] and already applied in [43]. The same boundary conditions can be derived from the Fick's first law for stationary fluids (under the assumptions of no net movement, no bulk motion and no coupling effect of more cargoes transported simultaneously), see the caption in Figure 2.3. Additional remarks and the specific BC used in the PDE model are in Section 5.2.4.

Passive transport of the species through the nuclear membrane is determined by the diffusion and the permeability coefficient (itself dependent on the diffusion), see the caption of Fig. 2.3. Note that mRNA export from the nucleus to the cytoplasm can take 10–30 minutes depending on the mRNA [16] which is likely caused not only by a relatively small diffusion but also a highly complex mRNA translocation through the nuclear envelope [32]. This induces another delay in the response to transcriptional activation, since the mRNA can be translated into a protein only once it is exported from the nucleus and binds to the ribosomes.

ATM is assumed to be strictly nuclear, thus we assume that p53 phosphorylation by ATM can occur only in the nucleus. Although Mdm2 is reported to be nuclear we assume that it can freely migrate between the compartments in the ODE model (but not in the PDE models where it is assumed to move from the translation site in the cytoplasm to the nucleus) and it also can ubiquitinate unphosphorylated p53 in both compartments. Unlike p53-P, which is assumed to be localised to the nucleus only, p53 can freely migrate between the compartments. The phosphatase Wip1 is assumed to move from the cytoplasm to the nucleus only since it is predominantly found to be the nuclear protein.

All the diffusion and permeability coefficients considered in our PDE simulations are listed in Table 5.2.

2.5 Overview of other p53 models

There are several mathematical models describing the p53-Mdm2 dynamics, for example the already mentioned model by Lev Bar-Or *et al.* [86] which shows (numerically and experimentally) the presence of damped oscillations. The model developed by Batchelor *et al.* [15], which is actually based on the former models of Geva-Zatorsky *et al.* [56], includes nuclear concentrations of the proteins, more or less, of all four species as we do, i.e. *a signal* (including ATM) that initiates p53 signalling and *an inhibitor* (including Wip1) that inhibits p53. The models [15, 56] rely on Delayed Differential Equations (DDE). However, DDE models may generate artificial rhythms in systems, which do not appear naturally, see [69] and references therein, so that the biological significance of the introduced delays in modelling protein networks is most often far from obvious in those DDE models. Avoiding DDEs, the authors in [69] convert the DDE system [15] into a system of ODEs. However, they still need to involve a positive feedback to obtain oscillations (they chose a recently observed positive feedback involving Rorα).

Ma *et al.* [94, 151] also use DDE to simulate particular delays in representing the transcription of Mdm2 mRNA and translation of the mRNA into Mdm2. Their models contain p53 activation by ATM kinase and nuclear species are considered only.

Ciliberto *et al.* [28] studies the negative feedback $p53 \to Mdm2 \dashv p53$ supplemented by a simplified positive feedback to reconstruct p53-Mdm2 oscillations. In the positive feedback, p53 initiates activation of a cascade of protein interactions (involving PTEN, PIP2, PIP3 and Akt) leading to a temporal inhibition of cytoplasmic Mdm2 translocation to the nucleus. T. Zhang *et al.* [160] explore the mechanism of p53-Mdm2 network of [28] and offer three other models simulating p53-Mdm2 dynamics which combine different positive feedbacks with

the p53-Mdm2 negative feedback. As we have already mentioned there exist several positive feedbacks between p53 and, e.g., PTEN, p14/19 ARF, Rb, Dapk1, c-Ha-Ras, DDR1 and Rorα which could be in principle combined with the p53-Mdm2 negative feedback loop and give a rise to oscillations[8]. In addition, the model in [160] proposes a mechanism enabling a cell to decide between cell cycle arrest and apoptosis, assuming that persistent p53 pulses trigger apoptosis. X.P. Zhang *et al.* [161] combine results of [28, 160] and develop a two-phase switch model, which includes p53-Mdm2, ATM-p53-Wip1 and p53-PTEN-Akt-Mdm2 feedback loops to simulate irreversible transition from cell cycle arrest to apoptosis[9].

Both ODE models of [160, 161] simulate cell fate decision by involving transcription of proarrest and proapoptotic proteins p21 and p53DINP1, respectively, the activation of which, however, is regulated by the p53 affinity for the genes. Following this affinity assumption, proarrest proteins are produced initially in an early cell response phase to DSB (controlled by a "p53-arrester") and proapoptotic proteins are produced later after a few p53 pulses (controlled by a "p53-killer")[10].

The p53-dependent transcriptional regulation of proteins is modelled by using Hill functions, mostly with coefficients 3 and 4, in the mentioned works [28, 94, 151, 160, 161].

Another model which simulates p53 signalling network through the p53-Mdm2 negative feedback combined with PTEN/Akt positive feedback and taking stochastic effects into account is proposed by Puszyński *et al.* [126]. In their recent work [125] (based on [126]) they explore pharmacodynamics of a small molecule Nutlin-3 which is able to inhibit p53-Mdm2 interactions. Sturrock *et al.* [141, 142, 143] and Dimitrio *et al.* [42, 43] study the sole p53-Mdm2 negative feedback (without active roles of ATM and Wip1) in maintaining p53 oscillatory dynamics using spatial PDE models.

[8] This confirms the complexity of p53 signalling in the sense that whenever one path of the p53 network is inactivated for some reason, the proper oscillatory behaviour of p53 can be still triggered by another one or more paths which can contribute to the normal p53 signalling, *etc.*.

[9] A tricky part of the models using Akt/PTEN signalling is in an uncertainty in the experimental results, see BOX-1.

[10] However, as it is discussed in the biological review, such affinity-based preference of p53 for the downstream substrates was not shown in several studies.

3

Physiological and compartmental ODE model for the p53 network

We start our modelling with a physiological and compartmental ODE model which is an extension of the model of L. Dimitrio et al. *[43, 42]. Unlike in the originally proposed model, we integrate ATM and Wip1 into the p53-Mdm2 dynamics so that p53 activation and regulation can be modelled more plausibly with respect to the relevant biological observations discussed in the biological overview. Thus, in contrast to the model in [43, 42], which took into account the sole p53-Mdm2 negative feedback only, we consider all four species including ATM activating the DDR in response to DSB and Wip1 acting to maintain homeostasis in the DDR.*

Organisation of the chapter is as follows: A short introduction to ODE modelling for p53 is in Section 3.1. Section 3.2 which presents the ODE model is then followed by numerical simulations in Section 3.3 and concluding remarks in Section 3.4.

Results presented in this chapter were published in [47],

> [47] *J. Eliaš, L. Dimitrio, J. Clairambault, and R. Natalini. The p53 protein and its molecular network: Modelling a missing link between DNA damage and cell fate. Biochimica et Biophysica Acta (BBA) - Proteins and Proteomics, 1844(1, Part B):232–247, 2014.*

3.1 Introduction to the ODE model

Most of the existing models describing p53 activation and regulation in single cells following their exposure to DNA damaging stress agents rely on either DDEs or ODEs modelling the p53-Mdm2 negative feedback alone or in combination with a positive feedback. We show that p53 oscillations that have been observed in individual cells can be reconstructed and predicted by compartmentalising cellular events occurring after DNA damage, either in the nucleus or in the cytoplasm, and by describing network interactions, using ODEs, between the ATM, p53, Mdm2 and Wip1 proteins, in each compartment, nucleus or cytoplasm, and between the two compartments.

The compartmental p53-Mdm2 model developed by L. Dimitrio *et al.* [42, 43] is extended by considering the ATM and Wip1 proteins, since in the light of new evidence from single cell experiments, the p53-Mdm2 negative feedback should not be sufficient for triggering oscilla-

tions. Instead, initiation and regulation of p53 must involve the ATM and Wip1 proteins, the dynamics of which should be fully described by mathematical variables, solutions of ODEs, rather than represented by constant parameters. As previously discussed, ATM is interpreted as an identifier of DNA DSB, although it is not a direct DNA DSB sensor [117]. In our context, a special signal denoted by E acts as a transmitter of information about the presence of DNA DSBs, and it is assumed to be a constant positively correlated with the DNA damage dose[1]. In the original model, compartmentalisation of cellular events together with the p53-Mdm2 feedback ($p53 \to Mdm2 \dashv 53$) led to the desired p53 oscillatory behaviour even with a constant ATM (considered as a measure of DNA damage). Under our new assumptions, ATM and Wip1 concentration are considered as continuous time-dependent functions, and we show that the feedbacks $p53 \to Mdm2 \dashv p53$ and $ATM \to p53 \to Wip1 \dashv ATM$ together with compartmental distribution of proteins can then reconstruct the oscillatory dynamics of these proteins.

3.2 ATM-p53-Mdm2-Wip1 compartmental model

In this section, we design and analyse a mathematical model that can successfully be used to reconstruct *in silico* experimentally observed dynamics of proteins, namely, the main cellular actor p53, ATM as a protein transferring the DNA damage signal, Wip1 as a dephosphorylation factor of both p53 and ATM, and Mdm2 that tags p53 for degradation. Note that our model is compartmental in the sense that we strictly distinguish the activities of proteins occurring in the nucleus from those occurring in the cytoplasm, as it is shown on Figure 3.1.

3.2.1 Modelling ATM activation and deactivation

ATM activation, i.e. its autophosphorylation and consequent dissociation of ATM dimers into (active) monomers, can be modelled in several ways. The simplest way is through the dissociation reaction

$$ATM\text{-}D \underset{k_{-m}}{\overset{k_m}{\rightleftharpoons}} ATM\text{-}P + ATM\text{-}P, \tag{3.1}$$

where ATM-D denotes a compound of two ATM kinases and ATM-P is active (phosphorylated) ATM. In our model, ATM in inactivate state is considered in the form of dimers only. The constants k_m and k_{-m} denote, respectively, the monomerisation (forward) and dimerisation (reverse) rates of the reaction. Reaction (3.1) involves monomerisation (dissociation) of a dimer complex ATM-D to the two active ATM species with the rate k_m and dimerisation of two ATM-P monomers to produce ATM-D with the rate k_{-m}. The Law of Mass Action then can give mathematical relations between ATM-D and ATM-P, with the production of ATM-D being equal to the half degradation of ATM-P [68]. A disadvantage of presenting the activation/deactivation of ATM as in (3.1), however, is that it does not mention any *signal* initiating ATM-D dissociation, whereas such a signal is thought to be produced by changes in the chromatin structures after DNA damage [7] and/or by the MRN complex as a DNA strand breaks sensor [117].

Hence, a more convenient way to represent ATM activation with the perspective of further analysis is to involve a hypothetical, likely molecular and so far biologically (*in vivo*) unidentified DNA damage signal E, produced by DNA damage recognition sensors, transmitted to and sensed by ATM, resulting in the dissociation of ATM dimers into two molecules

[1] We assume that the higher doses a cell is exposed to, the bigger number of DSB is caused, the stronger activation signal E is produced.

of ATM-P, i.e.

$$ATM\text{-}D + E \underset{k_{-i}}{\overset{k_i}{\rightleftharpoons}} Complex \xrightarrow{k_{ph2}} E + 2\,ATM\text{-}P \tag{3.2}$$

with the corresponding kinetic rates k_i, k_{-i} and k_{ph2}. This reaction is not a typical enzymatic reaction since the enzyme-like signal E in this approach is a non-specified signal corresponding to DNA damage; it is not necessarily an enzyme; however, we assume that E is not amplified, reduced nor changed otherwise in a short time interval.

ATM deactivation by Wip1 is modelled similarly as

$$Wip1 + 2\,ATM\text{-}P \underset{k_{-j}}{\overset{k_j}{\rightleftharpoons}} Complex \xrightarrow{k_{dph2}} ATM\text{-}D + Wip1. \tag{3.3}$$

Here, it is assumed that phosphatase Wip1 exists in a sufficient concentration to dephosphorylate ATM active monomers in the sense that whenever one ATM-P protein is dephosphorylated, another dephosphorylated ATM protein is present, so that they are immediately bound to the dimeric ATM-D. Kinetic rates are denoted by k_j, k_{-j} and k_{dph2}.

Note that ATM activation and deactivation by Wip1 occur in the nucleus.

The Law of Mass Action (LMA) and the QSSA [68, 133] then yield differential equations for (3.2) and (3.3); in particular, changes of concentrations in time of ATM-D and ATM-P are, respectively,

$$\begin{aligned}
\frac{d[ATM\text{-}D]}{dt} &= -k_{ph2}E\frac{[ATM\text{-}D]}{K_{ph2} + [ATM\text{-}D]} + k_{dph2}[Wip1]\frac{[ATM\text{-}P]^2}{K_{dph2} + [ATM\text{-}P]^2},\\
\frac{d[ATM\text{-}P]}{dt} &= 2k_{ph2}E\frac{[ATM\text{-}D]}{K_{ph2} + [ATM\text{-}D]} - 2k_{dph2}[Wip1]\frac{[ATM\text{-}P]^2}{K_{dph2} + [ATM\text{-}P]^2},
\end{aligned} \tag{3.4}$$

since the rate of change of ATM-D is half that of ATM-P. Here $K_{ph2} = \dfrac{k_{-i} + k_{ph2}}{k_i}$ and $K_{dph2} = \dfrac{k_{-j} + k_{dph2}}{k_j}$ are the Michaelis rates of reactions (3.2) and (3.3), and k_{ph2} and k_{dph2} are the velocities of these reactions.

Indeed, using the Law of Mass Action and the QSSA, the loss of ATM-D derived from the first reaction (3.2) can be written in the form

$$\frac{d[ATM\text{-}D]}{dt} = -k_{ph2}E\frac{[ATM\text{-}D]}{K_{ph2} + [ATM\text{-}D]}. \tag{3.5}$$

However, the equation for the loss of ATM-P is not so straightforward, since as a substrate we now have two ATM-P proteins. Let us write

$$s = [ATM\text{-}P],\ e = [Wip1],\ p = [ATM\text{-}D] \quad \text{and} \quad c = [Complex]$$

for the concentrations of the reactants in (3.3). Then the Law of Mass Action applied to (3.3) leads to the following equation for the substrate s,

$$\frac{ds}{dt} = -2k_j s^2 e + 2k_{-j}c, \tag{3.6}$$

since in every c that is made, two of s are used, and every time c is degraded, two of s are produced; and for the other reactants,

$$\begin{aligned}
\frac{de}{dt} &= -k_j s^2 e + (k_{-j} + k_{dph2})c,\\
\frac{dc}{dt} &= k_j s^2 e - (k_{-j} + k_{dph2})c,\\
\frac{dp}{dt} &= k_{dph2}c.
\end{aligned} \tag{3.7}$$

The initial conditions are $e(0) = e_0, s(0) = s_0$ and $c(0) = p(0) = 0$. With the conservation property of the enzyme e, $\frac{de}{dt} + \frac{dc}{dt} = 0$, and so with $e(t) = e_0 - c(t)$, we have the system of ordinary differential equations (ODEs) reduced to

$$\begin{aligned} \frac{ds}{dt} &= -2k_j s^2(e_0 - c) + 2k_{-j}c, \\ \frac{dc}{dt} &= k_j s^2(e_0 - c) - (k_{-j} + k_{dph2})c. \end{aligned} \tag{3.8}$$

The quasi-steady-state approximation then assumes $\frac{dc}{dt} \approx 0$. Hence, from the second equation in (3.8) we can explicitly write c in terms of s, in particular,

$$c = \frac{e_0 s^2}{K_{dph2} + s^2} \tag{3.9}$$

where $K_{dph2} = \frac{k_{-j} + k_{dph2}}{k_j}$ is the Michaelis rate of the reaction. Substituting c in the equation for s, we finally can write

$$\frac{ds}{dt} = -2k_{dph2}e_0 \frac{s^2}{K_{dph2} + s^2}, \tag{3.10}$$

where e_0 is replaced by e in numerical simulations. By coming back to our original problem reaction (3.3), we get the equation for the loss of ATM-P,

$$\frac{d[ATM\text{-}P]}{dt} = -2k_{dph2}[Wip1]\frac{[ATM\text{-}P]^2}{K_{dph2} + [ATM\text{-}P]^2}. \tag{3.11}$$

Finally, the combination of (3.5) and (3.11) gives (3.4).

Note that it is not necessary to use both equations (3.4) in numerical simulations, and actually, both equations involved in the system lead to the Jacobian matrix of the ODE system (composed of the all other equations describing p53-Mdm2 dynamics, see Section 3.2.3), which is singular for $E = 0$, i.e. for the value for which the system achieves equilibrium (no DNA damage is assumed). This is because the derivative of the right-hand side of the first equation in (3.4) with respect to the variable $[ATM\text{-}D]$ is zero for $E = 0$, similarly the derivatives of all other right-hand sides of the equations describing the dynamics of proteins are zeros as well (simply because these equations do not contain $[ATM\text{-}D]$, i.e. they are constants with respect to $[ATM\text{-}D]$); see the equations in (3.16) and (3.17). To calculate the equilibrium for $E = 0$ is a straightforward algebraic exercise; the problem, however, the continuation of the equilibrium curve starting at the computed equilibrium for $E = 0$ fails, since continuation techniques require non-singular Jacobian matrices.

By recalling the conservation the ATM protein, i.e.

$$[ATM\text{-}P] + 2[ATM\text{-}D] = const = ATM_{TOT}$$

and thus by writing $[ATM\text{-}D] = \frac{1}{2}(ATM_{TOT} - [ATM\text{-}P])$ in the second equation in (3.4), we actually have the mathematical equation for $[ATM\text{-}P]$ in the form

$$\begin{aligned} \frac{d[ATM\text{-}P]}{dt} =& 2k_{ph2}E\frac{\frac{1}{2}(ATM_{TOT} - [ATM\text{-}P])}{K_{ph2} + \frac{1}{2}(ATM_{TOT} - [ATM\text{-}P])} \\ &- 2k_{dph2}[Wip1]\frac{[ATM\text{-}P]^2}{K_{dph2} + [ATM\text{-}P]^2}. \end{aligned} \tag{3.12}$$

3.2.2 Modelling p53 pathway by ODEs: assumptions

The dynamics of p53-Mdm2-Wip1 in the nucleus can be expressed by the following reactions:

$$\begin{aligned}
&\text{p53} + Mdm2 \underset{k-}{\overset{k}{\rightleftharpoons}} Complex \xrightarrow{k_{ub}} p53_{ub} + Mdm2 \\
&\qquad\qquad\qquad\qquad \ldots \text{for p53 ubiquitination by Mdm2,} \\
&ATM\text{-}P + p53 \underset{k_{-2}}{\overset{k_2}{\rightleftharpoons}} Complex \xrightarrow{k_{ph1}} p53\text{-}P + ATM\text{-}P \\
&\qquad\qquad\qquad\qquad \ldots \text{for p53 phosphorylation by ATM,} \\
&Wip1 + p53\text{-}P \underset{k_{-4}}{\overset{k_4}{\rightleftharpoons}} Complex \xrightarrow{k_{dph1}} p53 + Wip1 \\
&\qquad\qquad\qquad\qquad \ldots \text{for p53 dephosphorylation by Wip1,}
\end{aligned} \tag{3.13}$$

with the corresponding kinetic constants.

Again, the application of the LMA and the QSSA yields the equations for time changes of the nuclear inactive p53 and active p53-P concentrations, i.e.,

$$\begin{aligned}
\frac{d[p53]}{dt} &= \underbrace{k_{dph1}[Wip1]\frac{[p53\text{-}P]}{K_{dph1} + [p53\text{-}P]}}_{\text{dephosphorylation of p53-P by Wip1}} - \underbrace{k_{ub}[Mdm2]\frac{[p53]}{K_{ub} + [p53]}}_{\text{ubiquitination of p53 by Mdm2}} \\
&\quad \underbrace{-k_{ph1}[ATM\text{-}P]\frac{[p53]}{K_{ph1} + [p53]}}_{\text{phosphorylation of p53 by ATM-P}} \\
\frac{d[p53\text{-}P]}{dt} &= \underbrace{k_{ph1}[ATM\text{-}P]\frac{[p53]}{K_{ph1} + [p53]}}_{\text{phosphorylation of p53 by ATM-P}} - \underbrace{k_{dph1}[Wip1]\frac{[p53\text{-}P]}{K_{dph1} + [p53\text{-}P]}}_{\text{dephosphorylation of p53-P by Wip1}} .
\end{aligned} \tag{3.14}$$

We do not consider $p53$ gene expression and its mRNA in this model, since, as it has been already mentioned, the principal means of control on p53 concentration by the cell is through the degradation of the protein, dominantly through the multiple Mdm2-dependent ubiquitination [111]. For simplicity, p53 degradation is rather modelled as an enzymatic reaction and the ubiquitination of p53 in (3.14) is thus interpreted as the loss of mass (i.e. we do not consider another variable for $p53_{ub}$). Note that although p53 degradation controlled by Mdm2 is a preferential way of p53 degradation reported in cells, natural (dominantly cytoplasmic) degradation also occurs, however, with no significant contribution to the overall p53 degradation [61, 97]. Thus, in parallel to Mdm2 ubiquitination labelling of p53, we add a normal decay term for the degradation of the cytoplasmic p53.

As described in Section 2.2, the $Mdm2$ and $Wip1$ genes coding for Mdm2 and Wip1 are dominantly expressed in a p53-dependent manner, which is model by a Hill function with the coefficient 4, since the transcriptionally active p53 appears in tetrameric form [152]. Note that other choices of the coefficient can be used; however, different Hill coefficients may result in different dynamical responses of the studied system. Denoting the basal Mdm2 mRNA production rate k_{Sm}, the protein transcription of the $Mdm2$ gene to its mRNA, $Mdm2_{RNA}$, can be written as

$$\frac{d[Mdm2_{RNA}]}{dt} = k_{Sm} + \underbrace{k_{S_{pm}}\frac{[p53\text{-}P]^4}{[p53\text{-}P]^4 + K_{S_{pm}}^4}}_{\text{Mdm2 gene transcription}}, \tag{3.15}$$

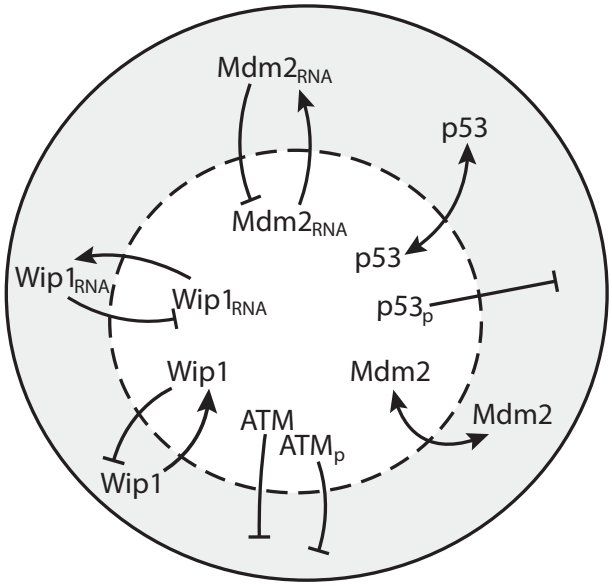

Figure 3.1. Assumptions on the localisation and exchange of the considered proteins between the nucleus and the cytoplasm made in our model. mRNA variables are denoted on this figure by the additional subscript RNA, and similarly the subscript p denotes a phosphorylated protein. The proteins p53 and Mdm2 are assumed to migrate freely (i.e., without diffusion limitations, resulting in homogeneous concentrations) within each of the two compartments. T-shaped lines mean impossible transport in the T-end direction.

where $k_{S_{pm}}$ and $K_{S_{pm}}$ are, respectively, mRNA transcription velocity and Michaelis rate of the p53-dependent transcription of Mdm2 mRNA. The mRNA of Mdm2 then moves to the cytoplasm where it is translated with the constant translation rate k_{tm}. The produced protein Mdm2 can then freely migrate between the cytoplasm and the nucleus, and ubiquitinate p53 in both compartments.

Transcription and translation of the $Wip1$ gene run similarly with the corresponding reaction constants $k_{S_{pw}}$ and $K_{S_{pw}}$, the production rate k_{Sw}, and the translation rate k_{tw}. Unlike Mdm2, the Wip1 protein is assumed to move to, and not from, the nucleus. Other regulation of both proteins is represented by considering degradation terms for the proteins and their mRNA.

Note that the equations (3.17) for the cytoplasmic concentrations of mRNAs describe the concentrations of the mRNAs unbound to ribosomes. In other words, the mRNA of Mdm2 (similarly, the mRNA of Wip1) already used in the translation is modelled as the loss of the free mRNA available in the cytoplasm, and thus it is subtracted from the total mRNA[2].

The compartment-specific physiological roles of the proteins, already mentioned in Section 1.7.3, translate into mathematical simulations in the model that explicitly take into account cell compartmentalisation. Our assumptions about the localisation of these proteins are shown on Figure 3.1. Most of the kinetic velocities and Michaelis constants shown in Table 3.1 appearing in the reactions are taken from the scientific literature and collected in the thesis of L. Dimitrio [42]; ATM and p53 dephosphorylation rates by Wip1 are taken from works of Shreeram *et al.* [136, 137]. Other unknown parameters (in Wip1 expression, ATM activation) are chosen by exploring the space of parameters so that the system exhibit oscillatory dynamics for the proteins.

[2]This is later changed in the PDE modes that is we consider equations for the total concentrations of mRNA not only for its "free" fraction.

These biologically observed facts together with specific boundary conditions for the exchange of species through the nucleocytoplasmic membrane finally result in the ODE system (c.f., equations (3.16) and (3.17)) presented in the following Section 3.2.3, which is solved numerically in Section 3.3.

3.2.3 Modelling p53 pathway by ODEs: equations

Section 3.2 contains the description of all processes and reactions which we have considered in the model. All the mentioned facts can be collected in the following equations, divided into those describing events occurring, respectively, in the nucleus and in the cytoplasm.

Let us remark that the protein/mRNA exchange throughout the nuclear membrane is modelled as a linear contribution of the difference between the averaged nuclear and cytoplasmic concentrations closely determined by the permeability rates (see Section 2.4). For example, the rate of change of p53 because of its nucleocytoplasmic exchange is modelled by the term $p_{p53}V_r([p53]^{(n)} - [p53]^{(c)})$ in the first equation of (3.16) where the superscripts n and c stand for the nuclear and cytoplasmic concentration of p53; V_r is a special volume ratio introduced in [28] to underline the fact that the reactions are V_r-times faster in the nucleus than in the cytoplasm provided that the nucleus is V_r-times smaller than the cytoplasm; and p_{p53} is the permeability coefficient for p53 translocation. Boundary conditions for the special cases, e.g., when a species (mRNA or Wip1) moves from one compartment to another only, can be easily derived from the above equation, see also Section 5.2.4.

Thus we consider the following equations for the nuclear species,

$$
(N)\begin{cases}
\dfrac{d[p53]^{(n)}}{dt} = k_{dph1}[Wip1]^{(n)}\dfrac{[p53\text{-}P]^{(n)}}{K_{dph1}+[p53\text{-}P]^{(n)}} - k_{ub}[Mdm2]^{(n)}\dfrac{[p53]^{(n)}}{K_{ub}+[p53]^{(n)}} \\
\qquad\qquad - k_{ph1}[ATM\text{-}P]^{(n)}\dfrac{[p53]^{(n)}}{K_{ph1}+[p53]^{(n)}} - p_{p53}V_r([p53]^{(n)} - [p53]^{(c)}), \\
\dfrac{d[Mdm2]^{(n)}}{dt} = -p_{mdm2}V_r([Mdm2]^{(n)} - [Mdm2]^{(c)}) - \delta_{mdm2}[Mdm2]^{(n)}, \\
\dfrac{d[Mdm2_{RNA}]^{(n)}}{dt} = k_{Sm} + k_{S_{pm}}\dfrac{([p53\text{-}P]^{(n)})^4}{K_{S_{pm}}^4+([p53\text{-}P]^{(n)})^4} - p_{mRNA}V_r[Mdm2_{RNA}]^{(n)} \\
\qquad\qquad - \delta_{mRNA}[Mdm2_{RNA}]^{(n)}, \\
\dfrac{d[p53\text{-}P]^{(n)}}{dt} = k_{ph1}[ATM\text{-}P]^{(n)}\dfrac{[p53]^{(n)}}{K_{ph1}+[p53]^{(n)}} - k_{dph1}[Wip1]^{(n)}\dfrac{[p53\text{-}P]^{(n)}}{K_{dph1}+[p53\text{-}P]^{(n)}}, \\
\dfrac{d[ATM\text{-}P]^{(n)}}{dt} = 2k_{ph2}E\dfrac{\frac{1}{2}(ATM_{TOT}-[ATM\text{-}P]^{(n)})}{K_{ph2}+\frac{1}{2}(ATM_{TOT}-[ATM\text{-}P]^{(n)})} \\
\qquad\qquad - 2k_{dph2}[Wip1]^{(n)}\dfrac{([ATM\text{-}P]^{(n)})^2}{K_{dph2}+([ATM\text{-}P]^{(n)})^2}, \\
\dfrac{d[Wip1]^{(n)}}{dt} = p_{wip1}V_r[Wip1]^{(c)} - \delta_{wip1}[Wip1]^{(n)}, \\
\dfrac{d[Wip1_{RNA}]^{(n)}}{dt} = k_{Sw} + k_{S_{pw}}\dfrac{([p53\text{-}P]^{(n)})^4}{K_{S_{pw}}^4+([p53\text{-}P]^{(n)})^4} - p_{wRNA}V_r[Wip1_{RNA}]^{(n)} \\
\qquad\qquad - \delta_{wRNA}[Wip1_{RNA}]^{(n)},
\end{cases}
\tag{3.16}
$$

and their cytoplasmic counterparts,

$$(C)\begin{cases} \dfrac{d[p53]^{(c)}}{dt} = k_S - k_{ub}[Mdm2]^{(c)}\dfrac{[p53]^{(c)}}{K_{ub}+[p53]^{(c)}} - p_{p53}([p53]^{(c)} - [p53]^{(n)}) \\ \qquad\qquad - \delta_{p53}[p53]^{(c)}, \\ \dfrac{d[Mdm2]^{(c)}}{dt} = k_{tm}[Mdm2_{RNA}]^{(c)} - p_{mdm2}([Mdm2]^{(c)} - [Mdm2]^{(n)}) \\ \qquad\qquad - \delta_{mdm2}[Mdm2]^{(c)}, \\ \dfrac{d[Mdm2_{RNA}]^{(c)}}{dt} = p_{mRNA}[Mdm2_{RNA}]^{(n)} - k_{tm}[Mdm2_{RNA}]^{(c)} \\ \qquad\qquad - \delta_{mRNA}[Mdm2_{RNA}]^{(c)}, \\ \dfrac{d[Wip1]^{(c)}}{dt} = k_{tw}[Wip1_{RNA}]^{(c)} - p_{wip1}[Wip1]^{(c)} - \delta_{wip1}[Wip1]^{(c)}, \\ \dfrac{d[Wip1_{RNA}]^{(c)}}{dt} = p_{wRNA}[Wip1_{RNA}]^{(n)} - k_{tw}[Wip1_{RNA}]^{(c)} - \delta_{wRNA}[Wip1_{RNA}]^{(c)}. \end{cases} \tag{3.17}$$

The ODE system is nondimensionalised before it is solved in a way that the number of parameters appearing in the equation for ATM activation is reduced to minimum.

All the numerical results presented in the text are, if not specified otherwise, produced by simulations with the constants listed in Table 3.1.

3.2.4 Modelling p53 pathway by ODEs: one-compartment model

In Section 3.3.3 we will demonstrate the necessity of the two negative feedbacks together with the compartmental distribution of cellular events between the nucleus and cytoplasm in maintaining sustained p53 oscillations (c.f., Fig. 3.10(b)). The one-compartmental ODE system which is considered there reads the following equations:

$$\begin{aligned} \frac{d[p53]}{dt} &= k_S + k_{dph1}[Wip1]\frac{[p53\text{-}P]}{K_{dph1}+[p53\text{-}P]} - k_{ub}[Mdm2]\frac{[p53]}{K_{ub}+[p53]} \\ &\quad - k_{ph1}[ATM\text{-}P]\frac{[p53]}{K_{ph1}+[p53]} - \delta_{p53}[p53], \\ \frac{d[Mdm2]}{dt} &= k_{tm}[Mdm2_{RNA}] - \delta_{mdm2}[Mdm2], \\ \frac{d[Mdm2_{RNA}]}{dt} &= k_{Sm} + k_{S_{pm}}\frac{([p53\text{-}P])^4}{K_{S_{pm}}^4+([p53\text{-}P])^4} - \delta_{mRNA}[Mdm2_{RNA}] - k_{tm}[Mdm2_{RNA}], \\ \frac{d[p53\text{-}P]}{dt} &= k_{ph1}[ATM\text{-}P]\frac{[p53]}{K_{ph1}+[p53]} - k_{dph1}[Wip1]\frac{[p53\text{-}P]}{K_{dph1}+[p53\text{-}P]}, \\ \frac{d[ATM\text{-}P]}{dt} &= 2k_{ph2}E\frac{\frac{1}{2}(ATM_{TOT}-[ATM\text{-}P])}{K_{ph2}+\frac{1}{2}(ATM_{TOT}-[ATM\text{-}P])} \\ &\quad - 2k_{dph2}[Wip1]\frac{([ATM\text{-}P])^2}{K_{dph2}+([ATM\text{-}P])^2}, \end{aligned}$$

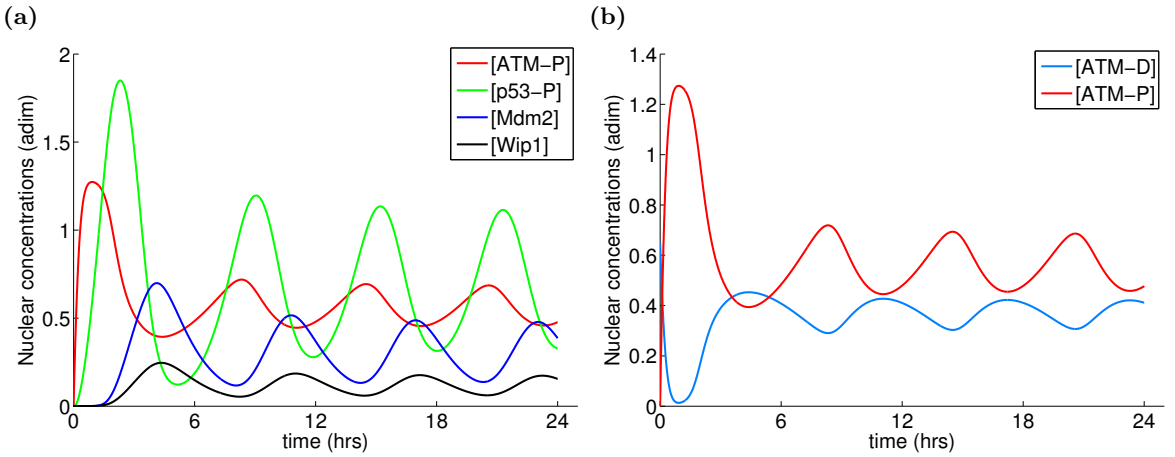

Figure 3.2. (a) Nuclear ATM, p53, Mdm2 and Wip1 (adim) concentrations over a 24 hour-long time interval. (b) Evolution of the ATM monomerisation and dimerisation with the total concentration of ATM, $ATM_{TOT} = 1.3\,\mu M$, and $E = 0.1\,\mu M$ (where E is a hypothetical damage signalling molecule launching ATM activation).

$$\begin{aligned}\frac{d[Wip1]}{dt} &= k_{tw}[Wip1_{RNA}] - \delta_{wip1}[Wip1],\\ \frac{d[Wip1_{RNA}]}{dt} &= k_{Sw} + k_{S_{pw}}\frac{([p53\text{-}P])^4}{K_{S_{pw}}^4 + ([p53\text{-}P])^4} - \delta_{wRNA}[Wip1_{RNA}] - k_{tw}[Wip1_{RNA}].\end{aligned} \tag{3.18}$$

3.3 Numerical simulations and discussion

3.3.1 The ODE model reproduces the oscillatory response of p53 to DNA damage

Under specified circumstances, the model ODE system yields expected pulsatile behaviour for the proteins. Pulses of the involved proteins are illustrated on Figure 3.2. Figure 3.2(a) confirms that the model can be used to reconstruct experimental observations [15]. After DNA damage producing a (likely molecular) signal E with concentration $E = 0.1\,\mu M$ (in this particular simulation), ATM is firstly activated. Then ATM-P phosphorylates p53 and thus, the peak on the curve of p53-P evolution is observed later than the peak of ATM-P. Mdm2 and Wip1 are the targets of active p53-P, hence the corresponding peaks appear after the p53 peak. Mdm2 and Wip1 then regulate p53, which leads to p53-P dephosphorylation and degradation. Wip1 also dephosphorylates ATM-P with the subsequent formation of ATM dimers. The period of the first pulse for nuclear p53-P is ∼5.16 hours and for ATM-P it is ∼4.4 hours which fits experimental observations [15, 77]. The evolution of ATM can be seen on Figure 3.2(b). The amount of activated ATM-P at the peaks of the evolution curve exceeds 50% of all ATM protein, as it has been observed in biological experiments [7]. Note that the total concentration of ATM is set to $ATM_{TOT} = 1.3\,\mu M$ in this simulation.

The pulses of the proteins on Figure 3.2 are, apart from a couple of first pulses, of the same amplitude, i.e., the model quickly produces sustained (undamped) oscillations [15, 77]. This can be seen from the phase planes in Figures 3.3 and 3.4 which show orbits of the solutions

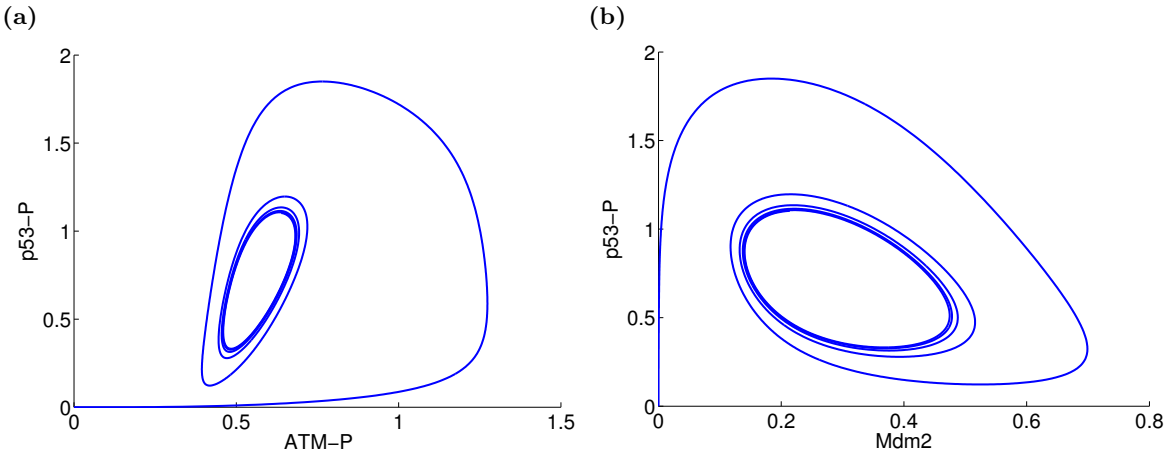

Figure 3.3. Phase plane curves relative to the involved nuclear proteins with $E = 0.1\,\mu M$ (where E is a hypothetical damage signalling molecule launching ATM activation): (a) ATM-P and p53-P (b) Mdm2 and p53-P.

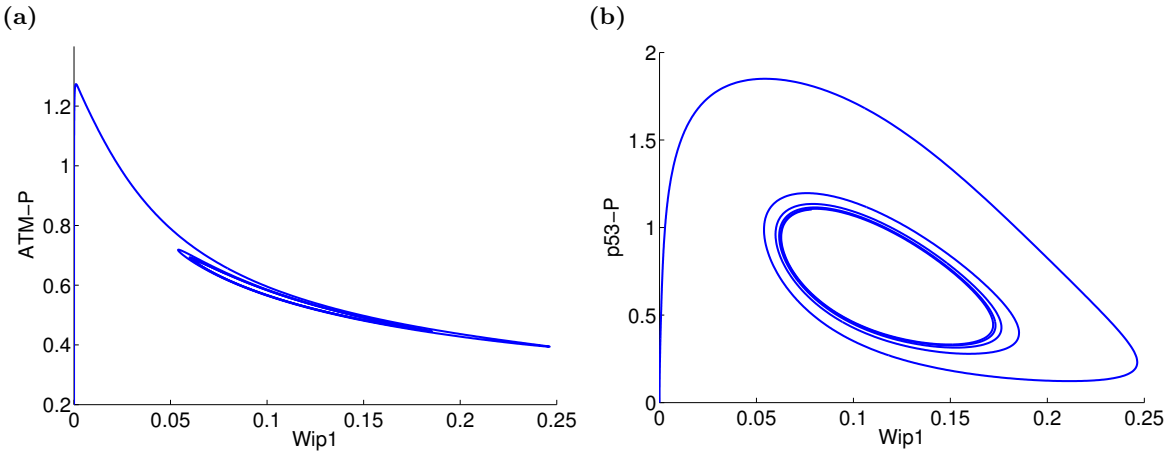

Figure 3.4. Phase planes relative to the involved nuclear proteins within $E = 0.1\,\mu M$ (a) Wip1 and ATM-P (b) Wip1 and p53-P.

converging fast towards the respective stable limit cycles. The first pulses in Figure 3.2(a) are of higher amplitude mainly because of the choice of initial concentrations of proteins; all initial concentrations of proteins are set to be zero in our simulations, and since Wip1 and Mdm2 are not initially present in the cell, the concentrations of p53 and ATM increase until the regulators Wip1 and Mdm2 start to accumulate in the nucleus and thus inhibit further ATM-P activation and p53 production.

The proposed ODE model is "noise-free" and we do not consider any stochasticity in the protein gene expression, nor noise in protein production rates. The amplitudes of experimentally observed pulses in the extended research works of Geva-Zatorsky *et al.* [56] are found to vary widely from peak to peak and from cell to cell (even within the same irradiation dose), mainly due to noise in protein production rates. It is also worth mentioning that the periods of biologically measured oscillations are affected by noise, so that the duration of one pulse may be different from another; however, this difference comes with a variability of (at most) 20% in contrast to the 70% variability in amplitudes [56]. Our ODE model shows variability

in periods in the first couple of pulses, simulated with $E = 0.1\,\mu M$ (Figure 3.5). The first pulse is of length 5.16 hours, the period of the stable limit cycle for $E = 0.1\,\mu M$ is ∼6 hours.

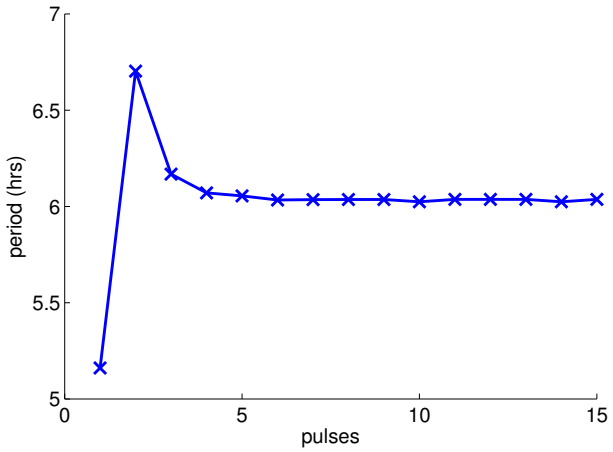

Figure 3.5. The periods of the fifteen p53-P pulses produced by the ODE model within $E = 0.1\,\mu M$. The length of the first pulse is 5.16 hours, the p53-P stable limit cycle is of the period ∼6 hours.

3.3.2 Bifurcation analysis of the system reveals two supercritical Hopf bifurcation points that correlate with DNA damage levels

With $E = 0$ we can easily calculate the equilibrium point of the studied system. Forward continuation, using the Matlab package MATCONT [41], of the equilibrium curve starting from the previously computed equilibrium point, numerically reveals two Hopf bifurcation points with negative Lyapunov coefficients [75] p. 120, i.e., corresponding to supercritical Hopf bifurcations. These Hopf bifurcation points are obtained for the values $E_1 = 2.5 \times 10^{-5}\,\mu M$ and $E_2 = 0.97\,\mu M$. Note that the computed equilibria are hyperbolic, [75] p. 67, except for the two Hopf bifurcation points, since the Jacobian matrix of the system has eigenvalues with non-zero real parts for all values of E except E_1 and E_2. A special situation appears in case of the Hopf points where a pair of complex eigenvalues crosses the imaginary axis, see Figure 3.6(a). For values below E_1 the equilibrium of the system is stable (all eigenvalues have negative real parts) and the concentrations of proteins tend to their steady states very quickly. By passing through this value, the equilibrium becomes unstable (the pair of complex eigenvalues crossing the imaginary axis change the real parts from negative to positive) and stable limit cycles appear; the equilibrium of the ODE system is stable again for $E > E_2$ (all eigenvalues have negative real parts again).

The periods of the stable limit cycles vary between 5.92 and 6.26 hours with varying E, as illustrated on Figure 3.6(b). Bifurcation diagrams of p53-P and ATM-P with respect to E and the phase planes p53-P vs. Mdm2 and p53-P vs. ATM-P are plotted on Figure 3.7. The amplitudes of p53-P and ATM-P of the stable limit cycles are small for the values of E close to E_1 and E_2, respectively (as expected in the case of supercritical Hopf bifurcations), which is illustrated on Figures 3.7(a) and 3.7(b). This does not, however, mean that the amplitudes of concentrations are of such small values throughout the whole time period. In fact, it may take several days until the limit cycle is reached; compare, for example, Figures 3.7(a) with 3.8(a) and 3.8(b), which show the concentrations of species for very small and large E.

In our ODE settings, E is considered as the measure of DNA damage. Interesting situations appear whenever E is small and close to the first Hopf bifurcation point (which may

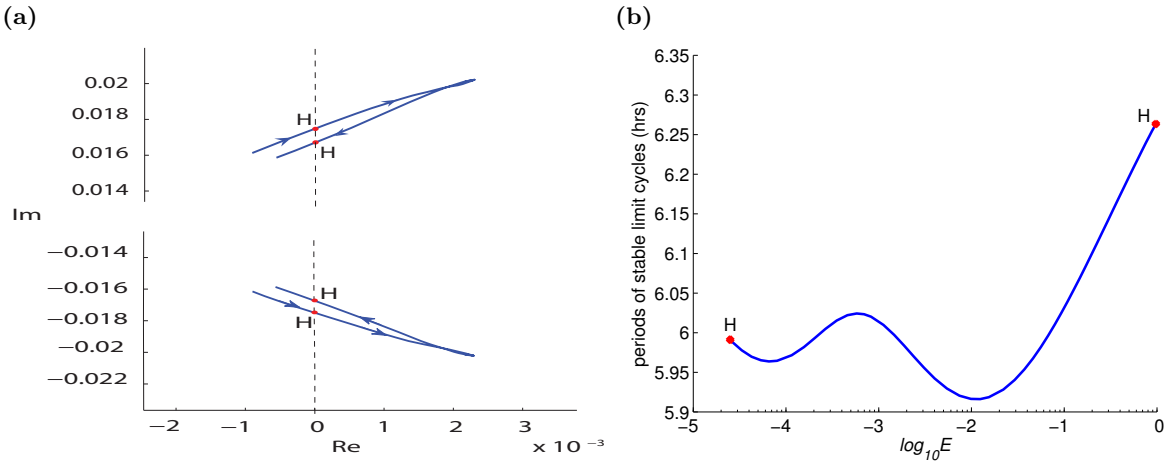

Figure 3.6. (a) A pair of eigenvalues crossing the imaginary axis for $E = 2.5 \times 10^{-5}$ and $E = 0.97$, revealing thus the existence of two Hopf bifurcation points. (b) Evolution of the period of stable limit cycles maintaining between the two Hopf bifurcation points; E is in the logarithmic scale.

correspond to a few DSB only) and when E is very big (which may correspond to serious DNA damage and many DSB). In the first case, the concentration of ATM-P does not even oscillate for the values of E close to E_1, see Figure 3.8(a). The ATM trajectory on Fig. 3.8(a) tends to a steady state of low level; however, this small concentration of ATM-P can still elicit p53-P pulses (rather moderate compared to Fig. 3.2(a)). This may contradict experimental observations that show oscillating ATM in the DDR [15]; note, however, that those experiments were performed with the exposure of cells to 10 Gy of γ-irradiation and not to doses causing only a few DSB (which may correspond to E as small as E_1). On the other hand, other works show evidence that only very small amounts of ATM (even not detectable) can still elicit relevant p53 signalling [13, 159]. Indeed, DNA damage at $E \approx E_1$ may correspond to occasional DNA DSB which do not need ATM for DNA repair and only moderate ATM is produced which is still efficient in p53 activation.

ATM oscillations are damped and disappear for E greater than E_2. Once the oscillations have vanished, they do not appear again with further increasing values of E. Figure 3.8(b), for example, shows the protein dynamics for $E = 10\,\mu M$. In this case ATM is almost fully activated and only small deviations in ATM concentration can be seen. Hence, we can speculate that if E is high and it is impossible to repair DNA DSB, then Wip1 phosphatase activities towards ATM are inhibited, the active ATM achieves its maxima and apoptosis is initiated. However, the latter suggestion is not supported by experimental observations; in fact, there is no paper in the literature, to our best knowledge, clarifying ATM activity and location in single cells committing apoptosis. Thus, ATM may oscillate whenever it is necessary for a proper cell response to DNA damage of an alive cell, and once E becomes too high, oscillations disappear and the cell dies. Such interpretation, however, may require E to be dependent not only on DNA damage levels but also on other factors amplifying the abundance of E, possibly with the contribution of proapoptotic proteins.

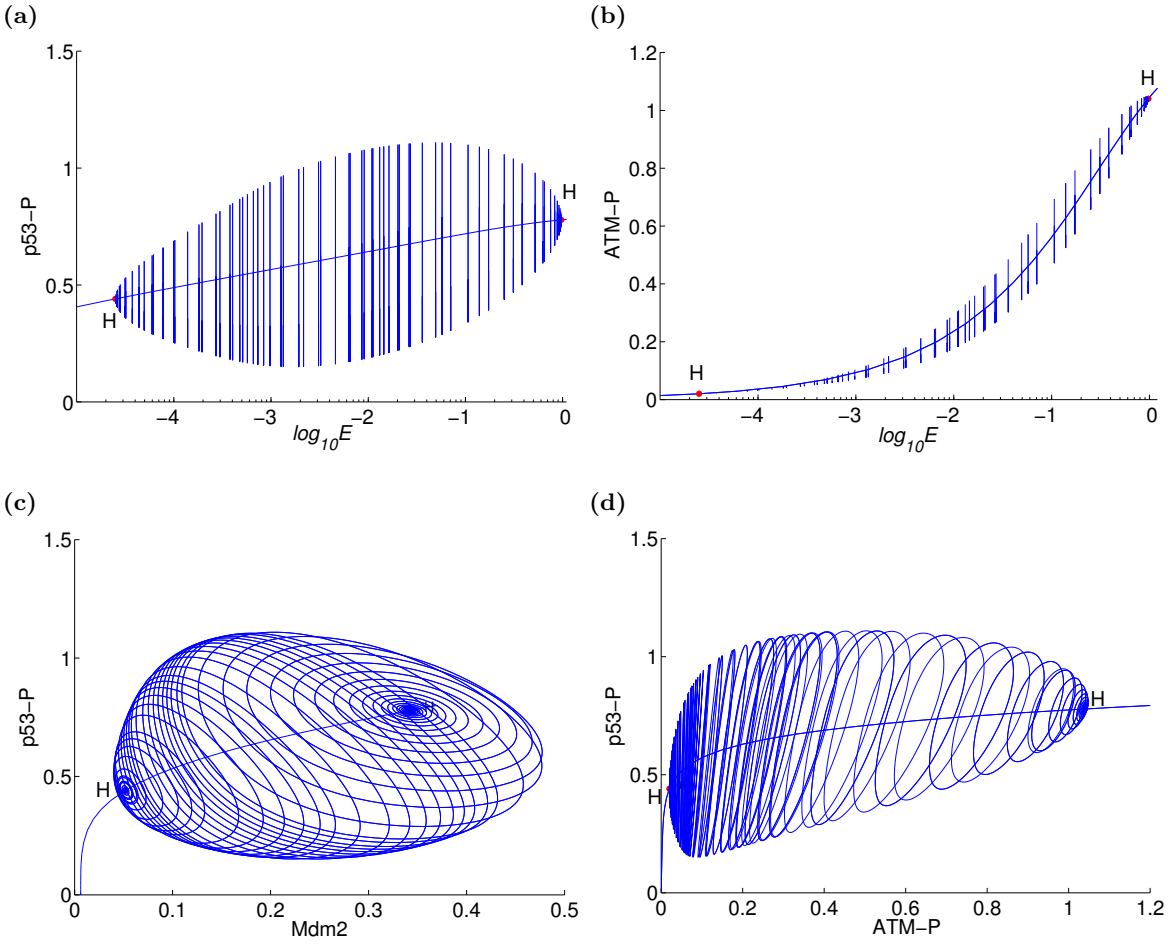

Figure 3.7. (a) Bifurcation diagram for the nuclear p53-P and (b) for the nuclear ATM-P with respect to increasing E; E is in the logarithmic scale. Bars plotted on figures (a) and (b) are the heights (showing maximum and minimum) of the amplitudes of stable limit cycles. (c) p53-P vs. Mdm2 limit cycles occurring for values of the damage signal E between the two Hopf bifurcation points. (d) The same in the p53-P vs. ATM-P phase plane. The equilibrium curves in (c) and (d) are the curves joining the two Hopf bifurcation points H, constituting stable, then unstable, and then stable equilibrium branch again, with the stable limit cycles surrounding the unstable equilibrium points. The plotted concentrations are dimensionless.

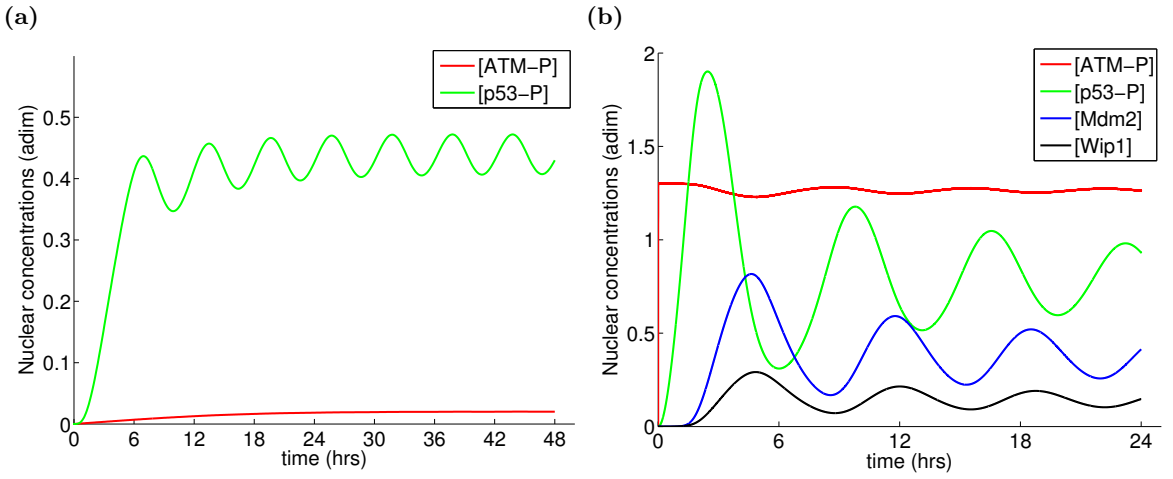

Figure 3.8. (a) Nuclear p53-P and ATM-P (adim) concentrations from the ODE system for $E = E_1 = 2.5 \times 10^{-5}\,\mu M$. The concentration of ATM-P converges to the equilibrium point (which is equal to 0.02) and the concentration of p53-P tends to a stable limit cycle. (b) Nuclear ATM-P, p53-P, Mdm2 and Wip1 (adim) concentrations for $E = 10\,\mu M$. The oscillations of ATM-P are of small amplitude, getting even smaller with further increasing E; $ATM_{TOT} = 1.3\,\mu M$.

3.3.3 Two negative feedback loops and a compartmental distribution of cellular processes produce sustained oscillations

In order to show that the oscillating ATM protein plays an active role in achieving p53 pulses we made several simulations to test different possibilities and thus we explored the system in more details. For example, the model can be used to mimic the observed inhibition of p53 (an Mdm2) pulses following one full ATM pulse [15]; this is illustrated on Figures 3.9, where ATM is inhibited after one pulse. We can see one complete pulse of ATM followed by the pulses in p53, Mdm2 and Wip1 concentration. Wip1 then blocks further ATM activation (in the corresponding equation (3.4) of ATM dephosphorylation by Wip1, the Michaelis rate K_{dph2} is set to be very small, $K_{dph2} = 0.0001$). Although the first pulses of the p53 and Mdm2 proteins are induced they are not sufficient to produce subsequent pulses if ATM signalling is impeded.

Other tests when we inhibit, respectively,

- the negative feedback $Wip1 \dashv ATM$ ($k_{dph2} = 0$ in (3.4), Figure 3.12(a)),
- the positive feedback $ATM \to p53$ ($k_{ph1} = 0$ in (3.14), Figure 3.12(b)),
- the negative feedback $Wip1 \dashv p53\text{-}P$ ($k_{dph1} = 0$ in (3.14), Figure 3.12(c)),
- the positive feedback $p53\text{-}P \to Wip1$ ($k_{S_{pw}} = 0$, Figures 3.12(d) and (e)),

produce either damped oscillations or do not produce oscillations at all. The ATM and Wip1 proteins must thus be involved in the p53-Mdm2 dynamics in order to produce sustained p53 oscillations.

The p53-Mdm2 negative feedback cannot be omitted either, since the inhibition of Mdm2 activity on p53 ($k_{ub} = 0$ in (3.14), see Figure 3.10(a)) or the inhibition of the transcriptional activity of p53-P on Mdm2 ($k_{S_{pm}} = 0$ in (3.15), Figures 3.12(f)) does not produce oscillations.

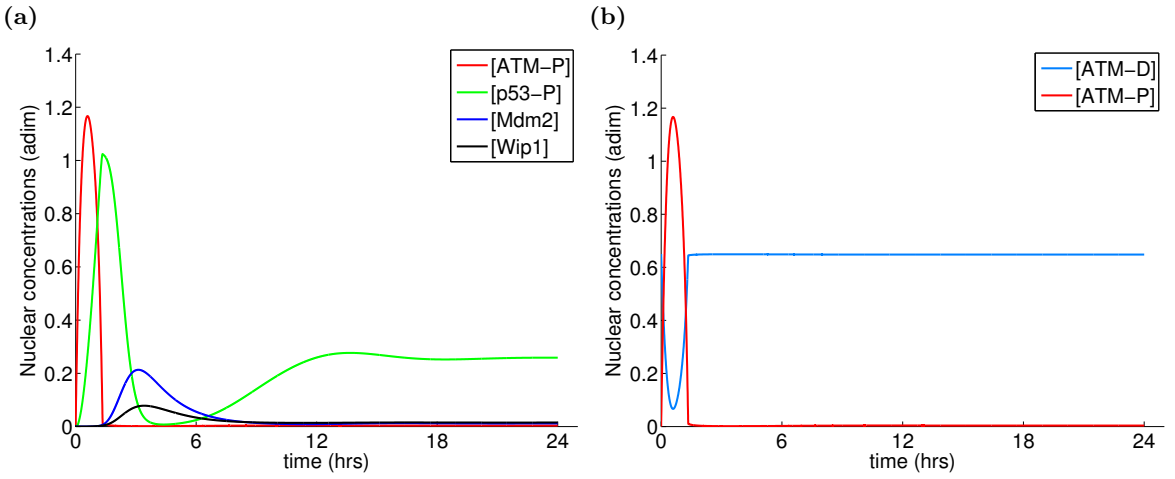

Figure 3.9. (a) Nuclear ATM, p53, Mdm2 and Wip1 (adim) concentrations over a 24 hour-long time interval following ATM inhibition after one full pulse. (b) Evolution of the ATM monomerisation and dimerisation with the total concentration of ATM, $ATM_{TOT} = 1.3\,\mu M$, and $E = 0.1\,\mu M$, following ATM inhibition after one full pulse.

We can further ask whether the two feedback loops without strict location of proteins in the compartments can lead to p53 oscillations. Merging protein dynamics into one compartment (the whole cell), i.e. omitting exchange of the species between the nucleus and the cytoplasm but rather considering both compartments as the one where proteins and their mRNA can freely migrate, is not, however, sufficient in producing sustained oscillations. Figure 3.10(b) shows the concentrations of proteins in the case of $E = 0.1\,\mu M$. Similarly, other choices of E exhibit concentrations of proteins converging to their steady states (bifurcation analysis does not reveal any significant point).

Hence, the feedbacks $p53 \to Mdm2 \dashv p53$ and $ATM \to p53 \to Wip1 \dashv ATM$ together with compartmental distribution of proteins result in sustained oscillations, and neglecting any part of these three components fails to produce sustained oscillations.

3.3.4 ATM threshold required for initiation of p53 pulses

Note again that there are two significant points in the range of the signal E. In particular, these are the two Hopf bifurcation points, $E_1 = 2.5 \times 10^{-5}\,\mu M$ and $E_2 = 0.97\,\mu M$: values of E starting from E_1 are sufficient to elicit sustained oscillations in the concentration of p53, and the second Hopf bifurcation point E_2 is the critical point at which stable limit cycles (otherwise said, sustained oscillations of the proteins) disappear. This point thus may mark a decision for the cell not to go on in DNA DSB repairing processes, and rather to start apoptosis. A relation to a supposed apoptotic threshold which is proposed in [73] remains to be further established.

The hypothetical substrate E is supposed to be produced by DNA DSB sensors (e.g., the MRN complex bound to the DNA break sites) and/or by some changes in the chromatin structure; E may be also affected by other prosurvival and proapoptotic factors. Then E is delivered to the ATM dimers and promotes ATM activation. Interestingly, an amount of E as small as E_1 can (for the value of total ATM protein $ATM_{TOT} = 1.3\,\mu M$) activate ATM at the concentration $\sim$0.02 μM, Figure 3.8(b), that is sufficient to produce oscillations in p53.

Note, however, that the Hopf bifurcation points are dependent on the total nuclear con-

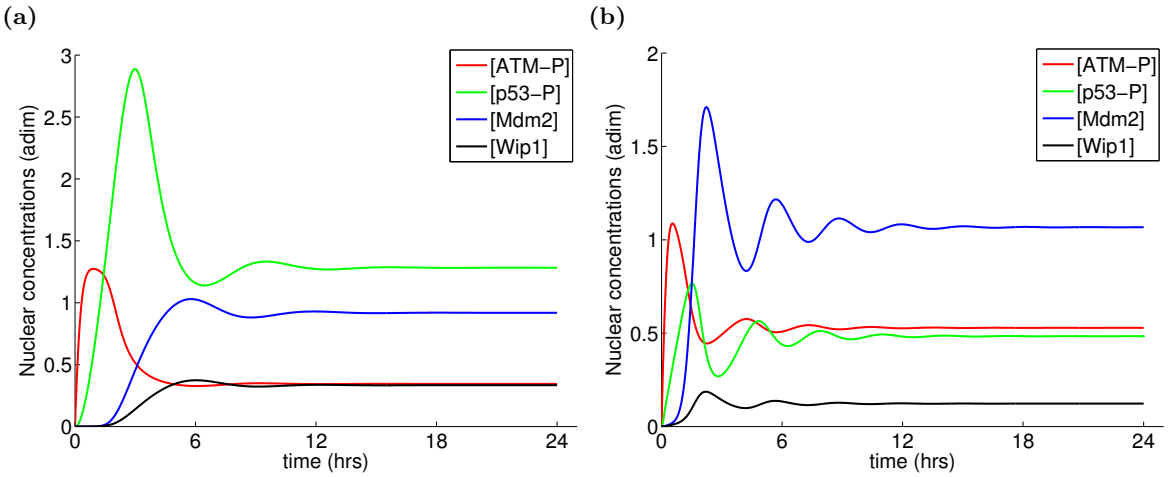

Figure 3.10. (a) Nuclear ATM, p53, Mdm2 and Wip1 (adim) concentrations over a 24 hour-long time interval, $E = 0.1\,\mu M$, in the case when Mdm2-mediated ubiquitination of p53 is inhibited, $k_{ub} = 0$. (b) Nuclear ATM, p53, Mdm2 and Wip1 (adim) concentrations over a 24 hour-long time interval and $E = 0.1\,\mu M$ in the case when only one compartment is considered.

centration of ATM, which is denoted by ATM_{TOT}. Indeed, Figure 3.11(a) shows the evolution of the Hopf bifurcation points with respect to ATM_{TOT} (on the y-axis). We can see that the values of the first Hopf point E_1 do not change dramatically and they range between $1,17 \times 10^{-5}$ (which corresponds to $ATM_{TOT} = 10\,\mu M$) and 3.5×10^{-5} (which corresponds to $ATM_{TOT} = 0.78\,\mu M$). The dependence of E_2 on ATM_{TOT} seems to be more intriguing. Similarly to E_1, the Hopf bifurcation point E_2 increases with decreasing ATM_{TOT}, and asymptotically reaches values corresponding to $ATM_{TOT} \approx 0.77\,\mu M$, Figure 3.11(a). In other words, the system has two Hopf bifurcation points for $ATM_{TOT} > 0.77\,\mu M$ (with similar bifurcation diagrams between these points Figure 3.11(b)). The system possesses only one Hopf bifurcation point between $ATM_{TOT} = 0.082$ and $0.77\,\mu M$ which determines stable solution and unstable solution (stable limit cycle). The system does not have any Hopf bifurcation point for $ATM_{TOT} < 0.082\,\mu M$.

This suggests that there is a threshold in the concentration of ATM that is necessary for the proper oscillatory response of p53. Indeed, p53 can exhibit oscillations in the cells with the total amount of ATM exceeding $0.082\,\mu M$ (in our modelling setting). Notably, when these cell are exposed to agents causing DNA damage which corresponds to $E = E_1$, that is the smallest value of E for which p53 shows oscillations, the activated ATM-P converges to a steady state which is independent of the total ATM molecules in the system. This equilibrium value of ATM-P is $\sim$0.02 μM. See, for example, Figure 3.8(a) where the dynamics of p53 is shown for $E = E_1 = 2.5 \times 10^{-5}\,\mu M$ and $ATM_{TOT} = 1.3\,\mu M$. Note that it has been observed that only a fraction of ATM molecules can be sufficient to activate p53 and thus to initiate DDR [159]. However, a certain threshold for initial ATM concentration is supposed to exist to initiate the ATM signalling pathway [15]. Our model confirms this hypothesis and, in addition, we propose that the value of activated ATM-P is independent of the total ATM molecules in the cell.

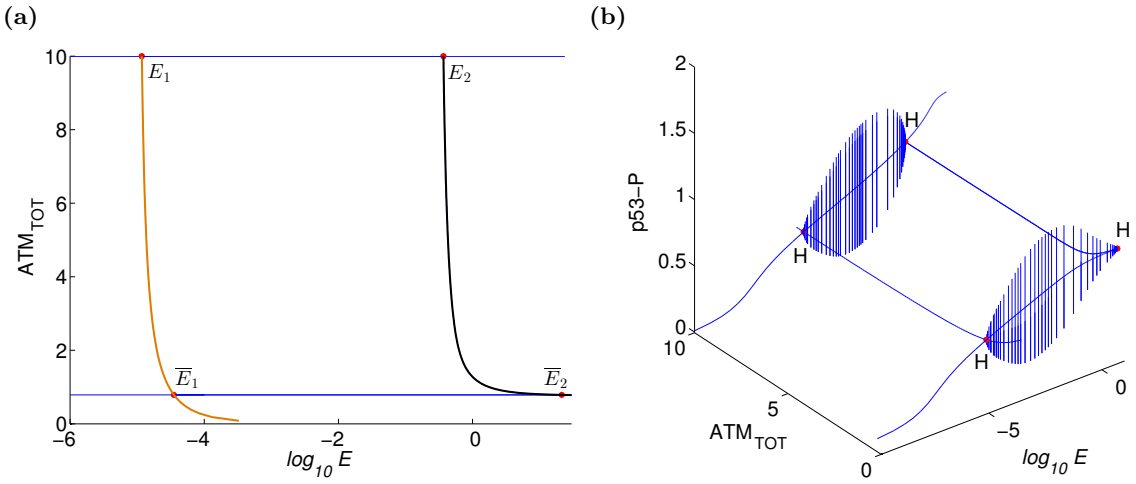

Figure 3.11. (a) The evolution curves of both Hopf bifurcation points (curves in brown and black colours). The plotted Hopf points E_1 and E_2 are computed for $ATM_{TOT} = 10\,\mu M$, the Hopf points $\overline{E}_1$ and $\overline{E}_2$ are computed for $ATM_{TOT} = 0.78\,\mu M$. E is in the logarithmic scale. (b) Bifurcation diagram of p53-P with respect to changing ATM_{TOT} and E.

3.4 Conclusion from the ODE modelling

Explaining experimentally observed p53 oscillations in human cancer cells after exposure of the cells to γ-irradiation [15, 77, 56] is a mathematical modelling challenge, especially in the perspective of proposing p53-mediated anticancer drug-induced cell cycle arrest/apoptotic predictions. The ODE model presented here is the extension of a previous work by Dimitrio *et al.* [42, 43]. It presents the dynamics of the "guardian of the genome" p53, that plays essential parts in cell responses to DNA damage and checkpoint signalling. The compartmental distribution of proteins in a cell is taken into account and it is shown that such compartmental recognition of cellular events allows to reconstruct the pulsatile behaviour of proteins without the need to introduce any time delay in their dynamics.

The oscillatory dynamics of the involved proteins can be speculatively explained as periodical testing of the presence of DNA damage: if unrepaired DNA DSB still exist, additional pulses of both phosphorylated ATM and p53 are triggered. More precisely, the level of phosphorylated ATM-P increases in response to DSB and ATM-dependent phosphorylation of p53 leads to its nuclear stabilisation and activation. p53 acts as a transcription factor of a bench of proteins employed in the cell cycle arrest and DNA damage repair, but also proteins initiating an irreversible decision (such as senescence or apoptosis) and prosurvival proteins which are trying to terminate the DDR and release the cell from the cell cycle arrest. Wip1 and Mdm2 proteins are such homeostatic agents since they act, respectively, through dephosphorylation and ubiquitination of ATM and p53, thus rendering them inactive. When p53 levels are reduced, ATM is released to re-examine the DNA. If the number of DSB remains above a certain threshold, the pathway becomes reactivated, leading to a second pulse of ATM and p53, and this continues until the DNA is repaired or until the cell decides to start apoptosis [15].

The original models of Dimitrio *et al.* [42, 43] involve ATM as a direct measure of DNA damage, in the form of a parameter that remains constant in the studied time interval. It has been experimentally shown, however, that a pulsatile behaviour of p53 cannot be reached without the active and oscillating ATM [15]. In addition, there exist biological

studies that confirm a role of ATM in cancer cell apoptosis induced, for example, by ionising radiations [83]. Hence, in this extended modelling work we consider ATM as an essential part of the DNA damage signalling pathway, varying with the time, that after ATM dimer dissociation and activation phosphorylates p53 and thus initiates p53 transcriptional activity towards proarrest and proapoptotic genes (for example, p21 and 14-3-3σ on the proarrest side, and Pig3, Apaf1 and PUMA on the proapoptotic side). It was shown here that a certain threshold of ATM-P is required for the p53 oscillations (as proposed by experimentalists) and that this threshold does not depend on the total abundance of ATM in the cell.

The p53 protein responds to a variety of cellular stresses (such as those causing DNA strand breaks, e.g., cytotoxic drug insults) through the transcription mode of protein production. Despite the complexity of all signalling pathways occurring in the stressed cells and the production of proteins involved therein, we can conclude that the pathway including p53 activation can be successfully reconstructed by our compartmental model that, in particular, takes into account the ATM-p53-Mdm2-Wip1 dynamics as it has been observed in the scientific literature on the subject [15, 136, 7, 13], and as it is summarised in details in the biological background.

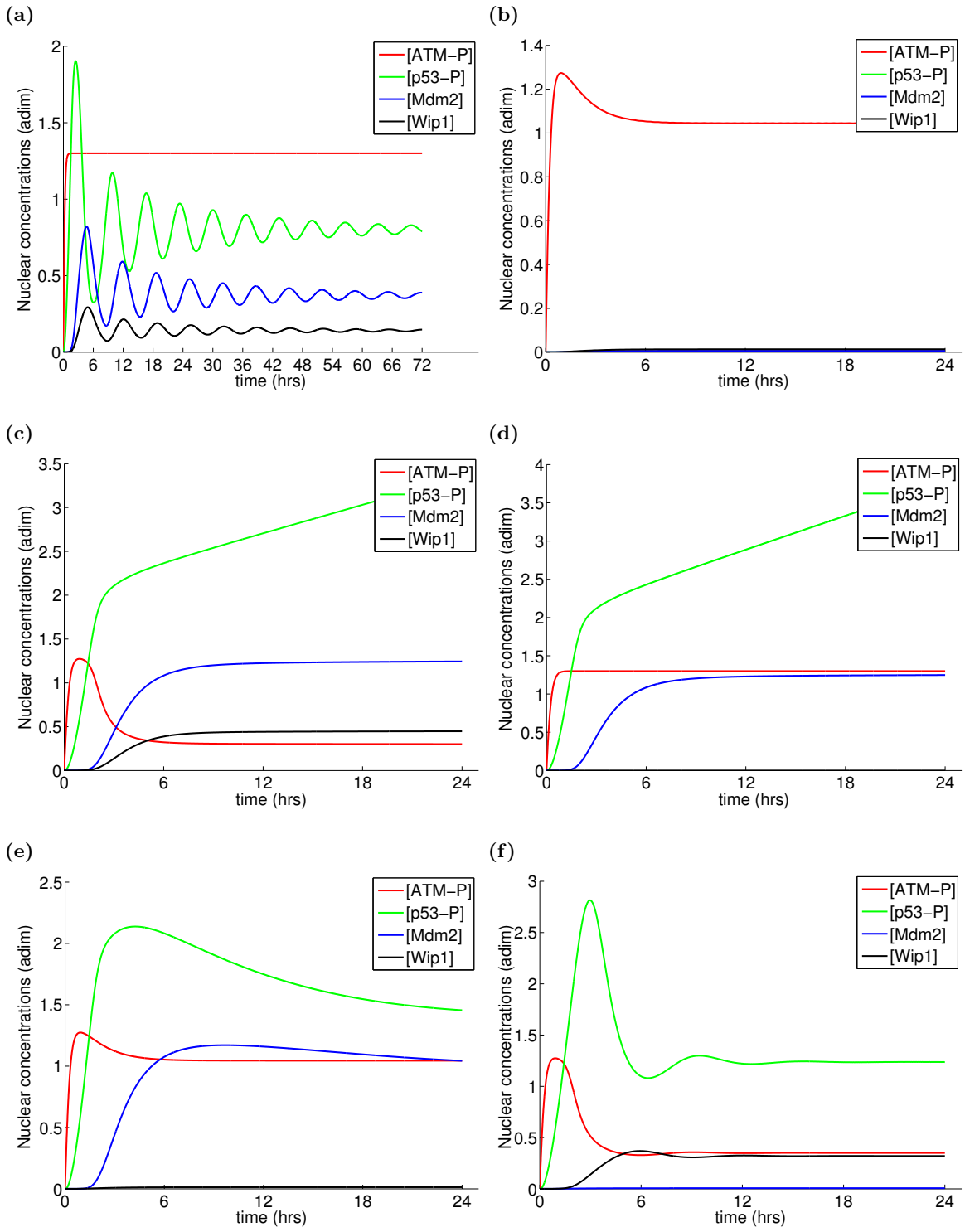

Figure 3.12. Nuclear ATM, p53, Mdm2 and Wip1 (adim) concentrations in the case of (a) inhibition of the negative feedback $Wip1 \dashv ATM$, $k_{dph2} = 0$ in (3.4); (b) inhibition of the positive feedback $ATM \to p53$, $k_{ph1} = 0$ in (3.14); (c) inhibition of the negative feedback $Wip1 \dashv p53\text{-}P$, $k_{dph1} = 0$ in (3.14); (d) inhibition of the positive feedback $p53\text{-}P \to Wip1$, $k_{S_{pw}} = 0$ and $k_{S_w} = 0$; (e) inhibition of the positive feedback $p53\text{-}P \to Wip1$, $k_{S_{pw}} = 0$ and $k_{S_w} = 0.03$; and (f) inhibition of the positive feedback $p53\text{-}P \to Mdm2$, $k_{S_{pm}} = 0$ and $k_{S_m} = 0.005$.

Parameter	Value	Units	Description
k_{ph1}	3	min^{-1}	velocity of ATM-P-dep. ph. of p53
K_{ph1}	0.1	μM	Michaelis rate of ATM-P-dep. ph. of p53
k_{dph1}	78	min^{-1}	velocity of Wip1-dep. deph. of p53-P
K_{dph1}	25	μM	Michaelis rate of Wip1-dep. deph. of p53-P
k_{ub}	10	min^{-1}	velocity of Mdm2-dep. ubiq. of p53
K_{ub}	1.01	μM	Michaelis rate of Mdm2-dep. ubiq. of p53
k_S	0.015	$\mu M/min$	basal synthesis rate of p53
k_{Sm}	0.005	$\mu M/min$	basal synthesis rate of Mdm2 mRNA
$k_{S_{pm}}$	1	$\mu M/min$	velocity of Mdm2 mRNA transcription
$K_{S_{pm}}$	0.1	μM	Michaelis rate of Mdm2 mRNA transcription
k_{tm}	1	min^{-1}	translation rate for Mdm2
k_{Sw}	0.03	$\mu M/min$	basal synthesis rate of Wip1 mRNA
$k_{S_{pw}}$	1	$\mu M/min$	velocity of Wip1 mRNA transcription
$K_{S_{pw}}$	0.1	μM	Michaelis rate of Wip1 mRNA transcription
k_{tw}	1	min^{-1}	translation rate for Wip1
k_{ph2}	15	min^{-1}	velocity of ATM activation by E
K_{ph2}	1	μM	Michaelis rate of ATM activation by E.
k_{dph2}	96	min^{-1}	velocity of Wip1-dep. deph. of ATM-P
K_{dph2}	26	μM	Michaelis rate of Wip1-dep. deph. of ATM-P
δ_{p53}	0.2	min^{-1}	p53 degradation rate
δ_{mdm2}	0.16	min^{-1}	Mdm2 degradation rate
δ_{mRNA}	0.0001	min^{-1}	Mdm2 mRNA degradation rate
δ_{wip1}	0.2	min^{-1}	Wip1 degradation rate
δ_{wRNA}	0.001	min^{-1}	Wip1 mRNA degradation rate
V_r	10	$adim$	nucleus:cytoplasm volume ratio
p_{p53}	0.083	min^{-1}	permeability rate for p53
p_{mdm2}	0.04	min^{-1}	permeability rate for Mdm2
p_{mRNA}	0.083	min^{-1}	permeability rate for Mdm2 mRNA
p_{wip1}	0.083	min^{-1}	permeability rate for Wip1
p_{wRNA}	0.083	min^{-1}	permeability rate for Wip1 mRNA
E	0.1	μM	concentration of "the damage signal"
ATM_{TOT}	1.3	μM	total ATM concentration

Table 3.1. Set of parameter values for the compartmental ODE model (3.16) and (3.17) published in [47]. Most of the parameters for the ODE model are taken from [42, 43], some other are taken from [136, 137]. In the table, "dep." stands for dependent, "ubiq." for ubiquitination, "ph." for phosphorylation and "deph." for dephosphorylation.

4

Reaction-diffusion systems for protein networks

Spatio-temporal dynamics of a variety of proteins is, among other things, regulated by post-translational modifications of these proteins. Such modifications can thus influence stability and biochemical activities of the proteins, activity and stability of their upstream targets within specific signalling pathways. Commonly used mathematical tools for such protein-protein (and/or protein-mRNA) interactions in single cells such as Michaelis-Menten and Hill kinetics, yielding a system of ordinary differential equations (as we have seen in the previous chapter), can be extended into partial differential equations by taking into account a more realistic spatial representation of the environment where these reactions occur. This chapter aims to connect physiological ODE models with their PDE counterparts in the simplest possible case—by involving a space variable and allowing species to diffuse across a domain under consideration.

Organisation of the chapter is as follows: The first of two sections in this chapter, Section 4.2, gives a rather general introduction to reaction-diffusion equations for a protein pathway occurring in a cell composed of two compartments: nucleus and cytoplasm. Section 4.3 presents the Leloup–Goldbeter model for the FRQ protein. Reaction-diffusion models for the p53 protein are left to other chapters. Note that to our best knowledge, the reaction-diffusion Leloup–Goldbeter model is newly presented here.

Partial results presented in this chapter were published in [45],

> [45] *J. Eliaš and J. Clairambault. Reaction-diffusion systems for spatio-temporal intracellular protein networks: A beginners guide with two examples. Computational and Structural Biotechnology Journal, 10(16):12–22, 2014.*

4.1 Introduction to spatio-temporal modelling

In the modelling framework under consideration, all interactions occur in a cell divided into two compartments, the nucleus and the cytoplasm, connected by the semipermeable nuclear membrane and bounded by the impermeable cell membrane, Figure 4.1. Passive transport mechanism discussed in Section 2.4 is modelled by the Kedem–Katchalsky boundary condi-

tions (which can be derived from the Fick's first law). Thus, in addition to the diffusion of species across a compartment, species can migrate from one compartment to another through the nuclear membrane. As an example, the circadian rhythm for concentration of the FRQ protein in *Neurospora crassa* is presented.

One of the simplest 'protein-mRNA' models is a nonlinear biochemical oscillator proposed by Goodwin in 1965 [57] that simulates expression of a single gene controlled by its protein product P, thus, closing the negative feedback loop. In particular, the equations appearing in the original Goodwin model are, respectively,

$$\frac{\mathrm{d}[mRNA]}{\mathrm{d}t} = \frac{a_1}{A_1 + k_1[P]} - \delta_1,$$
$$\frac{\mathrm{d}[P]}{\mathrm{d}t} = a_2[mRNA] - \delta_2,$$

reporting here only production (transcription in the first equation and translation in the second) and degradation terms (δ_1 and δ_2).

Based on this model, a compartmental ODE model for the circadian clock rhythm of the FRQ protein expressed during a day in *Neurospora crassa* was proposed by Leloup and Goldbeter [85]. The model includes expression of the *frq* gene in the nucleus, a process that is influenced by available light, and translation of FRQ mRNA into FRQ in the cytoplasm that, afterwards, enters the nucleus and negatively regulates the transcription of its gene, as it is observed *in vivo* in [4].

The spatial organisation of the cell, however, suggests to consider migration of the involved species in the cytosol and between the compartments, and thus to model a protein signalling more realistically by including diffusivities of the species and by setting particular translocation conditions to model exchanges of the species between the compartments. Thus, one has to deal with coupled systems of nonlinear evolution partial differential equations (PDEs) for the concentrations of the species in the nucleus and in the cytoplasm with transmission boundary conditions (BC) imposed on the inner nuclear envelope and on the outer cellular membrane (Robin-like and zero-flux BC in our modelling setting).

The aim of this chapter is to attract attention to reaction-diffusion equations for protein spatio-temporal signalling rising from protein-protein (and/or protein-mRNA) interactions in the two compartments of a cell, nucleus and cytoplasm, and from migration of the species in and between these compartments. Since it is impossible in general to derive analytical solutions for such coupled systems, numerically, passing to a weaker notion of solution, it can be proved to exist (e.g., in Lipschitz domains as the cellular domains are assumed to be in our approach), for instance by the Rothe method. This method is applied to a reversible enzyme reaction in Appendix B and can be easily adapted to more sophisticated problems, as the Leloup–Goldbeter FRQ model in this chapter and ATM-p53-Wip1-Mdm2 models in the chapters that follow.

4.2 Reaction-diffusion models for protein intracellular networks

Having in mind to represent the signalling of any protein in individual cells whose activity is determined by its post-translational modifications, one can write as many reactions as necessary to sufficiently describe a desired protein dynamics. The Law of Mass Action, Michaelis-Menten and Hill kinetics turn protein-protein interactions and transcription of genes into proteins into a system of ODEs. Since the spatial representation of signalling pathways can reveal diffusion patterns that are hidden in ODEs, one might consider a system of PDEs

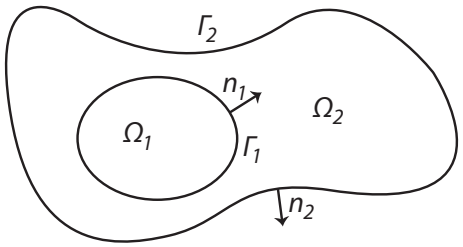

Figure 4.1. Cell scheme: the nucleus Ω_1, the cytoplasm Ω_2, the nuclear membrane Γ_1 and the cell membrane Γ_2; n_1 and n_2 are the unit normal vectors oriented outward from Ω_1 and Ω_2, respectively.

instead of ODEs. In PDEs, the protein dynamics in cells is particularly endowed with diffusivity rates and with some transmission conditions on the nuclear and cell (possibly other) membranes to represent, respectively, migration of species in and their exchange between the cellular compartments and between cells themselves. In the sections that follow we show two examples of oscillators given by reaction-diffusion PDEs [22, 110]. The first one is based on the commonly known and used Leloup–Goldbeter ODE model for circadian rhythms of the protein FRQ in *Neurospora* [85] (Section 4.3)[1]. The second one is a PDE model for the p53 intracellular dynamics following DNA damage in mammalian cells (Chapters 5 and 6). Another example of a signal transduction modelled by reaction-diffusion equations, more precisely, a model of Ran-driven transport process was studied in [134].

In cellular settings, a general coupled reaction diffusion system can be written as follows,

$$\begin{aligned} &\frac{\mathrm{d}u}{\mathrm{d}t} - div(D\nabla u) = f(u) \quad \text{in} \quad [0,T]\times\Omega_1, \\ &\frac{\mathrm{d}v}{\mathrm{d}t} - div(D\nabla v) = g(v) \quad \text{in} \quad [0,T]\times\Omega_2, \\ &+ \text{boundary conditions on } \Gamma_1 \text{ and } \Gamma_2 \end{aligned} \tag{4.1}$$

where $u = (u_1, \ldots, u_N)^T$, $u_i = u_i(t,x) : [0,T]\times\Omega_1 \to \mathbb{R}$ and $v = (v_1, \ldots, v_N)^T$, $v_i = v_i(t,x) : [0,T]\times\Omega_2 \to \mathbb{R}$ for $i = 0, 1, \ldots, N-1$ are the nuclear and cytoplasmic concentrations of N chemicals, $N > 0$, $T > 0$, $f : \mathbb{R}^N \to \mathbb{R}^N$ and $g : \mathbb{R}^N \to \mathbb{R}^N$ collect reaction and production/degradation terms for all N species (some of them can be equal to zero); avoiding any cross-diffusion, D is a diagonal N-by-N matrix with the diffusivities on the diagonal, and div is the divergence operator. The domains Ω_1 and Ω_2 represent the nucleus and the cytoplasm, respectively, assumed to be Lipschitz domains [130], Γ_1 is the nuclear membrane and Γ_2 is the cell membrane. The geometry of a cell under consideration is sketched in Figure 4.1, that in our very simplified framework represents a cell as big as $10-100\,\mu m$ or so, which is able to proliferate and which can have heterogeneous shape. However, we exclude cells of complicated structures and morphologies such as neurons or muscle cells.

As previously outlined, we will consider zero-flux boundary conditions on the outer cell membrane Γ_2, i.e. $\dfrac{\partial v_i}{\partial n_2} = 0$ for $i = 0, 1 \ldots, N-1$ where n_2 is the unit normal vector oriented outward from the cell, Figure 4.1. Although species with molecular weight over $40kDa$ usually use active transport mechanisms to be translocated from one compartment to another, for the sake of simplicity, only passive transport process driven by the difference in concentrations

[1]The Leloup–Goldbeter model for FRQ in *Neurospora* has been later slightly modified by the authors, adding two phosphorylation equations, to represent circadian rhythms of the protein PER in *Drosophila* [84, 31].

at both sides of the nuclear membrane, modelled by the Kedem–Katchalsky BC, is used here [23, 43, 46, 112], for additional details see Section 2.4. In particular, export/import of the nuclear species is modelled by

$$-D_i\frac{\partial u_i}{\partial n_1} = -p_i(v_i - u_i) \tag{4.2}$$

and export/import of the cytoplasmic species by

$$D_i\frac{\partial v_i}{\partial n_1} = -p_i(u_i - v_i), \tag{4.3}$$

where n_1 is the unit normal vector oriented outward from the nucleus (therefore, the BC in (4.3) come with a different sign), and p_i are the permeabilities of the membrane for each species $i = 0, 1, \ldots, N-1$. Recall that if a chemical is assumed to migrate between the compartments in one direction only, e.g. mRNA is supposed to move from the transcription sites in the nucleus to the cytoplasm and not the other way round, then this can easily be modelled by omitting either v_i or u_i in (4.2) and (4.3), cf. (4.6)-(4.8) below.

In addition to the boundary conditions, we will assume initial conditions for each species $i = 0, 1, \ldots, N-1$ to be non-negative functions $u_i(t = 0, x) = u_i^0(x) \geq 0$ and $v_i(t = 0, x) = v_i^0(x) \geq 0$ belonging to $L^2(\Omega_1)$ and $L^2(\Omega_2)$, respectively.

4.3 The Leloup–Goldbeter model for the *Neurospora crassa* circadian clock

4.3.1 The frequency protein and circadian clock

Circadian clock in *Neurospora* controls the pattern of asexual development [44] and a central component of sustained rhythms is the FRQ protein (a long form of 989 amino acids and a short form of 890 amino acids) encoded by the *frq* clock gene [4]. The oscillator consists of a self-control of frq transcription, i.e. a negative feedback loop in which *frq* is synthesised into the FRQ protein (both short and long forms are required for robust rhythmic responses) which, in turn, acts to reduce intensity of *frq* transcription into mRNA [44].

Making the *Neurospora* clock start at midnight when FRQ mRNA and the FRQ protein attain low levels in concentration, we see that transcription of the gene increases and mRNA reaches its peak in the midmorning about 4 hours before the peak of the total FRQ. FRQ enters the nucleus where it contributes to inhibit gene transcription through the interaction with other factors (WC-1 and WC-2) required in the *frq* gene transcription [55, 44]. Partial phosphorylation of FRQ leads to its initial degradation as soon as it enters the nucleus. Degradation then increases with more extensive FRQ phosphorylation through the early night [157, 44].

4.3.2 Spatio-temporal Leloup–Goldbeter PDE model for FRQ

Circadian clock represented by sustainedly oscillating concentration of the FRQ protein is modelled by Leloup and Goldbeter [85] via the following ODE equations,

$$\begin{aligned}
\frac{\mathrm{d}[FRQmRNA]}{\mathrm{d}t} &= V_s\frac{K^r}{K^r + ([FRQ]^{(n)})^r} - V_m\frac{[FRQmRNA]}{K_m + [FRQmRNA]},\\
\frac{\mathrm{d}[FRQ]^{(c)}}{\mathrm{d}t} &= k_s[FRQmRNA] - V_d\frac{[FRQ]^{(c)}}{K_d + [FRQ]^{(c)}} - k_1[FRQ]^{(c)} + k_2[FRQ]^{(n)},\\
\frac{\mathrm{d}[FRQ]^{(n)}}{\mathrm{d}t} &= k_1[FRQ]^{(c)} - k_2[FRQ]^{(n)}.
\end{aligned} \tag{4.4}$$

The first term in the first equation in (4.4) models the transcription of the *frq* gene that is negatively controlled (in a steep way if the Hill coefficient r is high; $r = 4$ here and in [85]) by the expression level of the nuclear FRQ protein, and where the rate of gene transcription V_s is a function of the light available during the day which changes in the time, $V_s = V_s(t, light)$. The second term represents mRNA degradation with the rate V_m. The first term in the second equation stands for gene translation into the cytoplasmic protein, and it is followed by the degradation term and the terms modelling exchange of the protein between the compartments. The equation for the nuclear concentration of the protein contains terms for its exchange between the compartments only.

The model of Leloup and Goldbeter [85] is based on the Goodwin model [57] and Hill functions are used to simulate production/degradation events occurring in the cell. Starting with the model (4.4), we can formulate reaction-diffusion equations for the nuclear and cytoplasmic FRQ protein and its nuclear and cytoplasmic mRNA. To our best knowledge, this is the first attempt to model the classical Leloup–Goldbeter circadian oscillator [85] via partial differential equations. For simplicity, let us simplify notations and write

$$u_0 = [FRQmRNA]^{(n)}, v_0 = [FRQmRNA]^{(c)}, u_1 = [FRQ]^{(n)} \text{ and } v_1 = [FRQ]^{(c)}$$

for the nuclear and cytoplasmic concentrations of FRQ and mRNA of FRQ (distinguished by the superscripts (n) and (c), respectively). The PDE equations may become

$$\begin{aligned} &\frac{\partial u_0}{\partial t} - D_0\Delta u_0 = V_s\frac{K^r}{K^r + u_1^r} - V_m^{(n)}\frac{u_0}{K_m^{(n)} + u_0}, \quad \frac{\partial u_1}{\partial t} - D_1\Delta u_1 = -V_d^{(n)}\frac{u_1}{K_d^{(n)} + u_1}, \\ &\frac{\partial v_0}{\partial t} - D_0\Delta v_0 = -V_m^{(c)}\frac{v_0}{K_m^{(c)} + v_0}, \qquad \frac{\partial v_1}{\partial t} - D_1\Delta v_1 = k_s v_0\chi_{tra} - V_d^{(c)}\frac{v_1}{K_d^{(c)} + v_1}, \end{aligned} \tag{4.5}$$

where, compared with (4.4), degradation of FRQ and its mRNA is considered to occur in both compartments with the (possibly different) rates of degradation $V_m^{(n)}$, $V_m^{(c)}$ and $V_d^{(n)}$, $V_d^{(c)}$ and the corresponding affinity constants in both compartments (distinguished by the superscripts (n) and (c) for the nucleus and the cytoplasm, respectively). As it is discussed in Section 2.2, translation of mRNA is assumed to occur at distance from the nucleus that is outside of the endoplasmic reticulum, i.e. in a subdomain of the cytoplasm denoted by χ_{tra}; cf. Figure 4.3.

Migration of the FRQ protein can be modelled in both directions from the nucleus to the cytoplasm, and the other way round, by the Kedem–Katchalsky BC

$$-D_1\frac{\partial u_1}{\partial n_1} = -p_1(v_1 - u_1) = -D_1\frac{\partial v_1}{\partial n_1}. \tag{4.6}$$

The flux in (4.6) is determined by the difference between the nuclear and cytoplasmic concentrations at the nuclear membrane, to be compared with translocation in the ODE model in (4.4), 2nd and 3rd equation, that runs in both directions with generally different rates k_1 and k_2. In addition, there is also a biological evidence [93] that FRQ is localised mainly in the nucleus so we can also assume that it can only move from the translation sites in the cytoplasm (ribosomes) into the nucleus. In this case the Kedem–Katchalsky BC are

$$-D_1\frac{\partial u_1}{\partial n_1} = -p_1 v_1 = -D_1\frac{\partial v_1}{\partial n_1}. \tag{4.7}$$

The mRNA is assumed to move from the nucleus to the cytoplasm where it binds free ribosomes localised outside of the ER, thus the boundary conditions on the nuclear membrane are set to

$$-D_0\frac{\partial u_0}{\partial n_1} = p_0 u_0 = -D_0\frac{\partial v_0}{\partial n_1} \tag{4.8}$$

where n_1 is the unit normal vector pointing outward from the nucleus and p_0 and p_1 are the permeabilities for FRQ mRNA and its protein product, FRQ. Zero-flux boundary conditions on the cell membrane $\dfrac{\partial v_i}{\partial n_2} = 0$, $i = 0, 1$ are still assumed.

Nuclear and cytoplasmic concentrations as solutions to the PDE model (4.5) with (4.7) and (4.8) are shown in Figure 4.2 for V_s set to $1.6\,nM\,h^{-1}$ in the continuous darkness, Figure 4.2(a), and for V_s defined as a piecewise constant function attaining values $2\,nM\,h^{-1}$ and $1.6\,nM\,h^{-1}$ every 12 hours in the 12:12 light:dark simulations, Figure 4.2(c). Periods of oscillations are 21.5 hours and ∼24 hours in constant darkness and 12:12 light:dark simulations, respectively, that can be compared with the periods of oscillations in the Leloup–Goldbeter ODE model and experimentally observed periods in *Neurospora*, [85] and citations therein. Figures 4.2(b) and (d) show stable limit cycles reached in the FRQ and its mRNA concentrations.

Parameter	Value [Units]	Parameter	Value [Units]
$V_m^{(n)}$	$0.005\,[nM\,h^{-1}]$	$K_m^{(n)}, K_m^{(c)}$	$0.5\,[nM]$
$V_m^{(c)}$	$0.5\,[nM\,h^{-1}]$	$K_d^{(n)}, K_d^{(c)}$	$0.13\,[nM]$
$V_d^{(n)}$	$0.4\,[nM\,h^{-1}]$	D_0	$108\,[\mu m^2 h^{-1}]$
$V_d^{(c)}$	$0.06\,[nM\,h^{-1}]$	D_1	$43200\,[\mu m^2\,h^{-1}]$
k_s	$0.9\,[h^{-1}]$	p_0	$1\,[\mu m\,h^{-1}]$
K	$1.01\,[nM]$	p_1	$2.7\,[\mu m\,h^{-1}]$
r	4	V_s (in Fig. 4.2(a))	$1.6\,nM\,h^{-1}$
		V_s (in Fig. 4.2(c))	$1.6 - 2\,nM\,h^{-1}$

Table 4.1. Parameters for the FRQ PDE model similar to those used in the ODE model in [85]. The diffusivity of the mRNA-protein complex is $D_0 = 108\,\mu m^2\,h^{-1}$ as suggested in [20] and the diffusivity of FRQ is $D_1 = 43200\,\mu m^2\,h^{-1}$ that corresponds to the diffusivity of a protein with the weight $110\,kDa$ [23, 46], while FRQ has the molecular weight in the range $97 - 160\,kDa$ depending on its form [55, 35]. The permeabilities $p_0 = 1\,\mu m\,h^{-1}$ and $p_1 = 2.7\,\mu m\,h^{-1}$ are tuned by hand so that the system gives oscillations.

4.3.3 Discussion and conclusion: RD system for protein networks

In this short chapter we have raised the question of replacing commonly used ODE models for protein-protein interactions by reaction-diffusion models which are well studied [22, 48, 130] and which not only contain reaction terms coming from the protein interactions but also describe the spatial distribution of species involved in the reactions over the cellular compartments. We have proposed the simpler Leloup–Goldbeter circadian model for FRQ in *Neurospora* that contains two equations for the nuclear and cytoplasmic FRQ protein and its mRNA in a single cell. The model, and more generally reaction-diffusion PDE models for intracellular protein dynamics, are likely to be more realistic than ODE models.

As an example of such possibly more realistic models, let us consider the slightly more complicated PER model in *Drosophila* of Leloup and Goldbeter [84, 31], that relies on the same principles as the FRQ model. Indeed, two additional phosphorylations are considered, and this first PER model (more sophisticated models of PER have been published by Leloup and Goldbeter) is proposed to be amenable to describe two Drosophila mutants for PER, with shorter or longer period of oscillations, by lower and higher values, respectively, of the maximum degradation rate v_d of cytoplasmic diphosphorylated PER. But is this sole

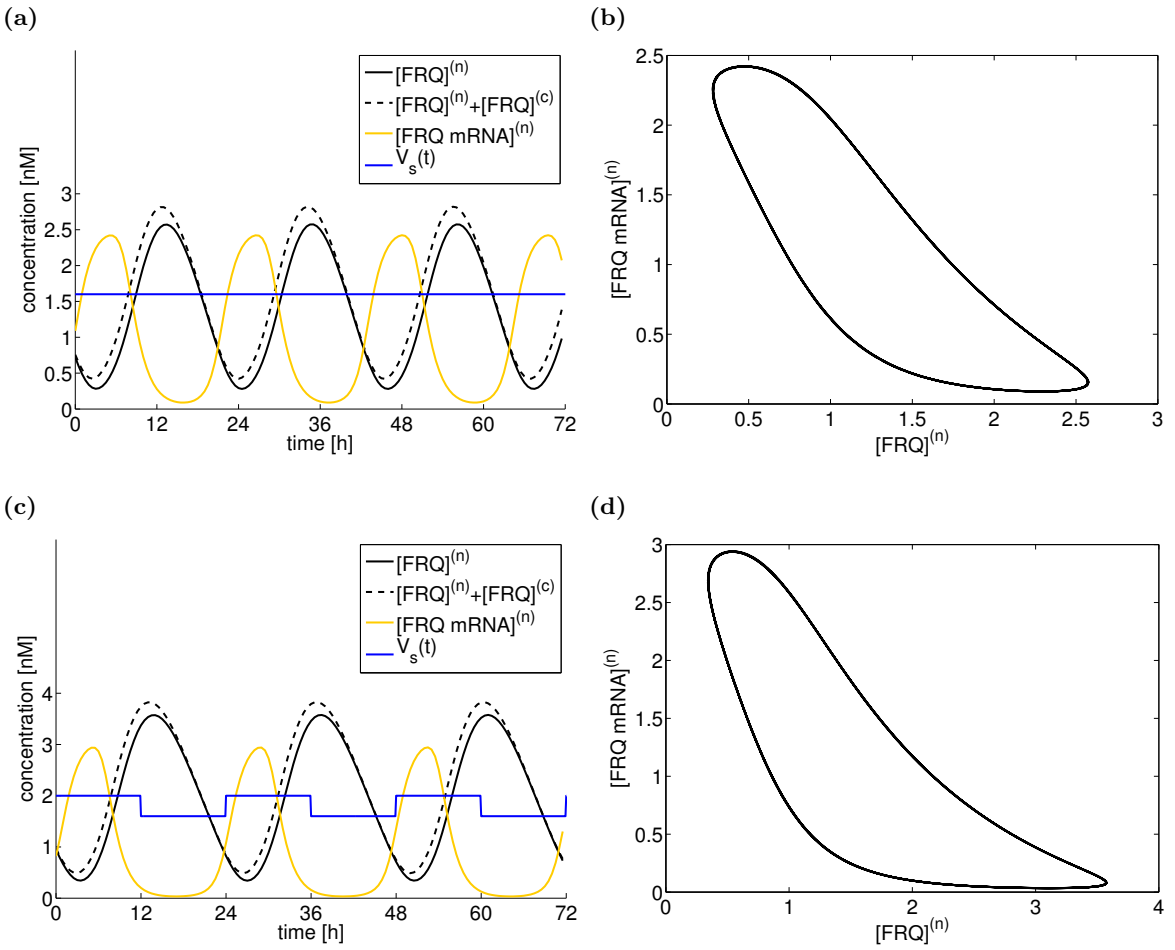

Figure 4.2. The concentrations of the nuclear FRQ, its mRNA, and the sum of the nuclear and cytoplasmic FRQ in (a) continuous darkness, $V_s = 1.6\,nM\,h^{-1}$, and in (c) 12:12 light:dark cycle, $V_s = 2\,nM\,h^{-1}$ and $1.6\,nM\,h^{-1}$ every 12 hours. Concentrations are solutions to the PDE model (4.5) with the Kedem–Katchalsky BC (4.7) and (4.8). Received period in (a) is 21.5 hours, in (c) 23.5 hours. Subplots in (b) and (d) show stable limit cycles of the concentrations. The parameters used in the PDE model (4.5) are in Table 4.1. The plotted concentrations are scaled over the total volume of the computational domain (nucleus or cytoplasm).

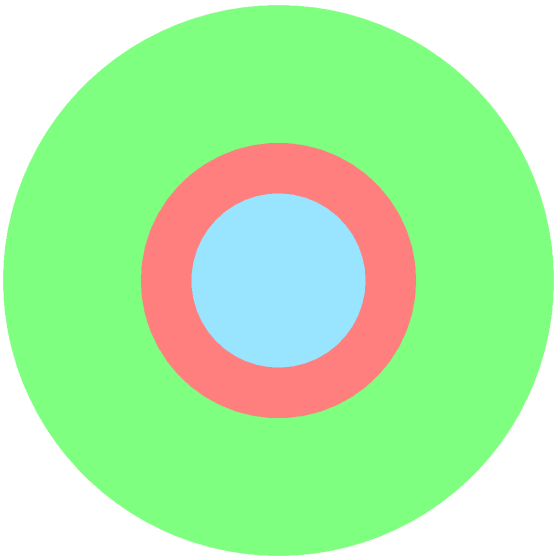

Figure 4.3. 2D cell used in simulations of the Leloup–Goldbeter PDE model. The cell is represented by the nucleus (central zone, blue) and the cytoplasm constituted of the endoplasmic reticulum (perinucleic annulus, red) where no translation is allowed and the translation zones (peripheral, green) denoted by χ_{tra} in (4.5). The nucleus, thus shown as an inner disc, has radius $\sqrt{10}\,\mu m$ in this case. The endoplasmic reticulum is an annulus with radii $\sqrt{10}\,\mu m$ and $5\,\mu m$. The rest of the cytoplasm is an annulus with radii $5\,\mu m$ and $10\,\mu m$.

change of constants the best reason, in a more physiological model, for the change in periods? Could it be related to transcription of genes, to species diffusion, to translation into protein products, to cytosolic/nucleic degradation, to nucleocytoplasmic transport, to the extension of the "dead zone" around the nucleus where translation occurs (Fig. 4.3)? The same questions can be posed when one considers p53 and drugs amenable to electively modify specific parts of its intracellular dynamics. This can be rendered optimally in PDE models, that are much more physiological than (rougher) ODE models since they are naturally able to take intracellular spatial features into account including possible space heterogeneities in the intracellular medium (not considered in the examples, apart from the above mentioned dead zone of non-translation in the cytoplasm).

We have shown how easy it is in principle to start from an ODE compartmental model, add diffusion terms - which in their simplest version are mere laplacians - and slightly modify the representation of exchanges between the compartments to adapt them to the new setting, to obtain a ready-made reaction-diffusion PDE model. However, dependence on spatial patterns, such as oscillations in concentration, on the diffusivities and the (nuclear membrane) permeabilities has to be better studied, with precise identification of the underlying biological parameters, to understand their roles properly. To obtain more realistic PDEs one can consider effects of different viscosities of buffers on different diffusivities of molecules or adjunction of advection terms when knowledge of aided transport makes it relevant (e.g., transport through microtubules). To support these ideas, different mobility of molecules in the nucleus and the cytoplasm caused by limited diffusions has led to biphasic caspase activation kinetics, see [153] and citations therein. In some circumstances it might be convenient to include specific spatial structures, such as position and density of ribosomes and thus to model gene expression more specifically [148, 6].

Note also that the oscillatory patterns are self-organised not only due to reaction events

occurring in the nucleus or in the cytoplasm but that they are also tightly connected to boundary conditions on the membranes. Thus physiological delays maintained due to the semipermeability of the nuclear membrane are more typical for PDEs than for ODEs (if one does not want to deal with artificial delays represented by DDEs). We examined the Kedem–Katchalsky as representing passive transport mechanisms with the difference of concentrations at both sides of the membrane as the driving force for exchanges; however, bigger species are rather transported actively, which should be taken into account in more sophisticated models of nucleocytoplasmic transport [23].

The simple RD systems could be certainly considered as an alternate solution to classical ODEs which may put some light on protein signalling and will be of some help to biologists and modellers who want to describe intracellular spatio-temporal dynamics of proteins in a faithful yet more demanding (in terms of parameter estimation) way. Such reaction-diffusion PDE models are also amenable to describe spatio-temporal dynamics at the level of cell populations and that, by introducing intercellular signalling, it is in principle possible to connect the two observation levels. This perspective still remains a challenge to mathematicians and modellers in biology.

5

Reaction-diffusion model for the p53 network

Recently observed oscillatory behaviour of p53 in single cells under stress conditions inspires several research groups in simulating and studying the dynamics of the protein with the perspective of a proper understanding of physiological meanings of the oscillations. In this chapter, we propose a reaction-diffusion PDE model of p53 activation and regulation in single cells following DNA damage and we show that the p53 oscillations can be retrieved by plainly involving p53-Mdm2 and ATM-p53-Wip1 negative feedbacks, which are sufficient for oscillations experimentally, with no further need to introduce any delays into the protein responses and without considering additional positive feedback.

Organisation of the chapter is as follows: Spatio-temporal model for p53 is introduced in Sections 5.1 and 5.2. Numerical simulations are presented in Section 5.3 and a discussion with conclusions in Section 5.4.

Partial results presented in this chapter were published in [46],

[46] *J. Eliaš, L. Dimitrio, J. Clairambault, and R. Natalini. The dynamics of p53 in single cells: physiologically based ODE and reaction–diffusion PDE models. Physical Biology, 11(4):045001, 2014.*

5.1 Rationale for a p53 PDE modelling

Let us briefly recall basic features of the dynamics of p53 which are described more extensively in Chapter 1. Following DNA damage, an information signalising the presence of DSB is transmitted to the inactive ATM dimers through an upstream signal E (begin either the MRN complex or any other signal produced by the chromatin). Activated ATM then phosphorylates p53 (on Ser15) which disrupts binding to its main regulator, the E3 ligase Mdm2, a transcription target for p53. The regulation of p53 by Mdm2 is predominantly achieved through (multiple-)ubiquitination, followed by nuclear export of p53 and its subsequent degradation. Such regulation by Mdm2 is possible due to previous p53 deactivation, i.e., Ser15 dephosphorylation by the phosphatase Wip1, which also dephosphorylates ATM, rendering the proteins inactive, see Figure 5.1.

The most pioneering works revealing experimentally spatio-temporal dynamics of p53 in

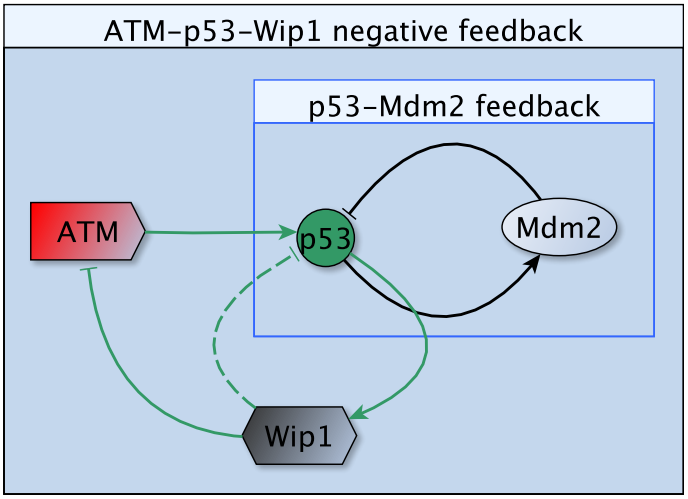

Figure 5.1. p53 dynamics in response to DNA damage: activated ATM targets p53 for phosphorylation, which results in inhibition of the p53-Mdm2 compound formation; p53 accumulates in the nucleus and acts as a transcription factor for Mdm2 and Wip1; Wip1 dephosphorylates ATM and p53 keeping them inactive and enabling Mdm2 to bind p53 again, Mdm2 initiates ubiquitination of p53, its nuclear export and degradation. This dynamics follows two negative feedback loops: the first one between p53 and Mdm2 and the second one between ATM and Wip1 through the intermediate p53.

single cells have been performed by the research group of Galit Lahav, see for example [15, 56, 77, 91, 123, 124]. In particular, it has been shown that the negative feedbacks p53-Mdm2 and ATM-p53-Wip1 are essential to maintain sustained oscillations in the p53 concentration [15], observed in the majority of cells following exposure of γ-radiation doses and other stress agents (e.g. neocarzinostatin) [77]. The p53-Mdm2 negative feedback, however, primarily functions to gain homeostasis in the DDR (keeping the concentration of p53 at low levels) rather than oscillations [147], Figure 5.2. The second negative feedback, i.e. ATM-p53-Wip1, is between ATM and Wip1 with an intermediate substrate p53 (Figure 5.1). Wip1 regulates both ATM and p53 levels through dephosphorylation. However, since ATM is the activator of p53 response and the ATM-dependent phosphorylation of p53 is critical for its escape from Mdm2, the inactivation of both protein by Wip1 and structural representation of cellular processes (e.g., gene transcription and translation) may impose time delays which could be sufficient to reproduce sustained oscillations. Other mathematical models simulating p53 through the p53-Mdm2 negative feedback either directly impose delays onto the equations and thus use Delayed Differential Equations (DDEs) or involve inter-compartmental transport of species, often coupled by a positive feedback (primarily via ODEs), see the overview of the existing models in Section 2.5.

We have shown in Chapter 3 that whenever classical Michaelis–Menten kinetics is used to mathematically describe protein reactions in a modelling setting where compartmental localisation of cellular events nor any positive feedback is considered, the two negative feedbacks did not produce oscillations (and eventually led to p53 homeostasis). Instead of involving any of the observed positive feedback loops, we show that it is sufficient to distinguish between cellular events occurring either in the nucleus or in the cytoplasm to obtain sustainedly oscillating p53 concentration (due to its nuclear accumulation and nuclear clearance) that is compatible with experimental observations. Note that different positive feedbacks may play prime roles in different phases of the p53 signalling and may depend on highly specific con-

ditions [60, 111], thus they should not be ruled out completely; however, none of them has been reported as necessary for oscillations in [15].

Compartmental distribution of the cellular events between the nucleus (e.g., gene transcription, p53 activation by ATM and its deactivation by Wip1) and the cytoplasm (e.g., mRNA translation into proteins, p53 degradation) suggests to involve spatial variables [43]. Thus, based on our compartmental ODE model introduced in Chapter 3, we propose to model the ATM-p53-Mdm2-Wip1 protein dynamics following DNA damage (depicted in Fig. 5.3) as a 2D and 3D reaction–diffusion problem with the transmission of species between the nucleus and the cytoplasm, as we have seen in the example of the FRQ model in Chapter 4. To our best knowledge, the only spatio-temporal p53-Mdm2 models formulated by PDEs are proposed in [43, 142]; however, they contain neither ATM nor Wip1 signalling.

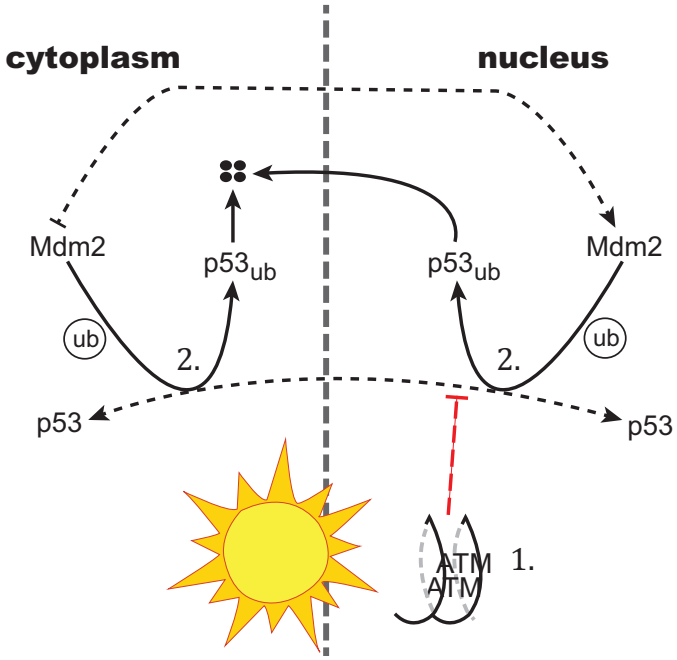

Figure 5.2. p53 dynamics in a normal unstressed cell: 1. The protein ATM in its inactive form is dimerised, unable to phosphorylate p53, which subsequently cannot act as a transcription factor. p53 is assumed to freely migrate between the compartments, Mdm2 moves from the translation sites to the nucleus. Mdm2-ubiquitin dependent degradation in the nucleus, 2., and in the cytoplasm, 3., retains the concentration of p53 at low levels in the compartments (mainly in the nucleus). *Dashed arrows indicate directions of molecule migrations, uni- or bidirectional, T-shaped lines meaning impossible nucleocytoplasmic transport in the T-end direction; solid arrows show schematically reactions in the signalling pathways. Red dashed T-shaped line shows inhibition of ATM-dependent phosphorylation of p53.*

5.2 Modelling p53 dynamics: physiological ODE and reaction-diffusion PDE models

5.2.1 Mathematical formalism and notation

A simplified cell model consists of two compartments, the nucleus Ω_1 and the cytoplasm Ω_2 with the nuclear membrane Γ_1 and the cellular membrane Γ_2, as it is schematically shown on Figure 4.1.

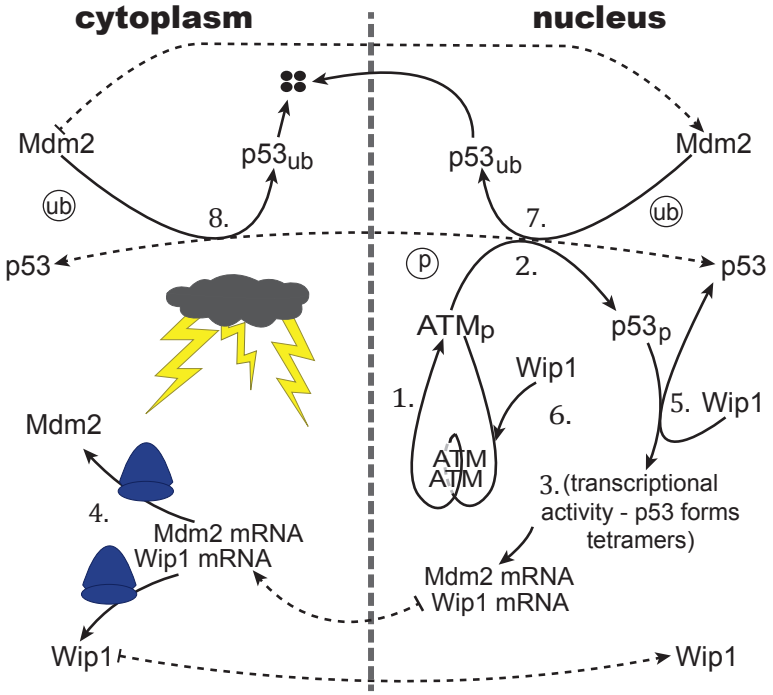

Figure 5.3. p53 dynamics under stress conditions: 1. ATM autophosphorylation (a consequence of the exposure to stress conditions, e.g., γ-radiation) results in ATM dimer dissociation into active monomers ATM-P (denoted by ATM_p in the sketch), which, 2., can phosphorylate p53 (denoted by $p53_p$ in the sketch), ATM-P and p53-P do not leave the nucleus. 3. Phosphorylated p53 forms tetramers which bind DNA and act transcriptionally for Mdm2 and Wip1. 4. The mRNAs of the proteins leave the nucleus, bind ribosomes outside of the endoplasmic reticulum and they are translated into proteins; both Mdm2 and Wip1 moves into the nucleus from the cytoplasm. 5. Wip1 dephosphorylates p53-P, making it visible for Mdm2. 6. Wip1 also dephosphorylates ATM-P which dimerises with another dephosphorylated ATM molecule. Dephosphorylated p53 can freely migrate between the compartments, where, 7. and 8., it can be ubiquitinated by Mdm2 and subsequently degraded. *Dashed arrows indicate directions of molecule migrations, uni- or bidirectional, T-shaped lines meaning impossible nucleocytoplasmic transport in the T-end direction; solid arrows show schematically reactions in the signalling pathways.*

For simplicity, let us denote the concentrations of species in their nuclear and cytoplasmic states (distinguished by the superscripts (n) and (c), respectively) as follows

$$\begin{aligned} u_0 = [p53]^{(n)}, u_1 = [Mdm2]^{(n)}, u_2 = [Mdm2_{mRNA}]^{(n)}, u_3 = [p53\text{-}P]^{(n)}, \\ u_4 = [ATM\text{-}P]^{(n)}, u_4^D = [ATM\text{-}D]^{(n)}, u_5 = [Wip1]^{(n)}, u_6 = [Wip1_{mRNA}]^{(n)}, \\ v_0 = [p53]^{(c)}, v_1 = [Mdm2]^{(c)}, v_2 = [Mdm2_{mRNA}]^{(c)}, v_3 = [p53\text{-}P]^{(c)}, \\ v_4 = [ATM\text{-}P]^{(c)}, v_4^D = [ATM\text{-}D]^{(c)}, v_5 = [Wip1]^{(c)}, v_6 = [Wip1_{mRNA}]^{(c)} \end{aligned} \tag{5.1}$$

where $u_i = u_i(t, \mathbf{x})$, $u_i : [0, T] \times \Omega_1 \to \mathbb{R}$ $\forall i = 0, 1, \ldots, 6$, and $v_j = v_j(t, \mathbf{x})$, $v_j : [0, T] \times \Omega_2 \to \mathbb{R}$, $\forall j = 0, 1, \ldots, 6$; $\Omega_1 \subset \mathbb{R}^d$, $\Omega_2 \subset \mathbb{R}^d$, $d = 2, 3$, are open and bounded domains with smooth boundaries Γ_1 (common to both domains; i.e. the nuclear membrane) and Γ_2 (exclusive to Ω_2; i.e. the cellular membrane).

In unstressed cells the levels of ATM and p53 are very low, even not detectable in some cells, thus initially we set $u_i(0, \mathbf{x}) = u_i^0 = 0$ and $v_j(0, \mathbf{x}) = v_j^0 = 0$ $\forall i, j = 0, 1, \ldots, 6$ (even for

Mdm2 which can be presented in cells keeping p53 at low concentrations). Reaction terms of the considered reactions, transmission conditions through Γ_1 and boundary conditions on Γ_2 are specified in the following sections. Note that, although based on our assumptions we have $v_3 = 0$, $v_4 = 0$ and $v_4^D = 0$, we will involve these species in the equations to make overall notation easier to follow.

5.2.2 Compartmental ODE model

The physiological ODE model for the dynamics of p53 network is developed and examined in Chapter 3. This compartmental ODE model consists of equations (3.16) and (3.17). The transmission conditions through Γ_1 are expressed as differences of the concentrations of species in both compartments controlled by the permeability coefficients and a special volume ratio V_r due to different velocities of reactions occurring either in the nucleus or in the cytoplasm [28].

Let us write $\mathbf{u} = (u_0, u_1, \ldots, u_6)^T$ and $\mathbf{v} = (v_0, v_1, \ldots, v_6)^T$ for the concentrations of species and $\mathbf{f} = (f_0, f_1, \ldots, f_6])^T$, $f_i = f_i(\mathbf{u}, \mathbf{v})$, and $\mathbf{g} = (g_0, g_1, \ldots, g_6)^T$, $g_i = g_i(\mathbf{u}, \mathbf{v})$, $i = 0, \ldots, 6$, for the reaction terms rising from the LMA, Michaelis-Menten and Hill kinetics and the transmission-like terms, i.e. the terms standing on the right-hand side of the ODE equations in (3.16) and (3.17). Thus, we can write equations for the compartmental ODE setting as a coupled system

$$\frac{\mathrm{d}\mathbf{u}}{\mathrm{d}t} = \mathbf{f}(\mathbf{u}, \mathbf{v}) \quad \text{and} \quad \frac{\mathrm{d}\mathbf{v}}{\mathrm{d}t} = \mathbf{g}(\mathbf{u}, \mathbf{v}) \tag{5.2}$$

with the initial conditions $\mathbf{u}(0) = \mathbf{u}^0 = \mathbf{0}$ and $\mathbf{v}(0) = \mathbf{v}^0 = \mathbf{0}$.

5.2.3 Reaction-diffusion PDE model

Based on the ODE model (5.2), by adding a diffusion term in each equation we can formulate a reaction–diffusion model describing the evolution of the concentrations of proteins as functions of time and space in a cell composed of the two compartments, Figure 4.1. The dynamics of the proteins including directions of their migration through the nuclear membrane is discussed in the biological overview and it is schematically shown on Figure 5.3.

The reaction–diffusion model for the nuclear and cytoplasmic concentrations $\mathbf{u}(t, \mathbf{x}) = (u_0, \ldots, u_6)^T(t, \mathbf{x})$ and $\mathbf{v}(t, \mathbf{x}) = (v_0, \ldots, v_6)^T(t, \mathbf{x})$, respectively, can be written (in the vector form) by

$$\frac{\partial \mathbf{u}}{\partial t} - div(D\nabla \mathbf{u}) = \mathbf{r}_{\mathbf{\Omega_1}}(\mathbf{u}) \quad \text{on} \quad (0, T) \times \Omega_1, \tag{5.3}$$

and

$$\frac{\partial \mathbf{v}}{\partial t} - div(D\nabla \mathbf{v}) = \mathbf{r}_{\mathbf{\Omega_2}}(\mathbf{v}) \quad \text{on} \quad (0, T) \times \Omega_2, \tag{5.4}$$

with the initial conditions $\mathbf{u}(0, \mathbf{x}) = \mathbf{u}^0 = \mathbf{0}$ and $\mathbf{v}(0, \mathbf{x}) = \mathbf{v}^0 = \mathbf{0}$ and boundary conditions on Γ_1 and Γ_2 specified in the next section. In (5.3) and (5.4), D is a diagonal matrix with the diffusion coefficients on the diagonal (Table 5.2), which are equal for both compartments; and $\mathbf{r}_{\mathbf{\Omega_i}}$, $i = 1, 2$, store the (nonlinear) reaction and production/degradation terms. The p53 basal production rate and the terms related to the translation of the mRNAs into the proteins are multiplied by the characteristic functions χ_C and χ_{CD} defining areas of the cytoplasm where the protein production events occur. These functions are defined and illustrated on Figure 5.4 in Section 5.2.7, see also Figure 2.2.

The corresponding equations of the RD system (5.3) and (5.4), are as follows:

$$(N)\begin{cases}
\dfrac{\partial u_0}{\partial t} = D_{p53}\Delta u_0 + k_{dph1}u_5\dfrac{u_3}{K_{dph1}+u_3} - k_{ub}u_1\dfrac{u_0}{K_{ub}+u_0} - k_{ph1}u_4\dfrac{u_0}{K_{ph1}+u_0}\\
\dfrac{\partial u_1}{\partial t} = D_{mdm2}\Delta u_1 - \delta_{mdm2}u_1\\
\dfrac{\partial u_2}{\partial t} = D_{mRNA}\Delta u_2 + k_{Sm} + k_{S_{pm}}\dfrac{(u_0+u_3)^4}{K_{S_{pm}}^4+(u_0+u_3)^4} - \delta_{mRNA}u_2\\
\dfrac{\partial u_3}{\partial t} = D_{p53}\Delta u_3 + k_{ph1}u_4\dfrac{u_0}{K_{ph1}+u_0} - k_{dph1}u_5\dfrac{u_3}{K_{dph1}+u_3}\\
\dfrac{\partial u_4}{\partial t} = D_{ATM}\Delta u_4 + 2k_{ph2}u_4^D\dfrac{E^2}{K_{ph2}^2+E^2} - k_{dph2}u_5\dfrac{u_4}{K_{dph2}+u_4}\\
\dfrac{\partial u_4^D}{\partial t} = D_{ATM}\Delta u_4^D - k_{ph2}u_4^D\dfrac{E^2}{K_{ph2}^2+E^2} + \dfrac{1}{2}k_{dph2}u_5\dfrac{u_4}{K_{dph2}+u_4}\\
\dfrac{\partial u_5}{\partial t} = D_{wip1}\Delta u_5 - \delta_{wip1}u_5\\
\dfrac{\partial u_6}{\partial t} = D_{wRNA}\Delta u_6 + k_{Sw} + k_{S_{pw}}\dfrac{(u_0+u_3)^4}{K_{S_{pw}}^4+(u_0+u_3)^4} - \delta_{wRNA}u_6
\end{cases} \tag{5.5}$$

$$(C)\begin{cases}
\dfrac{\partial v_0}{\partial t} = D_{p53}\Delta v_0 + k_S\chi_C - k_{ub}v_1\dfrac{v_0}{K_{ub}+v_0} - \delta_{p53}v_0\\
\dfrac{\partial v_1}{\partial t} = D_{mdm2}\Delta v_1 + k_{tm}v_2\chi_{CD} - \delta_{mdm2}v_1\\
\dfrac{\partial v_2}{\partial t} = D_{mRNA}\Delta v_2 - \delta_{mRNA}v_2\\
\dfrac{\partial v_3}{\partial t} = D_{p53}\Delta v_3\\
\dfrac{\partial v_4}{\partial t} = D_{ATM}\Delta v_4\\
\dfrac{\partial v_4^D}{\partial t} = D_{ATM}\Delta v_4^D\\
\dfrac{\partial v_5}{\partial t} = D_{wip1}\Delta v_5 + k_{tw}v_6\chi_{CD} - \delta_{wip1}v_5\\
\dfrac{\partial v_6}{\partial t} = D_{wRNA}\Delta v_6 - \delta_{wRNA}v_6
\end{cases} \tag{5.6}$$

Note that there are some differences between the ODE and PDE models. In particular, we consider both equations for the monomeric u_4, v_4 and dimeric u_4^D, v_4^D forms of ATM both diffusing with the same diffusion rate D_{ATM} (but still satisfying the conservation law: $\int u_4 + 2u_4^D\,\mathrm{d}x = const = ATM_{TOT}$), see discussion in Section 2.2.1. In addition, the Hill function with the coefficient 2 is used for ATM activation by E and ATM-P dephosphorylation by Wip1 is modelled as a simple enzyme reaction $ATM\text{-}P + Wip1 \rightleftharpoons C \xrightarrow{k_{dph2}}$ "$\frac{1}{2}ATM\text{-}D$"$+Wip1$ when compared to (3.3). Then the equations for the mRNAs v_2 and v_6 represent the evolution of the total amount of the mRNA and not the *free* mRNA molecules considered in the ODE model. Mdm2 is assumed to move from the cytoplasm to nucleus only, as its main function is to remove p53 from the DNA sites. Finally, we assume that both p53 and p53-P appear in the transcription process for its substrate genes[1].

[1]In the ODE model we assumed that only p53-P, which is hidden from Mdm2, is able to form tetramers

All the kinetic parameters used in simulations are shown in Table 5.5, permeabilities (translocation) and diffusion coefficients in Table 5.2.

5.2.4 Nucleocytoplasmic transmission BC: Kedem–Katchalsky boundary conditions

Boundary conditions applied for a passive transmission of the species through the nuclear membrane are discussed in Section 2.4. Let us recall that a driving force for the diffusive transport in the Kedem–Katchalsky BC is the difference in concentrations at both sides of the membrane, which is the simplification of a more realistic driving force standing behind most of the passive transport processes — a chemical potential gradient — which depends not only on concentrations but also on pressure, temperature, electric field and other quantities. The same BC can be derived easily from Fick's first law for stationary fluids (i.e. with no net movement, no bulk motion and no coupling effect of more cargoes transported simultaneously); see also Figure 2.3.

In particular, a contribution to the overall concentration (increase or decrease) of a chemical with the nuclear concentration u_i, for some i, throughout Γ_1 is defined by

$$-D_i \frac{\partial u_i}{\partial \mathbf{n}_1} = -p_i(v_i - u_i). \tag{5.7}$$

where v_i is the cytoplasmic concentration of the same chemical, p_i is the permeability. Equation (5.7) says that the flux (LHS of (5.7)) is equal to the difference of the concentrations across the nuclear membrane for the direction of flow from u_i to v_i if $u_i > v_i$, and the other way round if $u_i < v_i$, which is in agreement with the assumption for the particle flow (Fick's first law) to be directed from a compartment with higher concentration of the chemical to a compartment with its smaller concentration.

Similar condition, particularly,

$$D_i \frac{\partial v_i}{\partial \mathbf{n}_1} = -p_i(u_i - v_i), \tag{5.8}$$

is written for the cytoplasmic concentration of the chemical, however, with the minus sign because of the orientation of the normal vector $\mathbf{n}_1$ which points outward from the nucleus Ω_1 to the cytoplasm Ω_2, see Figure 4.1.

The Kedem–Katchalsky BC (5.7) and (5.8) satisfy the continuity of the flux condition on the boundary (what goes out from one compartment must come in to the second compartment),

$$D_i \frac{\partial u_i}{\partial \mathbf{n}_1} = D_i \frac{\partial v_i}{\partial \mathbf{n}_1}, \tag{5.9}$$

however, usually, $u_i \neq v_i$ on both sides of the nuclear membrane because of the permeability of the nuclear membrane (non-zero membrane "conductance"). In contrast, continuous translocation of species throughout the nuclear membrane modelled by the transmission conditions $u_i = v_i$ together with (5.9) are considered in [142] (i.e. no limits on perviousness of the membrane are taken into account in [142]).

Equations (5.7) and (5.8) are applied to the chemicals which migrate between Ω_1 and Ω_2 (i.e., the protein p53). Other particular cases when a chemical translocates from one compartment to another in one direction only, e.g. Mdm2 and Wip1 mRNAs which move from the nucleus to the cytoplasm and not back, and the proteins Mdm2 and Wip1, that

and bind the DNA. However, the phosphorylation status of p53 does not likely determine tetramerisation of p53. In fact, tetramerisation represents another mechanism how p53 can escape from Mdm2.

Chemical	nuclear changes	cytoplasmic changes
p53	$-D_{p53}\frac{\partial u_0}{\partial \mathbf{n}_1} = -p_{p53}(v_0 - u_0)$	$D_{p53}\frac{\partial v_0}{\partial \mathbf{n}_1} = -p_{p53}(u_0 - v_0)$
Mdm2	$-D_{mdm2}\frac{\partial u_1}{\partial \mathbf{n}_1} = -p_{mdm2}(v_1 - u_1)$	$D_{mdm2}\frac{\partial v_1}{\partial \mathbf{n}_1} = -p_{mdm2}(u_1 - v_1)$
Mdm2 mRNA	$-D_{mRNA}\frac{\partial u_2}{\partial \mathbf{n}_1} = p_{mRNA}u_2$	$D_{mRNA}\frac{\partial v_2}{\partial \mathbf{n}_1} = -p_{mRNA}u_2$
p53-P	$-D_{p53}\frac{\partial u_3}{\partial \mathbf{n}_1} = 0$	$D_{p53}\frac{\partial v_3}{\partial \mathbf{n}_1} = 0$
ATM-P	$-D_{ATM}\frac{\partial u_4}{\partial \mathbf{n}_1} = 0$	$D_{ATM}\frac{\partial v_4}{\partial \mathbf{n}_1} = 0$
ATM-D	$-D_{ATM}\frac{\partial u_4^D}{\partial \mathbf{n}_1} = 0$	$D_{ATM}\frac{\partial v_4^D}{\partial \mathbf{n}_1} = 0$
Wip1	$-D_{wip1}\frac{\partial u_5}{\partial \mathbf{n}_1} = -p_{wip1}v_5$	$D_{wip1}\frac{\partial v_5}{\partial \mathbf{n}_1} = p_{wip1}v_5$
Wip1 mRNA	$-D_{wRNA}\frac{\partial u_6}{\partial \mathbf{n}_1} = p_{wRNA}u_6$	$D_{wRNA}\frac{\partial v_6}{\partial \mathbf{n}_1} = -p_{wRNA}u_6$

Table 5.1. The Kedem–Katchalsky transmission boundary conditions on Γ_1 with the diffusion coefficients D_i and the translocation (permeability) rates p_i for each specie $i \in \{p35, mdm2, mRNA, ATM, wip1, wRNA\}$.

move from the cytoplasm to the nucleus, and, finally, the cases of ATM and phosphorylated p53-P, which do not leave the nucleus, are simple modifications of (5.7) and (5.8) and are listed in Table 5.1.

In the vector form, the Kedem–Katchalsky BC can be uniquely written by

$$-D\frac{\partial \mathbf{u}}{\partial \mathbf{n}_1} = P\mathbf{g}_{\Omega_1}(\mathbf{u}, \mathbf{v}) \quad \text{and} \quad D\frac{\partial \mathbf{v}}{\partial \mathbf{n}_1} = P\mathbf{g}_{\Omega_2}(\mathbf{u}, \mathbf{v}), \tag{5.10}$$

where D and P are diagonal matrices with the diffusion and permeability coefficients on the diagonals, and $\mathbf{g}_{\Omega_1} = \mathbf{g}_{\Omega_1}(\mathbf{u}, \mathbf{v})$ and $\mathbf{g}_{\Omega_2} = \mathbf{g}_{\Omega_2}(\mathbf{u}, \mathbf{v})$ collect the terms on the right hand sides of the boundary conditions as they are stated in Table 5.1; note that $\mathbf{g}_{\Omega_1} = -\mathbf{g}_{\Omega_2}$.

Finally, we do not assume exchange of the species between cells. Thus, we set

$$D\frac{\partial \mathbf{v}}{\partial \mathbf{n}_2} = \mathbf{0} \tag{5.11}$$

on the cell membrane, where $\mathbf{n}_2$ is the normal vector pointed outward from the cell membrane.

5.2.5 Diffusion and permeability coefficients for the RD model

Transport of the species through the nuclear membrane Γ_1 is determined by the diffusion and the permeability coefficients in (5.10). All the permeability and diffusion coefficients considered in our simulations are listed in Table 5.2. Note that due to the similar nuclear and cytoplasmic cytosol viscosity we will consider the same diffusion values for both compartments. Note also that there are other possibilities how to approximate diffusion coefficients of proteins, for example, by using Einstein's formula [23] which, however, requires Stokes radii of the proteins, which are often not known.

Chemical	Diffusion	$[\mu m^2/min]$	Permeability	$[\mu m/min]$	Weight $[kDa]$
GFP	—	2500 [64, 65]	—	—	26.9 [64]
p53-GFP	—	900 [64, 65]	—	—	∼80 [64]
p53 (dimer)	D_{p53}	1000 [64, 65]	p_{p53}	1 [est.]	53 [158]
Mdm2	D_{mdm2}	1000 [est.]	p_{mdm2}	1 [est.]	90 [109, 154]
Mdm2 mRNP	D_{mRNA}	1.8 [20]	p_{mRNA}	0.1 [est.]	≤1600 [34]
p53-P (dimer)	D_{p53}	1000 [64, 65]	$p_{p53\text{-}P}$	0	53 [158]
ATM (monomer)	D_{ATM}	300 [est.]	p_{ATM}	0	370 [7]
Wip1	D_{wip1}	1000 [est.]	p_{wip1}	1 [est.]	61 [52]
Wip1 mRNP	D_{wRNA}	1.8 [20, 146]	p_{wRNA}	0.1 [est.]	≤1600 [34]

Table 5.2. (Estimated) diffusion and translocation (permeability) coefficients used in the PDE model. We assume that p53-P and ATM-P do not leave nor enter the nucleus. Although we consider ATM in its monomer and dimer we assume that both conformations diffuse with the same diffusion rate. Similarly, we assume that the diffusivity for p53 and p53-P is the same. The diffusion rates could be roughly estimated by comparison of the known diffusions and the molecular weights of the species. Due to the lack of data on permeabilities, we have run several simulations and tested various permeability rates for which oscillations appear. In this table are those rates we have chosen as the reference ones. Note that in the ODE model proposed in Chapter 3 we considered different permeabilities than in the PDE model.

5.2.6 Nondimensionalisation

The PDE system (5.3) and (5.4), more precisely equations (5.5) and (5.6)) with the Kedem–Katchalsky BC (5.10) explicitly listed in Tables 5.1 and with the parameters in Tables 5.5 and 5.2, are nondimensionalised before they are solved. See [132] for more details on advantages and the necessity of nondimensionalisation.

For the reference concentration α_i, $i = 0, \dots, 7$, the scaled nuclear and cytoplasmic concentrations of the species are defined by, respectively,

$$\bar{u}_i = \frac{u_i}{\alpha_i} \quad \text{and} \quad \bar{v}_i = \frac{v_i}{\alpha_i}. \tag{5.12}$$

By setting

$$\bar{t} = \frac{t}{\tau}, \bar{x}_j = \frac{x_j}{L}, \, j = 1, \dots, d \tag{5.13}$$

and

$$\begin{aligned}
\bar{k}_{dph1} = \tau k_{dph1}(\alpha_5/\alpha_0), \bar{K}_{dph1} = K_{dph1}/\alpha_3, \bar{k}_{ph1} = \tau k_{ph1}(\alpha_4/\alpha_0), \\
\bar{K}_{ph1} = K_{ph1}/\alpha_0, \bar{k}_{ub} = \tau k_{ub}(\alpha_1/\alpha_0), \bar{K}_{ub} = K_{ub}/\alpha_0, \\
\bar{\delta}_{p53} = \tau\delta_{p53}, \bar{\delta}_{mdm2} = \tau\delta_{mdm2}, \bar{\delta}_{mRNA} = \tau\delta_{mRNA}, \bar{\delta}_{wip1} = \tau\delta_{wip1}, \bar{\delta}_{wRNA} = \tau\delta_{wRNA}, \\
\bar{k}_{Sm} = \tau k_{Sm}/\alpha_2, \bar{k}_{S_{pm}} = \tau k_{S_{pm}}/\alpha_2, \bar{K}_{S_{pm}} = K_{S_{pm}}/\alpha_3, \\
\bar{k}_{Sw} = \tau k_{Sw}/\alpha_6, \bar{k}_{S_{pw}} = \tau k_{S_{pw}}/\alpha_6, \bar{K}_{S_{pw}} = K_{S_{pw}}/\alpha_3, \\
\bar{k}_{dph2} = \tau k_{dph2}(\alpha_5/\alpha_4), \bar{K}_{dph2} = K_{dph2}/\alpha_4^2, \bar{k}_{ph2} = \tau k_{ph2}, \bar{K}_{ph2} = K_{ph2}/\alpha_4 \\
\bar{k}_S = \tau k_S/\alpha_0, \bar{k}_{tm} = \tau k_{tm}, \bar{k}_{tw} = \tau k_{tw}, \bar{E} = E/\alpha_4, \\
\bar{p}_i = \tau p_i/L, \bar{D}_i = \tau D_i/L^2 \; \forall i,
\end{aligned} \tag{5.14}$$

we finally arrive at the systems used in our simulations. The nondimensionalised equations

of the PDE model are not shown here, since they are very similar to the nonscaled equations except for the entries replaced by their nondimensionalised substitutions.

We have chosen $\tau = 1\,min$, $\alpha_i = 1\,\mu M$ for each i and $L = 10\,\mu m$ in the following simulations[2].

5.2.7 Numerical simulations of PDEs in 2 and 3 dimensions

The nondimensionalised reaction–diffusion problem derived from (5.3) and (5.4) with the zero initial conditions and the Kedem–Katchalsky BC (5.10) is solved numerically in 2 and 3 dimensions on the triangulations shown on Figure 5.4 by *the semi-implicit Rothe method*, see Appendix B and, e.g., [130], implemented in the FreeFem++ solver [62]. The cell under consideration on Figure 5.4 has radius equal to 1 length unit, thus, by considering the scaling length $L = 10\,\mu m$, the cell model represents a real cell with size $20\,\mu m$ in diameter[3].

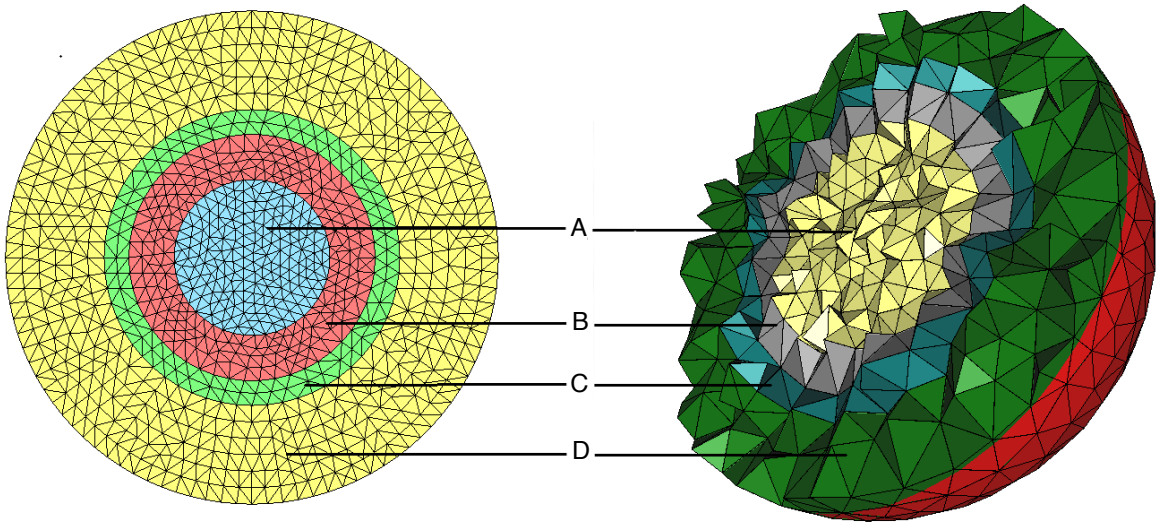

Figure 5.4. The 2D and 3D cell is represented by a disc and by a 3D ball, respectively, with radius $10\,\mu m$. The nucleus, A, is shown as an inner disc and an inner ball, respectively, with radius $3\,\mu m$. The endoplasmic reticulum B, where no production of the proteins occurs, is an annulus with radii $3\,\mu m$ and $5\,\mu m$; the ring-shaped area C, where the basal production of p53 is assumed to occur, is an annulus with radii 5 and $6\,\mu m$, respectively, and the rest of the cytoplasm, D, is an annulus with radii 6 and $10\,\mu m$. Translation of the mRNAs is supposed to occur in C+D. The 2D and 3D cell triangulations are generated by *FreeFem++*, [62].

As already mentioned in Section 2.2, the total net production of p53 determined by the basal production rate k_S is restricted to a narrow ring-shaped area within the cytoplasm (denoted by C on Figure 5.4) separated from the nucleus by the endoplasmic reticulum (ER, denoted by B on Figure 5.4). Numerically, we multiply k_S by the characteristic function

[2]Other choices for the reference concentrations can be obviously chosen, for instance, such that some unknown parameters are eliminated, in our particular case we nevertheless use all the reference concentrations to be equal to each other; we used different reference concentrations α_i for different species i in [46].

[3]Note that a diameter of an average eukaryotic cell is between $10 - 20\,\mu m$ and a diameter of the nucleus ranges from $3 - 10\,\mu m$ [105]. The cell under our consideration is of a diameter $20\,\mu m$ with the nucleus of $6\,\mu m$ in diameter.

$\chi_C = \chi_C(\bar{\mathbf{x}})$, $\bar{\mathbf{x}} \in \Omega_2 \subset \mathbb{R}^d$, $d = 2, 3$, defined by

$$\chi_C(\bar{\mathbf{x}}) = \begin{cases} 1 & \text{for} \quad 0.5 \leq \|\bar{\mathbf{x}}\| \leq 0.6, \\ 0 & \text{otherwise.} \end{cases}$$

Similarly, translation of the Mdm2 and Wip1 mRNAs into the proteins is allowed to occur in the cytoplasm except for the ER, i.e. only in the regions C and D on Figure 5.4. Thus, the translation terms with the rates k_{tm} and k_{tw} are multiplied by $\chi_{CD} = \chi_{CD}(\bar{\mathbf{x}})$

$$\chi_{CD}(\bar{\mathbf{x}}) = \begin{cases} 1 & \text{for} \quad 0.5 \leq \|\bar{\mathbf{x}}\| \leq 1, \\ 0 & \text{otherwise.} \end{cases}$$

Details about solving reaction-diffusion problems rising in molecular biology (as the particular one) by the semi-implicit Rothe method is omitted. Nonetheless, a special section in the appendix is dedicated to the Rothe method, giving a proof of the existence and uniqueness of the solution to a RD for the reversible enzyme reaction. The proof relying on the Rothe method is constructive which gives us hints on how to solve numerically not only that enzyme reaction problem but also more complicated problems as the one in this chapter. Note that we have chosen the Rothe method rather than the commonly used Newton method for nonlinear PDEs because it gives accurate results computationally faster than the Newton method and, in addition, it has been found easier to implement when dealing with the systems of equations. The FreeFem++ [62] solver has been used for our simulations.

5.3 Numerical simulations of PDEs: results

5.3.1 Oscillations of p53 in the PDE model

The 2D and 3D PDE systems (5.3) and (5.4) with the boundary conditions (5.10) and (5.11) and parameters in Tables 5.5 and 5.2 give oscillatory responses of the p53 protein to the damage signal with $E = 1$. This is shown in Figures 5.6, 5.7(a) and 5.8(a), where, respectively, the dimensionless nuclear and cytoplasmic concentrations of the proteins in 2D and 3D, and the phase plane of the nuclear concentrations of p53 and p53-P with respect to Mdm2 as well as the reached limit cycle are shown[4].

In normal conditions, i.e. when $E = 0$, the Mdm2-dependent ubiquitination keeps p53 at a low level, since there is no need for its activation (although the equilibrium reached by p53 is bigger than the equilibria of its regulators[5]). Figure 5.5(a) shows the total nuclear concentrations of the species from 2D simulations, Fig. 5.5(b) from 3D simulations.

The obtained p53 oscillations for $E = 1$ are of the period $\sim 6\,hrs$, the value which is in agreement with the experimentally observed periods (ranging between 4.5 to 7 hours) [15, 56]. Further, we can see rapid ATM activation in response to E which is observed to be almost fully activated in $5 - 15$ minutes post-irradiation [7]. Mdm2-independent degradation of p53 corresponds to the 7 hours long half-life of p53. Figure 5.7(b) and 5.8(b) then show that the actual degradation due to the active ubiquitination of Mdm2 corresponds to the half-lives 15 and 30 minutes in 2D and 8 and 25 minutes in 3D in the first and second (and other) pulses which perfectly agrees with the notion of p53 being a short-lived protein (with the half-life $20 - 30$ minutes [116]). Note that the difference in the first two pulses is caused by the *zero* initial conditions. Indeed, no regulators in the system allow p53 to accumulate at a

[4]Note that in the following we will show mostly 2D results since those in 3D are qualitatively similar to the 2D results.

[5]As discussed in Section 1.5, no excess of Mdm2 is necessary for efficient degradation of p53.

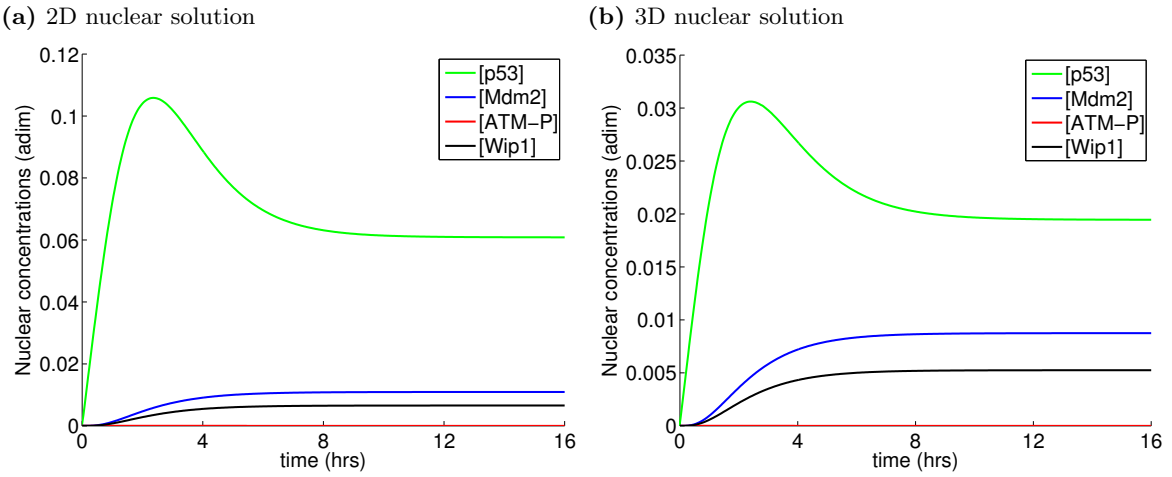

Figure 5.5. Solution of the PDE system within 16 hrs under normal conditions, $E = 0$, for the fixed set of parameters in Tables 5.5 and 5.2: nondimensionalised nuclear (a) 2D, (b) 3D concentrations. The plotted concentrations are the total concentrations in the nucleus and cytoplasm, respectively. Without any ATM-P in the system, there is obviously no p53-P produced, thus unphosphorylated p53 is plotted only.

high concentration. p53 then transcribes a higher amount of Wip1 and Mdm2 mRNA, thus yielding a higher level of Wip1 and Mdm2, which in turn lead to a more rapid degradation (that is why $t_{1/2} = 15\,min$ and $8\,min$ in the first pulse in 2D and 3D, respectively). Then the second wave of p53 is limited by the presence of some Wip1 and Mdm2 in the system and thus it peaks at a smaller level compared to the first pulse.

Note that the timing of pulses is in perfect agreement with the experimentally observed dynamics of p53 discussed in Section 1.7.1. The first pulse of p53 peaks at the 2 hour time point after damage in 2D simulations and slightly sooner in 3D (which is in agreement with the observations made in [27, 61, 15]). Mdm2 does not change for some time after DNA damage, after 1.5 hr it starts to grow and peaks at the $\sim 4\,hrs$ (in 2D, and slightly sooner in 3D) time point thus in about 2 hours later than p53 (see [27, 61]) and the maximal Mdm2 coincides with rapid p53 loss (see [61]). The second pulse is triggered (since the damage signal E is still present) and p53 peaks $\sim 8\,hrs$ after damage (see [15]). To illustrate these features, Figures 5.9 and 5.10 show samples from the spatial oscillatory evolutions of the total p53 (p53-P and p53) and Mdm2 concentrations in the 3D model of the cell captured at six time points: at the initial time 0 and the times when either p53 or Mdm2 reach its maximum. The remaining pulses in the concentrations of all proteins have the same timing in the 2D and 3D simulation. In fact, the dynamics of p53 does not differ qualitatively in 2D and 3D simulations (except for the achieved amplitudes which are affected). For this reason we will present 2D simulations if not mentioned otherwise.

5.3.2 Parameter sensitivity analysis: activation "stress" signal E

Bifurcation analysis of the 2D PDE system with respect to the activation signal E, the main bifurcation parameter under consideration (see Section 2.2.1 for the introduction of E) reveals a supercritical Hopf bifurcation point $E_1 = 0.015$ in the equilibrium curve starting at $E = 0$ within the fixed set of parameters. Similarly we can find a supercritical Hopf point in the activation signal E in 3D model. Recall that the equilibrium changes from stable to unstable by passing through the Hopf point E_1. This means that the solution bifurcates between two

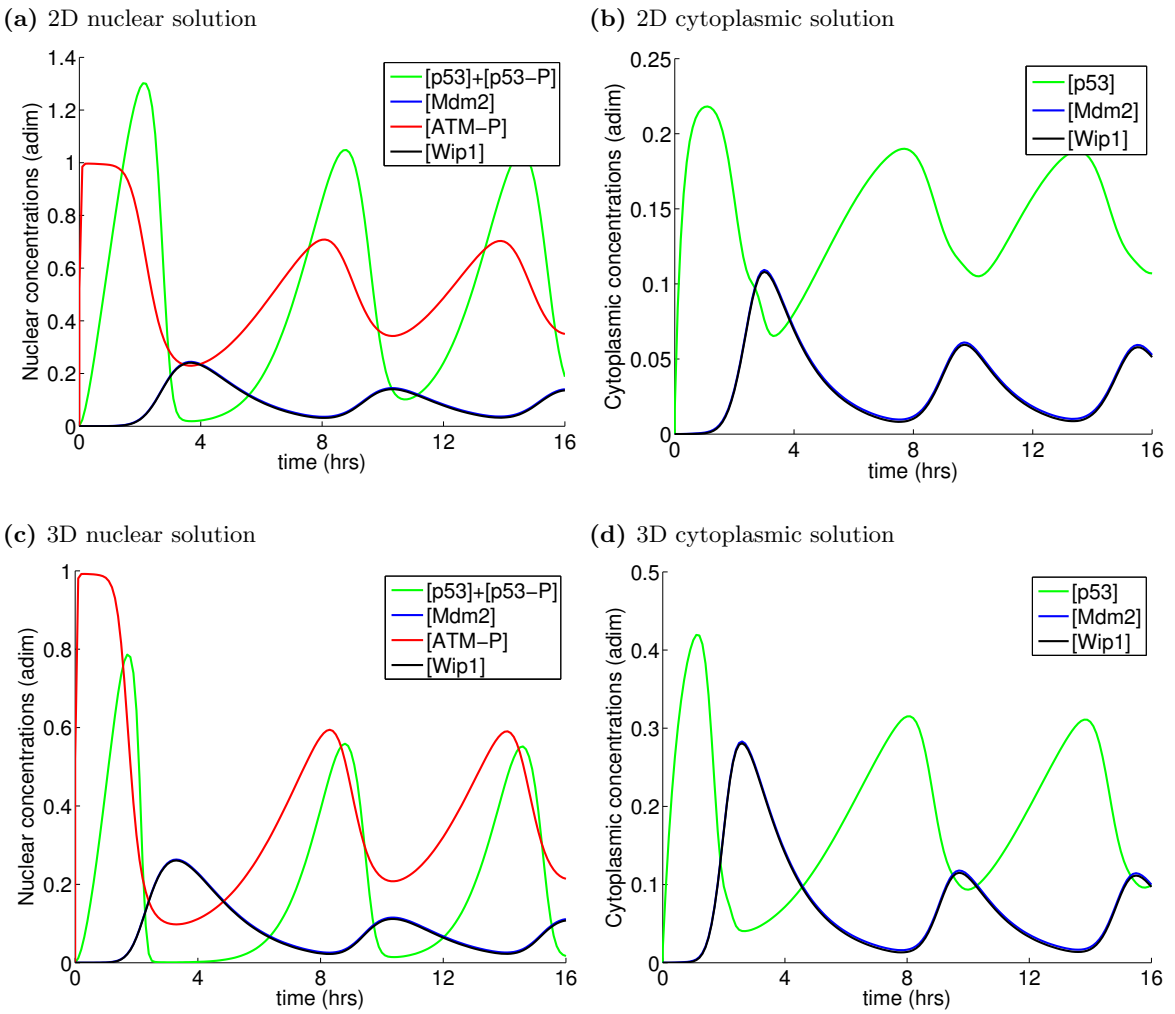

Figure 5.6. Solution of the PDE system within 16 hrs of DDR in response to the stress signal $E = 1$ for the fixed set of parameters in Tables 5.5 and 5.2: nondimensionalised (a) 2D nuclear, (b) 2D cytoplasmic, (c) 3D nuclear and (d) 3D cytoplasmic concentrations. The plotted concentrations are the total concentrations in the nucleus and cytoplasm, respectively.

qualitatively different states: convergence to a steady state for $E < E_1$, and convergence to a stable limit cycle for $E > E_1$, (with respect to the fixed set of parameters in Tables 5.5 and 5.2), see Figure 5.11.

This significant point is small, confirming that ATM and p53 activation is sensitive even to damage producing such a small E, [7, 13, 159], which, in turn, is able to activate ATM, and so p53, with concentrations that sustainedly oscillate in time. Furthermore, solutions of the PDE system remain in the oscillatory regime for all $E > E_1$. Recall again in this place that the activation signal E is considered here to be a measure of the DNA damage in cells exposed to stress conditions and we assume positive correlation between the damage dose (of γ-radiation, cytotoxic drugs) and the DNA damage (number of DSB) E. Thus our results are in agreement with the experiments saying that p53 oscillations are independent of the damage dose and that the number of cells which show oscillatory response increases with the increasing damage dose, [77, 91]. In particular, the amplitudes and duration of oscillations are independent of the damage dose: indeed, the amplitudes firstly increase rapidly for the

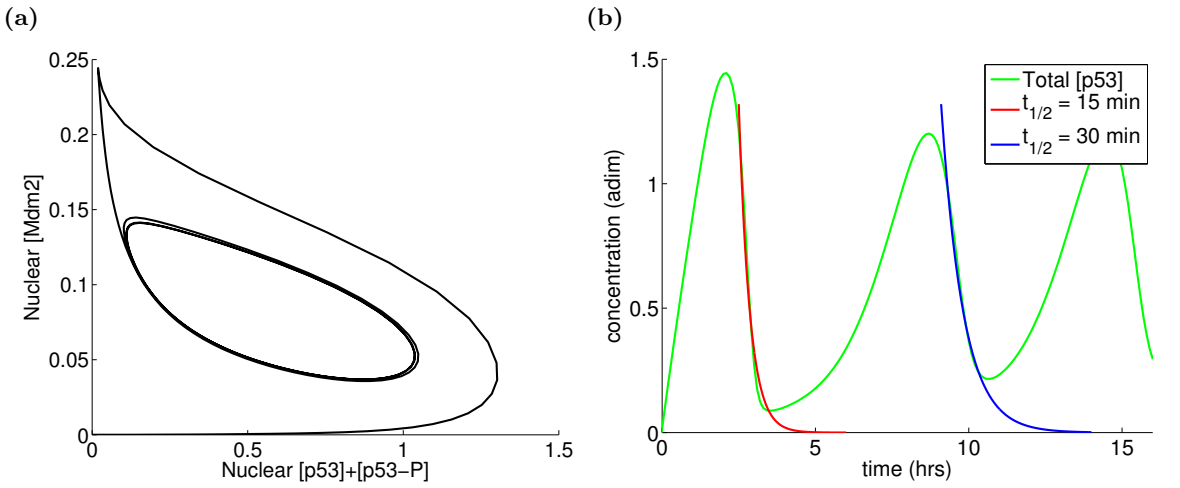

Figure 5.7. Solution of the 2D PDE system for the fixed set of parameters in Tables 5.5 and 5.2: (a) phase portrait of dimensionless nuclear concentrations of p53 (p53 and p53-P) with respect to Mdm2; (b) decay of the total (nuclear and cytoplasmic) p53 concentration in the cell with wt Mdm2 corresponds to the half-life of 15 and 30 minutes, respectively, in the first and the second pulse.

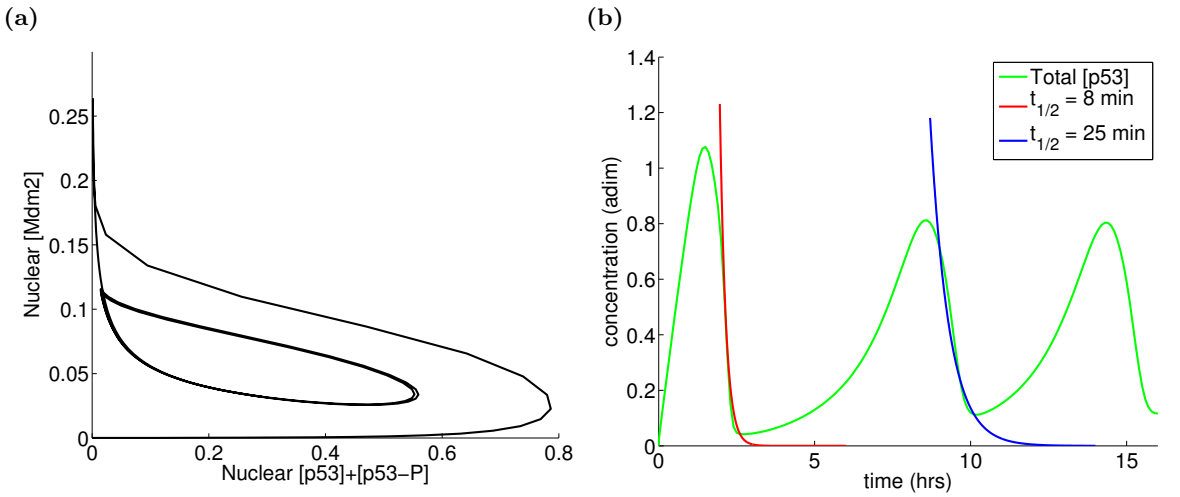

Figure 5.8. Solution of the 3D PDE system for the fixed set of parameters in Tables 5.5 and 5.2: (a) phase portrait of dimensionless nuclear concentrations of p53 (p53 and p53-P) with respect to Mdm2; (b) decay of the total (nuclear and cytoplasmic) p53 concentration in the cell with wt Mdm2 corresponds to the half-life of 8 and 25 minutes, respectively, in the first and the second pulse.

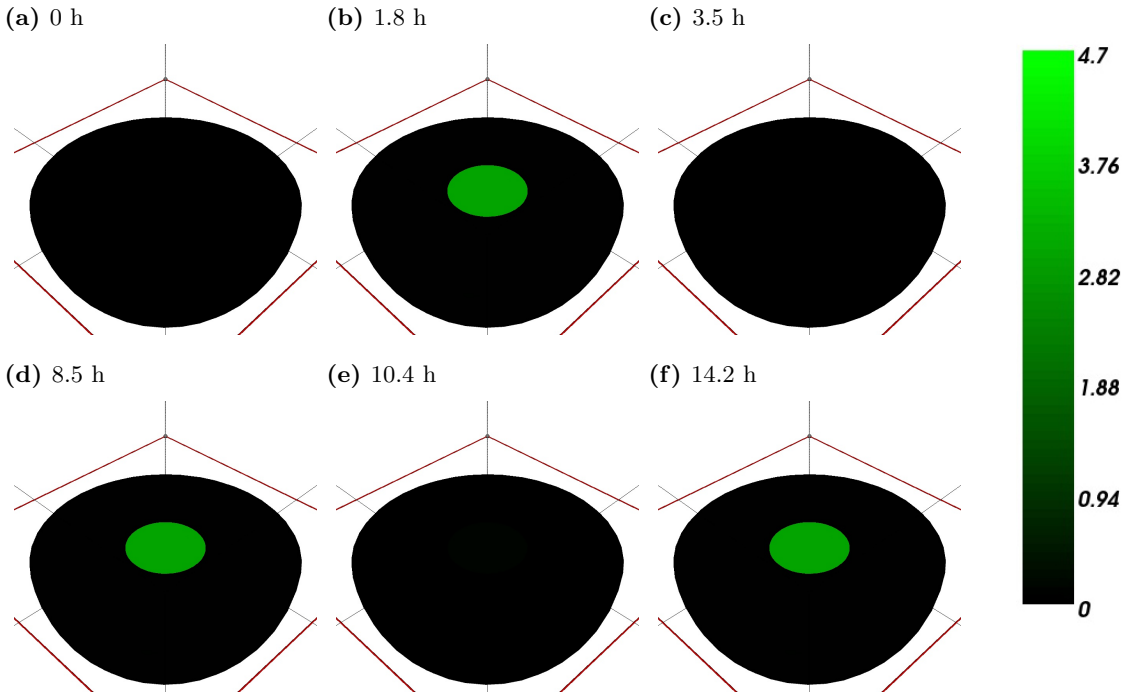

Figure 5.9. 3D visualisation of the solution of the PDE system for the fixed set of parameters in Tables 5.5 and 5.2: nondimensionalised concentration of p53 (p53-P and p53). The chosen samples are captured at the times when p53 and Mdm2 reach peaks in their concentrations.

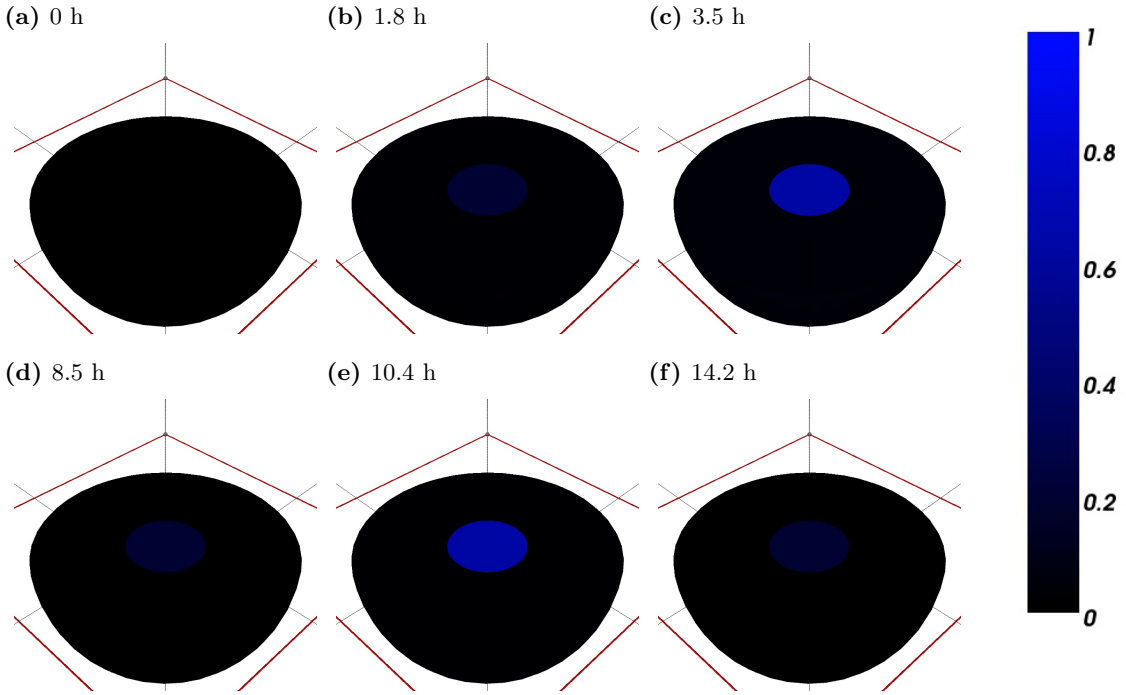

Figure 5.10. 3D visualisation of the solution of the PDE system for the fixed set of parameters in Tables 5.5 and 5.2: nondimensionalised concentration of Mdm2. The chosen samples are captured at the times when p53 and Mdm2 reach peaks in their in concentrations.

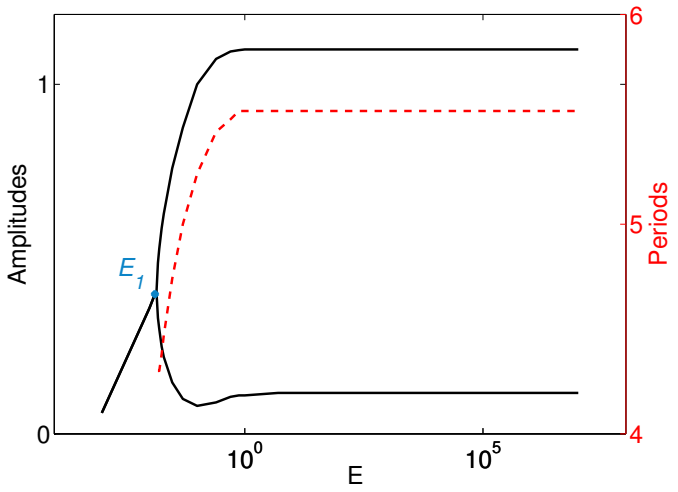

Figure 5.11. Bifurcation diagram for nuclear p53 (p53 and p53-P) with respect to the varying signal E in the 2D PDE system with the parameters in Tables 5.5 and 5.2; E is plotted in the logarithmic scale. The bifurcation point E_1 is the point on the black curve where the curve bifurcates into two paths. The curve for $E < E_1$ shows attained steady states and plotted two curves for $E > E_1$ are the heights (showing maximum and minimum) of the amplitudes of stable limit cycles. The red curve shows periods of oscillations depending on E.

values of E between $E = E_1 = 0.015$ and $E = 0.25$, then do not change for $E > 0.25$, Figure 5.11.

5.3.3 Parameter sensitivity analysis: diffusivity and permeability parameters

Once the oscillatory mode is established for the particular set of parameters, robustness of the PDE system to spatial perturbations can be examined, i.e. one can vary the spatial parameters, namely, diffusivity and permeability. For the purpose of a clearer notation we will use only in this section the following subscripts: 0 for p53, 1 for mdm2, 2 for mRNA, 3 for p53-P, 4 for ATM, 5 for wip1 and 6 for wRNA.

The reference diffusion coefficients for proteins $D_{0,1,3,5} = 1000\,\mu m^2/min$ and $D_4 = 300\,\mu m^2/min$ and for mRNPs $D_{2,6} = 1.8\,\mu m^2/min$ (Table 5.2) are partially obtained from experiments and can thus be considered as the realistic ones. On the other side, the reference permeabilities $p_{0,1,5} = 1\,\mu m/min$ and $p_{2,6} = 0.1\,\mu m/min$ (Table 5.2) have been chosen based on our simulations. Recall that p53-P and ATM-P are assumed not to be transported from the nucleus and thus the permeabilities for these two proteins are taken to be zero, i.e. $p_{3,4} = 0\,\mu m/min$. The parameters from Table 5.5 are fixed in the sequel.

Let us now fix the reference permeability coefficients, i.e. let us assume that the nuclear membrane has its "carrying capacity" fixed and cargoes are allowed to be transported through the membrane in the same manner whatever cargo cytosol diffusivities are. For the fixed protein diffusivities (1000 and $300\,\mu m^2/min$), oscillations can be obtained for the diffusivity of mRNPs greater than 0.01 in 2D and $0.1\,\mu m^2/min$ in 3D simulations. Conversely, when the diffusivity rate for mRNPs is fixed to $1.8\,\mu m^2/min$, then the system exhibits oscillations for $D_{0,1,3,5} : D_4 \geq 2 : 0.6\,\mu m^2/min$ in 2D and for $D_{0,1,3,5} : D_4 \geq 1 : 0.3\,\mu m^2/min$ in 3D, respectively, whilst the ratio between the diffusivities for p53 (Mdm2, Wip1) and ATM is

Diffusion values for oscillations	Description	Dim.
$0.01 \leq D_{2,6}$	$D_{0,1,3,5} = 1000, D_4 = 300$ fixed	2D
$2 : 0.6 \leq D_{0,1,3,5} : D_4$	ratio $D_{0,1,3,5} : D_4$ and $D_{2,6} = 1.8$ fixed	2D
$1 : 0.3 : 0.0018 \leq D_{0,1,3,5} : D_4 : D_{2,6}$	ratio $D_{0,1,3,5} : D_4 : D_{2,6}$ fixed	2D
$0.1 \leq D_{2,6}$	$D_{0,1,3,5} = 1000, D_4 = 300$ fixed	3D
$1 : 0.3 \leq D_{0,1,3,5} : D_4$	ratio $D_{0,1,3,5} : D_4$ and $D_{2,6} = 1.8$ fixed	3D
$5 : 1.5 : 0.009 \leq D_{0,1,3,5} : D_4 : D_{2,6}$	ratio $D_{0,1,3,5} : D_4 : D_{2,6}$ fixed	3D

Table 5.3. Ranges for the diffusion parameters (in $\mu m^2/min$) for which the 2D and 3D PDE systems give oscillations, assuming that the considered ratios and the unmentioned parameters from Tables 5.5 and 5.2 are fixed. As for the reference values, $D_{0,1,3,5} = 1000$, $D_4 = 300$ and $D_{2,6} = 1.8\,\mu m^2/min$ for the p53 (Mdm2, Wip1), ATM and mRNPs, respectively, have been taken. Subscripts: 0 for p53, 1 for mdm2, 2 for mRNA, 3 for p53-P, 4 for ATM, 5 for wip1 and 6 for wRNA; Dim. stands for dimension.

kept constant. Whenever the ratio between the proteins and mRNPs is kept fixed (equal to the ratio between the reference diffusivities), then oscillations appear for $D_{0,1,3,5} : D_4 : D_{2,6} \geq 1 : 0.3 : 0.0018\,\mu m^2/min$ in 2D and for $D_{0,1,3,5} : D_4 : D_{2,6} \geq 5 : 1.5 : 0.009\,\mu m^2/min$ in 3D simulations. Computed lower bounds for the diffusion rates are listed in Table 5.3. Interestingly, no upper bounds on the diffusivities are found where our simulations were executed for the diffusivities up to order 10^7. Higher diffusivities ($\sim 10^4\,\mu m^2/min$ and higher for the p53 protein) in any of the tested cases lead to oscillations with rather uniform shape, i.e., oscillations with constant amplitudes and periods.

Let us now fix the reference diffusion parameters and examine the PDE model with respect to the varying permeability rates. Firstly, let us fix the permeability for the proteins $p_{0,1,5} = 1\,\mu m/min$; then the oscillations appear for the mRNAs permeabilities $p_{2,6} \geq 0.05\,\mu m/min$ in 2D and $p_{2,6} \geq 0.02\,\mu m/min$ in 3D, respectively. When $p_{2,6} = 0.1\,\mu m/min$ is fixed, then the system yields oscillations for $p_{0,1,5} \geq 0.2\,\mu m/min$ in 2D and for $p_{0,1,5} \geq 0.15\,\mu m/min$ in 3D simulations. Finally, if the ratio between the permeabilities for the proteins and mRNAs is constant (equal to the ratio between the reference permeabilities), then the oscillations can be attained for $p_{0,1,5} : p_{2,6} \geq 0.15 : 0.054\,\mu m/min$ in 2D and 3D. Again, no upper bounds have been detected. Computed ranges for the permeabilities which give a rise to oscillations are listed in Table 5.4.

Simulations thus show that the oscillations can be obtained for a broad range of spatial parameters. In particular, there are lower bounds for the diffusion coefficients, below which we do not receive any oscillations. The oscillatory response can be then maintained for all diffusions larger than these bounds. This is expected, since fast diffusion makes the solutions of the reaction-diffusion system homogenous in space and thus, roughly speaking, the PDE system resembles the compartmental ODE model which is able to produce oscillations in the p53 concentration.

5.3.4 Sole p53-Mdm2 negative feedback does not trigger oscillations

As expected from the ODE model, the sole p53-Mdm2 negative feedback is not sufficient to produce any oscillations.

Clearly, without the active role of Wip1 in dephosphorylation of p53-P, Mdm2 itself is not able to sufficiently label p53 for degradation. This is depicted on Figure 5.12(a) where Wip1 dephosphorylation of p53-P is inhibited by setting the dephosphorylation rate to zero

Permeability values for oscillations	Description	Dim.
$0.05 \leq p_{2,6}$	$p_{0,1,5} = 1$ fixed	2D
$0.2 \leq p_{0,1,5}$	$p_{2,6} = 0.1$ fixed	2D
$0.15 : 0.054 \leq p_{0,1,5} : p_{2,6}$	ratio $p_{0,1,5} : p_{2,6}$ fixed	2D
$0.02 \leq p_{2,6}$	$p_{0,1,5} = 1$ fixed	3D
$0.15 \leq p_{0,1,5}$	$p_{2,6} = 0.1$ fixed	3D
$0.15 : 0.054 \leq p_{0,1,5} : p_{2,6}$	ratio $p_{0,1,5} : p_{2,6}$ fixed	3D

Table 5.4. Ranges for the permeability parameters (in $\mu m/min$) for which the 2D and 3D PDE systems give oscillations, assuming that the considered ratios and the unmentioned parameters from Tables 5.5 and 5.2 are fixed. As for the reference values, $p_{0,1,5} = 1$ and $p_{2,6} = 0.1\,\mu m/min$ for the p53 (Mdm2, Wip1) and mRNPs, respectively, have been taken. Subscripts: 0 for p53, 1 for mdm2, 2 for mRNA, 5 for wip1 and 6 for wRNA; Dim. stands for dimension.

(i.e., $k_{dph1} = 0$). As a result, the dynamics of p53 resemble the UV response to DNA damage, i.e., following DNA damage caused by UV radiation, p53 exhibits one prolonged pulse in its concentration [14], c.f. Fig. 6.9. Oscillatory behaviour could be partially restored if we allow Mdm2 to ubiquitinate p53-P. Recall that phosphorylation of p53 by ATM (and other kinases) reduce ability of Mdm2 to bind p53 which, in turn, leads to its stabilisation and nuclear accumulation (Figure 5.6(a)); however, in our model we assume that a single phosphorylation event inhibits interactions between p53 and Mdm2 completely.

On the other side our model shows that inhibition of Wip1-dependent dephosphorylation of ATM-P (by setting $k_{dph2} = 0$; which results to the full activation of ATM-P) does not change significantly the dynamics of p53. Indeed we can observe damped oscillations in Figure 5.12(b). However, as it is claimed in [14], the feedback from Wip1 to ATM should be necessary for the repeated fixed oscillations since otherwise the sustained p53 signalling is maintained. Our results suggest that sustained signalling is a consequence of the strong inhibition of the p53-Mdm2 negative loop rather than inactivation of the Wip1-dependent dephosphorylation of ATM, since the fully activated ATM can still compete with Wip1 for p53 which leads consequently to damped oscillations. Inhibition of both negative loops (from Mdm2 to p53 and from Wip1 to ATM) establishes sustained p53 signalling as well (Fig. 5.12(c)).

Figure 5.12(d) (and partially (a)) shows that even when one full pulse of ATM-P is produced in response to DNA damage and Mdm2 and Wip1 can negatively regulate p53, then this is not sufficient for sustained p53 oscillations. This is in agreement with experimental observations in [15].

5.3.5 One compartmental model does not trigger oscillations

We can further merge both compartments into one and see if the PDE model can produce oscillations as we did in the ODE model. This merging consists in removal of the nuclear membrane and thus allowing species freely migrate over one domain, the transcription and translation of proteins is allowed in the whole domain, otherwise the model assumptions remain unchanged compared with the 2-compartmental model.

Figure 5.13 confirms that under the new physiological setting the model is not able to trigger any oscillations[6]. This suggests that spatial representation of the cell which allows

[6]Even if we modified parameters, still no oscillatory response could be found.

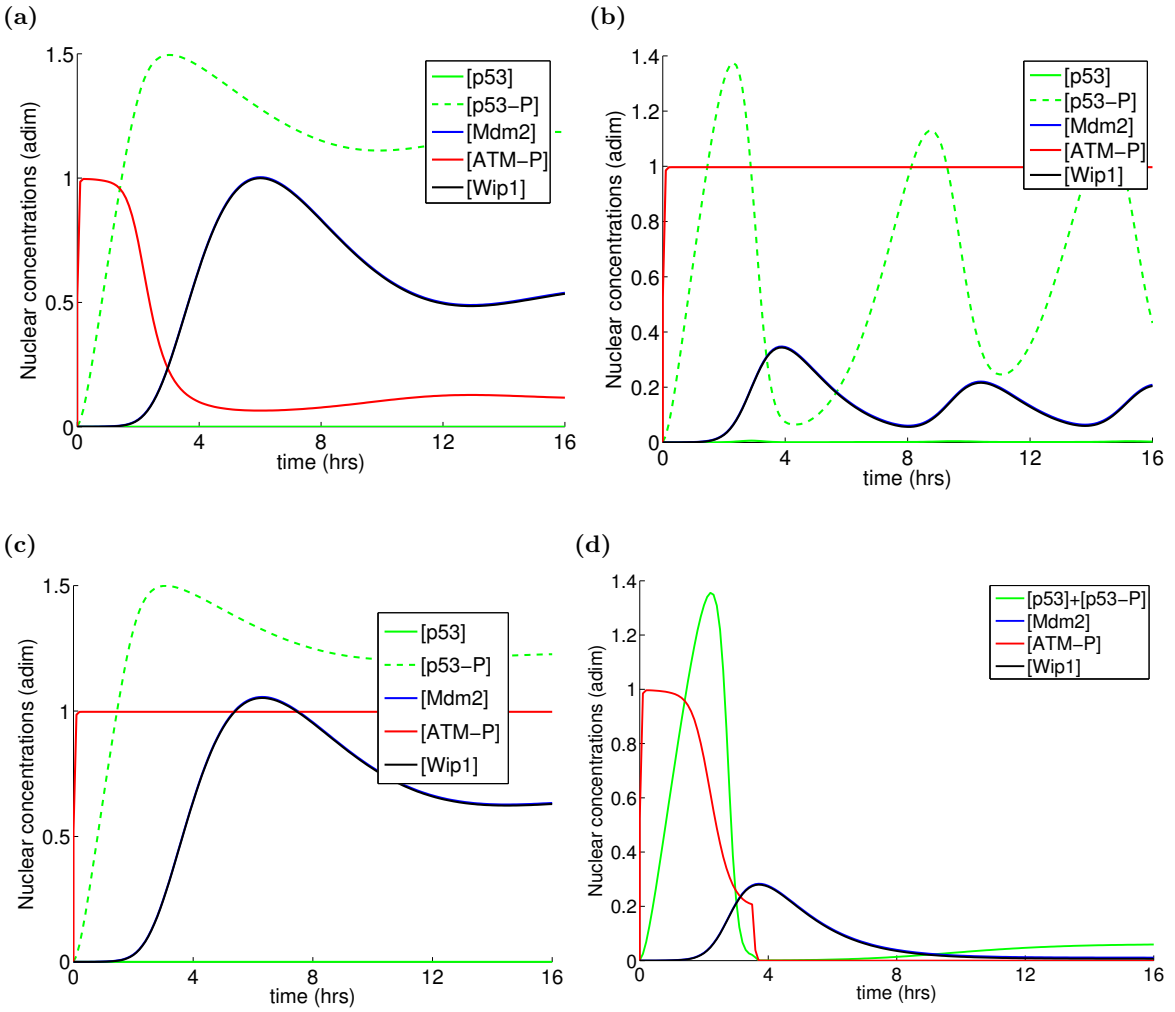

Figure 5.12. Solution of the 2D PDE system where (a) Wip1-dependent dephosphorylation of p53-P is inhibited ($k_{dph1} = 0$); (b) Wip1-dependent dephosphorylation of ATM-P is inhibited ($k_{dph2} = 0$); (c) Wip1-dependent dephosphorylation of both p53-P and ATM-P is inhibited ($k_{dph1} = 0$ and $k_{dph2} = 0$); (d) ATM-P is inhibited after one full pulse, Mdm2 and Wip1 signalling is unaffected. The plotted concentrations are the total concentrations of the species in the nucleus.

p53 to accumulate and stabilise in the nucleus, specific localisation of the negative regulators Mdm2 and Wip1 inside or outside the nucleus and/or mRNA transmission from the DNA sites to the cytoplasm, could be indeed necessary for triggering oscillations.

5.3.6 Oscillations in cells of complicated structures

Besides the very simple cell model used in simulations (represented by a disc and a sphere), oscillations can be obtained even in very complicated cell structures. As an example, a 2D Hela cell has been considered, Figure 5.14(a) and (b). The cell under consideration has an elliptic-like nucleus. The ER and an area for p53 basal production and mRNA translation have been chosen with the similar shape as the nucleus (not shown).

The PDE model (5.3) and (5.4) with the Kedem–Katchalsky boundary conditions (5.10) applied on the nuclear membrane and the zero flux boundary conditions (5.11) on the outer

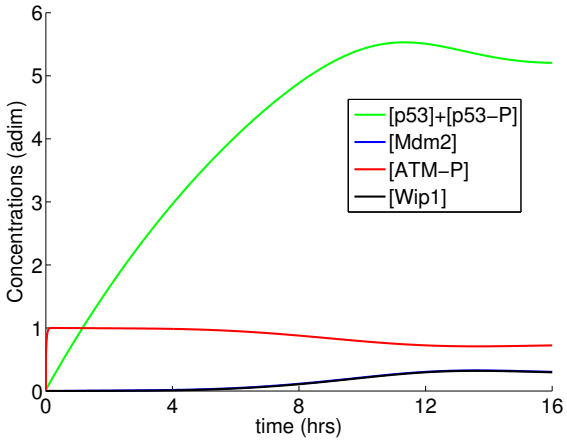

Figure 5.13. Solution of the 2D PDE system following DNA damage producing the transiting signal $E = 1$ in the case when both compartments are merged together. The plotted concentrations are the total concentrations in the nucleus.

cellular membrane is then solved on the triangulation generated by FreeFem++. The kinetic rates, diffusion and translocation parameters remain the same as in Tables 5.5 and 5.2 (except for the p53 basal production rate which is set to $0.03\,\mu M/min$). The semi-implicit Rothe method then gives oscillations in the p53 dynamics following exposition to a stress signal of the amount of $E = 1$, see Figures 5.15(a) and (b) where the nuclear and cytoplasmic (dimensionless) concentrations of the proteins are plotted, Fig. 5.15(c) for a particular phase plane that confirm existence of (stable) limit cycles in the protein evolutions, and also Figures 5.16 and 5.17 where six different samples from the concentrations of p53 and Mdm2 are captured: at the initial time 0 and the times when either p53 or Mdm2 reach its maximum. In the simulation the obtained solutions show oscillations of the period ∼6.3 hours.

5.4 Discussion and conclusions from the PDE model #1

Based on the recently observed oscillations of the p53 protein in single cells [15, 56, 77], we have proposed a spatio-temporal RD model counting the negative feedback p53-Mdm2 together with ATM-p53-Wip1 and compartmental distinction of cellular events between the nucleus and the cytoplasm.

We have shown that spatial variables and the PDE model can be used to simulate the behaviour of the p53 intracellular network in the stressed cells as well as by ODE models. The oscillations obtained from PDEs are driven by a spatial representation, diffusivities and permeabilities of the species, since in the PDE model they have to overcome distances diffusively to reach targets and particular areas in the cell, e.g. to reach the translations sites for mRNAs to be translated into proteins, which is not the case of ODEs. Translocation through the nuclear membrane, which is modelled by the Kedem–Katchalsky BC, is also affected by diffusivity of the species. For example, Mdm2, which acts only in the nucleus, diffusively spreads over the entire cytoplasm after leaving the translation sites, which decreases its abundance at the nuclear membrane and so the level of the protein at the membrane that can be potentially translocated into the nucleus. Notably, a single mRNA export from the nucleus to the cytoplasm may take 10–30 minutes [16]. Thus, diffusive motion and membrane translocation impose a delay in the protein/mRNA translocation between the compartments which, afterwards, affects the dynamics (amplitudes and periods) of their concentration. Transloca-

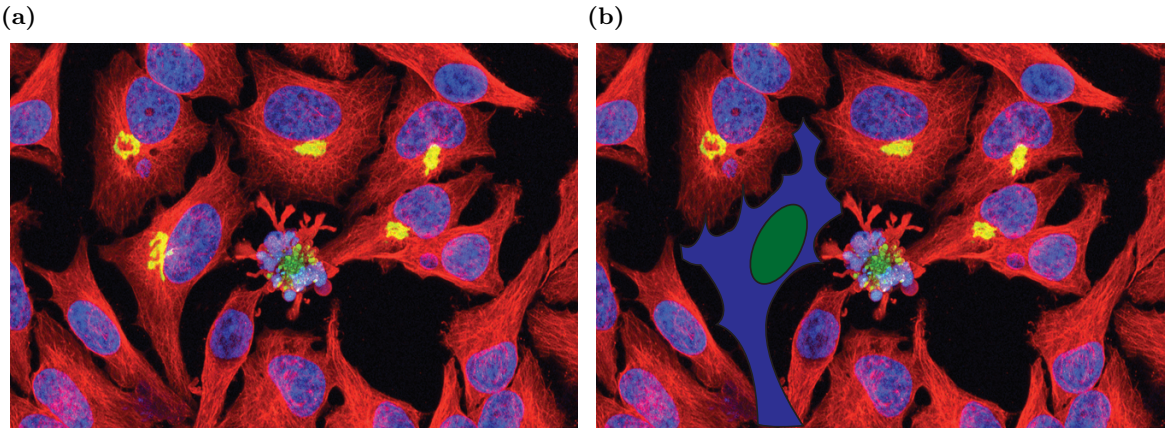

Figure 5.14. (a) Healthy HeLa cells surrounding apoptotic HeLa cell (center). Visible parts are the nucleus (blue), fibres (red) and Golgi's apparatus (yellow). (b) One particular cell chosen for simulations (nucleus is in green, cytoplasm in blue). Image courtesy of Thomas Deerinck and Mark Ellisman (NCMIR and UCSD) [33].

tion in ODEs is simplified in the way that the actual concentrations at the nuclear membrane are the concentrations in the whole compartments thus independent of the effect of diffusive movement. Hence, diffusivity, the time the species need to reach membranes, compartments and the translation zones within the cytoplasm, translocation through the nuclear membrane (controlled by the permeability of the membrane), *etc.*, regulate p53 dynamics by imposing sufficient physiological delays, resulting in sustained oscillations.

The diffusion rates chosen here ($\sim 1000 \mu m^2/min$ for p53, Mdm2 and Wip1) lie at the upper bound of the estimated range of acceptable diffusion coefficients for p53 and Mdm2 for which simulations in [43] yield oscillations. The estimated range of the diffusion parameters, for which our PDE system gives oscillations, is rather wide (even with no upper bounds in 2D and 3D simulations, Table 5.3) compared with the range $10 - 1000\,\mu m^2/min$ for the protein diffusivity obtained in [43] and the range $4.44 - 150\,\mu m^2/min$ given by the PDE model in [142] for the diffusivities of both proteins and mRNAs.

Sustained oscillations can be reproduced in cells with complicated morphologies as in those in Figure 5.14, however, with some restrictions on the permeability of the nuclear membrane. These restrictions can be partially abolished by the inclusion of the well defined ER, although the ER does not necessarily have to present smooth boundaries. Hence, the ER around the nucleus may set limits on the range of acceptable permeabilities needed for oscillations; the narrower the ER is, the smaller range of permeabilities for oscillations could be used.

Unlike with the chosen set of parameters in the ODE model shown in Table 3.1, in the PDE model presented here we have slightly changed some rates, in particular, unknown parameters in the expression of Wip1 by p53 so that Wip1 and Mdm2 transcription by p53 runs with no affinity of p53 for these target genes. The are also some other differences between the ODE and PDE models. In particular, unlike the ODE model, the PDE model contains also two variables for the ATM monomer and ATM dimer (with different reaction terms), equations of which were not merged to one using the conservation of the total amount of ATM. In addition, we do not consider equations for the"free" but rather for the total Wip1 and Mdm2 mRNA, Mdm2 is assumed to be strictly nuclear and transcription of $Mdm2$ and $Wip1$ genes is mediated by phosphorylated and unphosphorylated p53.

Bearing in mind the expected behaviour of p53, i.e. turning off its oscillations at some

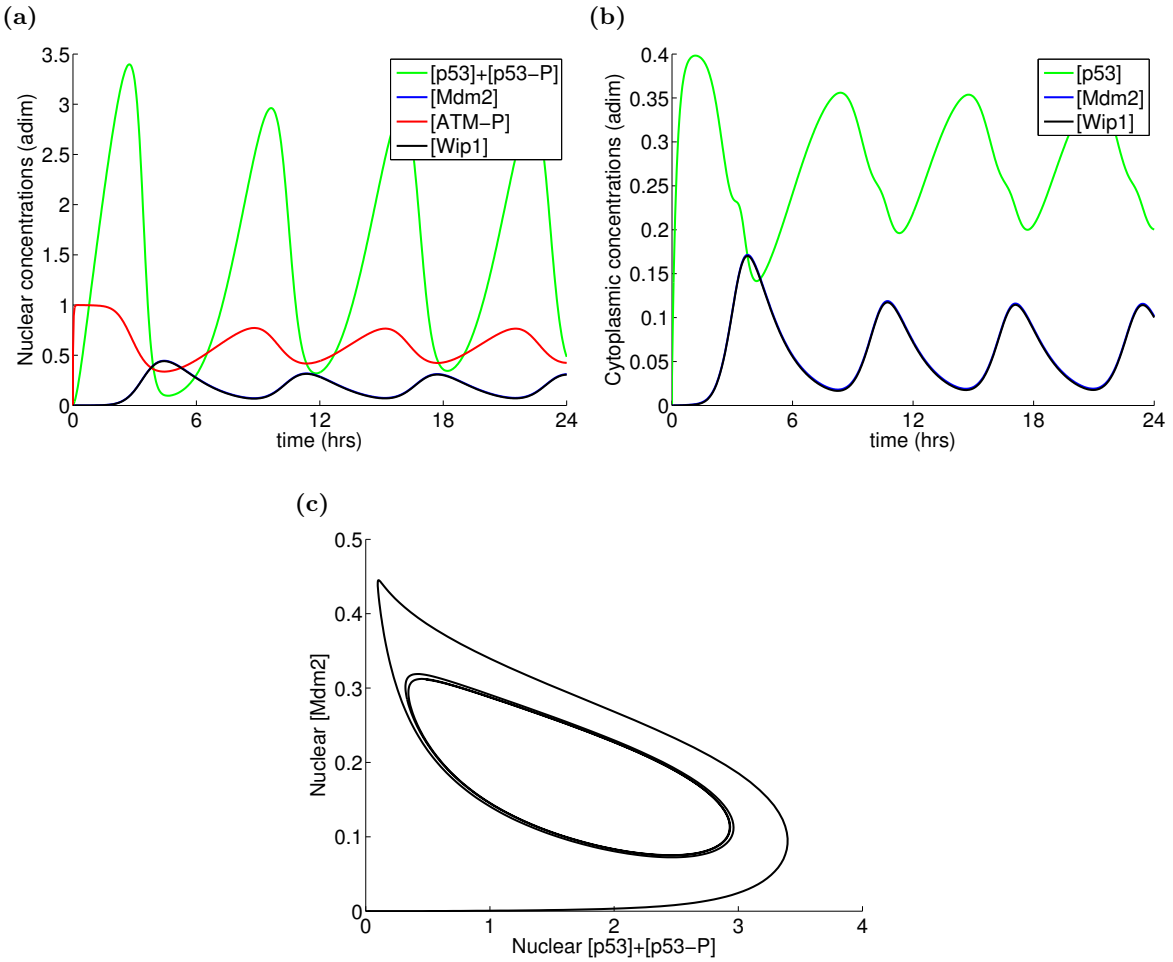

Figure 5.15. Solution of the 2D system on the HeLa cell: nondimensionalised (a) nuclear and (b) cytoplasmic concentrations of p53 (p53 and p53-P), Mdm2, ATM-P and Wip1 proteins. The plotted concentrations are the total concentrations in the nucleus and cytoplasm, respectively; (c) phase portrait of the nuclear concentration of p53 (p53 and p53-P) with respect to the nuclear concentration of Mdm2.

point and establishing a steady state of high levels signalising started apoptosis, the parameter set, just mentioned differences between the models, and the chosen reference concentrations for the proteins used in nondimensionalisation in the ODE system turned the system to exhibit two Hopf bifurcation points signalising two qualitatively different states for the damage signal E, the main bifurcation parameter under consideration (see Section 2.2.1 for the introduction of E). Indeed, a bifurcation analysis of the ODE system in Chapter 3 with respect to E reveals two supercritical Hopf bifurcation points in the equilibrium curve starting at $E = 0$. The equilibrium changed from stable to unstable by passing through the first Hopf point E_1 and then back from being unstable to stable when E crosses the second Hopf point E_2. This means that the solution bifurcates between two qualitatively different states: convergence to a steady state for $E < E_1$ and $E > E_2$, and convergence to a stable limit cycle for $E_1 < E < E_2$.

We speculate that these Hopf points E_1 and E_2 may represent in a very summarised form key points in the p53-mediated cell fate decisions. In particular, whenever p53 oscillatory signalling is necessary for DNA repair, the damaged DNA signal E is produced so that

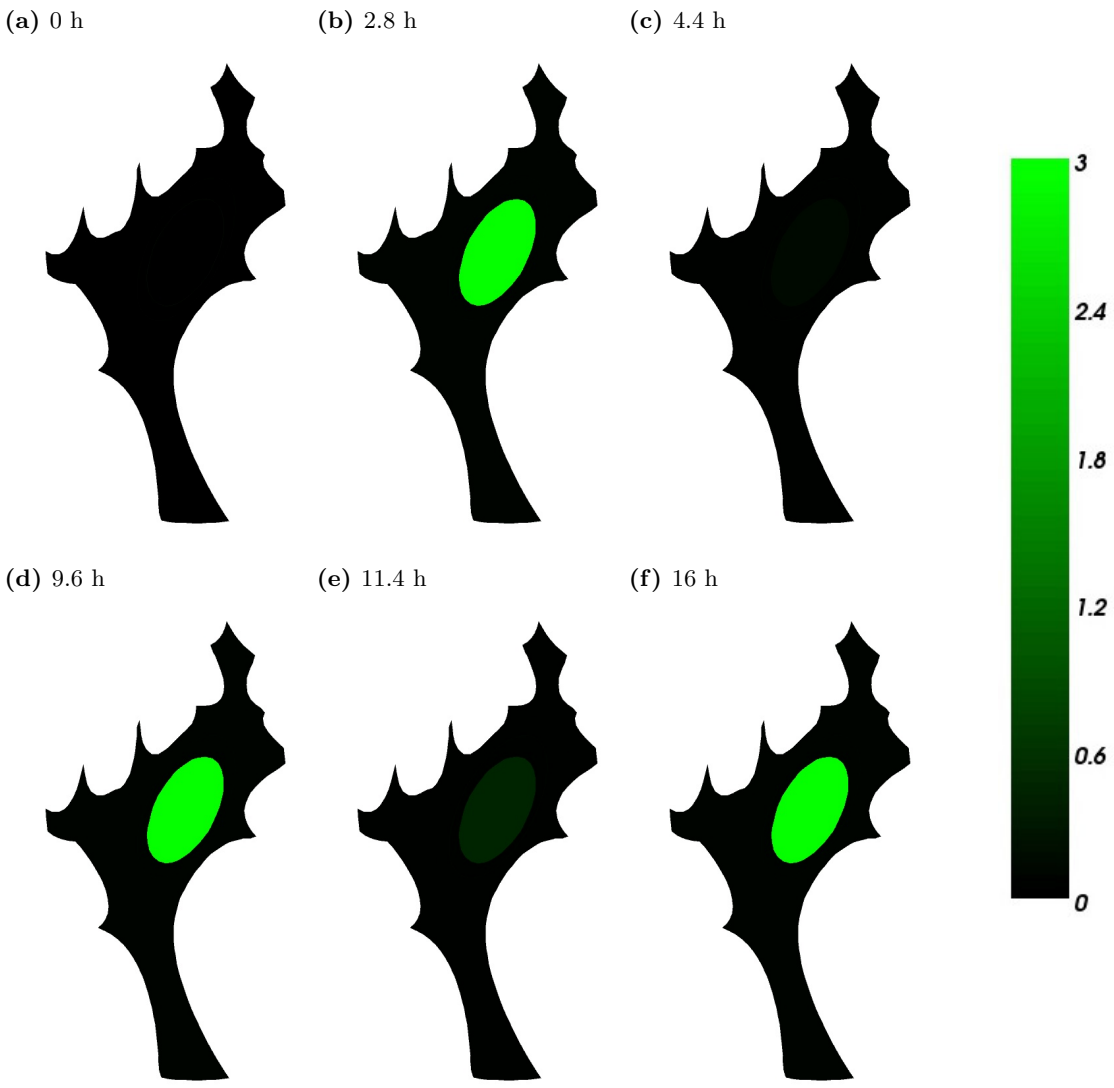

Figure 5.16. 2D visualisation of the solution of the PDE system for the HeLa cell: nondimensionalised concentration of p53-P and p53. The chosen samples are captured at 6 time points when p53 and Mdm2 reach peaks in the concentration.

$E_1 < E < E_2$. For these values of E, p53 sustainedly oscillates with a possible physiological interpretation of the oscillations as a periodical examination of persistence of DNA DSB as proposed in [15, 77]. If the number of DSB decreases in repair processes and p53 oscillations are not needed anymore, then also E might decrease, and become potentially smaller than E_1 or completely extinct if the DNA damage is successfully fixed. Therefore, E might turn off the oscillations of the proteins. This speculation can be partially supported by some experiments, for example, it has been reported in [13] that transient and temporal DNA DSB (as the occasional ones occurring in DNA synthesis) do not result in ATM and p53 oscillations, and these occasional DSB may be related to $E < E_1$. However, if DSB persist, even more when their number increases, and/or it is impossible to repair them, then the cell might decide to launch apoptosis with amplified E so that E trespasses the threshold E_2. In apoptotic cells then the concentration of p53 leaves oscillations and approaches its steady state of high values, for example, due to the compartmental regulation of the proteins in the

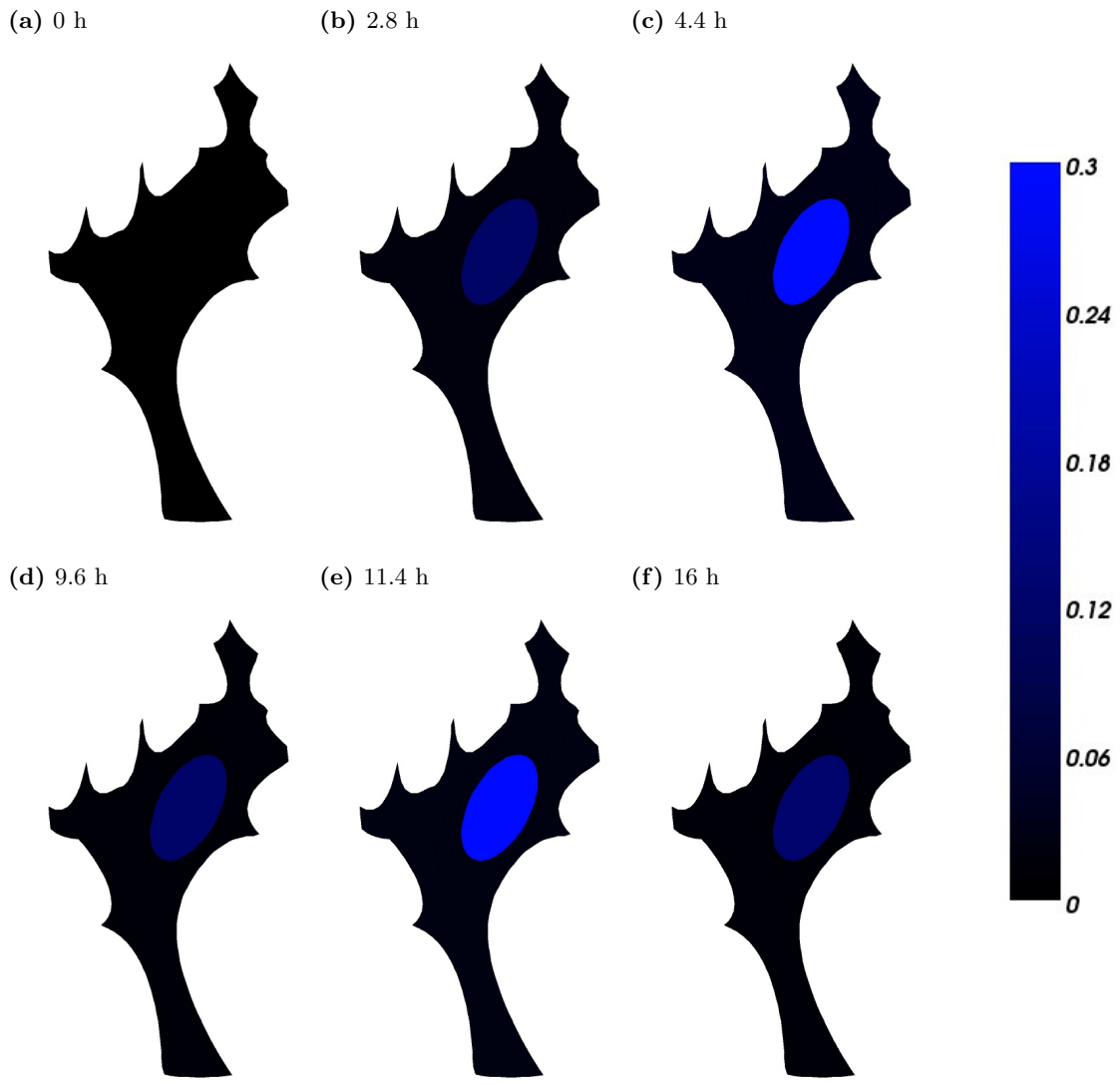

Figure 5.17. 2D visualisation of the solution of the PDE system for the HeLa cell: nondimensionalised concentration of Mdm2. The chosen samples are captured at 6 time points when p53 and Mdm2 reach peaks in the concentration.

p53 pathway, as an Akt-dependent inhibition of Mdm2 translocation into the nucleus in such cells [24, 58].

The activation signal E is understood as the measure of the DNA damage, and we assume that it is positively correlated with the damage doses (the higher doses a cell is exposed to, the bigger number of DSB is caused, the stronger activation signal E is produced; although closer identification of E with the number of DSB is not resolved in our works). Experiments on the p53 signalling network in single cells show that the oscillations can be observed independently of the damage dose and that the probability for starting pulsatile response becomes greater with the increasing number of DSB [56, 91]. Thus, based on such strong evidence, the oscillations of the system should not become extinct with increasing E as it was modelled by the ODE model provided that E corresponds to the damage dose. The signal E in the ODE model apparently plays a stronger role in the p53 signalling since "it can turn off the oscillations by itself". However, further studies need to be done to somehow give a biological

basis to our abstract parameter E and either accept or reject our speculations.

The PDE system presented in this chapter and the ODE model in the previous exhibit a supercritical Hopf point starting from which, when E increases, the solution maintains sustained oscillations instead of converging to a steady state. This bifurcation point can have a biological explanation as above. However, the second point for which sustained oscillations are switched back into the convergence to a steady state by crossing this point does not appear anymore in the present study as illustrated in Figures 5.11. Thus, as it has been reported in [56, 77], p53 oscillations can be modelled as a response of the cell to stress agents independently of the abundance of such agents, i.e. the oscillations are not turned off just by considering increased DNA damage.

Apoptosis of the cell can still be accompanied by the concentration of p53 switched from the oscillatory response to the DNA damage to a stable steady state of high levels. Note that the p53 sustained oscillations observed in [15, 56, 77], which can persist as long as 3 days (and possibly longer), have been demonstrated in breast cancer cells MCF-7 lacking functional PTEN protein, thus, indeed, the p53-PTEN-PIP3-Akt positive feedback may play an essential role in cell fate decisions [24, 58]. The compartmental ODE models [126, 161] consider effects of this particular positive feedback. It is, for example, proposed in [126] that the p53-PTEN-PIP3-Akt positive feedback works as a clock behind the p53-Mdm2 negative feedback, which gives some time ($\sim$15 hours) to repairing processes to fix the DNA damage, otherwise, irreversible apoptosis is launched. In addition, the p53-Mdm2 negative feedback alone is used to gain sustained oscillations in [126], however, it has been shown inefficient to produce oscillations *in vivo* [15]. The ODE model in [161] consists of the two negative feedbacks as they are considered in our models. A cell fate decision is determined by one of the two different p53 states, p53-arrester and p53-killer, the latter overcoming the former. The p53-arrester firstly transcribes proarrest genes ($Wip1$ and $p21$) and subsequently blocks the cell cycle, while p53-killer transcribes proapoptotic genes ($PTEN$, $p53DINP1$ and $p53AIP1$) later on, thus directing the cell to death. Note that this concept is based on the affinity of p53 for the target genes that contradicts recently published observations in [73, 102].

At this step of modelling we have represented and simulated p53 immediate responses to various stress conditions disrupting the integrity of the genome, such as γ-radiation or drugs in chemotherapies causing DNA DSB. In such cases, the DNA damage sensor ATM activates p53, thus endowing it with the ability to subsequently act as a transcription factor. Such responses to stress agents can be very sensitive in mammalian cells and our models also show sensitivity in producing oscillatory responses for very low values of the damage signal, E. On the other side, the duration of the oscillatory response is not terminated purely by increasing E.

Parameter	Value [Units]	Description
k_{ph1}	10 $[min^{-1}]$	velocity of ATM-P-dep. ph. of p53, [est.]
K_{ph1}	0.1 $[\mu M]$	Michaelis rate of ATM-P-dep. ph. of p53, [est.])
k_{dph1}	78 $[min^{-1}]$	velocity of Wip1-dep. deph. of p53-P, [136]
K_{dph1}	25 $[\mu M]$	Michaelis rate of Wip1-dep. deph. of p53-P, [136]
k_{ub}	5 $[min^{-1}]$	velocity of Mdm2-dep. ubiq. of p53, [78]
K_{ub}	1 $[\mu M]$	Michaelis rate of Mdm2-dep. ubiq. of p53, [78]
$k_S^\star$	0.015 $[\mu M/min]$	basal synthesis rate of p53, [15]
$k_{Sm}^\star$	0.000005 $[\mu M/min]$	basal synthesis rate of Mdm2 mRNA, [est.]
$k_{S_{pm}}$	0.03 $[\mu M/min]$	velocity of Mdm2 mRNA transcription, [est.]
$K_{S_{pm}}$	10 $[\mu M]$	Michaelis rate of Mdm2 mRNA transcription, [est.]
k_{tm}	1 $[min^{-1}]$	translation rate for Mdm2, [16]
$k_{Sw}^\star$	0.000003 $[\mu M/min]$	basal synthesis rate of Wip1 mRNA, [est.]
$k_{S_{pw}}$	0.03 $[\mu M/min]$	velocity of Wip1 mRNA transcription, [est.]
$K_{S_{pw}}$	10 $[\mu M]$	Michaelis rate of Wip1 mRNA transcription, [est.]
k_{tw}	1 $[min^{-1}]$	translation rate for Wip1, [16]
k_{ph2}	1 $[min^{-1}]$	velocity of ATM activation by E, [est.]
K_{ph2}	0.3 $[\mu M]$	Michaelis rate of ATM activation by E, [est.]
k_{dph2}	96 $[min^{-1}]$	velocity of Wip1-dep. deph. of ATM-P, [136]
K_{dph2}	26 $[\mu M]$	Michaelis rate of Wip1-dep. deph. of ATM-P, [136]
E	1 $[\mu M]$	concentration of "the damage signal", [chosen]
ATM_{TOT}	1 $[\mu M]$	total ATM concentration, [chosen]

Table 5.5. Parameter values for the RD PDE system (5.5)-(5.6) modelling p53 dynamics. Degradation terms are collected in Table 2.1. In the table, "dep." stands for dependent, "ubiq." for ubiquitination, "ph." for phosphorylation and "deph." for dephosphorylation.
*The constant rates represent the total net production in a certain area of the cell, e.g., the basal rates k_{Sm} and k_{Sm} produce the assigned values (in $\mu M/min$) over the whole nucleus, the basal rate k_S represents the total net production of the assigned value (in $\mu M/min$) over the cytoplasmic ring-shaped area denoted by C in Figure 5.4.
Note that the parameters in this table may be different from the ones used in the ODE model which were mostly taken from [42, 43]. Based on our recent search in the available biological articles, we have decided to replace some of them by more accurate parameters.

6

Novel mechanism for p53 oscillations: positive role of the negative regulator Mdm2

It is generally accepted that Mdm2 is a dominant negative regulator of p53 establishing its homeostasis in DNA damage response [147]. As it is mentioned in the previous sections, there exist several negative feedback loops regulating p53, most of them between p53 and Mdm2 [60]. However and somehow surprisingly, in addition to targeting p53 for degradation, Mdm2 in tight cooperation with MdmX can control expression levels of p53 through the enhanced induction of p53 synthesis in response to DNA damage [54, 96]. Whilst ATM-dependent phosphorylation of p53 is not observed to be important in this enhanced synthesis, ATM-dependent phosphorylation of Mdm2 (as well as MdmX) is essential for its dual role which is accompanied with widely oscillating p53. In the light of these new observations we formulate a novel mechanism for p53-Mdm2 dynamics and show that this mechanism is sufficient to trigger p53 oscillations. Notably, p53 excitable response to a transient input [15] can be explained by this dual function of Mdm2.

Organisation of the chapter is as follows: Section 6.1 introduces new biological observations and a dual function of Mmd2 to p53. A model of p53 dynamics taking into account positive and negative role of Mdm2 towards p53 is developed and examined in Section 6.2. Section 6.3 is then devoted to a phenomena of p53 excitability which is shown to occur in response to DSB caused by γ-irradiation or drugs.

6.1 Mdm2's dual function toward p53 in DDR

Recent observations suggest that Mdm2 can regulate p53 synthesis. In particular, Mdm2 can induce translation of p53 mRNA from two alternative initiation sites, giving a full-length p53 and an isoform of p53 with a relative molecular mass of approximately $47\,kDa$. This isoform does not contain the Mdm2-binding site and it lacks the amino-terminal transcriptional-activation domain of p53, however, its abundance positively regulates stabilisation of the full-length p53 in the presence of Mdm2. In addition, the p53 translation induction can be affected by Mdm2 and this regulation of p53 synthesis requires Mdm2 to interact directly with the nascent p53 mRNA [158].

In the more recent studies [54, 96], R. Fåhraeus and his colleagues discovered and described the precise molecular mechanism of a positive role of Mdm2 and its homolog MdmX

in the regulation of p53. In particular, they observed that Mdm2 as well as MdmX[1] can bind and form complexes with p53 mRNA following phosphorylation of Mdm2 at Ser395 [54] and MdmX at Ser403 [96] both by ATM. ATM-dependent phosphorylation of Mdm2 was not followed by Mdm2-P rapid degradation in [54] as it was observed in [139], but this phosphorylation event led to its nucleoli accumulation where Mdm2 changed its function from being a negative to a positive regulator of p53 [54]. In the first instance, the phosphorylated MdmX binds the nascent p53 mRNA and promotes its conformational changes in a way that favours attraction of the phosphorylated Mdm2 to the complex [96].

Action of MdmX-P on p53 mRNA following DNA damage relies on specific folding of the mRNA and MdmX-P can bind to a newly born mRNA at the DNA site only. In the p53 mRNA-MdmX-Mdm2 complexes MdmX acts as the "RNA chaperone" during its transportation from the nucleus to the cytoplasm [96]. Further, Mdm2 bound to the complex is much less capable to ubiquitinate p53 for degradation and, on the other hand, it stimulates p53 mRNA translation after genotoxic stress [54, 96]. In fact Mdm2-P induces more than three-fold increase in the rate of p53 synthesis after cells were exposed to doxorubicin [54, 96]. In addition, the wild-type p53 protein expressed from a non-Mdm2 binding mRNA is hyperunstable in the presence of Mdm2 in DDR. Thus the significance of the p53 mRNA-MdmX-Mdm2 complexes is not only in increasing p53 levels (through the enhanced p53 synthesis) but also in preventing p53 degradation following genotoxic stress (through the suppressed p53 ubiquitination) [54].

ATM-dependent phosphorylation of Mdm2 and MdmX is required for p53 mRNA-MdmX-Mdm2 interactions. Indeed, while phosphorylation of Mdm2 by ATM promoted its interaction with p53 mRNA, nonphosphorylated Mdm2 had weak affinity for p53 mRNA [54]. Phosphorylation of either of the two proteins supports formation of Mdm2-MdmX oligomers; nonphosphorylated Mdm2 interacts with MdmX and prevents its RNA chaperone activity [96]. In addition, Mdm2's Ser395[2] phosphorylation site is sufficient and necessary for the stability of p53 mRNA-Mdm2 complexes with a 3-5 fold increased abundance of p53 mRNA [54]. ATM-mediated phosphorylation of MdmX at Ser403 induces a highly specific binding to the p53 which is similar to that of Mdm2, however, MdmX does not stimulate its translation [96].

As described in Section 1.2.2, the generally accepted model for stabilisation of p53 requires phosphorylation of p53 by ATM, which enables p53 to escape from Mdm2-mediated degradation. Nevertheless, ATM-mediated phosphorylation of p53 was not observed to be necessary in the stabilisation of p53 and in order for Mdm2 to enhance p53 activity in response to DNA damage in [54]. In the line with this observation, close examination of all possible phosphorylation sites of p53 revealed that the site Ser15 may not have any direct effects on binding p53 to Mdm2 (although it is still necessary for the transcriptional activation of p53). Phosphorylation of p53's Thr18 is the only event found to significantly inhibit the ability of Mdm2 to bind p53 [131].

Thus, all these results demonstrate how ATM activity can switch between the two opposite roles of Mdm2 in the regulation of p53: depending on its phosphorylations status Mdm2 targets either p53 mRNA or p53, see Figure 6.1. This also suggests a novel mechanism which could possibly explain p53 oscillations after genotoxic stress. In the following section we

[1]It is known from previous studies that MdmX can form a complex with p53, bind to the same domain as Mdm2 (thus it competes with Mdm2 binding), yet it possesses no E3 activity and does not target p53 for degradation. However, p53 which accumulates in the presence of MdmX is biochemically and biologically inactive [106].

[2]Importance of this site for the increased activity of p53 is also evident from a significant reduction in apoptosis in several cell lines following the treatment with doxorubicin, including AT5-BIVA, H1299, and DKO cells which express ATM and wt p53 (of a smaller amount compared to wt Mdm2) but with Mdm2 mutated at Ser395 [54].

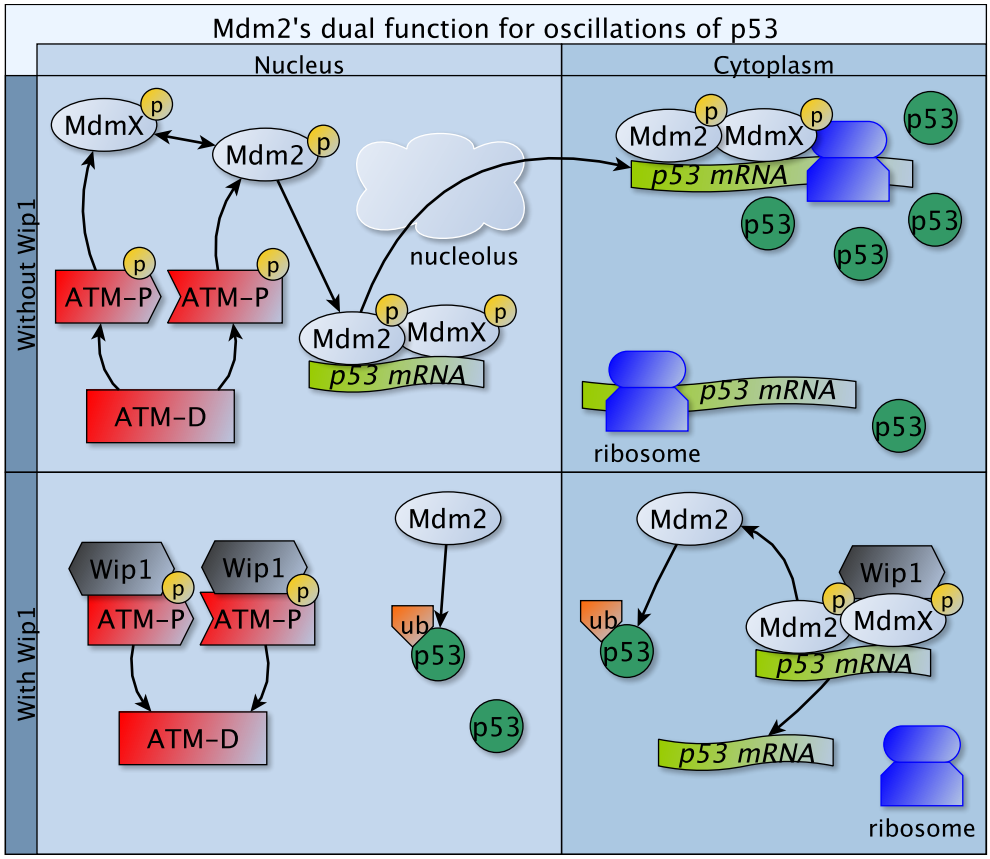

Figure 6.1. Positive effect of Mdm2 and MdmX towards p53: In the presence of DNA damage, ATM dimers dissociate into active monomers which phosphorylate Mdm2 at Ser395 and MdmX at Ser403 in the nuclear compartment. Phosphorylated Mdm2 and MdmX then form a complex with a nascent p53 mRNA, fold it and move from the nucleus to the cytoplasm, passing likely through the nucleolus where Mdm2 switches into a positive regulator of p53 by increasing p53 synthesis and, at the same time, suppressing Mdm2-dependent degradation of p53. This all enables p53 to accumulate in the nucleus where it acts as a transcription factor for the *Mdm2* and *Wip1* (and other) genes. The phosphatase Wip1 targets ATM-P for inactivation. Wip1 reverses also Mdm2 and MdmX phosphorylation status so that Mdm2 promotes ubiquitination and degradation of p53. The persistent DNA damage signal can trigger another pulse of p53 by ATM dimer monomerisation again.

propose a model for this mechanism. It is based on a simple conclusion from the observations above: as long as the ATM signalling is active, Mdm2 serves as a positive regulator of p53, whilst p53 is rapidly degraded by Mdm2 when the DDR is terminated (via the action of Wip1 [52, 92]).

6.2 A novel mechanism for p53 oscillations

A model for the molecular network composed of the negative feedback loops $p53 \to Mdm2 \dashv p53$ and $ATM\text{-}P \to Mdm2 \to p53 \to Wip1 \dashv ATM\text{-}P$ situated in the spatial PDE framework is presented in this section. The model is simplified in the sense that MdmX, which acts in the tight cooperation with Mdm2, is omitted from further considerations[3].

[3]Partly because MdmX and possibly its mRNA would represent another variables in the model.

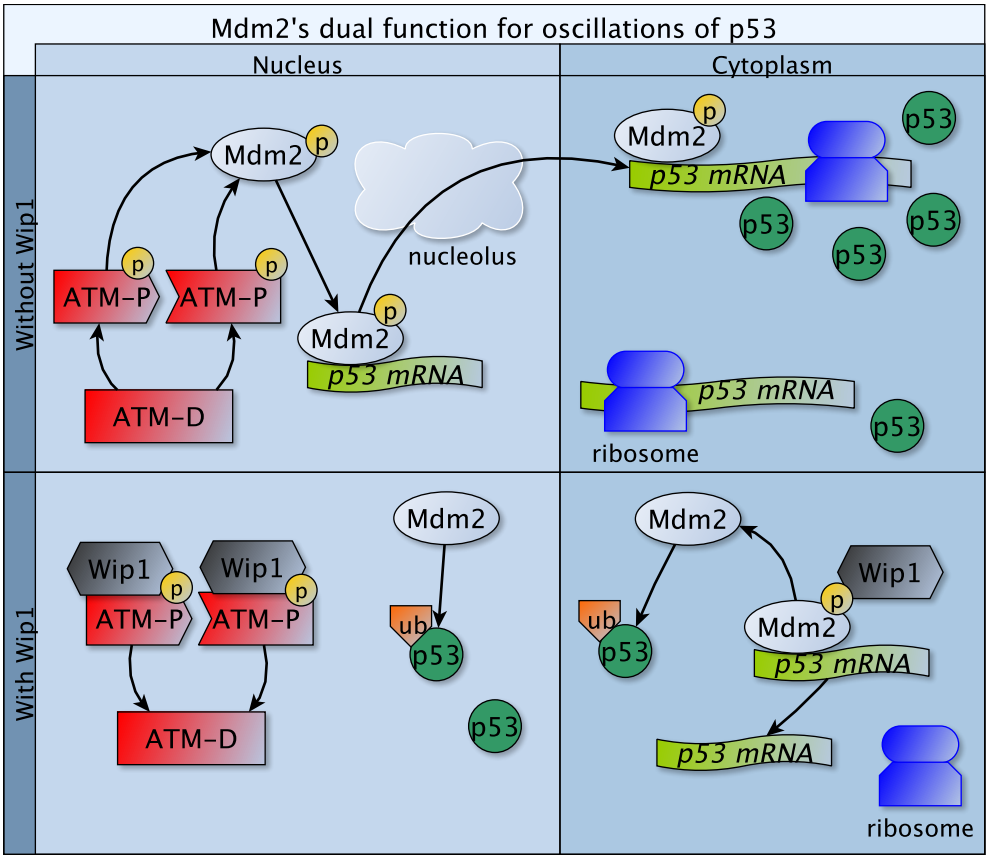

Figure 6.2. A simplified positive effect of Mdm2 towards p53: ATM dimers dissociate into active monomers ATM-P after DNA damage which then phosphorylate Mdm2 in the nuclear compartment. Phosphorylated Mdm2 switches into a positive regulator of p53, binds to a nascent p53 mRNA at the DNA site and moves with mRNA from the nucleus to the cytoplasm. In the cytoplasm, p53 mRNA from the complex is translated with a higher translation rate than p53 from "non-complex mRNA". At the same time, Mdm2-dependent degradation of p53 is decreased. p53 then translocates to the nucleus where it acts as a transcription factor for the *Mdm2* and *Wip1* (and other) genes. The phosphatase Wip1 targets ATM-P for inactivation. Wip1 also dephosphorylates Mdm2 so that Mdm2 promotes ubiquitination and degradation of p53. The persistent DNA damage signal can trigger another pulse by ATM dimer monomerisation again.

A novel model for p53 oscillations which we propose runs as follows, see also Figure 6.2: Following DNA damage, Mdm2 is phosphorylated by ATM and the phosphorylated Mdm2-P targets p53 mRNA instead of the protein p53. Mdm2-P acts as a chaperone for the mRNA, moves with it to the cytoplasm and together with p53 mRNA binds to free ribosomes. The mRNA is then translated with an increased synthesis rate giving the p53 protein. Meanwhile, p53 accumulates in the nucleus where it acts as a TF for the $Mdm2$ and $Wip1$ genes. In turn, Wip1 dephosphorylates Mdm2-P and the dephosphorylated Mdm2 targets p53 for degradation. Wip1 also dephosphorylates ATM-P trying to establish homeostasis in the DDR. This closes the first cycle between the antagonists. We do not consider any DNA repair mechanism here, thus persistent DNA damage signal E[4] triggers another wave of ATM-P and consequent pulses in all the other proteins under consideration.

[4]See Section 2.2.1 for the introduction of the substrate E.

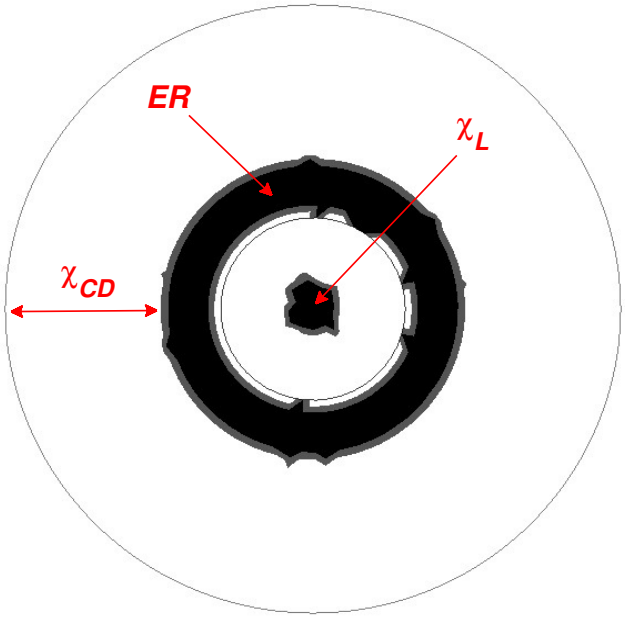

Figure 6.3. A scheme of the cell used in the model: the cell is represented by a disc with radius $10\,\mu m$. It consists of the nucleus represented by an inner disc of radius $3\,\mu m$ and the cytoplasm containing the rest of the cell. Within the cytoplasm there is an endoplasmic reticulum (ER) where no translation of the mRNAs occurs. The ER is represented by an annulus with radii $3\,\mu m$ and $5\,\mu m$. Translation of the mRNAs is supposed to occur outside of the ER, thus in an annulus χ_{CD} with radii 5 and $10\,\mu m$. Inside the nucleus there is a small disc χ_L of radius $1\,\mu m$ which represents the DNA locus where production of all mRNA content occurs.

6.2.1 Modelling Mdm2's dual function: assumptions

In contrast to the previous p53 PDE model (equations (5.5) and (5.6), hereafter denoted by Model 1) where we did not consider p53 mRNA, the new model relies on the synthesis of the mRNA either bound or unbound to the phosphorylated Mdm2 protein. Following ATM-dependent phosphorylation of Mdm2, Mdm2-P binds nascent p53 mRNA at the DNA sites in the nucleus thus, for simplicity, we specify a small area inside the nucleus as a "DNA locus" (denoted by χ_L on Fig. 6.3) where p53 mRNA is produced with a constant rate, and we assume that the reaction

$$p35\ mRNA + Mdm2\text{-}P \xrightarrow{k_a} C$$

with an association rate k_a occurs in this area χ_L only[5]. Here C denotes the p53 mRNA-Mdm2-P complex which moves to the cytoplasm where it binds free ribosomes, and similarly to the previous model, ribosomes are assumed to be located outside of the endoplasmic reticulum. The complex C can dissociate back into p53 mRNA and Mdm2-P in the cytoplasm, thus following the reaction

$$C \xrightarrow{k_d} p35\ mRNA + Mdm2\text{-}P$$

with a dissociation rate k_d. When it is released from C, p53 mRNA can be again used in the translation process; however, Mdm2-P cannot bind such mRNA again nor any other p53

[5]The Law of Mass action is then used to rewrite this reaction into mathematical terms.

mRNA outside the DNA locus χ_L in the nucleus.

The half-life of the complex C is set to 1 hour in this model which is the same as the half-lives of Mdm2 and Wip1 mRNA and 3-fold longer than the half-life of "free" p53 mRNA not bound to C (i.e., 20 minutes in accord with [1] who claim that the half-lives of mRNA of short-lived proteins such as transcription factors is often shorter than 30 minutes).

Since p53 produced from the mRNA bound to Mdm2-P is more stable (hereafter denoted by p53-2) when compared with the stability of p53 produced from the "free" mRNA (which was not bound to Mdm2-P; hereafter denoted by p53-1), the turnover constant for ubiquitination of p53-2 by both Mdm2 and Mdm2-P, i.e., $k_{ub\text{-}2} = 1\, min^{-1}$, is chosen to be 5-fold smaller than the ubiquitination rate ($k_{ub\text{-}1} = 5\, min^{-1}$) reported in [78]. The "unstable" p53-1 is targeted for ubiquitination by Mdm2 with the rate $k_{ub\text{-}1}$ and by Mdm2-P with the rate $k_{ub\text{-}2}$[6]. The Michaelis constant of the ubiquitination process is the same ($K_{ub} = 1\, \mu M$) for both p53-1 and p53-2 ubiquitination. Natural and Mdm2-independent degradation rates for both p53-1 and p53-2 correspond to the half-life of 7 hours. Natural degradation rates for Mdm2 and Mdm2-P are the same (Table 2.1).

Both proteins p53-1 and p53-2 are translated with different rates, since the synthesis of p53-2, when produced from p53 mRNA bound to the complex C, is enhanced 3–4-fold due to the active role of Mdm2-P. Thus we will consider two translation rates: $k_{tp\text{-}1}$ for p53-1 which is equal to the translation rates for Mdm2 and Wip1 (as they are used in the previous Model 1) and $k_{tp\text{-}2}$ for p53-2 which is 3-times larger than $k_{tp\text{-}1}$. In the transcription process of the $Mdm2$ and $Wip1$ genes, both proteins p53-1 and p53-2 act in a synergistic way, i.e., we do not distinguish between them whenever they are supposed to do the transcription job. Rates for p53-dependent synthesis of Mdm2 and Wip1 are the same as in the previous model. Transcription of the genes is supposed to occur in the DNA locus χ_L.

We will also assume that all proteins under consideration are nuclear proteins in the sense that they move from the translation sites in the cytoplasm (outside the ER) to the nucleus. On the other side, mRNAs and the complex C move from the nucleus to the cytoplasm. All these translocations are unidirectional.

We do not consider p53 phosphorylation by ATM in this model, and as in the previous model we include both equations for the nuclear monomeric and dimeric ATM protein. While the parameters (k_{ph3} and K_{ph3}) for ATM-dependent phosphorylation of Mdm2 are not known (and thus were tuned by hand), the rates k_{dph3} and K_{dph3} for newly added Wip1-dependent dephosphorylation of Mdm2-P are taken from [155]. Other relevant parameters are the same as in the previous PDE model and all kinetic rates are listed in Table 6.2, natural degradation rates in Table 2.1. As far as we are concerned with the diffusion and permeability rates for the complex C and p53 mRNA unbound to C, we assume that they are equal to the diffusion and permeability rate of an average mRNP compound (i.e., $D_C = D_{pRNA} = 1.8\, \mu m^2/min$ and $p_C = p_{pRNA} = 0.1\, \mu m/min$, pRNA stands for p53 RNA); diffusions and permeabilities are also the same for the pairs p53-1 and p53-2, and Mdm2 and Mdm2-P, respectively. All the relevant diffusion and permeability rates are listed in Table 5.2.

Protein-protein interactions are modelled as the enzyme reactions and thus, using the LMA and QSSA, the specific terms in the equations are composed from Michaelis functions. Transcription of the $Mdm2$ and $Wip1$ genes is modelled by Hill functions with the coefficient 4. Thus new equations, as shown in the following section, resemble equations (5.5) and (5.6) from the previous PDE model.

[6]Thus, we assume a certain level of a lowered affinity of Mdm2-P for p53 (both p53-1 and p53-2). In other words, ATM-dependent phosphorylation of Mdm2 reduces the ability of Mdm2-P to ubiquitinate both p53-2 (more stable) and p53-1 (less stable). Increased stability of p53-2 is achieved through a decreased ability of non-phosphorylated Mdm2 to ubiquitinate p53-2.

6.2.2 Modelling Mdm2's dual function: RD equations

For a simplified notation, we denote the concentrations of species in their nuclear and cytoplasmic states (distinguished by the superscripts (n) and (c), respectively) by

$$\begin{aligned} u_0 = [ATM\text{-}P]^{(n)}, u_0^D = [ATM\text{-}D]^{(n)} \\ u_1 = [p53\ mRNA]^{(n)}, u_2 = [C]^{(n)}, u_3 = [p53\text{-}1]^{(n)}, u_4 = [p53\text{-}2]^{(n)}, \\ u_5 = [Wip1\ mRNA]^{(n)}, u_6 = [Wip1]^{(n)}, \\ u_7 = [Mdm2\ mRNA]^{(n)}, u_8 = [Mdm2]^{(n)}, u_9 = [Mdm2\text{-}P]^{(n)}, \end{aligned} \tag{6.1}$$

and

$$\begin{aligned} v_0 = [ATM\text{-}P]^{(c)}, v_0^D = [ATM\text{-}D]^{(c)} \\ v_1 = [p53\ mRNA]^{(c)},, v_2 = [C]^{(c)}, v_3 = [p53\text{-}1]^{(c)}, v_4 = [p53\text{-}2]^{(c)}, \\ v_5 = [Wip1\ mRNA]^{(c)}, v_6 = [Wip1]^{(c)}, \\ v_7 = [Mdm2\ mRNA]^{(c)}, v_8 = [Mdm2]^{(c)}, v_9 = [Mdm2\text{-}P]^{(c)}, \end{aligned} \tag{6.2}$$

where, for each i, $u_i = u_i(t, \mathbf{x})$ and $v_i = v_i(t, \mathbf{x})$ are real functions of the time $t > 0$ and the space $\mathbf{x} \in \Omega \subset \mathbb{R}^2$ for a domain Ω as on Fig. 4.1. The nuclear species satisfy the following equations:

$$(N) \begin{cases} \dfrac{\partial u_0}{\partial t} = D_{ATM}\Delta u_0 + 2k_{ph2}u_0^D \dfrac{E^2}{K_{ph2}^2 + E^2} - k_{dph2}u_6 \dfrac{u_0}{K_{dph2} + u_0} \\ \dfrac{\partial u_0^D}{\partial t} = D_{ATM}\Delta u_0^D - k_{ph2}u_0^D \dfrac{E^2}{K_{ph2}^2 + E^2} + \dfrac{1}{2}k_{dph2}u_6 \dfrac{u_0}{K_{dph2} + u_0} \\ \dfrac{\partial u_1}{\partial t} = D_{pRNA}\Delta u_1 + k_S\chi_L - k_a u_1 u_9 \chi_L - \delta_{pRNA}u_1 \\ \dfrac{\partial u_2}{\partial t} = D_C\Delta u_2 + k_a u_1 u_9 \chi_L - \delta_C u_2 \\ \dfrac{\partial u_3}{\partial t} = D_{p53}\Delta u_3 - (k_{ub-1}u_8 + k_{ub-2}u_9)\dfrac{u_3}{K_{ub} + u_3} - \delta_{p53}u_3 \\ \dfrac{\partial u_4}{\partial t} = D_{p53}\Delta u_4 - k_{ub-2}(u_8 + u_9)\dfrac{u_4}{K_{ub} + u_4} - \delta_{p53}u_4 \\ \dfrac{\partial u_5}{\partial t} = D_{wRNA}\Delta u_5 + k_{Sw}\chi_L + k_{S_{pw}}\dfrac{(u_3 + u_4)^4}{K_{S_{pw}}^4 + (u_3 + u_4)^4}\chi_L - \delta_{wRNA}u_5 \\ \dfrac{\partial u_6}{\partial t} = D_{wip1}\Delta u_6 - \delta_{wip1}u_6 \\ \dfrac{\partial u_7}{\partial t} = D_{mRNA}\Delta u_7 + k_{Sm}\chi_L + k_{S_{pm}}\dfrac{(u_3 + u_4)^4}{K_{S_{pm}}^4 + (u_3 + u_4)^4}\chi_L - \delta_{mRNA}u_7 \\ \dfrac{\partial u_8}{\partial t} = D_{mdm2}\Delta u_8 - k_{ph3}u_0 \dfrac{u_8}{K_{ph3} + u_8} + k_{dph3}u_6 \dfrac{u_9}{K_{dph3} + u_9} - \delta_{mdm2}u_8 \\ \dfrac{\partial u_9}{\partial t} = D_{mdm2}\Delta u_9 + k_{ph3}u_0 \dfrac{u_8}{K_{ph3} + u_8} - k_{dph3}u_6 \dfrac{u_9}{K_{dph3} + u_9} - k_a u_1 u_9 \chi_L \\ \qquad - \delta_{mdm2}u_9 \end{cases} \tag{6.3}$$

while the species in the cytoplasm satisfy:

$$(C)\begin{cases} \dfrac{\partial v_0}{\partial t} = D_{ATM}\Delta v_0 \\ \dfrac{\partial v_0^D}{\partial t} = D_{ATM}\Delta v_0^D \\ \dfrac{\partial v_1}{\partial t} = D_{pRNA}\Delta v_1 + k_d v_2 - \delta_{pRNA} v_1 \\ \dfrac{\partial v_2}{\partial t} = D_C\Delta v_2 - k_d v_2 - \delta_C v_2 \\ \dfrac{\partial v_3}{\partial t} = D_{p53}\Delta v_3 + k_{tp-1} v_1 \chi_{CD} - (k_{ub-1} v_8 + k_{ub-2} v_9)\dfrac{v_3}{K_{ub}+v_3} - \delta_{p53} v_3 \\ \dfrac{\partial v_4}{\partial t} = D_{p53}\Delta v_4 + k_{tp-2} v_2 \chi_{CD} - k_{ub-2}(v_8+v_9)\dfrac{v_4}{K_{ub}+v_4} - \delta_{p53} v_4 \\ \dfrac{\partial v_5}{\partial t} = D_{wRNA}\Delta v_5 - \delta_{wRNA} v_5 \\ \dfrac{\partial v_6}{\partial t} = D_{wip1}\Delta v_6 + k_{tw} v_5 \chi_{CD} - \delta_{wip1} v_6 \\ \dfrac{\partial v_7}{\partial t} = D_{mRNA}\Delta v_7 - \delta_{mRNA} v_7 \\ \dfrac{\partial v_8}{\partial t} = D_{mdm2}\Delta v_8 + k_{tm} v_7 \chi_{CD} + k_{dph3} v_6 \dfrac{v_9}{K_{dph3}+v_9} - \delta_{mdm2} v_8 \\ \dfrac{\partial v_9}{\partial t} = D_{mdm2}\Delta v_9 - k_{dph3} v_6 \dfrac{v_9}{K_{dph3}+v_9} - \delta_{mdm2} v_9 \end{cases} \tag{6.4}$$

Boundary conditions (Kedem–Katchalsky BC) which take into account our new assumptions on the movement of species are listed in Table 6.1. We will consider zero initial conditions for almost all species except for Mdm2 and p53 mRNA which are assumed to be 0.1 and 0.01 (μM), respectively, at the initial time 0, i.e., we consider

$$\begin{gathered} \int u_1(0,\mathbf{x}) + v_1(0,\mathbf{x})\,\mathrm{d}x = 0.01 \quad \text{and} \int u_8(0,\mathbf{x}) + v_8(0,\mathbf{x})\,\mathrm{d}x = 0.1. \\ u_i(0,\mathbf{x}) = v_i(0,\mathbf{x}) = 0, \text{ otherwise.} \end{gathered} \tag{6.5}$$

The system (6.3)-(6.4) is then nondimensionalised in a similar way as the PDE system in the previous chapter[7]. Equations are solved numerically in 2D in FreeFem++, [62].

6.2.3 Numerical simulations

The nondimensionalised RD PDE system (6.3)-(6.4) for the p53 dynamics with a dual function of Mdm2 toward p53 is solved with the boundary conditions in Table 6.1, diffusion and permeability rates in Table 5.2 and other kinetic parameters in Tables 6.2 and 2.1.

Figure 6.4(a) shows oscillations in the p53 protein (plotted as the sum of concentrations of both p53-1 and p53-2) and confirms thus that the previously described mechanism for the dual function of Mdm2 towards p53 can trigger oscillations. Importantly, the dynamics of p53 in this model is similar to the dynamics from the previous model when compared to Fig. 5.6(a). A difference can be clearly seen in the achieved p53 amplitudes which are twice as big as the reached amplitudes in the previous Model 1. The amplitudes in the Mdm2 and Wip1 concentrations are fairly the same in both models (the peaks of the second pulses are

[7]The system is nondimensionlised with the reference values $\tau = 1\,min$, $\alpha_i = 1\,\mu M$ for each i and $L = 10\,\mu m$.

Chemical	nuclear changes	cytoplasmic changes
ATM-P	$-D_{ATM}\frac{\partial u_0}{\partial \mathbf{n}_1}=0$	$D_{ATM}\frac{\partial v_0}{\partial \mathbf{n}_1}=0$
ATM-D	$-D_{ATM}\frac{\partial u_0^D}{\partial \mathbf{n}_1}=0$	$D_{ATM}\frac{\partial v_0^D}{\partial \mathbf{n}_1}=0$
p53 mRNA	$-D_{pRNA}\frac{\partial u_1}{\partial \mathbf{n}_1}=p_{pRNA}u_1$	$D_{pRNA}\frac{\partial v_1}{\partial \mathbf{n}_1}=-p_{pRNA}u_1$
C	$-D_C\frac{\partial u_2}{\partial \mathbf{n}_1}=p_C u_2$	$D_C\frac{\partial v_2}{\partial \mathbf{n}_1}=-p_C u_2$
p53-1	$-D_{p53}\frac{\partial u_3}{\partial \mathbf{n}_1}=-p_{p53}v_3$	$D_{p53}\frac{\partial v_3}{\partial \mathbf{n}_1}=p_{p53}v_3$
p53-2	$-D_{p53}\frac{\partial u_4}{\partial \mathbf{n}_1}=-p_{p53}v_4$	$D_{p53}\frac{\partial v_4}{\partial \mathbf{n}_1}=p_{p53}v_4$
Wip1 mRNA	$-D_{wRNA}\frac{\partial u_5}{\partial \mathbf{n}_1}=p_{wRNA}u_5$	$D_{wRNA}\frac{\partial v_5}{\partial \mathbf{n}_1}=-p_{wRNA}u_5$
Wip1	$-D_{wip1}\frac{\partial u_6}{\partial \mathbf{n}_1}=-p_{wip1}v_6$	$D_{wip1}\frac{\partial v_6}{\partial \mathbf{n}_1}=p_{wip1}v_6$
Mdm2 mRNA	$-D_{mRNA}\frac{\partial u_7}{\partial \mathbf{n}_1}=p_{mRNA}u_7$	$D_{mRNA}\frac{\partial v_7}{\partial \mathbf{n}_1}=-p_{mRNA}u_7$
Mdm2	$-D_{mdm2}\frac{\partial u_8}{\partial \mathbf{n}_1}=-p_{mdm2}v_8$	$D_{mdm2}\frac{\partial v_8}{\partial \mathbf{n}_1}=p_{mdm2}v_8$
Mdm2-P	$-D_{mdm2}\frac{\partial u_9}{\partial \mathbf{n}_1}=-p_{mdm2}v_9$	$D_{mdm2}\frac{\partial v_9}{\partial \mathbf{n}_1}=p_{mdm2}v_9$

Table 6.1. The Kedem–Katchalsky transmission boundary conditions on Γ_1 with the diffusion coefficients D_i and the translocation rates p_i for the RD PDE system (6.3)-(6.4) modelling p53 dynamics with a dual function of Mdm2 towards p53. Whilst neither ATM dimers (ATM-D) nor ATM-P are allowed to leave nucleus, the complex C, p53, Wip1 and Mdm2 mRNAs move from the nucleus to the cytoplasm and the proteins p53-1, p53-2, Mdm2 and Wip1 from the cytoplasm to the nucleus as well as Mdm2-P unless it is bound to C.

equal to 0.14 in both models). One may think that the p53-dependent transcription is then different in both models, and it really is in the sense that the transcription sites are reduced to the DNA locus in this model whereas the transcription was allowed in the whole nucleus in Model 1. Otherwise the parameters for the transcription of genes used in this model are the same as in Model 1. The level of p53 (p53-1 and p53-2) appearing in the DNA locus is shown by the green dashed line in Fig. 6.4(a).

Timing of the pulses is also similar to each other in both models. The first two peaks in the p53 concentration are reached at 2.4 and 8.6 hrs after damage and the period of p53 oscillations in this specific example is 5.7 hours. Figure 6.5(b) further shows that the half-life of p53 in the cell in the presence of wt Mdm2 is 15 and 20 minutes when estimated from the first and second pulse, respectively. Obtained oscillations are confirmed by a limit cycle plotted on Fig. 6.5(a).

We started this simulation with a non-zero initial condition for Mdm2 and as it can be seen from Fig. 6.4(a), the Mdm2 level decreases in the first two hours. This was not caused by its degradation due to autoubiquitination (after the previous phosphorylation by ATM-P) clearly because our equations do not contain terms reflecting this phenomena. Instead,

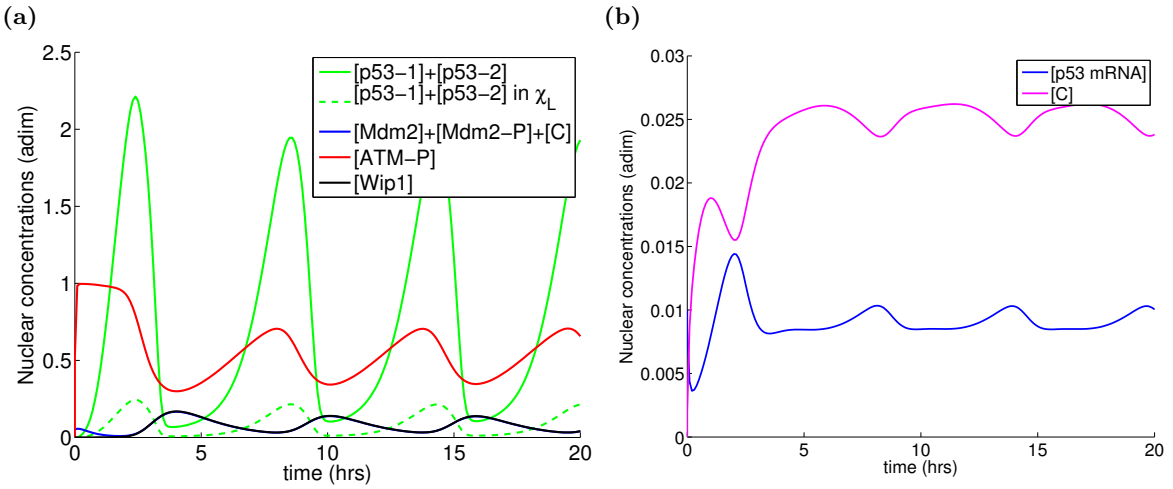

Figure 6.4. Solution of the RD PDE system (6.3)-(6.4) modelling p53 dynamics with a dual function of Mdm2 toward p53. Plotted curves are the concentrations in 20 hrs of DDR in response to the stress signal $E = 1$ for the fixed set of parameters in Tables 6.2 and 5.2: nondimensionalised (a) nuclear concentrations of total p53 (p53-1 and p53-2), total Mdm2 (Mdm2, free Mdm2-P and Mdm2-P bound to C), ATM-P and Wip1; green dashed line shows the concentration of p53 in the DNA locus χ_L (that is the transcriptionally active p53); (b) total cellular "free" p53 mRNA and p53 mRNA bound to the complex C. The plotted concentrations are the total concentrations in the nucleus and cell, respectively.

Mdm2 is degraded simply because of its short half-life and new Mdm2 molecules depend transcriptionally on p53 (its nuclear accumulation and activity). More than 2 hours after damage, the level of Mdm2 starts to increase and peaks at the 4 hrs time point after damage, at the point when p53 is found at its minimum.

Figure 6.4(b) shows the total intracellular concentration of p53 mRNA either bound to the complex C or "free" mRNA (unbound to C). In this case, the mRNA level in the complex C is 2.5-fold of the level of free mRNA.

In this specific case the enhanced translation from p53 mRNA bound to the complex C is necessary for oscillations. If we either do not allow the p53 mRNA-Mdm2-P complex formation (the association constant k_a is set to zero) or $k_a > 0$ remains as reported in Table 6.2 but the translation rates for both p53-1 and p53-2 are the same (i.e., $k_{tp\text{-}2} = k_{tp\text{-}1} = 1\, min^{-1}$), then we loose sustained oscillations. Instead, in the first case we observe convergence to a steady-state Figure 6.6, the p53 pattern which resembles p53 response to UV irradiation as depicted on Fig. 6.9. In the second case (when $k_{tp\text{-}2} = k_{tp\text{-}1}$), we obtain damped oscillations in the p53 concentration, Figure 6.7. Sustained oscillations can be retrieved for the value of $k_{tp\text{-}2} \geq 1.4\, min^{-1}$ and they are observed for the values of $k_{tp\text{-}2}$ as big as $500\, min^{-1}$ (in the latter case, the difference between the maxima in the p53 and Mdm2 nuclear levels is of several orders of magnitude, which confirms that a low concentration of Mdm2 can sufficiently remove over-expressed p53 from the nucleus).

Decreased ability of Mdm2 to target p53-2 for degradation, that is the p53 protein synthesised from the mRNA bound to the complex C, is essential for oscillations. The admissible rates $k_{ub\text{-}2}$ of the Mdm2-dependent ubiquitination of p53-2 yielding sustained oscillations are in the range $0.02 - 3.5$ min^{-1} which is less that the reported turnover rate $k_{ub\text{-}1} = 5\, min^{-1}$ in [78]. The rate $k_{ub\text{-}1}$ is used in the ubiquitination of p53-1.

Finally, Figure 6.8 shows dependence of the p53 concentration on varying stress signal E

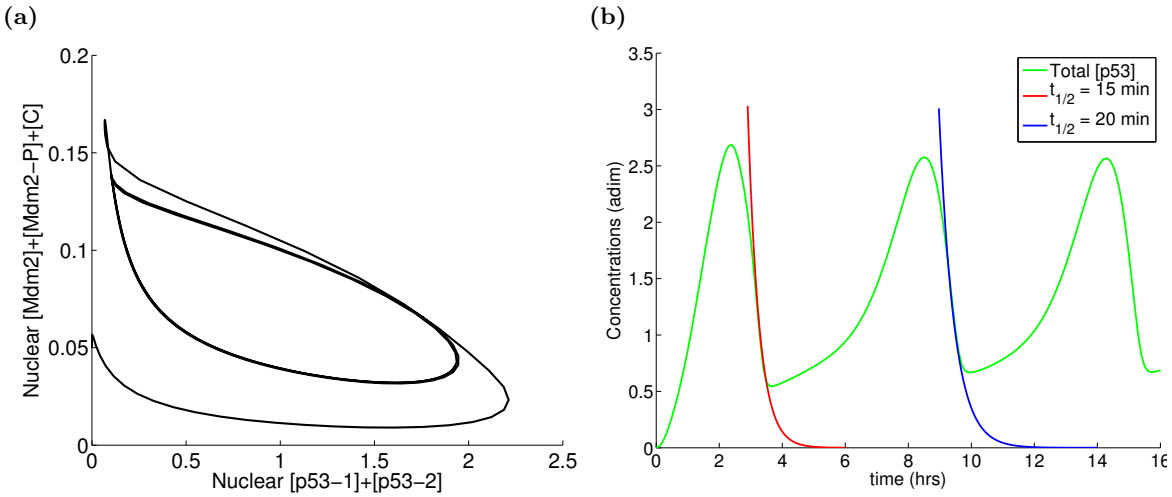

Figure 6.5. Solution of the RD PDE system (6.3)-(6.4) modelling p53 dynamics with a dual function of Mdm2 toward p53. Plotted curves are the concentrations in 20 hrs of DDR in response to the stress signal $E = 1$ for the fixed set of parameters in Tables 6.2 and 5.2: (a) phase portrait of dimensionless nuclear concentrations p53 (p53-1 and p53-2) with respect to the total concentration of Mdm2; (b) decay of the total (nuclear and cytoplasmic) p53 concentration in the cell with wt Mdm2 corresponding to the half-life of 15 and 20 minutes, respectively, in the first and the second pulse.

starting at $E = 0$ (normal conditions) where the concentrations of all the four species converge to their respective steady states, Fig. 6.8(a). Note that the reached steady state by p53 is higher than the steady states of its regulators when (but similar to the states maintained by Model 1 in Fig. 5.5(a)). However as it is pointed out in Section 1.5, a moderate level of Mdm2 can efficiently degrade p53 (see also [61]), and the actual reduction of p53 in normal conditions and in stress is about two orders of magnitude. With increasing E, Fig. 6.8(b), the dynamics of p53 changes from the convergence to equilibrium to the convergence to a (stable) limit cycle by passing through a bifurcation point $E_1 = 0.011$ (similar as in Model 1). The amplitudes and periods of the limit cycles do not change for $E > 0.25$ confirming that they are independent of the damage dose.

The similar dynamics of p53 arising from this model when compared to the previous one is important, since in this case the molecular mechanism explaining p53 excitability in the following section has realistic basis.

6.3 Excitability of p53

The response of p53 to DSB is excitable in the sense that a transient stimulus (for one hour) is sufficient for triggering a full p53 response (one full pulse of p53). This is the behaviour just in opposite to the p53 response to UV radiation, which is thus not excitable, Figure 6.9. Indeed, cells treated with ATM's inhibitor wortmannin one hour after DNA damage caused by γ-IR or drugs still exhibit one full p53 pulse. On the other side, if the kinase ATR, which is the activator of p53 pathway able to sense single strand breaks (SSB) caused by UV radiation, is inhibited one hour post-irradiation, then the inhibition of ATR results in inhibition of p53 levels which remain fairly constant in the following time course [14], see Figure 6.9.

It is proposed in [14] that a possible mechanism responsible for generating excitable

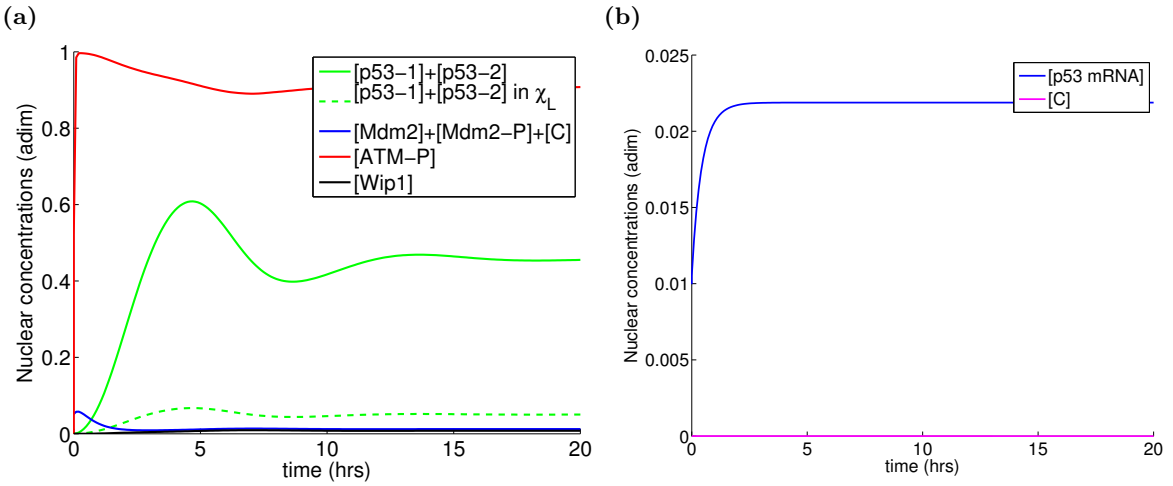

Figure 6.6. Solution of the RD PDE system (6.3)-(6.4) modelling p53 dynamics with a dual function of Mdm2 toward p53. Plotted curves are the concentrations in 20 hrs of DDR in response to the stress signal $E = 1$ in the case when no complex C formation is allowed (i.e., $k_a = 0$) for the parameters in Tables 6.2 and 5.2: nondimensionalised (a) nuclear concentrations of total p53-1 (no p53-2 is produced), total Mdm2 (Mdm2 and Mdm2-P), ATM-P and Wip1; green dashed line shows the concentration of p53 in the DNA locus χ_L (that is the transcriptionally active p53); (b) total cellular "free" p53 mRNA and p53 mRNA bound to the complex C. The plotted concentrations are the total concentrations in the nucleus and cytoplasm, respectively.

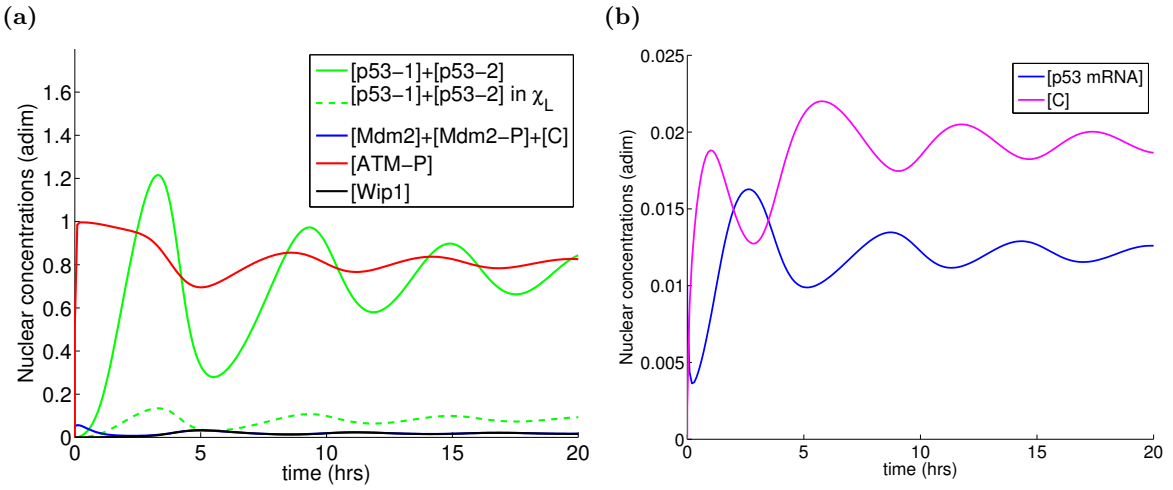

Figure 6.7. Solution of the RD PDE system (6.3)-(6.4) modelling p53 dynamics with a dual function of Mdm2 toward p53. Plotted curves are the concentrations in 20 hrs of DDR in response to the stress signal $E = 1$ for the decreased translation rate for p53-2 so that $k_{tp\text{-}1} = k_{tp\text{-}2} = 1$, other fixed parameters in Tables 6.2 and 5.2: nondimensionalised (a) nuclear concentrations of total p53 (p53-1 and p53-2), total Mdm2 (Mdm2, free Mdm2-P and Mdm2-P bound to C), ATM-P and Wip1; green dashed line shows the concentration of p53 in the DNA locus χ_L (that is the transcriptionally active p53); (b) total cellular "free" p53 mRNA and p53 mRNA bound to the complex C. The plotted concentrations are the total concentrations in the nucleus and cytoplasm, respectively.

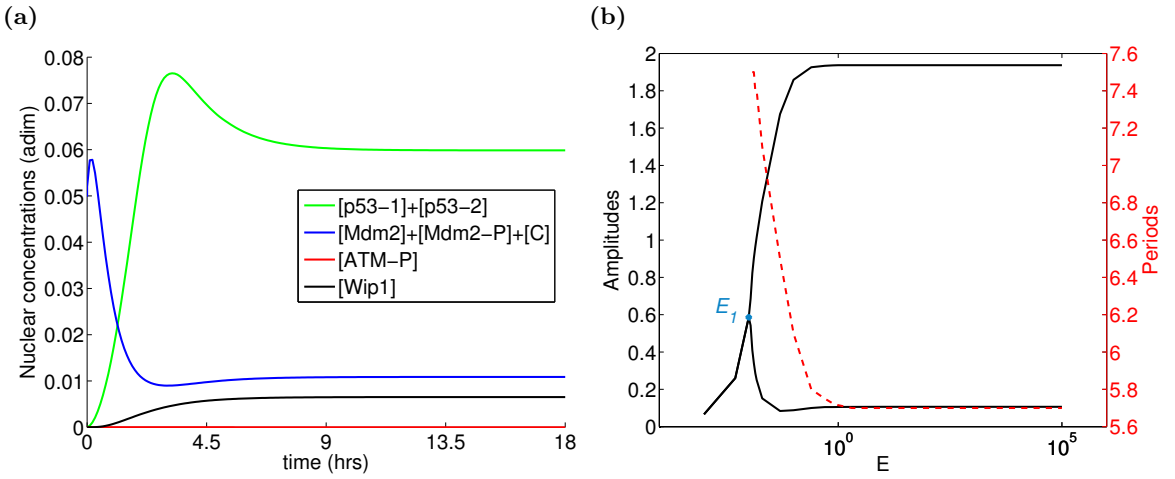

Figure 6.8. (a) Solution of the RD PDE system (6.3)-(6.4) modelling p53 dynamics with a dual function of Mdm2 toward p53 in normal conditions ($E = 0$); (b) Bifurcation diagram for the nuclear p53 concentration (p53-1 and p53-2) with respect to the varying signal E (plotted in the logarithmic scale). The bifurcation point E_1 is the point on the black curve where the curve bifurcates into two paths. The curve for $E < E_1$ shows attained steady states and plotted two curves for $E > E_1$ are the heights (showing maximum and minimum) of the amplitudes of stable limit cycles. The red curve shows periods of oscillations depending on E. The plotted nondimensionalised concentrations are the total concentrations in the nucleus. The used parameters are in Tables 6.2 and 5.2.

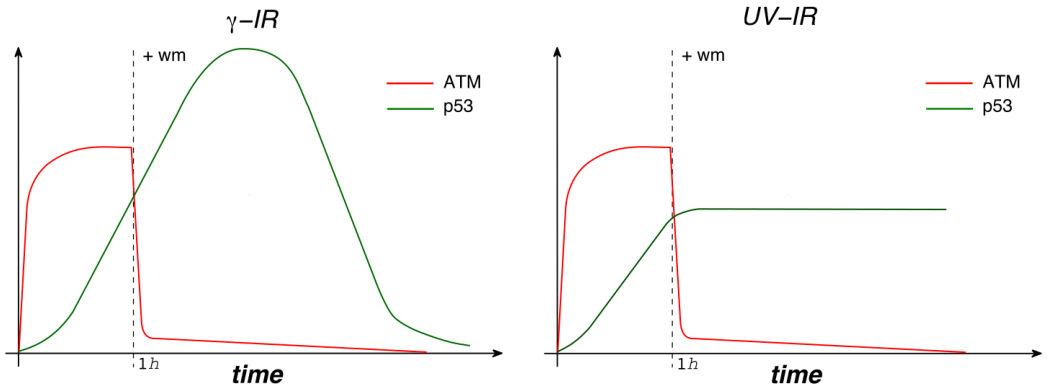

Figure 6.9. The dynamics of p53 is excitable, i.e., in response to γ-IR a transient input for one hour is sufficient to trigger one full pulse of p53 [14]. Following UV IR, a transient input results to a sustained p53 response.

behaviour of p53 relies likely on the fast removal of p53 inhibitors, such as Mdm2. Following phosphorylation by ATM [98], Mdm2 is observed to be rapidly degraded in response to NCS [139, 14] and this transient removal of Mdm2 may be sufficient for full p53 pulse. The excitability could be possibly caused by a fast positive feedback which, for instance, inhibits interaction of p53 with its negative regulators (Mdm2 and Wip1) or sequesters the regulators from the nucleus. To disfavour this hypothesis, it is pointed out in [14] that all known positive feedbacks in the p53 response to DSB depend on a transcriptional activity of p53 (see also [60]). Thus none of them could be fast enough to explain excitability.

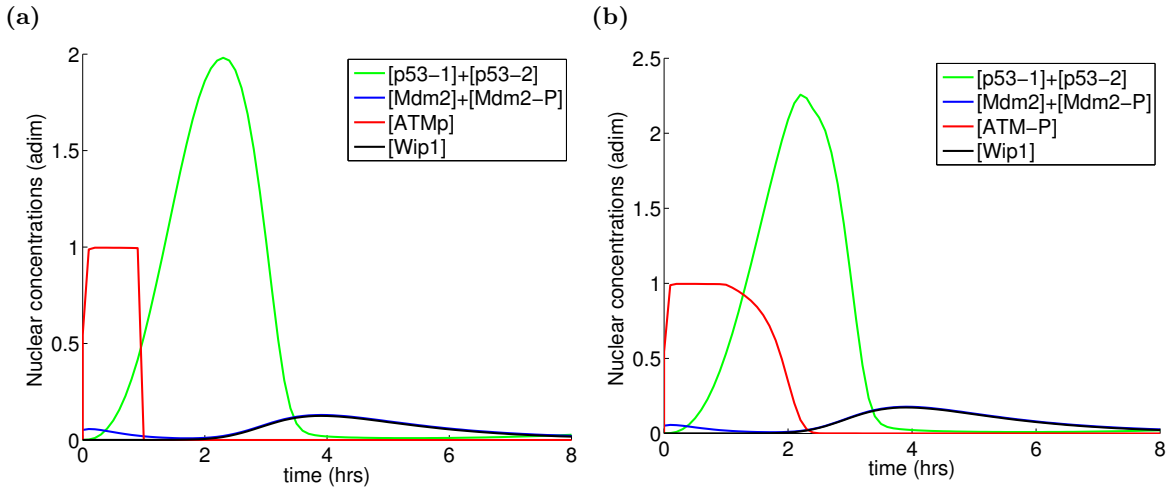

Figure 6.10. Solution of the RD PDE system (6.3)-(6.4) modelling p53 dynamics with the dual function of Mdm2 toward p53 when (a) ATM-P signalling is inhibited 1 hour after damage and (b) the damage-transmitting signal E is inhibited after one hour. The plotted nondimensionalised concentrations are the total concentrations in the nucleus.

The molecular pathways in [54, 96], as they were shown to be sufficient to trigger oscillations in the p53 concentration, however, suggest a different mechanism for the excitability. Notably the experimental results in [54, 96] do not confirm any degradation of Mdm2 after phosphorylation by ATM following DNA damage as it is observed in [139, 14]. On the other side, such phosphorylation events resulted in a positive effect of Mdm2 towards p53, [54, 96], see Section 6.1. Although both events, i.e., degradation of Mdm2-P and positive role of Mdm2-P after phosphorylation by ATM, seem to be exclusive to each other, we cannot exclude a possibility that they occur simultaneously. It could be also MdmX which is responsible for the different fate of Mdm2-P, once it is phosphorylated by ATM, since it is equally required for Mdm2-P to bind p53 mRNA. Thus we can speculate that if MdmX-P is not successful in the attraction of Mdm2-P to the complexes with mRNA, Mdm2-P initiates its own ubiquitination and degradation.

Nonetheless, the positive role of Mdm2-P can efficiently explain excitability of p53. In particular, Fig. 6.10(a) shows one full p53 pulse in the case when ATM-P signalling is inhibited 1 hour after damage (1 hour after damage, the equation for ATM-P was "removed" from the system; this can simulate ATM-P inhibition by wortmannin). Fig. 6.10(b) then shows a full p53 pulse when ATM-P signalling was gradually silenced by Wip1 (the damage signal E was set to 0 one hour after damage). The mechanism for the excitability we propose here relies on the prolongation of the half-life of p53 mRNA bound to the complex with Mdm2-P (we assume that the half-life of the complex is 1 hour whilst the half-life of the "free" p53 mRNA 20 minutes) which together with the enhanced p53 synthesis (the synthesis rate for the translation of p53 mRNA bound to Mdm2-P is 3-fold the translation rate for p53 from the "free" p53 mRNA in the model) can serve as a source of p53 for a longer period of time. The excitability can be thus achieved through a specificity of the ATM-dependent phosphorylation of Mdm2, thus through the positive role of Mdm2-P towards enhanced p53 synthesis. In fact, it is not caused by any positive feedback but the negative feedback between ATM and Wip1 with the intermediate substrates Mdm2 and p53 (i.e., $ATM\text{-}P \to Mdm2 \to p53 \to Wip1 \dashv ATM\text{-}P$).

Note that the excitability cannot be reproduced by Model 1 (Eqs. (5.5) and (5.6)), see

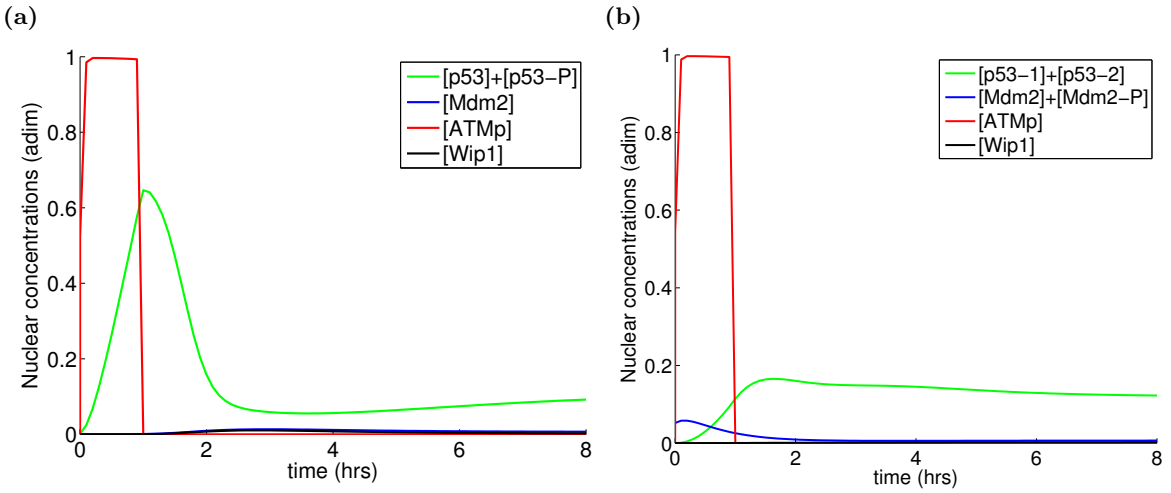

Figure 6.11. (a) Solution of the RD PDE system (5.5)-(5.6) modelling p53 dynamics *without* the dual function of Mdm2 towards p53 when ATM-P signalling is inhibited 1 hour after damage. (b) Solution of the RD PDE system (6.3)-(6.4) modelling p53 dynamics *with* the dual function of Mdm2 towards p53 when $k_a = 0$, i.e., no complexes between p53 mRNA and Mdm2-P are allowed and ATM-P signalling is inhibited 1 hour after damage. The plotted nondimensionalised concentrations are the total concentrations in the nucleus.

Figure 6.11(a). When we compare Figure 6.10(a) with 6.11(a) we see that p53 increases with the same slope in both figures but at 1 hour when ATM-P is completely inhibited, p53 continues to grow in the new model, Fig. 6.10(a), while p53 levels immediately start to decrease in the old model, Fig. 6.11(a). The excitability is not observed even in the new model when the association constant for the complex induction $k_a = 0$, i.e. p53 mRNA-Mdm2-P complexes are not produced in the DDR. This is shown on Figure 6.11(b).

6.4 Discussion and conclusions from the PDE model #2

We have shown that depending on the phosphorylation status of Mdm2, its dual role for p53 can lead to oscillations in the p53 concentration whenever ATM signalling towards Mdm2 is active. In fact, the new model for p53 oscillations (hereafter referred to as Model 2) uses almost the same two negative feedbacks (as we used in the previous model) as well as spatial representation of the cell which, when put together, represent a new oscillator.

The negative feedback loops used in the old models are between p53 and Mdm2 ($p53 \to Mdm2 \dashv p53$) and ATM and Wip1 through the intermediate p53 ($ATM\text{-}P \to p53 \to Wip1 \dashv ATM\text{-}P$). Notably, the ATM-dependent phosphorylation of p53 was necessary for breaking bounds between p53 and Mdm2 and enabling thus p53 to accumulate in the nucleus. In the new model, we have imposed another intermediate substrate into the latter feedback that is Mdm2 ($ATM\text{-}P \to Mdm2 \to p53 \to Wip1 \dashv ATM\text{-}P$), as shown on Figure 6.12, and we have excluded phosphorylation of p53 by ATM. Mdm2 involved in the second loop changes significantly effects of both negative feedbacks. Depending on the phosphorylation status of Mdm2, when Mdm2 is phosphorylated by ATM the first negative loop is weakened since Mdm2-P does not target sufficiently p53 for degradation and the second strengthened since Mdm2-P positive stimulates p53 synthesis induction with more stable p53 and higher level of p53 mRNA. If Mdm2 is not phosphorylated by ATM, then the first negative loop is

strengthened since Mdm2 targets p53 for degradation (independently on the phosphorylation status of p53, i.e., whether p53 is phosphorylated by ATM or not), and the second loop is weakened since the non-phosphorylated Mdm2 cannot (or it can but with very low affinity) bind p53 mRNA and thus it does not contribute to its synthesis.

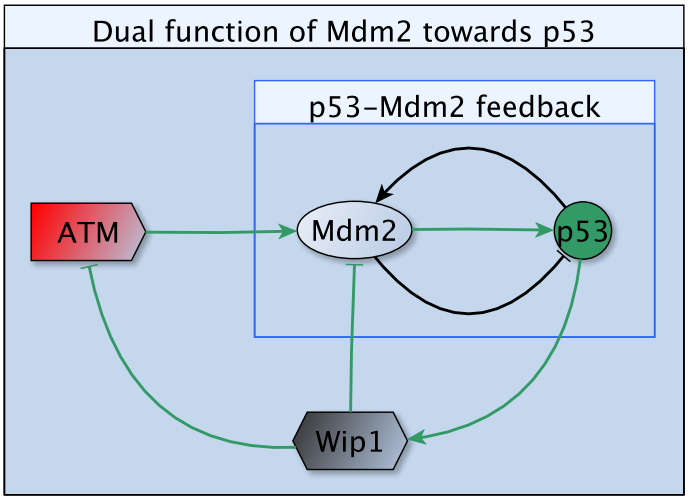

Figure 6.12. The model for the dual function of Mdm2 towards p53 relies on the two negative feedback loop: the classical $p53 \to Mdm2 \dashv p53$ where p53 transcriptionally induces Mdm2 and Mdm2 in turn degrades p53, and the loop between ATM and Wip1 through the cascade involving p53 and Mdm2, i.e. $ATM\text{-}P \to Mdm2 \to p53 \to Wip1 \dashv ATM\text{-}P$, where Mdm2, after being phosphorylated by ATM, enhances synthesis of p53 which in turn transcriptionally activates Wip1 (and also Mdm2) which inactivates ATM.

The level of p53 as well as its nuclear stability is determined by Mdm2-dependent stimulation of p53 synthesis. This is a new mechanism of regulation of p53 by its negative regulator Mdm2, [54, 96].

The new model is able to reproduce (and thus to suggest a mechanism explaining) excitable p53 response to a transient input. Such response would be surprising in the first Model 1, since the model does not contain either a positive feedback or ATM-dependent degradation of Mdm2—the two hypotheses proposed in [14]. We do not reject these hypotheses explaining p53 excitability. However, in Model 1, which does not trigger a full pulse in response to a transient ATM-P signal (Fig. 6.11(a)), we started our simulations with the zero initial state for Mdm2, thus there is no Mdm2 in the pool to be phosphorylated and the appearance of Mdm2 in the nucleus is delayed due to p53-dependent transcription. The picture is not different (when compared to Fig. 6.11(a)) even if we start simulations of Model 1 from a non-zero initial datum for Mdm2 and/or we include ATM-dependent degradation of Mdm2 (due to auto-ubiquitination). This suggests that either Model 1 misses some parts necessary for the excitability or that the removal of Mdm2 from the nucleus (due to enhanced autoubiquitination) is a complementary effect of an unknown path that actually triggers p53 excitability (e.g., the role of MdmX as discussed above).

Parameter	Value [Units]	Description
$k_{ub\text{-}1}$	5 $[min^{-1}]$	velocity of Mdm2-dep. ubiq. of p53-1, [78]
$k_{ub\text{-}2}$	1 $[min^{-1}]$	velocity of Mdm2-dep. ubiq. of p53-2, [est.]
K_{ub}	1 $[\mu M]$	Michaelis rate of Mdm2-dep. ubiq. of p53, [78]
$k_S^\star$	0.0005 $[\mu M/min]$	basal synthesis rate of p53 mRNA, [est.]
$k_{tp\text{-}1}$	1 $[min^{-1}]$	translation rate for p53-1, [16]
$k_{tp\text{-}2}$	3 $[min^{-1}]$	translation rate for p53-2, [54, 96]
$k_{Sm}^\star$	0.000005 $[\mu M/min]$	basal synthesis rate of Mdm2 mRNA, [est.]
$k_{S_{pm}}$	0.03 $[\mu M/min]$	velocity of Mdm2 mRNA transcription, [est.]
$K_{S_{pm}}$	10 $[\mu M]$	Michaelis rate of Mdm2 mRNA transcription, [est.]
k_{tm}	1 $[min^{-1}]$	translation rate for Mdm2, [16]
$k_{Sw}^\star$	0.000003 $[\mu M/min]$	basal synthesis rate of Wip1 mRNA, [est.]
$k_{S_{pw}}$	0.03 $[\mu M/min]$	velocity of Wip1 mRNA transcription, [est.]
$K_{S_{pw}}$	10 $[\mu M]$	Michaelis rate of Wip1 mRNA transcription, [est.]
k_{tw}	1 $[min^{-1}]$	translation rate for Wip1, [16]
k_{ph2}	1 $[min^{-1}]$	velocity of ATM activation by E, [est.]
K_{ph2}	0.3 $[\mu M]$	Michaelis rate of ATM activation by E, [est.]
k_{dph2}	96 $[min^{-1}]$	velocity of Wip1-dep. deph. of ATM-P, [136]
K_{dph2}	26 $[\mu M]$	Michaelis rate of Wip1-dep. deph. of ATM-P, [136]
k_{ph3}	1 $[min^{-1}]$	velocity of ATM-dep. ph. of Mdm2, [est.]
K_{ph3}	1 $[\mu M]$	Michaelis rate of ATM-dep. ph. of Mdm2, [est.]
k_{dph3}	84 $[min^{-1}]$	velocity of Wip1-dep. deph. of Mdm2-P, [155]
K_{dph3}	23 $[\mu M]$	Michaelis rate of Wip1-dep. deph. of Mdm2-P, [155]
k_a	20 $[min^{-1}]$	association rate for the complex C, [est.]
k_d	0.01 $[\mu M^{-1}\, min^{-1}]$	dissociation rate from the complex C, [est.]
E	1 $[\mu M]$	concentration of "the damage signal", [chosen]
ATM_{TOT}	1 $[\mu M]$	total ATM concentration, [chosen]

Table 6.2. Parameter values for the RD PDE system (6.3)-(6.4) modelling p53 dynamics with a dual function of Mdm2 toward p53. Degradation terms are collected in Table 2.1. In the table, "dep." stands for dependent, "ubiq." for ubiquitination, "ph." for phosphorylation and "deph." for dephosphorylation.
*The constant rates represent the total net production in a certain area of the cell: the basal rates k_S, k_{Sm} and k_{Sm} produce substrates of the assigned values over the whole DNA locus.

7

Summary of the p53 modelling and follow-up work

7.1 Physiological ODE and PDE models for p53

The aim of our modelling, rather simple compared with the overall complexity of p53 signalling network in cell fate decisions between survival and death, is to simulate activation of p53 in single cells, the concentration of which shows sustained oscillations under stress conditions, the duration of oscillations being independent of the damage signal. Thus, we simplified the p53 network by neglecting (hundreds of) possible target proteins and kept only those proteins that are actually experimentally justified to be necessary and sufficient for oscillations [15]. Therefore, four proteins, particularly, p53, Mdm2, Wip1 and ATM were chosen. Plausible effects of any positive feedback are not disputed in our work. We have developed the compartmental ODE model which became basis for the two spatial RD PDE models simulating the p53 protein in a single cell in response to DNA DSB (caused by γ-radiation, cytotoxic drugs used in chemotherapy or by other means).

Basic features of the models are: compartmental distribution of the cellular processes between those occurring in the nucleus and those in the cytoplasm, the negative feedback loop $p53 \to Mdm2 \dashv 53$ and then either the negative loop $ATM \to p53 \to Wip1 \dashv ATM$ (in the ODE model and the PDE Model 1) or $ATM \to Mdm2 \to p53 \to Wip1 \dashv ATM$ (in the PDE Model 2 with the dual function of Mdm2). It was confirmed that the sole p53-Mdm2 negative feedback is not sufficient for triggering oscillations. Instead, activation and regulation of p53 must involve the ATM and Wip1 proteins considered as continuous time- and space-dependent (in the PDE models) functions, the dynamics of which is fully described by mathematical equations rather than being represented by constant parameters. In our context, a special signal denoted by E acts as a transmitter of information about the presence of the DNA DSBs; E is assumed to be a constant positively correlated with the DNA damage dose. We assume that the higher doses a cell is exposed to, the bigger number of DSB is caused, the stronger activation signal E is produced, and we have shown by the PDE models that the amplitudes and periods of p53 oscillations are, as expected from experiments, independent of the damage dose (that is independent of E).

In principle, one can similarly model intracellular pathways of any other proteins, i.e., write as many reactions as necessary just by employing simple tools such as The Law of Mass Action, Michaelis-Menten and Hill kinetics. Since the spatial representation of the signalling pathways can reveal diffusion-driven patterns that are hidden in ODE, we aimed to attract attention to reaction-diffusion equations. Our models are still simple since, in contrast to the ODE setting, the spatial models are placed into a structural framework of the cell composed

of the two compartments only, nucleus and cytoplasm, and the diffusive motion of the species in and between these compartments is further considered. However, we believe that the PDE models are much more physiological than (rougher) ODE models since they are naturally able to take intracellular spatial features into account including possible space heterogeneities in the intracellular medium. For instance, the oscillatory patterns in the p53 concentration are self-organised not only due to the reactions in the nucleus or in the cytoplasm but that they are also tightly connected to the boundary conditions on the membranes and to the diffusions of the species. The physiological delays maintained due to the semipermeability of the nuclear membrane are more typical for PDEs than for ODEs (if one does not want to deal with artificial delays represented by DDEs). The second specific property of the PDE models, which affects amplitudes, periods and the timing of pulses, is diffusive motion of the species. Although, we were able to find some lower bounds for the diffusion coefficients, below which we do not receive any oscillations, oscillations can be maintained for any other diffusions larger than these bounds. One may expect such results since fast diffusions make solutions of the RD system homogenous in space and thus, roughly speaking, the PDE system resembles the compartmental ODE model which describes the dynamics of proteins with the same reaction terms and thus it is able to produce oscillations in the p53 concentration.

Further, intracellular signalling in our modelling setting is restricted to the cells of physiology and morphology where a molecular network in question is, at least, partially understood. What does the p53 signal transduction in response to DNA damage in a nerve cell or in a polynucleic muscle cell look like? What is the role of diffusion in a cell where a signal is spread over long distances and in very small cells? These and other questions should be further addressed and spatial PDE models might fruitfully be used for this purpose.

Reaction-diffusion systems could be thus considered as an alternative approach to classical ODEs which may put some light on protein signalling and will be of some help to biologists and modellers who want to describe intracellular spatio-temporal dynamics of proteins in a faithful yet more demanding (in terms of parameter estimation) way. Such reaction-diffusion PDE models are also amenable to describe spatio-temporal dynamics at the level of cell populations and that, by introducing intercellular signalling, it is in principle possible to connect the two observation levels. This perspective still remains a challenge to mathematicians and modellers in biology.

7.2 p53 as a chemotherapeutic target

The protein p53 is a well studied protein due to its role in the protection of the genome. Furthermore, because p53 can elicit life or death decisions in cells, it has recently become a therapeutic target in cancer treatment. Therapeutic effort in p53-aimed treatments focuses mainly on either substitution of the p53 lost functionality and destabilisation of oncogenic p53 mutants or restoration of p53 function by targeting upstream proteins in the p53 signalling pathway, in particular the negative regulators Mdm2 and Wip1 which, in some cancer cells, are over-expressed and thus suppress the p53 functionality, see [66, 79] and citations therein.

There have been developed and already used in clinical testing several protocols and p53-based anti-cancer therapies including retrovirus- or adenovirus-mediated gene therapy (to restore p53 function), targeting p53-deficient cells with modified adenoviruses, pharmacological modulation of p53 (and also p63 and p73) protein functions, identification and design of small-molecule inhibitors of the Mdm2-p53 (and Wip1-p53) interactions (potential therapeutic agents: nutlins, RITA, spiro-oxindoles, quinolinols). However, there are not yet clear clinical studies confirming successful applications of the therapies in the treatment of cancers. In addition, the described therapeutic efforts were accompanied with unwanted side effects

in normal tissues, appearance of p53-resistant tumours or premature aging. Thus, optimisation of doses and time of treatment, application of combined therapies, and efficacy of the treatments with small-molecule inhibitors have to be further elucidated [36].

For example, tissue-specific deletion of Mdm2 in cardiomyocytes, smooth muscle cells, and the central nervous system was accompanied with p53-dependent apoptosis. Thus, the loss of Mdm2 can be sufficient to induce p53-dependent apoptosis in these (and likely in other) cell types, [12] and citations therein. On the other side, experiments on small-molecule inhibitors against Mdm2-p53 complex formation suggest that Mdm2 action toward p53 cannot be completely restrained, since in normal cells this can have fatal consequences. This was highlighted, for example, by the embryonic lethality of Mdm2 null mice which were rescued by the elimination of p53, i.e. p53 became lethally hyperactive in the absence of Mdm2, [106] and citations therein.

7.3 p53 dynamics in blocking proliferation and launching apoptosis

Single cell experiments and observed distinct p53 dynamics in response to γ-radiation or drugs (DSB) and UV radiation (SSB) encouraged G. Lahav and her colleagues to explore further consequences of the specific dynamical patterns on the cell fate decision with possible applications in the cancer treatment [124]. Notably, they observed that p53 pulses following γ-irradiation resulted in transient cell-cycle arrest and DNA damage recovery, whilst artificially sustained p53 oscillations by inhibiting Mdm2's activity by Nutlin-3 led to cellular irreversible fate, preferentially to senescence, following γ-irradiation [123], Figure 7.1. A delayed wave of p53 of high level triggered several days post-irradiation, as the consequence of persistent genomic injury, associated with p21-dependent activation of senescence and suppression of apoptosis is observed also in [108]. The cells were not treated with nutlin in [108]. On the other side, one single pulse of p53 triggered after UV radiation induced apoptosis [123, 124]. This suggests that the dynamics of p53 can be associated with specific cellular outcomes, i.e. it may be considered as the marker of the chosen reversible or irreversible cell fate. Dynamical patterns of p53 can be also modulated by a combination of two or more stimuli with synergistic effects on downstream signalling (prosurvival, proapotosis, *etc.*) proteins.

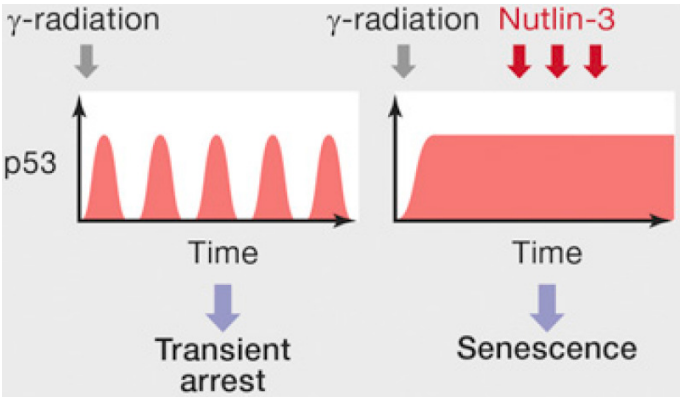

Figure 7.1. Information about the cell fate can be encoded in the dynamics of p53: the cell is arrested in the cell cycle whenever p53 oscillates and the cell initiates senescence whenever p53 shows a sustained signalling. Reprinted from [124], Copyright (2013), with permission from Elsevier.

A stressed cell likely evaluates the presence of both proarrest and proapoptotic proteins produced in a p53-dependent manner at any time during its response to DNA damage. The cell determines the so-called "apoptotic ratio"[1] with respect to protein concentrations, duration of their expression and other factors. Irreversible apoptosis is initiated whenever this ratio crosses a given threshold [73]. Expression of those apoptosis-launching proteins is complex process that depends on many factors (post-translational modifications, interactions with other cellular substrates, location). On the other side, it is observed that p53, its regulators and most of the apoptotic proteins are all short-lived proteins [106, 26]. This may suggest that these proteins exhibit a similar oscillatory behaviour in the (transient) cell cycle arrest and DNA damage repair, which does not allow them to accumulate sufficiently to cross the apoptotic ratio. In contrast, p53 switched to the sustained signalling may lead to sufficient accumulation and stabilisation of apoptotic agents which are then able to initiate apoptotic program. Although further studies have to be done in this line, it seems, however, that the dynamics of p53 could control the apoptotic threshold of individual cells in response to DNA damage. In this context, the oscillatory dynamics of the involved proteins can be possibly explained as a periodical testing of the presence of DNA damage: if unrepaired DNA DSB still exist, additional pulses of both phosphorylated ATM and p53 are triggered [15].

In an even more realistic vision of the processes leading a single cell to decision between survival and death, more than deterministic events, random molecule encounters and stochastic gene expression should be taken into consideration, and should be modelled by stochastic processes (as sketched in [141] for Hes1), from which deterministic equations (partial differential equations physiologically structured in variables, identified as biological "readouts" in a single cell model, representing relevant biological variability inside the cell population) should be further designed at the level of cell populations.

In the same way, in the perspective of connecting the proposed p53 modelling with existing PK–PD models, drug effects, measured only at the cell population level, can be represented as environmental factors exerting their influence on molecular targets, included as functions in stochastic processes, at the level of a single cell. Establishing such connections between stochastic events at the individual cell level and resulting deterministic effects at the cell population level is a challenge for mathematical modelling that we intend to tackle in future works. Readers interested in such interconnections between stochastic and deterministic mathematics in the Hes1 regulatory network are recommended to read the papers by M. Sturrock *et al.* [141, 140] to get acquainted with this challenge.

7.4 Cancer therapies and PK–PD models

Most cytotoxic and cytostatic drugs used in cancer treatments act in a selective manner, taking advantage of differences in tumour cell characteristics, compared to healthy cells, such as high proliferation rates, genome instability and tolerance to hypoxia. This results in proper targeting of chemotherapeutic agents on tumour cells. However, cancer therapies also have toxic side effects on healthy cells and can lead to the disruption of physiological functionality of tissues and organs. In the particular case of chronotherapeutic settings (i.e., hypothesising best treatment periods in the 24 hour span), physiologically based molecular pharmacokinetic-pharmacodynamic (PK–PD) models using ODEs have been proposed for the cytotoxic drugs Oxaliplatin [30], 5-Fluorouracil [30, 87] and Irinotecan [9, 8], all three drugs that are commonly used in the treatment of metastatic colorectal cancer. Moreover, to minimise such unwanted effects in more general (non chronotherapeutic) settings, most anti-

[1] The ratio which does not have to be necessarily associated with apoptosis but rather with any irreversible cell fate.

cancer drugs are delivered in the clinic in time interval-depending regimens to allow cells to recover their normal functions after pharmacological insult. However, time intervals between chemotherapy courses also allow tumour cells to recover, activating their survival mechanisms, and further resist subsequent therapeutic insults. Optimal scheduling strategies are currently being theoretically investigated [29, 30, 19] to obtain satisfying trade-offs between the objective of reducing the tumour burden without inducing neither intolerable side effects on healthy cells nor emergence of resistant clones in the tumour cell population.

Besides toxic side effects on healthy cells, tumour cells can indeed often develop multiple resistance to drugs. Moreover, *in vivo* observations in the tumour stromal tissue surrounding tumours of prostate, breast and ovary reveal the drug-induced production of a spectrum of secreted cytokines and growth factors, e.g., WNT16B, that promote tumour growth and survival of cancer cells after cytotoxic therapy, and further reduce chemotherapy sensitivity in tumour cells, resulting in tumour progression; otherwise said, among other constraints, one must take into account the fact that chemotherapy itself can positively influence the growth of tumours [144].

In order to take into account these different therapy-limiting constraints, optimal administration of anticancer agents should involve accurately representing the action of drugs at the molecular, i.e., intracellular, level, which means molecular PK–PD modelling for each drug used in a given treatment firstly at the level of a single cell and secondly at the level of cell populations, i.e., tissues and organs. The review of p53 molecular mechanisms of action, and their modelling, is positioned in continuity with, but downstream of, the action of cytotoxic anticancer drugs, when DNA damage is constituted, so that DNA damage is the interface between molecular PK–PD models and the models we proposed in the thesis.

7.5 Other concluding notes

The oscillatory dynamics of p53, "the guardian of the genome", has long been evidenced by biological recordings in experimental conditions representing cell stress due to, e.g. radiotoxic insult [77, 56]. In this sense, the biological question of identifying intracellular spatio-temporal dynamics is certainly crucial. Furthermore, since p53 disruptions are found in more than 50% of solid tumours, with various modifications of its stress-induced dynamics [149, 150, 111], it is also a crucial point in cancer therapy modelling to understand *how* p53 dynamics may be affected in disease, and to this aim, to have an accurate representation of how p53 is activated and regulated in physiological conditions, which was undertaken by our models.

Part II

Modelling enzyme reaction

8

Beyond the enzyme reaction model

As we have seen in the previous chapters, post-translational modifications (protein-protein interactions) can be modelled as the enzyme reactions, even though none of the proteins in question is a real enzyme. The Law of Mass Action (LMA) and particularly the quasi-steady state approximation (QSSA) can be used to reduce four equations for the species up to one composed of Michaelis function with two unknown parameters. These parameters can be sometimes found in the literature. In general, responses to a variety of stimuli consist of chains of successive protein interactions where enzymes play significant roles, mostly by speeding up reactions. Enzymes are catalysts that convert other molecules (proteins) called substrates into products, but the enzymes are not changed by the reaction [68]. In this chapter we deal with few mathematical problems related to the enzyme reaction.

Organisation of the chapter is as follows: A brief introduction to the enzyme reaction is given first in Section 8.1. It is followed by Section 8.2 where we review the QSSA and give a proof of its validity in the ODE case. Finally, Section 8.3 deals with the large-time behaviour of a reaction-diffusion system for the reversible enzyme reaction.

8.1 Introduction to enzyme reactions

In the reaction scheme proposed by Michaelis and Menten in 1913 [107], the enzyme E converts the substrate S into the product P through a two step process, schematically written as

$$S + E \underset{k_-}{\overset{k_+}{\rightleftharpoons}} C \xrightarrow{k_{p+}} E + P, \tag{8.1}$$

where C is the intermediate complex. Briggs and Haldane proposed in 1925 an ODE analysis of (8.1) which is now basis for the most current descriptions of enzyme reaction [21]. In their quasi-steady state approximation (QSSA), the complex is assumed to reach its steady state quickly. Thus by setting $\mathrm{d}n_C/\mathrm{d}t \approx 0$ in the equation for the complex concentration $n_C = [C]$, the analysis ends up with an algebraic expression (i.e., Michaelis function) for n_C and a simple (although nonlinear) equation for the substrate $n_S = [S]$ (called as Michaelis-Menten equation). The kinetics of enzyme reaction described by Briggs and Haldane is sometimes called Michaelis-Menten kinetics. A detailed analysis based on perturbation technique is further provided by Segel and Slemrod [133].

Importantly, P can also combine with E to form the complex C in (8.1), in fact, nearly all enzymes increase the speed of the reaction in both directions [68], which is schematically

written as

$$S + E \underset{k_-}{\overset{k_+}{\rightleftharpoons}} C \underset{k_{p-}}{\overset{k_{p+}}{\rightleftharpoons}} E + P. \tag{8.2}$$

The following two sections present two mathematical results related an ODE system for (8.1) in Section 8.2 and a reaction-diffusion PDE system for (8.2) in Section 8.3.

8.2 Michaelis-Menten Law and ODE system

In the framework of the irreversible enzyme reaction (8.1), the Law of Mass Action gives four equations for the concentrations of species $n_S = [S], n_E = [E], n_C = [C]$ and $n_P = [P]$, i.e.

$$\begin{aligned} \frac{\mathrm{d}n_S}{\mathrm{d}t} &= k_- n_C - k_+ n_S n_E, \qquad & \frac{\mathrm{d}n_E}{\mathrm{d}t} &= (k_- + k_{p+}) n_C - k_+ n_S n_E, \\ \frac{\mathrm{d}n_C}{\mathrm{d}t} &= k_+ n_S n_E - (k_- + k_{p+}) n_C, \qquad & \frac{\mathrm{d}n_P}{\mathrm{d}t} &= k_{p+} n_C, \end{aligned} \tag{8.3}$$

where, for simplicity, the initial conditions $(n_S(0), n_E(0), n_C(0), n_P(0)) = (n_S^0, n_E^0, 0, 0)$ are assumed.

The last equation for the product P is uncoupled from the others and it can be thus omitted from further considerations. In addition, two conservation laws hold, particularly, $n_E + n_C = n_E^0$ and $n_S + n_C + n_P = n_S^0$. Using the former one, we can reduce the above equations into

$$\frac{\mathrm{d}n_S}{\mathrm{d}t} = k_- n_C - k_+ n_S (n_E^0 - n_C), \tag{8.4}$$

$$\frac{\mathrm{d}n_C}{\mathrm{d}t} = k_+ [n_S (n_E^0 - n_C) - K_m n_C], \tag{8.5}$$

where $K_m = \dfrac{k_- + k_{p+}}{k_+}$ is the Michaelis constant.

After a transient pre-steady-state phase (where the depletion of n_S is assumed to be negligible), one can observe that $\dfrac{\mathrm{d}n_C}{\mathrm{d}t} = 0$ that is indeed true whenever the concentration of enzyme is small enough compared to the concentration of the substrate (where free enzyme molecule is immediately bound to another substrate molecule). Thus, in the standard QSSA (sometimes referred to as Michaelis-Menten law), we can replace the equation of the fast variable (complex), which reaches its equilibrium quickly, by an algebraic formula. In particular, we can write[1]

$$\frac{\mathrm{d}\overline{n_S}}{\mathrm{d}t} = k_- \overline{n_C} - k_+ \overline{n_S} (n_E^0 - \overline{n_C}), \tag{8.6}$$

$$0 = k_+ [\overline{n_S} (n_E^0 - \overline{n_C}) - K_m \overline{n_C}], \tag{8.7}$$

and in a more condensed way,

$$\frac{\mathrm{d}\overline{n_S}}{\mathrm{d}t} = -k_{p+} \overline{n_C} \tag{8.8}$$

where

$$\overline{n_C} = n_E^0 \frac{\overline{n_S}}{K_m + \overline{n_S}}. \tag{8.9}$$

Note that the assumption on negligible depletion of the initial concentration of n_S in the pre-steady state phase becomes important when we set $\overline{n_S}(0) = n_S(0) = n_S^0$.

[1] The different notation for the concentrations used in the following equations (8.6), (8.7) and so on, e.g., $\overline{n_S}$ and $\overline{n_C}$, is a matter of convenience only. In the proof of validity of the QSSA, we will need to distinguish between the "pre-QSSA" solution to (8.3) and "post-QSSA" solution to (8.6) and (8.7).

We prove the following

Proposition 8.1 (Validity of the QSSA)**.** *For n_E^0 small there is a constant $C = C(n_S^0)$ independent of n_E^0 such that*

$$\sup_{t\geq 0} |n_S(t) - \overline{n_S}(t)| \leq C n_E^0. \tag{8.10}$$

Remark 8.2. *To prove this result, one can introduce a scaling as in [119], i.e.*

$$\varepsilon = n_E^0,\ s = \varepsilon t,\ u_S(s) = n_S(t) \quad \text{and} \quad u_C(s) = \frac{n_C(t)}{\varepsilon}.$$

However, different scalings can be also found in the literature when the system (8.4)-(8.5) is studied, e.g., the scaling of Heineken et al. [63] (which is also used in the book of Keener & Sneyd [68]) and Segel & Slemrod's scaling [133], which is based on a detailed analysis of the duration of pre- and steady-state phases. For the convenience, they are summarised in the following table,

$$\begin{array}{c|c|c|c|l}
\varepsilon = n_E^0 & s = \varepsilon t & u_S(s) = n_S(t) & u_C(s) = \dfrac{n_C(t)}{\varepsilon} & \textit{in [119],} \\
\varepsilon = \dfrac{n_E^0}{n_S^0} & s = k_+ n_S^0 \varepsilon t & u_S(s) = \dfrac{n_S(t)}{n_S^0} & u_C(s) = \dfrac{n_C(t)}{\varepsilon n_S^0} & \textit{in [63],} \\
\varepsilon = \dfrac{n_E^0}{K_m + n_S^0} & s = k_{p+}\varepsilon t & u_S(s) = \dfrac{n_S(t)}{n_S^0} & u_C(s) = \dfrac{n_C(t)}{\varepsilon n_S^0} & \textit{in [133].}
\end{array}$$

By applying any of these scalings, one can reduce the system (8.4)-(8.5) to a slow-fast dynamics. Note, however, that the small parameter ε of Segel & Slemrod [133] allows also situation where n_E^0 does not have to be necessarily smaller than n_S^0. In such case, the complex concentration n_C must be smaller than n_S (i.e., K_m must be large enough). Although, Segel & Slemrod's condition $n_E^0 \ll K_m + n_S^0$ validates the enzyme dynamics for more initial states than the experimental condition $n_E^0 \ll n_S^0$, it still does not cover all possible initial states.

Proof. To cover all the three scalings, we can define

$$\varepsilon = \frac{n_E^0}{\alpha},\ s = \beta\varepsilon t,\ u_S(s) = \frac{n_S(t)}{\gamma} \quad \text{and} \quad u_C(s) = \frac{n_C(t)}{\delta\varepsilon} \tag{8.11}$$

for $\alpha, \beta, \gamma, \delta > 0$ constants[2] Using (8.11), the equations can be rescaled to

$$\frac{\mathrm{d}u_S}{\mathrm{d}s} = \frac{k_-\delta}{\beta\gamma} u_C - \frac{k_+}{\beta} u_S(\alpha - \delta u_C), \tag{8.12}$$

$$\varepsilon \frac{\mathrm{d}u_C}{\mathrm{d}s} = \frac{k_+}{\beta\delta}[\gamma u_S(\alpha - \delta u_C) - K_m \delta u_C], \tag{8.13}$$

with the initial conditions $(u_S(0), u_C(0)) = (n_S^0/\gamma, 0)$, and

$$\frac{\mathrm{d}\overline{u_S}}{\mathrm{d}s} = \frac{k_-\delta}{\beta\gamma}\overline{u_C} - \frac{k_+}{\beta}\overline{u_S}(\alpha - \delta\overline{u_C}), \tag{8.14}$$

[2]Thus, $\alpha = \beta = \gamma = \delta = 1$ in [119]; $\alpha = n_S^0$, $\beta = k_+ n_S^0$, $\gamma = \delta = n_S^0$ in [63]; and $\alpha = n_S^0 + K_m$, $\beta = k_{p+}$, $\gamma = \delta = n_S^0$ in [133]).

$$0 = \frac{k_+}{\beta\delta}[\gamma\overline{u_S}(\alpha - \delta\overline{u_C}) - K_m\delta\overline{u_C}], \tag{8.15}$$

with the initial condition $\overline{u_S}(0) = n_S^0/\gamma$. From (8.13), we can write

$$\overline{u_C} = \frac{\alpha}{\delta}\frac{\gamma\overline{u_S}}{\gamma\overline{u_S} + K_m} \quad \text{and} \quad \frac{\mathrm{d}\overline{u_S}}{\mathrm{d}s} = -k_p\frac{\alpha}{\beta}\frac{\overline{u_S}}{\gamma\overline{u_S} + K_m}. \tag{8.16}$$

Thus, instead of (8.10) we prove

$$\sup_{s\geq 0}|u_S(s) - \overline{u_S}(s)| \leq C\varepsilon. \tag{8.17}$$

Note, that when we compare equations in (8.16) we can obtain

$$\frac{\mathrm{d}\overline{u_S}}{\mathrm{d}s} = -k_p\frac{\delta}{\beta\gamma}\overline{u_C}, \tag{8.18}$$

the relation, that can be also immediately obtained by combining (8.14)$+\delta/\gamma$(8.15). We can also notice that

$$\frac{\mathrm{d}}{\mathrm{d}s}(u_S + \varepsilon\frac{\delta}{\gamma}u_C) = -k_p\frac{\delta}{\beta\gamma}u_C. \tag{8.19}$$

Further, it is not difficult to see that both pairs u_S, $\overline{u_S}$ and u_C, $\overline{u_C}$ are non-negative and bounded from above. Precisely, $0 \leq u_S(s) \leq n_S^0/\gamma$, $0 \leq \overline{u_S}(s) \leq n_S^0/\gamma$ $0 \leq u_C(s) \leq \alpha/\delta$ and $0 \leq \overline{u_C}(s) \leq \alpha/\delta$. In fact,

$$u_C(s), \overline{u_C}(s) \leq u^M, \text{ where } u^M = \frac{\alpha}{\delta}\frac{n_S^0}{n_S^0 + K_m}.$$

For $z(s) = \dfrac{\mathrm{d}u_C}{\mathrm{d}s}(s)$ we can write equation $\varepsilon\dfrac{\mathrm{d}z}{\mathrm{d}s} + \lambda(s)z(s) = \mu(s)z(s)$ where μ is bounded and $\lambda(s) = \dfrac{k_+}{\beta}(\gamma u_S + K_m) \geq \dfrac{k_+}{\beta}K_m$, which implies boundedness of z, i.e. we can find a constant K such that $\left|\dfrac{\mathrm{d}u_C}{\mathrm{d}s}\right| \leq K$.

Finally, using the properties above, we can show that $R(s) = u_S(s) + \varepsilon\dfrac{\delta}{\gamma}u_C(s) - \overline{u_S}(s)$ is bounded, i.e. $|R(s)| \leq C\varepsilon$ for some constant C, from where (8.17) follows.

To prove boundedness of R, let us define $r(s) = -\dfrac{\beta}{\delta}\dfrac{\mathrm{d}u_C}{\mathrm{d}s} + k_+u_C^2$ bounded. Multiplying R by k_+u_C and r by $\varepsilon\dfrac{\delta}{\gamma}$ yields, after some necessary calculations,

$$u_C = \frac{\varepsilon\delta r - k_+\gamma u_C R + k_+\alpha\gamma/\delta u_S}{k_+(\gamma\overline{u_S} + K_m)},$$

and (using (8.16) and $u_S - \overline{u_S}$ from the definition of R)

$$u_C - \overline{u_C} = \frac{\varepsilon\delta r - k_+\gamma(\dfrac{\alpha}{\delta} - u_C)R - \varepsilon k_+\alpha u_C}{k_+(\gamma\overline{u_S} + K_m)}.$$

Thus, using (8.18) and (8.19), we obtain

$$\frac{\mathrm{d}R}{\mathrm{d}s} = \frac{\mathrm{d}}{\mathrm{d}s}(u_S + \varepsilon\frac{\delta}{\gamma}u_C) - \frac{\mathrm{d}}{\mathrm{d}s}\overline{u_S} = -k_p\frac{\delta}{\beta\gamma}(u_C - \overline{u_C}),$$

and, after rearranging the terms, we have

$$\frac{\mathrm{d}R}{\mathrm{d}s} + k_p \frac{\delta}{\beta} \frac{\alpha/\delta - u_C}{\gamma \overline{u_S} + K_m} R = \varepsilon k_p \frac{\delta}{\beta\gamma} \left(\frac{-\delta/k_+ r + \alpha u_C}{\gamma \overline{u_S} + K_m} \right).$$

and thus R bounded. □

Note that this proof written for a specific choice of $\alpha = \beta = \gamma = \delta = 1$ can be found in the lecture notes of B. Perthame [119].

8.3 Reaction-diffusion system for the reversible enzyme reaction

The entire mathematical treatment of the enzyme reactions (8.1) and (8.2) is usually done by using ODEs. However, protein pathways occur in living cells, heterogenous spatial structure of which has an impact on the reaction efficiency, speed of the enzyme reaction and convergence to the respective equilibria. In the sequel, a reaction-diffusion system for the reversible enzyme reaction (8.2) is studied.

More precisely, by employing the LMA we obtain four equations which, equipped with the Laplacians for the diffusive motion of the species, describe the concentrations of the species in (8.2) in time and space. These equations are, respectively,

$$\begin{aligned}
\frac{\partial n_S}{\partial t} - D_S \Delta n_S &= k_- n_C - k_+ n_S n_E, \\
\frac{\partial n_E}{\partial t} - D_E \Delta n_E &= (k_- + k_{p+}) n_C - k_+ n_S n_E - k_{p-} n_E n_P, \\
\frac{\partial n_C}{\partial t} - D_C \Delta n_C &= k_+ n_S n_E - (k_- + k_{p+}) n_C + k_{p-} n_E n_P, \\
\frac{\partial n_P}{\partial t} - D_P \Delta n_P &= k_{p+} n_C - k_{p-} n_E n_P,
\end{aligned} \tag{8.20}$$

where n_i, $i \in \{S, E, C, P\}$, are the concentrations of the substrate S, enzyme E, intermediate complex C and product P. It is assumed that $n_i = n_i(t, x)$ are defined on an open bounded domain Ω with sufficiently smooth boundary and a time interval $I = [0, T]$ for $0 < T < \infty$, $Q_T = I \times \Omega$. Without loss of generality we will assume $|\Omega| = 1$. Diffusion coefficients D_i are assumed to be positive and different from each other. Further we assume that there exist non-negative functions n_i^0 such that

$$n_i(0, x) = n_i^0(x), \quad \int_\Omega n_i^0(x)\,\mathrm{d}x > 0, \quad \forall\, i \in \{S, E, C, P\}. \tag{8.21}$$

Finally, the system is coupled with the zero-flux boundary conditions

$$\nu \cdot \nabla n_i = 0, \quad \forall t \in I,\ x \in \partial\Omega,\ i \in \{S, E, C, P\}, \tag{8.22}$$

where ν is a unit normal vector pointed outward from the boundary $\partial\Omega$.

The species in the reaction (8.2) are conserved in the following way:

$$0 < M_1 = \int_\Omega (n_E + n_C)(t, x)\,\mathrm{d}x = \int_\Omega (n_E^0 + n_C^0)(x)\,\mathrm{d}x \quad \forall t \geq 0, \tag{8.23}$$

$$0 < M_2 = \int_\Omega (n_S + n_C + n_P)(t, x)\,\mathrm{d}x = \int_\Omega (n_S^0 + n_C^0 + n_P^0)(x)\,\mathrm{d}x \quad \forall t \geq 0, \tag{8.24}$$

with the total mass $M = M_1 + M_2$.

The conservations of masses (8.23) and (8.24) give L^1-bounds on the solutions of the reversible enzyme reaction system (8.20)-(8.22) uniformly in time. This is unfortunately insufficient to show the existence of solutions on $I = [0, T]$ for any $T < \infty$. Global existence of a weak solution of system (8.20)-(8.22) is a consequence of a combination of the duality argument (Appendix A), which provides L^2-estimates on the nonlinearities of the system (which are at most quadratic), and an "approximation method" of M. Pierre [120, 122, 40], which justifies rigorously the existence of the solutions of (8.20)-(8.22) (which are build up from the solutions of the approximated system). The existence of a global weak solution with the total mass conserved in the way as in (8.23) and (8.24) can also be showed by the Rothe method, which provides a constructive proof and thus it can be also used in numerical simulations, see Appendix B.

Here we prove the following

Proposition 8.3. *Let $n_i^0 \in L^2(\log L)^2(\Omega)$, then any weak solution n_i, $i \in \{S, E, C, P\}$ to (8.20)-(8.22) with the conserved mass according to (8.23) and (8.24) belongs to $L^2(Q_T)$ for each $T < \infty$. In particular, by a duality argument we obtain*

$$\|n_i(\log(\sigma_i n_i) - 1)\|_{L^2(Q_T)} \leq C(1+T)\Big\| \sum_{i\in\{S,E,C,P\}} n_i^0(\log(\sigma_i n_i^0) - 1)\Big\|_{L^2(\Omega)},$$

cf. (8.33) below, where σ_i are constants dependent on the kinetic rates k_j given by (8.27).

If in addition to the L^2-estimates arising from Proposition 8.3 the solution n_i of (8.20)-(8.22) satisfies uniform L^∞-bounds, we can deduce global existence in time of "classical" (strong) solutions[3], by the standard results for reaction-diffusion systems[4], i.e. we can show the smoothness of n_i (e.g., $n_i \in C^2([0, T] \times \overline{\Omega})$ or $n_i \in C^\infty([0, T] \times \overline{\Omega})$, for any $T < \infty$) for all smooth non-negative initial data, depending on the regularity of the boundary $\partial\Omega$ (being, respectively, $C^{2+\alpha}$ or C^∞). By using the properties of the heat kernel (c.f., Lemma 8.8) combined with a bootstrapping argument we can indeed prove

Proposition 8.4. *Let $n_i^0 \in L^\infty(\Omega)$, then $n_i \in L^\infty_{loc}([0, \infty) \times \overline{\Omega})$ (locally in time), $i \in \{S, E, C, P\}$.*

The large time behaviour of the solution n_i, $i \in \{S, E, C, P\}$, of the system (8.20)-(8.22) is studied by means of the relative entropy convergence. As the main result we prove

Theorem 8.5. *Let n_i be a solution to the system (8.20)-(8.22) satisfying the conservation laws (8.23) and (8.24). Then there exist two constants C_1 and C_2 such that*

$$\sum_{i\in\{S,E,C,P\}} \|n_i - n_{i,\infty}\|^2_{L_1(\Omega)} \leq C_2 e^{-C_1 t}$$

cf. (8.51) below, where $n_{i,\infty}$ are unique positive steady-states to (8.20)-(8.22) defined in (8.35).

[3]By classical solution we mean bounded solution, so that, by a regularity theory, a classical solution has classical derivatives at least *a.e.* and the equations (8.20) are understood pointwise.

[4]Smoothness is an easy consequence of general properties of the heat operator and the regularity with respect to a parameter of solutions of ODEs [38], p.11-12.

8.3.1 Entropy, entropy dissipation and first estimates

Let us first mention a simple result on the non-negativity of solutions to (8.20)-(8.22). It follows from the so-called quasi-positivity property of the right hand sides of (8.20). In particular, it can be proved

Lemma 8.6. *For $n_i^0(x) \geq 0$ in Ω, a solution n_i of the system (8.20)-(8.22) is non-negative for $t \in I$ and $x \in \Omega$, $i = \{S, E, C, P\}$, i.e.*

$$n_i(t, x) \geq 0 \text{ everywhere in } Q_T.$$

Proof. The r.h.s. of (8.20), denoted here by $f_i = f_i(n_S, n_E, n_C, n_P)$, $i \in \{S, E, C, P\}$, satisfies the quasi-positivity property, i.e. $f_i(n_i = 0) \geq 0$ for each $i \in \{S, E, C, P\}$, which implies the non-negativity of the solution, see, e.g., [121]. □

For the species n_i, $i \in \{S, E, C, P\}$, we will sometimes write shortly $\mathbf{n} = (n_S, n_E, n_C, n_P)$. The entropy functional $E(\mathbf{n}) : [0, \infty)^4 \to [0, \infty)$ and entropy dissipation $D(\mathbf{n}) : [0, \infty)^4 \to [0, \infty)$ are defined, respectively, by

$$E(\mathbf{n}(t, x)) = \int_\Omega \sum_{i=\{S,E,C,P\}} n_i(\log(\sigma_i n_i) - 1) + 1/\sigma_i \, \mathrm{d}x \tag{8.25}$$

where σ_S, σ_E, σ_C and σ_P are constants dependent on the kinetic rates k_j to be determined, and

$$\begin{aligned} D = &\int_\Omega \sum_{i=\{S,E,C,P\}} D_i \frac{|\nabla n_i|^2}{n_i} \, \mathrm{d}x \\ &+ \int_\Omega \left[(k_+ n_S n_E - k_- n_C) \left(\log(\sigma_S \sigma_E n_S n_E) - \log(\sigma_C n_C) \right) \right. \\ &\left. + (k_{p-} n_E n_P - k_{p+} n_C) \left(\log(\sigma_E \sigma_P n_E n_P) - \log(\sigma_C n_C) \right) \right] \mathrm{d}x. \end{aligned} \tag{8.26}$$

Note that the function $x \log(x) - x + 1$ is non-negative and strictly convex on $[0, \infty)$. Thus, E is non-negative as well for any $t \geq 0$. The dissipation D is also non-negative for all $t \geq 0$ and for any $\alpha, \beta > 0$ such that

$$\begin{aligned} \sigma_C = \alpha k_-, \quad \sigma_S \sigma_E = \alpha k_+, \\ \sigma_C = \beta k_{p+}, \quad \sigma_E \sigma_P = \beta k_{p-}. \end{aligned} \tag{8.27}$$

The non-negativity of D follows from the trivial inequality $(x - y)(\log x - \log y) \geq 0$ valid for all $x, y \in \mathbb{R}$. For example, we can choose $\alpha = 1$, $\beta = \dfrac{k_-}{k_{p+}}$, $\sigma_C = \sigma_E = k_-$, $\sigma_S = \dfrac{k_+}{k_-}$ and $\sigma_P = \dfrac{k_{p-}}{k_{p+}}$ in (8.27).

It is straightforward to verify that $D = -\dfrac{\mathrm{d}E}{\mathrm{d}t}$, which implies that E is decreasing as a function of the time t and that the limit $\lim\limits_{t \to \infty} E(\mathbf{n}(t, x))$ exists. By integrating this simple relation over $[t_1, t_2]$ $(t_2 > t_1 > 0)$ we obtain,

$$E(\mathbf{n}(t_1, x)) - E(\mathbf{n}(t_2, x)) = \int_{t_1}^{t_2} D(\mathbf{n}(s, x)) \mathrm{d}s$$

which implies

$$\lim_{T \to \infty} \int_T^\infty D(\mathbf{n}(s, x)) \mathrm{d}s = 0.$$

From above, we can also write

$$E(\mathbf{n}(t,x)) + \int_0^t D(\mathbf{n}(s,x))\mathrm{d}s = E(\mathbf{n}(0,x)). \tag{8.28}$$

From the definitions of entropy and entropy dissipation, by using their non-negativities and (8.28), we can deduce the following a-priori estimates for each species n_i, $i \in \{S, E, C, P\}$:

$$\sup_{t\in[0,\infty)} \|n_i \log(n_i)\|_{L^1(\Omega)} \leq C, \tag{8.29}$$

i.e., $n_i \in L^\infty([0,\infty); L(\log L)(\Omega))$; and using $\dfrac{|\nabla n_i|^2}{n_i} = 4|\nabla\sqrt{n_i}|^2$ we deduce

$$\|\nabla\sqrt{n_i}\|^2_{L^2([0,\infty);L^2(\Omega;\mathbb{R}^d))} \leq C, \tag{8.30}$$

i.e., $\sqrt{n_i} \in L^2([0,\infty); W^{1,2}(\Omega))$. In all these estimates $C = E(\mathbf{n}(0,x)$ independent of the time.

The conservation laws (8.23) and (8.24) imply $L^1(\Omega)$-bounds for n_i for all $t \geq 0$, that is $n_i \in L^\infty([0,\infty); L^1(\Omega))$ (and also trivially $\sqrt{n_i} \in L^\infty([0,\infty); L^2(\Omega))$), $i \in \{S, E, C, P\}$.

8.3.2 $L^2(\log L)^2$ estimates

Proposition 8.3 states the $L^2(\log L)^2$ estimate for n_i. This proposition can be proved by a duality argument of M. Pierre [122, 121] , see Appendix A, applied to the system (8.20)-(8.22). We obtain the following

Proof. (of Proposition 8.3) The system (8.20)-(8.22) can be rewritten in the terms of the non-negative entropy density variables $z_i = n_i(\log(\sigma_i n_i) - 1) + 1/\sigma_i$ to the form

$$\frac{\partial z}{\partial t} - \Delta(Az) \leq 0, \quad \nu \cdot \nabla(Az) = 0 \tag{8.31}$$

where $z = \sum z_i$, $z_d = \sum D_i z_i$ (sums go for $i \in \{S, E, C, P\}$) and $A = z_d/z \in \left[\underline{D}, \overline{D}\right]$ for $\underline{D} = \min_{i\in\{S,E,C,P\}}\{D_i\}$ and $\overline{D} = \max_{i\in\{S,E,C,P\}}\{D_i\}$. Indeed, after some calculation, we arrive to

$$\begin{aligned}\frac{\partial z}{\partial t} - \Delta(Az) = &- \sum D_i \frac{|\nabla n_i|^2}{n_i} \\ &- (k_+ n_S n_E - k_- n_C)\left(\log(\sigma_S\sigma_E n_S n_E) - \log(\sigma_C n_C)\right) \\ &- (k_{p-} n_E n_P - k_{p+} n_C)\left(\log(\sigma_E\sigma_P n_E n_P) - \log(\sigma_C n_C)\right).\end{aligned} \tag{8.32}$$

The right hand side of (8.32) is non-positive for σ_i as in (8.27), i.e. for σ_i which satisfy

$$\begin{aligned}\sigma_C = \alpha k_-, \quad \sigma_S\sigma_E = \alpha k_+, \\ \sigma_C = \beta k_{p+}, \quad \sigma_E\sigma_P = \beta k_{p-},\end{aligned}$$

for some $\alpha, \beta > 0$. The boundary condition in (8.31) is easy to be verified.

A duality argument, Lemma 8.18 from Appendix A, applied to (8.31) implies the estimate

$$\|n_i(\log(\sigma_i n_i) - 1)\|_{L^2(Q_T)} \leq C(1+T)\Big\| \sum_{i\in\{S,E,C,P\}} n_i^0(\log(\sigma_i n_i^0) - 1) + \frac{1}{\sigma_i}\Big\|_{L^2(\Omega)}, \tag{8.33}$$

which we wanted to prove. □

Remark 8.7. *Thus, $n_i \in L^2(\log L)^2(Q_T)$ whenever $n_i^0 \in L^2(\log L)^2(\Omega)$. Finally, since $L^2(\log L)^2(Q_T) \subset L^2(Q_T)$ for Ω bounded and $T < \infty$ (because of the trivial inequality $x \log x \geq x - 1$), there is a constant C dependent on the time T such that $\|n_i\|_{L^2(Q_T)} \leq C(T)$ for each $i \in \{S, E, C, P\}$.*

8.3.3 L^∞ estimates in 1-3D: bootstrapping argument

A bootstrapping argument[5] combined with the smoothing properties of the heat kernel (cf. Lemma 8.8) are used to show L^∞ bounds for the weak solution $n_i \in L^2(Q_T)$ of the system (8.20)-(8.22) in the space dimensions $d = 1, 2$ and 3. The smoothing property of the heat kernel in question can be stated as follows (see also [38]):

Lemma 8.8. *Consider $f = f(t,x) \in L^p(Q_T)$ and $u = u(t,x)$ a solution of*

$$\begin{aligned} \partial_t u - \Delta u &= f, \quad \forall t \in I,\ x \in \Omega, \\ \nu \cdot \nabla u &= 0, \quad \forall t \in I,\ x \in \partial\Omega, \\ u(0,x) &= u_0(x) \in L^\infty(\Omega). \end{aligned}$$

Then it holds that $u \in L^q(Q_T)$ for all $q \in [1,\infty]$ satisfying

$$\frac{1}{q} > \frac{1}{p} - \frac{2}{d+2}. \tag{8.34}$$

With this lemma in hand, we can proceed with the proof of Proposition 8.4.

Proof. (of Proposition 8.4) Since the system (8.20) satisfies

$$\begin{aligned} \frac{\partial n_S}{\partial t} - D_S \Delta n_S &\le k_- n_C, \\ \frac{\partial n_E}{\partial t} - D_E \Delta n_E &\le (k_- + k_{p+}) n_C, \\ \frac{\partial n_C}{\partial t} - D_C \Delta n_C &\le (k_+ n_S + k_{p-} n_P) n_E, \\ \frac{\partial n_P}{\partial t} - D_P \Delta n_P &\le k_{p+} n_C, \end{aligned}$$

then, for $u_C \in L^2_{loc}([0,\infty) \times \overline{\Omega})$ (locally in time), the property of the heat kernel (8.34) implies $n_S, n_P \in L^{q_0}_{loc}([0,\infty) \times \overline{\Omega})$ for all q_0 such that $\frac{1}{q_0} > \frac{1}{2} - \frac{2}{d+2} = \frac{d-2}{2(d+2)}$. Applying Hölder inequality with $n_E \in L^2_{loc}([0,\infty) \times \overline{\Omega})$ and $n_S, n_P \in L^{q_0}_{loc}([0,\infty) \times \overline{\Omega})$, we have $(k_+ n_S + k_{p-} n_P) n_E \in L^{r_0}_{loc}([0,\infty) \times \overline{\Omega})$ for $\frac{1}{r_0} > \frac{d}{d+2}$. As a consequence, the property of the heat kernel (8.34) gives $n_C \in L^{s_0}_{loc}([0,\infty) \times \overline{\Omega})$ for $\frac{1}{s_0} > \frac{1}{r_0} - \frac{2}{d+2} > \frac{d-2}{d+2}$. Finally, $n_E \in L^{s_0}_{loc}([0,\infty) \times \overline{\Omega})$ for the same s_0.

Thus, by the property of the heat kernel only (no bootstrapping is needed here), we obtain $n_S, n_P \in L^{q_0}_{loc}([0,\infty) \times \overline{\Omega})$ for $q_0 \in [1,\infty)$ and $n_C, n_E \in L^{s_0}_{loc}([0,\infty) \times \overline{\Omega})$ for $s_0 \in [1,\infty)$ in the simpler cases of $d = 1, 2$.

For $d = 3$, we apply a bootstrapping argument combined further with the property of the heat kernel (8.34). We can deduce from above that $n_S, n_P \in L^{q_0}_{loc}([0,\infty) \times \overline{\Omega})$ for $q_0 \in [1, 10)$, $(k_+ n_S + k_{p-} n_P) n_E \in L^{r_0}_{loc}([0,\infty) \times \overline{\Omega})$ for $r_0 \in [1, 5/3)$, and $n_C, n_E \in L^{s_0}_{loc}([0,\infty) \times \overline{\Omega})$ for $s_0 \in [1, 5)$. Since $\partial_t n_S - D_S \Delta n_S \le k_- n_C \in L^{s_0}$ and $\partial_t n_P - D_P \Delta n_P \le k_{p+} n_C \in L^{s_0}$, we have $n_S, n_P \in L^{q_1}_{loc}([0,\infty) \times \overline{\Omega})$ for q_1 such that $\frac{1}{q_1} > \frac{1}{s_0} - \frac{2}{5} > -\frac{1}{5}$, i.e. for $q_1 \in [1,\infty]$. As a consequence, $(k_+ n_S + k_{p-} n_P) n_E \in L^{r_1}_{loc}([0,\infty) \times \overline{\Omega})$ for $\frac{1}{r_1} > \frac{1}{5}$, and so $n_C \in L^{s_1}_{loc}([0,\infty) \times \overline{\Omega})$

[5] A bootstrapping argument, as it is used here, has been adapted from [38].

for $\frac{1}{s_1} > \frac{1}{r_1} - \frac{2}{5} > -\frac{1}{5}$, i.e., for all $s_1 \in [0, \infty]$. Finally, since $\partial_t n_E - D_E \Delta n_E \leq (k_- + k_{p+}) n_C \in L^{s_1}$, then also $n_E \in L^{s_1}_{loc}([0,\infty) \times \overline{\Omega})$ for $s_1 \in [0, \infty]$.

Thus, in the dimensions $d = 1, 2$ and 3, we have $n_i \in L^\infty(Q_T)$ for any $T < \infty$[6]. □

Note that we can proceed in a similar way to show L^∞ bounds for higher space dimensions. For more details, see [38].

By using simple arguments it can be easily shown that $\|\nabla n_i\|_{L^2(Q_T)} \leq C$ and thus we also have $n_i \in W^{1,2}(\Omega)$ for each $t \in I$.

8.3.4 Other properties of the EnR system

Let us also observe that for the positive diffusivities D_i, the system (8.20)-(8.22) possesses a unique constant steady state $\mathbf{n}_\infty = (n_{S,\infty}, n_{E,\infty}, n_{C,\infty}, n_{P,\infty})$.

Lemma 8.9. *For $M = M_1 + M_2$ and $K = \frac{k_-}{k_+} + \frac{k_{p+}}{k_{p-}}$, the system (8.20)-(8.22) has a unique constant strictly positive steady state $\boldsymbol{n}_\infty$,*

$$\begin{aligned} n_{C,\infty} &= \frac{1}{2}\left(M + K - \sqrt{(M+K)^2 - 4M_1M_2}\right), \\ n_{E,\infty} = M_1 - n_{C,\infty}, \quad n_{S,\infty} &= \frac{k_- n_{C,\infty}}{k_+ n_{E,\infty}}, \quad n_{P,\infty} = \frac{k_{p+} n_{C,\infty}}{k_{p-} n_{E,\infty}} \end{aligned} \tag{8.35}$$

Proof. The steady states for the system are uniquely determined by

$$n_{E,\infty} + n_{C,\infty} = M_1, \quad n_{S,\infty} + n_{C,\infty} + n_{P,\infty} = M_2, \tag{8.36}$$

and

$$k_- n_{C,\infty} = k_+ n_{S,\infty} n_{E,\infty}, \quad k_{p+} n_{C,\infty} = k_{p-} n_{E,\infty} n_{P,\infty}. \tag{8.37}$$

Easy computations, i.e. employing (8.36) in (8.37), lead to a quadratic equation for $n_{C,\infty}$, i.e.

$$(n_{C,\infty})^2 - (M+K) n_{C,\infty} + M_1 M_2 = 0 \tag{8.38}$$

which has two positive real solutions

$$(n_{C,\infty})_\pm = \frac{1}{2}\left(M + K \pm \sqrt{(M+K)^2 - 4M_1M_2}\right). \tag{8.39}$$

Note, however, that $(n_{C,\infty})_+$ does not satisfy the conservation laws (8.36) since $(n_{C,\infty})_+ > \max\{M_1, M_2\}$. In addition, $(n_{C,\infty})_+$ tends to infinity whilst $(n_{C,\infty})_-$ converges to zero in the limit for $k_{p-} \to 0$, i.e. $K \to \infty$).

The steady state $n_{i,\infty}$, $i \in \{S, E, C, P\}$, is spatially homogenous which follows from the fact that the entropy dissipation vanishes at it. More precisely, it holds that

$$D(\mathbf{n}(t,x)) = 0 \Longleftrightarrow \mathbf{n}(t,x) = \mathbf{n}_\infty. \tag{8.40}$$

Thus, using (8.36) and (8.36), we arrive to the steady state (8.35) which is unique and positive equilibrium state for the system (8.20)-(8.22) with the conserved mass according to (8.23) and (8.24). □

[6] We can indeed obtain $n_i \in L^p(Q_T)$ for all $p \in [1, \infty]$ in the case of $d = 1, 2$ just by using the bootstrapping argument as we have used in the case of $d = 3$. It is sufficient to take any large number, for example, $s_0 = 100$, etc., in the first step of the bootstrapping method.

As far as we are concerned with the uniqueness of the weak solutions, we can prove the following

Lemma 8.10. *Consider an open bounded domain Ω with sufficiently smooth boundary and a bounded weak solution $n_i \in L^\infty(\Omega)$, $i \in \{S, E, C, P\}$, to the problem (8.20)-(8.22). Then n_i is unique.*

Proof. Let us consider, as usual, two sets of bounded solutions $n_{i,1}$ and $n_{i,2}$, $i \in \{S, E, C, P\}$, to (8.20), both satisfying the initial conditions (8.21) and zero-flux boundary conditions (8.22). Then, by subtracting the corresponding equations, multiplying them by $n_{i,12} = n_{i,1} - n_{i,2}$ for each $i \in \{S, E, C, P\}$ and integrating over Ω, we arrive to

$$
\begin{aligned}
&\frac{1}{2}\frac{\partial}{\partial t}\left(\sum_{i\in\{S,E,C,P\}} \|n_{i,12}\|^2_{L^2(\Omega)}\right) + \sum_{i\in\{S,E,C,P\}} \|\nabla n_{i,12}\|^2_{L^2(\Omega;\mathbb{R}^d)} + (k_- + k_{p+})\|n_{C,12}\|^2_{L^2(\Omega)} \\
&\quad = \int_\Omega k_- n_{C,12} n_{S,12}\,\mathrm{d}x + \int_\Omega (k_- + k_{p+}) n_{C,12} n_{E,12}\,\mathrm{d}x + \int_\Omega k_{p+} n_{C,12} n_{P,12}\,\mathrm{d}x \\
&\qquad - \int_\Omega k_+ (n_{S,1} n_{E,12} n_{S,12} + n_{E,2} n^2_{S,12})\,\mathrm{d}x - \int_\Omega k_+ (n_{S,1} n^2_{E,12} + n_{E,2} n_{S,12} n_{E,12})\,\mathrm{d}x \\
&\qquad - \int_\Omega k_{p-} (n_{P,2} n^2_{E,12} + n_{E,1} n_{P,12} n_{E,12})\,\mathrm{d}x + \int_\Omega k_+ (n_{S,1} n_{E,12} n_{C,12} + n_{E,2} n_{S,12} n_{C,12})\,\mathrm{d}x \\
&\qquad + \int_\Omega k_{p-} (n_{E,1} n_{P,12} n_{C,12} + n_{P,2} n_{E,12} n_{C,12})\,\mathrm{d}x - \int_\Omega k_{p-} (n_{E,1} n^2_{P,12} + n_{P,2} n_{E,12} n_{P,12})\,\mathrm{d}x \\
&\quad \le k_- \|n_{C,12}\|_{L^2} \|n_{S,12}\|_{L^2} + (k_- + k_{p+}) \|n_{C,12}\|_{L^2} \|n_{E,12}\|_{L^2} + k_{p+} \|n_{C,12}\|_{L^2} \|n_{P,12}\|_{L^2} \\
&\qquad\quad + k_+ \|n_{S,1}\|_{L^\infty} \|n_{E,12}\|_{L^2} \|n_{S,12}\|_{L^2} + k_+ \|n_{E,2}\|_{L^\infty} \|n_{S,12}\|^2_{L^2} \\
&\qquad\quad + k_+ \|n_{S,1}\|_{L^\infty} \|n_{E,12}\|^2_{L^2} + k_+ \|n_{E,2}\|_{L^\infty} \|n_{S,12}\|_{L^2} \|n_{E,12}\|_{L^2} \\
&\qquad\quad + k_{p-} \|n_{P,2}\|_{L^\infty} \|n_{E,12}\|^2_{L^2} + k_{p-} \|n_{E,1}\|_{L^\infty} \|n_{P,12}\|_{L^2} \|n_{E,12}\|_{L^2} \\
&\qquad\quad + k_+ \|n_{S,1}\|_{L^\infty} \|n_{E,12}\|_{L^2} \|n_{C,12}\|_{L^2} + k_+ \|n_{E,2}\|_{L^\infty} \|n_{S,12}\|_{L^2} \|n_{C,12}\|_{L^2}, \\
&\qquad\quad + k_{p-} \|n_{E,1}\|_{L^\infty} \|n_{P,12}\|^2_{L^2} \|n_{C,12}\|^2_{L^2} + k_{p-} \|n_{P,2}\|_{L^\infty} \|n_{E,12}\|_{L^2} \|n_{C,12}\|_{L^2} \\
&\qquad\quad + k_{p-} \|n_{E,1}\|_{L^\infty} \|n_{P,12}\|^2_{L^2} + k_{p-} \|n_{P,2}\|_{L^\infty} \|n_{E,12}\|_{L^2} \|n_{P,12}\|_{L^2} \\
&\quad \le C(k_\cdot, \|n_{\cdot,\cdot}\|_{L^\infty}) \sum_{i\in\{S,E,C,P\}} \|n_{i,12}\|^2_{L^2(\Omega)},
\end{aligned}
$$

where we have used the non-negativity of n_i, the boundedness of $n_{S,1}$, $n_{E,1}$, $n_{E,2}$ and $n_{P,2}$ and Hölder's inequality. The constant $C = C(k_\cdot, \|n_{\cdot,\cdot}\|_{L^\infty})$ above is dependent on the rates k_+, k_-, k_{p+}, k_{p-} and the L^∞-norms of $n_{S,1}$, $n_{E,1}$, $n_{E,2}$ and $n_{P,2}$. Gronwall's inequality then yields for all $t \in I$

$$
\sum_{i\in\{S,E,C,P\}} \|n_{i,12}(t,\cdot)\|^2_{L^2(\Omega)} \le C(T) \sum_{i\in\{S,E,C,P\}} \|n_{i,12}(t=0,\cdot)\|^2_{L^2(\Omega)} = 0,
$$

i.e. $n_{i,12} = 0$ for each $i \in \{S, E, C, P\}$ in Q_T. □

Remark 8.11. *In the previous lemma we have assumed n_i bounded. In Lemma (8.8), by using the properties of the heat kernel combined with a bootstrap argument, we have shown that $n_i \in L^\infty(Q_T)$ for $i \in \{S, E, C, P\}$.*

8.3.5 Large-time behaviour: convergence in relative entropy

Before giving a proof of Theorem 8.5, let us mention some simplifications in the notation and some easily derived preliminary results. We will also state basic lemmas which will be used in the proof.

In the sequel, we will shortly write $\mathbf{n} = (n_S, n_E, n_C, n_P)$, $\mathbf{n}_\infty = (n_{S,\infty}, n_{E,\infty}, n_{C,\infty}, n_{P,\infty})$ and we will assume without loss of generality that $|\Omega| = 1$. By setting $\overline{n_i} = \int_\Omega n_i \,\mathrm{d}x$ for all i, we can rewrite the conservation laws as

$$\begin{aligned} M_1 &= n_{E,\infty} + n_{C,\infty} = \overline{n_E} + \overline{n_C}, \\ M_2 &= n_{S,\infty} + n_{C,\infty} + n_{P,\infty} = \overline{n_S} + \overline{n_C} + \overline{n_P}. \end{aligned} \tag{8.41}$$

We will also write shortly $E(f|g) = E(f) - E(g)$ for the relative entropy. Using the conservation laws (8.41) we can obtain

$$\sum_{i=\{S,E,C,P\}} \int_\Omega (n_i - n_{i,\infty}) \log(\sigma_i n_{i,\infty}) \,\mathrm{d}x = 0. \tag{8.42}$$

and also

$$E(\mathbf{n}(t,x)|\mathbf{n}_\infty) = \sum_{i=\{S,E,C,P\}} \int_\Omega n_i \log \frac{n_i}{n_{i,\infty}} - (n_i - n_{i,\infty}) \,\mathrm{d}x \geq 0. \tag{8.43}$$

The following lemma contains a rather general Cziszár-Kullback-Pinsker's inequality, known from information theory, and a proof of which can be found in [51].

Lemma 8.12 (Cziszár-Kullback-Pinsker's)**.** *Let Ω be a measurable domain in $\mathbb{R}^d$ and $f, g : \Omega \to \mathbb{R}_+$ measurable functions. Then*

$$\int_\Omega f \log \frac{f}{g} - (f - g) \,\mathrm{d}x \geq \frac{3}{2\|f\|_{L^1(\Omega)} + 4\|g\|_{L^1(\Omega)}} \|f - g\|^2_{L^1(\Omega)}. \tag{8.44}$$

A proof of the following logarithmic Sobolev inequality can be found in [39].

Lemma 8.13 (logarithmic Sobolev inequality)**.** *Let Ω be a bounded domain in $\mathbb{R}^d$, $|\Omega| \geq 1$. Then the logarithmic Sobolev inequality*

$$\int_\Omega \phi^2 \log \left(\frac{\phi^2}{\|\phi\|^2_{L^2(\Omega)}} \right) \mathrm{d}x \leq L \|\nabla \phi\|^2_{L^2(\Omega, \mathbb{R}^d)} \tag{8.45}$$

holds for some $L = L(\Omega, d) > 0$.

In addition, a continuous function $\Phi : (0, \infty)^2 \to \mathbb{R}$ defined by

$$\Phi(x, y) = \frac{x(\log x - \log y) - (x - y)}{(\sqrt{x} - \sqrt{y})^2} \tag{8.46}$$

will be useful when the estimate (8.48) on the entropy dissipation is derived. The function Φ, see Fig. 8.1, obeys properties summarised in the following lemma (a proof of which can be found in [37]).

Lemma 8.14. *For all $y > 0$, $\Phi(\cdot, y)$ is strictly increasing on $(0, \infty)$, and for all $x > 0$, $\Phi(x, \cdot)$ is strictly decreasing; $\lim_{x \to 0} \Phi(x, y) = 1$, $\Phi(y, y) = 2$ and $\Phi(x, y) \sim \log x$ for $x \to \infty$.*

Finally, we are ready state the proof of Theorem 8.5.

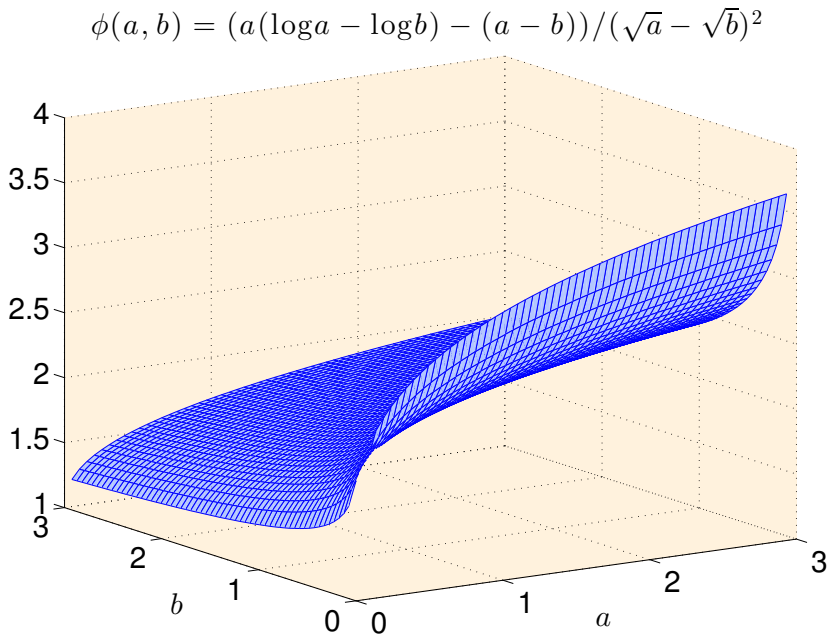

Figure 8.1. Graph of the function $\Phi(a,b)$ for $a,b \in [0,3]$.

Proof. (of Theorem 8.5)

The property (8.40) of the entropy dissipation, namely

$$D(\mathbf{n}(t,x)) = 0 \Longleftrightarrow \mathbf{n}(t,x) = \mathbf{n}_\infty$$

immediately implies that

$$D(\mathbf{n}(t,x)) = -\frac{\mathrm{d}}{\mathrm{d}t}E(\mathbf{n}(t,x)) = -\frac{\mathrm{d}}{\mathrm{d}t}E(\mathbf{n}(t,x)|\mathbf{n}_\infty). \tag{8.47}$$

We would like to show that the entropy dissipation controls relative entropy. In the simplest case[7] it means that we would like to find a constant C_1 such that

$$D(\mathbf{n}(t,x)) \geq C_1 E(\mathbf{n}(t,x)|\mathbf{n}_\infty), \tag{8.48}$$

which can be rewritten as

$$\frac{\mathrm{d}}{\mathrm{d}t}\left(E(\mathbf{n}(t,x)|\mathbf{n}_\infty)\right) \leq -C_1 E(\mathbf{n}(t,x)|\mathbf{n}_\infty).$$

By using Gronwall's inequality, this leads to an estimate

$$E(\mathbf{n}(t,x)|\mathbf{n}_\infty) \leq \left(E(\mathbf{n}(0,x)|\mathbf{n}_\infty)\right) e^{-C_1 t}, \tag{8.49}$$

i.e. the relative entropy $E(\mathbf{n}(t,x)|\mathbf{n}_\infty)$ exponentially decays as t tends to infinity (that is we obtain exponential "convergence in relative entropy"). Then we can apply Cziszar-Kullback-Pinsker's inequality (8.44) to estimate the l.h.s. of (8.49), which can be written as (8.43), from below and obtain

$$\begin{aligned} E(\mathbf{n}(t,x)|\mathbf{n}_\infty) \geq & \frac{1}{2M_2}\|n_S - n_{S,\infty}\|^2_{L^1(\Omega)} + \frac{1}{M_1+M_2}\|n_C - n_{C,\infty}\|^2_{L^1(\Omega)} \\ & + \frac{1}{2M_1}\|n_E - n_{E,\infty}\|^2_{L^1(\Omega)} + \frac{1}{2M_2}\|n_P - n_{P,\infty}\|^2_{L^1(\Omega)} \end{aligned} \tag{8.50}$$

[7] See [3] for a general discussion about entropy methods.

Thus, with $C_2 = \min\left\{\frac{1}{2M_1}, \frac{1}{2M_2}, \frac{1}{M_1+M_2}\right\}$ we finally get the estimate

$$C_2 \sum_{i\in\{S,E,C,P\}} \|n_i - n_{i,\infty}\|^2_{L_1(\Omega)} \leq (E(\mathbf{n}(0,x)|\mathbf{n}_\infty))\, e^{-C_1 t} \tag{8.51}$$

for the species appearing in the reversible enzyme reaction system (8.20)-(8.22). In other words we can show L^1-convergence of the solution of (8.20)-(8.22) to their respective steady state $n_{i,\infty}$ given by (8.35) at the suboptimal rate $C_1/2$.

Thus, it remains to show the entropy-entropy dissipation inequality (8.48). Firstly, we estimate the dissipation D given by (8.26) from below by using Poincaré-Wirtinger's inequality and the elementary estimate $(x-y)(\log x - \log y) \geq 4(\sqrt{x}-\sqrt{y})^2$ valid for $x, y \in \mathbb{R}_+$. We obtain

$$\begin{aligned} D = &\sum_{i=\{S,E,C,P\}} 4D_i \int_\Omega |\nabla\sqrt{n_i}|^2 \,\mathrm{d}x \\ &+ \int_\Omega (k_+ n_S n_E - k_- n_C)\left(\log(k_+ n_S n_E) - \log(k_- n_C)\right)\,\mathrm{d}x \\ &+ \int_\Omega (k_{p-} n_E n_P - k_{p+} n_C)\left(\log(k_{p-} n_E n_P) - \log(k_{p+} n_C)\right)\,\mathrm{d}x \\ \geq &\sum_{i=\{S,E,C,P\}} \frac{4D_i}{P(\Omega)} \|\sqrt{n_i} - \overline{\sqrt{n_i}}\|^2_{L^2(\Omega)} \\ &+ 4\|\sqrt{k_+ n_S n_E} - \sqrt{k_- n_C}\|^2_{L^2(\Omega)} + 4\|\sqrt{k_{p-} n_E n_P} - \sqrt{k_{p+} n_C}\|^2_{L^2(\Omega)}. \end{aligned} \tag{8.52}$$

On the other side, we can split the relative entropy as follows,

$$E(\mathbf{n}(t,x)|\mathbf{n}_\infty) = \underbrace{E(\mathbf{n}(t,x)|\overline{\mathbf{n}}(t))}_{(\star)} + \underbrace{E(\overline{\mathbf{n}}(t)|\mathbf{n}_\infty)}_{(\star\star)} \tag{8.53}$$

where we denote $\overline{\mathbf{n}}(t) = (\overline{n_S}, \overline{n_E}, \overline{n_C}, \overline{n_P})$. Following [39], we estimate $(\star)$ and $(\star\star)$ separately. Firstly, we can write for each $t \in I$

$$\begin{aligned} E(\mathbf{n}(t,x)|\overline{\mathbf{n}}(t)) &= \sum_{i=\{S,E,C,P\}} \int_\Omega n_i \log\frac{n_i}{\overline{n_i}}\,\mathrm{d}x \\ &= \sum_{i=\{S,E,C,P\}} \int_\Omega (\sqrt{n_i})^2 \log\frac{(\sqrt{n_i})^2}{\|\sqrt{n_i}\|^2_{L^2(\Omega)}}\,\mathrm{d}x \qquad (\star) \\ &\leq L \sum_{i=\{S,E,C,P\}} \|\nabla\sqrt{n_i}\|^2_{L^2(\Omega;\mathbb{R}^d)}, \end{aligned}$$

by recalling the logarithmic Sobolev inequality (8.45), which is clearly bounded by the entropy dissipation D.

We need to show that the second term $(\star\star)$ can be also bounded from above by D. The conservation laws (8.41) imply that $\Phi(\overline{n_i}, n_{i,\infty}) \leq C(M)$ for all $i \in \{S,E,C,P\}$, where Φ is defined in (8.46) and satisfies the properties of Lemma 8.14. Thus, using (8.42), we can write

$$\begin{aligned} E(\overline{\mathbf{n}}(t)|\mathbf{n}_\infty) &= \sum_{i=\{S,E,C,P\}} \overline{n_i}\log\frac{\overline{n_i}}{n_{i,\infty}} - (\overline{n_i} - n_{i,\infty}) \\ &= \sum_{i=\{S,E,C,P\}} \Phi(\overline{n_i}, n_{i,\infty})\left|\sqrt{\overline{n_i}} - \sqrt{n_{i,\infty}}\right|^2 \qquad (\star\star) \\ &\leq C(M) \sum_{i=\{S,E,C,P\}} \left|\sqrt{\overline{n_i}} - \sqrt{n_{i,\infty}}\right|^2, \end{aligned}$$

i.e.

$$\sum_{i=\{S,E,C,P\}} \left|\sqrt{\overline{n_i}} - \sqrt{n_{i,\infty}}\right|^2 \geq \frac{1}{C(M)} E(\overline{\mathbf{n}}(t)|\mathbf{n}_\infty). \tag{8.54}$$

Whence, we can conclude the proof once we are able to show the existence of constants C_3 and C_4 such that (by combining (8.52) and (8.54))

$$\begin{aligned} C_3 \sum_{i=\{S,E,C,P\}} \|\sqrt{n_i} - \overline{\sqrt{n_i}}\|^2_{L^2(\Omega)} + C_4 \Big(\|\sqrt{k_+ n_S n_E} - \sqrt{k_- n_C}\|^2_{L^2(\Omega)} \\ + \|\sqrt{k_{p-} n_E n_P} - \sqrt{k_{p+} n_C}\|^2_{L^2(\Omega)} \Big) \geq \sum_{i=\{S,E,C,P\}} \left|\sqrt{\overline{n_i}} - \sqrt{n_{i,\infty}}\right|^2 . \end{aligned} \tag{8.55}$$

With C_3 and C_4 at hand as well as with $\underline{D} = \min_{i\in\{S,E,C,P\}} D_i$, $P = P(\Omega)$ from Poincaré-Wirtinger's inequality used in (8.52), $L = L(\Omega, d)$ from the Log-Sobolev inequality applied in $(\star)$ and $C = C(M)$ from $(\star\star)$, the desired constants C_1 and C_2 appearing in (8.51) have the form, respectively,

$$\begin{aligned} C_1 &= 4 \min\left\{ \frac{\underline{D}}{L}, \frac{\underline{D}}{C_3\, C\, P}, \frac{1}{C_4\, C} \right\}, \\ C_2 &= \min\left\{ \frac{1}{2M_1}, \frac{1}{2M_2}, \frac{1}{M_1 + M_2} \right\}. \end{aligned} \tag{8.56}$$

The proof of (8.55) is a result of the following Lemma 8.16. □

Remark 8.15. *To avoid using function $\Phi(\cdot,\cdot)$ in the estimate $(\star\star)$, i.e., in*

$$E(\overline{\boldsymbol{n}}|\boldsymbol{n}_\infty) \leq \sum_i \Phi(\overline{n_i}, n_{i,\infty}) \left(\sqrt{\overline{n_i}} - \sqrt{n_{i,\infty}}\right)^2 \leq C \sum_i \left(\sqrt{\overline{n_i}} - \sqrt{n_{i,\infty}}\right)^2,$$

we can use the fact that $f(r) = r\log(\sigma r) - r + 1/\sigma$ is convex (and $f'(r) = \log(\sigma r)$).

In particular, we can write (with $\sigma = \sigma_i$)

$$E(\overline{\boldsymbol{n}}|\boldsymbol{n}_\infty) = E(\overline{\boldsymbol{n}}) - E(\boldsymbol{n}_\infty) = \sum_i f(\overline{n}_i) - f(n_{i,\infty}).$$

Since f is convex, $f(x) \geq f(y) + f'(y)(x-y)$ for $x, y \in \mathbb{R}_+$, and the substitution $x = n_{i,\infty}$ and $y = \overline{n}_i$ gives

$$f(n_{i,\infty}) - f(\overline{n}_i) \geq \log(\sigma_i \overline{n}_i)(n_{i,\infty} - \overline{n}_i),$$

i.e.

$$f(\overline{n}_i) - f(n_{i,\infty}) \leq \log(\sigma_i \overline{n}_i)(\overline{n}_i - n_{i,\infty}).$$

Summing this up over i yields

$$\sum_i f(\overline{n}_i) - f(n_{i,\infty}) \leq \sum_i \log(\sigma_i \overline{n}_i)(\overline{n}_i - n_{i,\infty}),$$

i.e.

$$E(\overline{\boldsymbol{n}}|\boldsymbol{n}_\infty) \leq \sum_i \log(\sigma_i \overline{n}_i)(\overline{n}_i - n_{i,\infty}). \tag{8.57}$$

The term (8.42) arising from the conservation laws, i.e.,

$$\sum_i (\overline{n_i} - n_{i,\infty}) \log(\sigma_i n_{i,\infty}) = 0$$

can be subtracted from (8.57) to obtain

$$E(\overline{\boldsymbol{n}}|\boldsymbol{n}_\infty) \le \sum_i (\overline{n}_i - n_{i,\infty})(\log(\overline{n}_i) - \log(n_{i,\infty})). \tag{8.58}$$

A trivial inequality $(x-y)(\log x - \log y) \le 5(\sqrt{x}-\sqrt{y})^2$ *for all* $x, y \in \mathbb{R}_+$, *see Figure 8.2, finally leads to*

$$E(\overline{\boldsymbol{n}}|\boldsymbol{n}_\infty) \le 5 \sum_i \left(\sqrt{\overline{n_i}} - \sqrt{n_{i,\infty}}\right)^2. \tag{8.59}$$

This suggests that the constant $C(M)$ *in (8.54) and (8.56) can be replaced by 5.*

In turn, the substitution $x = \overline{n}_i$ *and* $y = n_{i,\infty}$ *can be used to show that the relative entropy is non-negative, i.e.,* $E(\overline{\boldsymbol{n}}|\boldsymbol{n}_\infty) \ge 0$.

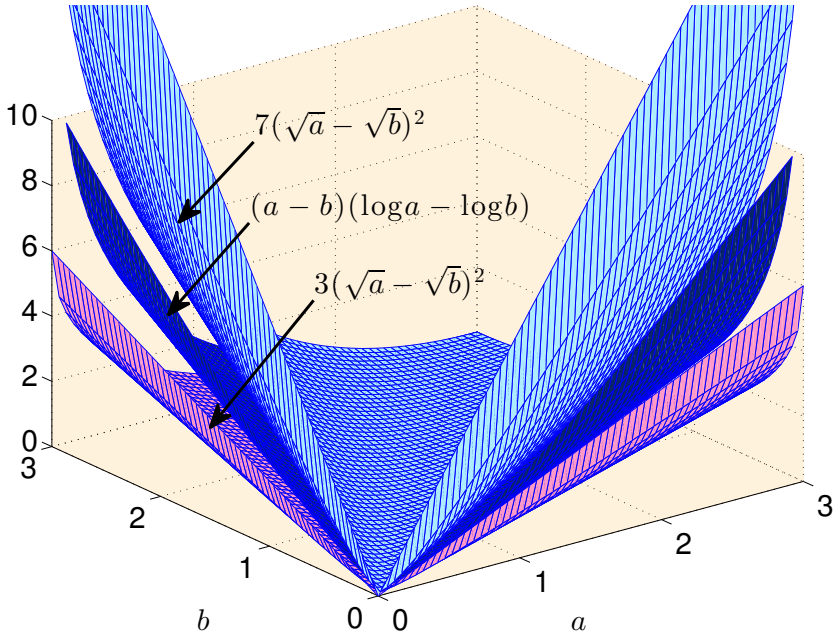

Figure 8.2. Plots of the three function appearing in the inequality $L_1(\sqrt{a}-\sqrt{b})^2 \le (a-b)(\log a - \log b) \le L_2(\sqrt{a}-\sqrt{b})^2$ for $L_1 = 3$ and $L_2 = 7$ for the clarity of the picture. The inequality is actually true for better rates, e.g., for $L_1 = 4$ and $L_2 = 5$ (the picture would not be very clear for these constants).

To proceed with Lemma 8.16, let us simplify notation by setting $N_i = \sqrt{n_i}$, (and so $\overline{N_i^2} = \overline{n_i}$) and $N_{i,\infty} = \sqrt{n_{i,\infty}}$. Thus we can rewrite (8.55) into the form

$$\begin{aligned} C_3 \sum_{i=\{S,E,C,P\}} \|N_i - \overline{N_i}\|^2_{L^2(\Omega)} + C_4 \Big(\|\sqrt{k_+} N_S N_E - \sqrt{k_-} N_C\|^2_{L^2(\Omega)} \\ + \|\sqrt{k_{p-}} N_E N_P - \sqrt{k_{p+}} N_C\|^2_{L^2(\Omega)} \Big) \ge \sum_{i=\{S,E,C,P\}} \left(\sqrt{\overline{N_i^2}} - N_{i,\infty} \right)^2. \end{aligned} \tag{8.60}$$

Lemma 8.16. *Let* N_i, $i \in \{S, E, C, P\}$, *be measurable functions from* Ω *to* $\mathbb{R}_+$ *satisfying the conservation laws (8.23) and (8.24), i.e.*

$$\overline{N_C^2} + \overline{N_E^2} = M_1 \quad \text{and} \quad \overline{N_S^2} + \overline{N_C^2} + \overline{N_P^2} = M_2, \tag{8.61}$$

and $n_{i,\infty} = N_{i,\infty}^2$ *defined in (8.35). Then there exist constants* C_3 *and* C_4 *such that the inequality (8.60) is satisfied.*

Proof. Let us use the expansion

$$N_i = \overline{N_i} + \delta_i(x), \quad \overline{\delta}_i = 0, \quad i \in \{S, E, C, P\}, \tag{8.62}$$

which also implies $\overline{N_i^2} = \overline{N_i}^2 + \overline{\delta_i^2}$. By Jensen's inequality $\overline{N_i} \leq \sqrt{\overline{N_i^2}}$, the *r.h.s.* of (8.60) can be estimated from above as follows:

$$\begin{aligned}\sum_{i=\{S,E,C,P\}} \left(\sqrt{\overline{N_i^2}} - N_{i,\infty}\right)^2 &= \sum_{i=\{S,E,C,P\}} \overline{N_i^2} - 2\sqrt{\overline{N_i^2}} N_{i,\infty} + N_{i,\infty}^2 \\ &\leq \sum_{i=\{S,E,C,P\}} \overline{N_i}^2 - 2\overline{N_i} N_{i,\infty} + N_{i,\infty}^2 + \overline{\delta_i^2} \\ &= \sum_{i=\{S,E,C,P\}} \left(\overline{N_i} - N_{i,\infty}\right)^2 + \sum_{i=\{S,E,C,P\}} \overline{\delta_i^2}.\end{aligned} \tag{8.63}$$

As far as we are concerned with the *l.h.s.* of (8.60), we immediately have

$$\sum_{i=\{S,E,C,P\}} \|N_i - \overline{N_i}\|^2_{L^2(\Omega)} = \sum_{i=\{S,E,C,P\}} \overline{\delta_i^2}. \tag{8.64}$$

With the expansion (8.62), we can also expand the other two terms on the *l.h.s.* of (8.60). In particular, we can write

$$\begin{aligned}\|\sqrt{k_+} N_S N_E - \sqrt{k_-} N_C\|^2_{L^2(\Omega)} &= \left(\sqrt{k_+}\overline{N_S N_E} - \sqrt{k_-}\overline{N_C}\right)^2 \\ &+ 2\sqrt{k_+}\left(\sqrt{k_+}\overline{N_S N_E} - \sqrt{k_-}\overline{N_C}\right)\overline{\delta_S \delta_E} \\ &+ \|\sqrt{k_+}\left(\overline{N_S}\delta_E + \overline{N_E}\delta_S + \delta_S\delta_E\right) - \sqrt{k_-}\delta_C\|^2_{L^2(\Omega)}.\end{aligned} \tag{8.65}$$

The conservation laws give us the following bounds $\overline{N_S}$, $\overline{N_P} \leq \sqrt{M_2}$, $\overline{N_E} \leq \sqrt{M_1}$ and $\overline{N_C} \leq \frac{1}{\sqrt{2}}\sqrt{M_1 + M_2}$. These bounds together with the trivial inequality $2ab \leq a^2 + b^2$ imply an estimate for the second term in (8.65), i.e.

$$\begin{aligned}2\sqrt{k_+}\left(\sqrt{k_+}\overline{N_S N_E} - \sqrt{k_-}\overline{N_C}\right)\overline{\delta_S\delta_E} &\geq -2\sqrt{k_+}\left|\sqrt{k_+}\overline{N_S N_E} - \sqrt{k_-}\overline{N_C}\right|\int_\Omega \delta_S\delta_E \,\mathrm{d}x \\ &\geq -\sqrt{k_+}K_1(\overline{\delta_S^2} + \overline{\delta_E^2}) \geq -\sqrt{k_+}K_1\sum_i \overline{\delta_i^2},\end{aligned} \tag{8.66}$$

where $K_1 = \sqrt{k_+ M_1 M_2} + \sqrt{k_-(M_1 + M_2)/2}$. From (8.65) and (8.66) we conclude

$$\|\sqrt{k_+} N_S N_E - \sqrt{k_-} N_C\|^2_{L^2(\Omega)} \geq \left(\sqrt{k_+}\overline{N_S N_E} - \sqrt{k_-}\overline{N_C}\right)^2 - \sqrt{k_+}K_1\sum_i \overline{\delta_i^2}. \tag{8.67}$$

We can similarly handle the remaining term in (8.60) and write

$$\|\sqrt{k_{p-}} N_P N_E - \sqrt{k_{p+}} N_C\|^2_{L^2(\Omega)} \geq \left(\sqrt{k_{p-}}\overline{N_P N_E} - \sqrt{k_{p+}}\overline{N_C}\right)^2 - \sqrt{k_{p-}}K_2\sum_i \overline{\delta_i^2} \tag{8.68}$$

for $K_2 = \sqrt{k_{p-} M_1 M_2} + \sqrt{k_{p+}(M_1 + M_2)/2}$.

We see from (8.63), (8.67) and (8.68) that we have to explore "how far" the spatial averages $\overline{N_i}$ could be from the equilibrium states $N_{i,\infty}$ for $i \in \{S, E, C, P\}$.

Let us define the following substitution for each $i \in \{S, E, C, P\}$

$$\overline{N_i} = N_{i,\infty}(1 + \mu_i), \tag{8.69}$$

for $-1 < \mu_i \leq \mu_{i,m}$ where

$$\mu_{E,m} = \frac{N_{C,\infty}^2}{2N_{E,\infty}^2}, \quad \mu_{C,m} = \frac{1}{2N_{C,\infty}^2} \max\left\{N_{E,\infty}^2, N_{C,\infty}^2 + N_{P,\infty}^2\right\},$$
$$\mu_{S,m} = \frac{N_{C,\infty}^2 + N_{P,\infty}^2}{2N_{S,\infty}^2}, \quad \mu_{S,m} = \frac{N_{C,\infty}^2 + N_{S,\infty}^2}{2N_{P,\infty}^2}.$$

The upper bounds are directly derived from the conservation laws which with (8.62) and (8.69) can be written as

$$N_{E,\infty}^2 + N_{C,\infty}^2 = N_{E,\infty}^2(1 + \mu_E)^2 + N_{C,\infty}^2(1 + \mu_C)^2 + \overline{\delta_E^2} + \overline{\delta_C^2} \tag{8.70}$$

and

$$N_{S,\infty}^2 + N_{C,\infty}^2 + N_{P,\infty}^2 = N_{S,\infty}^2(1+\mu_S)^2 + N_{C,\infty}^2(1+\mu_C)^2 + N_{P,\infty}^2(1+\mu_P)^2 + \overline{\delta_S^2} + \overline{\delta_C^2} + \overline{\delta_P^2}. \tag{8.71}$$

Note that if $\mu_i = 0$ for each $i \in \{S, E, C, P\}$, i.e. $\overline{N_i} = N_{i,\infty}$, then (8.60) is valid for $C_3 = 1$ and $C_4 \geq 0$ (just by looking at the terms (8.63) and (8.64)). Thus assume that $\mu_i \neq 0$ for at least one $i \in \{S, E, C, P\}$. Then using (8.69) we obtain

$$\sum_{i=\{S,E,C,P\}} \left(\overline{N_i} - N_{i,\infty}\right)^2 = \sum_{i=\{S,E,C,P\}} N_{i,\infty}^2 \mu_i^2 \tag{8.72}$$

from (8.63), and

$$\begin{aligned} \left(\sqrt{k_+}\overline{N_S N_E} - \sqrt{k_-}\overline{N_C}\right)^2 &= k_- N_{C,\infty}^2((1+\mu_S)(1+\mu_E) - (1+\mu_C))^2 \\ \left(\sqrt{k_{p-}}\overline{N_P N_E} - \sqrt{k_{p+}}\overline{N_C}\right)^2 &= k_{p+} N_{C,\infty}^2((1+\mu_P)(1+\mu_E) - (1+\mu_C))^2 \end{aligned} \tag{8.73}$$

from (8.67) and (8.68).

Putting together all the estimates above, we see that we need to find constants C_3 and C_4 such that

$$\left(C_3 - C_4(\sqrt{k_+}K_1 + \sqrt{k_{p-}}K_2)\right) \sum \overline{\delta_i^2} \geq \sum \overline{\delta_i^2}$$

and

$$C_4 K_3 \left(((1+\mu_S)(1+\mu_E) - (1+\mu_C))^2 + ((1+\mu_P)(1+\mu_E) - (1+\mu_C))^2\right) \geq \max_{i\in\{S,E,C,P\}} N_{i,\infty}^2 \sum \mu_i^2,$$

where $K_3 = \min\{k_-, k_{p+}\} N_{C,\infty}^2$. To this end, it is enough to show that there is a constant K_4 such that

$$K_4(\underbrace{((1+\mu_S)(1+\mu_E) - (1+\mu_C))^2}_{=I_1} + \underbrace{((1+\mu_P)(1+\mu_E) - (1+\mu_C))^2}_{=I_2}) \geq \sum \mu_i^2, \tag{8.74}$$

since in this case we can take

$$C_4 \geq \frac{\max_{i\in\{S,E,C,P\}} N_{i,\infty}^2}{K_4 K_3 N_{C,\infty}^2} \quad \text{and} \quad C_3 \geq 1 + C_4(\sqrt{k_+}K_1 + \sqrt{k_{p-}}K_2) \tag{8.75}$$

in the inequality (8.60).

Let us realise that the conservation laws possess some restrictions on"the deviations μ_i of spatial averages from their respective equilibria". In particular, it cannot happen that $\mu_E < 0$ and $\mu_C < 0$ at the same time since, otherwise, $\overline{N_E} > N_{E,\infty}$ and $\overline{N_C} > N_{C,\infty}$ imply that

$$M_1 = \overline{N_E^2} + \overline{N_C^2} \geq \overline{N_E}^2 + \overline{N_C}^2 > N_{E,\infty}^2 + N_{C,\infty}^2 = M_1$$

by (8.61) and Jensen's inequality. It cannot even happen that $\mu_E > 0$ and $\mu_C > 0$ at the same time since it can be easily deduced from (8.70) that

$$0 < N_{E,\infty}^2 \mu_E^2 \leq -2\mu_E N_{E,\infty}^2 - 2\mu_C N_{C,\infty}^2 < 0,$$

and similarly

$$0 < N_{C,\infty}^2 \mu_C^2 \leq -2\mu_E N_{E,\infty}^2 - 2\mu_C N_{C,\infty}^2 < 0.$$

Thus the only admissible cases are $\mu_E < 0$, $\mu_C > 0$ and $\mu_E > 0$, $\mu_C < 0$.

Similarly, the second conservation low, that is (8.71), yields that the only admissible cases for μ_S, μ_C and μ_P that may occur are, respectively,

$$\mu_S < 0, \mu_C < 0 \text{ and } \mu_P > 0, \quad \text{(I)}$$
$$\mu_S < 0, \mu_P < 0 \text{ and } \mu_C > 0, \quad \text{(II)}$$
$$\mu_P < 0, \mu_C < 0 \text{ and } \mu_S > 0, \quad \text{(III)}$$
$$\mu_S < 0, \mu_C > 0, \text{ and } \mu_P > 0, \quad \text{(IV)}$$
$$\mu_C < 0, \mu_S > 0, \text{ and } \mu_P > 0, \quad \text{(V)}$$
$$\mu_P < 0, \mu_C > 0, \text{ and } \mu_S > 0, \quad \text{(VI)}$$

where the specific cases (I)-(VI) have to be separately treated (for clarity they are summarised in Table 8.1).

μ_E	+			−		
μ_C	−			+		
μ_S	−	+	+	−	−	+
μ_P	+	−	+	−	+	−
	(I)	(III)	(V)	(II)	(IV)	(VI)

Table 8.1. Six quadruples of possible relations between μ_i, $i \in \{S, E, C, P\}$, given by the conservation laws (8.70) and (8.71). In the table + and − means the positiveness or negativeness of a quantity.

Since we assume now that at least one μ_i is non-zero[8], the *r.h.s.* of (8.74) is non-zero. The *l.h.s.* of (8.74) is non-zero as well. Indeed, it could be zero if and only if

$$\mu_S = \mu_P = \frac{\mu_C - \mu_E}{1 + \mu_E}.$$

The signs of μ_i, particularly the cases (II) and (V) in Table 8.1, however, exclude this possibility, unless $\mu_C = 0$. If $\mu_C = 0$, i.e. $\overline{N_C} = N_{C,\infty}$, then the only two options $\mu_S = \mu_P > 0 > \mu_E$ and $\mu_E > 0 > \mu_S = \mu_P$ could eventually occur. The conservation laws (8.61) (and (8.41)) with Jensen's inequality exclude these two options as well.

[8]Nevertheless, inequality (8.74) holds trivially for $\mu_i = 0$ for all $i \in \{S, E, C, P\}$.

Let us finish the proof by showing (8.74) for each of the six cases (I)–(VI):

Ad (I). Assume that $\mu_E > 0$, $\mu_C < 0$, $\mu_S < 0$ and $\mu_P > 0$. Then using trivial inequality $a^2 + b^2 \geq \frac{1}{2}(a+b)^2$ we easily obtain

$$I_1 + I_2 \geq \frac{1}{2}(\mu_S - \mu_P)^2(1+\mu_E)^2 > \frac{1}{2}(\mu_S - \mu_P)^2 > \frac{1}{2}(\mu_S^2 + \mu_P^2).$$

Further, it holds that $(1+\mu_P)(1+\mu_E) > (1+\mu_E)$ which implies

$$(1+\mu_P)(1+\mu_E) - (1+\mu_C) > \mu_E - \mu_C > 0$$

and thus

$$I_1 + I_2 > I_2 > (\mu_E - \mu_C)^2 > \mu_E^2 + \mu_C^2.$$

Altogether, $I_1 + I_2 > \frac{1}{4}\sum \mu_i^2$ and thus it is sufficient to take $K_4 = 4$ in (8.74).

Ad (III). Assume that $\mu_E > 0$, $\mu_C < 0$, $\mu_S > 0$ and $\mu_P < 0$. Similarly to the case (I), we can write

$$I_1 + I_2 \geq \frac{1}{2}(\mu_S^2 + \mu_P^2).$$

Since $(1+\mu_S)(1+\mu_E)-(1+\mu_C) > \mu_E - \mu_C > 0$, then also $I_1 + I_2 > I_1 > (\mu_E - \mu_C)^2 > \mu_E^2 + \mu_C^2$. Putting the two estimates together gives $I_1 + I_2 > \frac{1}{4}\sum \mu_i^2$ and $K_4 = 4$.

Ad (V). Assume that $\mu_E > 0$, $\mu_C < 0$, $\mu_S > 0$ and $\mu_P > 0$. Using the facts that $(1+\mu_S)(1+\mu_E) > (1+\mu_S)$, $(1+\mu_S)(1+\mu_E) > (1+\mu_E)$, $(1+\mu_P)(1+\mu_E) > (1+\mu_P)$ and $(1+\mu_P)(1+\mu_E) > (1+\mu_E)$ and since $\mu_i - \mu_C > 0$ for each $i \in \{S, E, P\}$, we can write

$$\begin{aligned} I_1 + I_2 &= ((1+\mu_S)(1+\mu_E) - (1+\mu_C))^2 + ((1+\mu_P)(1+\mu_E) - (1+\mu_C))^2 \\ &\geq \frac{1}{2}(\mu_S - \mu_C)^2 + (\mu_E - \mu_C)^2 + \frac{1}{2}(\mu_P - \mu_C)^2 \geq \frac{1}{2}\sum \mu_i^2. \end{aligned}$$

Thus $K_4 = 2$ in (8.74).

Ad (II). Assume that $\mu_E < 0$, $\mu_C > 0$, $\mu_S < 0$ and $\mu_P < 0$. As in the case (V) we can use $(1+\mu_S)(1+\mu_E) < (1+\mu_S)$, $(1+\mu_S)(1+\mu_E) < (1+\mu_E)$, $(1+\mu_P)(1+\mu_E) < (1+\mu_P)$ and $(1+\mu_P)(1+\mu_E) < (1+\mu_E)$ and $\mu_C - \mu_i > 0$ for each $i \in \{S, E, P\}$ to conclude $I_1 + I_2 > \frac{1}{2}\sum \mu_i^2$ and $K_4 = 2$.

Ad (IV). Assume that $\mu_E < 0$, $\mu_C > 0$, $\mu_S < 0$ and $\mu_P > 0$. Then, by the same argument as above, we can write

$$I_1 + I_2 > I_1 > \frac{1}{2}(\mu_C - \mu_S)^2 + \frac{1}{2}(\mu_C - \mu_E)^2 > \mu_C^2 + \frac{1}{2}\mu_S^2 + \frac{1}{2}\mu_E^2. \tag{8.76}$$

The difficulty comes from μ_C and μ_P both having the same sign and $\mu_E < 0$. Thus, for example, we cannot use neither the estimate

$$I_1 + I_2 > \frac{1}{2}(\mu_S - \mu_P)^2(1+\mu_E)^2,$$

unless we know that there exists a constant $C^\star$ such that $-1 < C^\star \le \mu_E < 0$, nor any estimates from the term I_2, e.g., the inequality

$$(1+\mu_C) - (1+\mu_P)(1+\mu_E) > (1+\mu_C) - (1+\mu_P) = \mu_C - \mu_P$$

since $\mu_C - \mu_P$ can be negative and positive, to obtain a bound for μ_P^2. Nevertheless, if we assume that $\mu_C \ge \mu_P$, then it follows trivially from (8.76) that $I_1 + I_2 > \mu_C^2 + \frac{1}{2}\mu_S^2 + \frac{1}{2}\mu_E^2 \ge \frac{1}{2}\sum \mu_i^2$. Otherwise if $0 < \mu_C < \mu_P$ then there can be found a constant $\overline{K}$, $0 < \overline{K} < 1$, such that $\mu_C \ge \overline{K}\mu_P$. Further we can notice that $(1+\mu_S)(1+\mu_E) < 1 < 1 + \frac{\overline{K}}{2}\mu_P$, for example. Thus,

$$(1+\mu_C) - (1+\mu_S)(1+\mu_E) > (1+\mu_C) - \left(1 + \frac{\overline{K}}{2}\mu_P\right) = \mu_C - \frac{\overline{K}}{2}\mu_P \ge \frac{\overline{K}}{2}\mu_P > 0,$$

which implies

$$I_1 = \left((1+\mu_C) - (1+\mu_S)(1+\mu_E)\right)^2 > \frac{\overline{K}^2}{4}\mu_P^2.$$

Altogether we obtain

$$\begin{aligned} I_1 + I_2 > I_1 &> \frac{1}{3}(\mu_C - \mu_S)^2 + \frac{1}{3}(\mu_C - \mu_E)^2 + \frac{\overline{K}^2}{12}\mu_P^2 \\ &> \frac{2}{3}\mu_C^2 + \frac{1}{3}\mu_S^2 + \frac{1}{3}\mu_E^2 + \frac{\overline{K}^2}{12}\mu_P^2 > \frac{\overline{K}^2}{12}\sum \mu_i^2. \end{aligned}$$

Irrespectively of the signs of μ_C and μ_P, we need to take $K_4 = \max\left\{2, \frac{12}{\overline{K}^2}\right\} = \frac{12}{\overline{K}^2}$ in (8.74). Note that we have not used any information from I_2 in this specific estimates.

Ad (VI). Finally, assume that $\mu_E < 0$, $\mu_C > 0$, $\mu_S > 0$ and $\mu_P < 0$. This case is symmetric to the previous case (IV) and the desired estimate can be obtain purely from I_2. Thus, similarly to the previous case, it can be verified that $I_1 + I_2 > \frac{1}{2}\sum \mu_i^2$ for $\mu_C \ge \mu_S > 0$ and $I_1 + I_2 > \frac{2}{3}\mu_C^2 + \frac{1}{3}\mu_S^2 + \frac{1}{3}\mu_E^2 + \frac{\widetilde{K}^2}{12}\mu_P^2 > \frac{\widetilde{K}^2}{12}\sum \mu_i^2$ for $0 < \widetilde{K} < 1$ whenever $\mu_C < \mu_S$. The constant $K_4 = \max\left\{2, \frac{12}{\widetilde{K}^2}\right\} = \frac{12}{\widetilde{K}^2}$ works in (8.74) in both specific sub-cases.

From all the six admissible quadruples we can take $K_4 = \max\left\{2, 4, \frac{12}{\overline{K}^2}, \frac{12}{\widetilde{K}^2}\right\}$ to find inequality (8.74) valid. Note that K_4 can be very large which, however, allows to choose C_4 small and thus to possibly obtain C_1 large (C_1 is the rate of exponential decay; C_1 however depends on other parameters and thus it can be still small). □

Remark 8.17. *Let us mention that the entropy method cannot be applied to the RD system for the irreversible enzyme reaction (8.1) as it has been applied in the case of the reversible enzyme reaction. For instance, the steady states for the irreversible system are not strictly positive ($n_{S,\infty} = n_{C,\infty} = 0$) and the entropy functional (8.25) is not even defined.*

Appendix

Appendix A: Duality principle

Let us recall the result of M. Pierre [122, 121] used to show L^2 bounds for the solution to (8.20)-(8.22).

Lemma 8.18 (Duality principle[9])**.** *Let $0 < T < \infty$ and Ω be a bounded, open and regular (e.g., C^2) subset of $\mathbb{R}^d$. Consider a non-negative weak solution u of the problem*

$$\begin{cases} \partial_t u - \Delta(au) \leq 0, \\ \nu \cdot \nabla(au) = 0, \quad \forall t \in I,\ x \in \partial\Omega, \\ u(0,x) = u_0(x), \end{cases} \tag{8.77}$$

where we assume that $0 < a_1 \leq a = a(t,x) \leq a_2 < \infty$ is smooth, a_1 and a_2 are strictly positive constants, $u_0 \in L^2(\Omega)$ and $\int u_0 \geq 0$. Then we have the following a-priori estimate

$$\|u\|_{L^2(Q_T)} \leq C(1+T)\|u_0\|_{L^2(\Omega)} \tag{8.78}$$

where $C = C(\Omega, \underline{a}, \overline{a})$ is independent of T.

Proof. Let us consider an adjoint problem: find $v \in C(I; L^2(\Omega))$ such that $v \geq 0$, it is regular in the sense that $\partial_t v, \Delta v \in L^2(Q_T)$ and satisfies

$$\begin{cases} -\partial_t v - a\Delta v = F, \\ \nu \cdot \nabla v = 0, \quad \forall t \in I,\ x \in \partial\Omega, \\ v(T,x) = 0, \end{cases} \tag{8.79}$$

for $F = F(t,x) \in L^2(Q_T)$ non-negative. The existence of such v follows from classical results on parabolic equations [76].

By combining equations for u and v, we can readily check that

$$-\frac{\mathrm{d}}{\mathrm{d}t}\int_\Omega uv \geq \int_\Omega uF$$

which, by using $v(T) = 0$, yields

$$\int_{Q_T} uF \leq \int_\Omega u_0 v_0. \tag{8.80}$$

By multiplying equation for v in (8.79) by $-\Delta v$, integrating per partes and using Young inequality, we obtain

$$-\frac{1}{2}\frac{\mathrm{d}}{\mathrm{d}t}\int_\Omega |\nabla v|^2 + \int_\Omega a(\Delta v)^2 = -\int_\Omega F\Delta v \leq \int_\Omega \frac{F^2}{2a} + \frac{a}{2}(\Delta v)^2,$$

[9] Formulation of the duality estimate, as it is stated here, is adapted from [17]. A more general result can be found in [40], Theorem 3.1.

i.e.

$$-\frac{\mathrm{d}}{\mathrm{d}t}\int_\Omega |\nabla v|^2 + \int_\Omega a(\Delta v)^2 \le \int_\Omega \frac{F^2}{a}.$$

Integrating this over $[0,T]$ and using $v(T)=0$ gives

$$\int_\Omega |\nabla v_0|^2 + \int_{Q_T} a(\Delta v)^2 \le \int_{Q_T} \frac{F^2}{a}.$$

Thus we obtain the a-priori bounds

$$\|\nabla v_0\|_{L^2(\Omega;\mathbb{R}^d)} \le \left\|\frac{F}{\sqrt{a}}\right\|_{L^2(Q_T)} \quad \text{and} \quad \|\sqrt{a}\Delta v\|_{L^2(\Omega)} \le \left\|\frac{F}{\sqrt{a}}\right\|_{L^2(Q_T)}. \tag{8.81}$$

From the equation for v we can also write (again, by integrating this equation over Ω and $[0,T]$ and using $v(T)=0$)

$$\int_\Omega v_0 = \int_{Q_T} a\Delta v + F,$$

which by using Hölder's inequality leads to the estimate

$$\begin{aligned}\int_\Omega v_0 = \int_{Q_T} \sqrt{a}\left(\sqrt{a}\Delta v + \frac{F}{\sqrt{a}}\right) &\le \|\sqrt{a}\|_{L^2(Q_T)}\left\|\sqrt{a}\Delta v + \frac{F}{\sqrt{a}}\right\|_{L^2(Q_T)} \\ &\le 2\|\sqrt{a}\|_{L^2(Q_T)}\left\|\frac{F}{\sqrt{a}}\right\|_{L^2(Q_T)},\end{aligned} \tag{8.82}$$

just by applying the latter estimate from (8.81).

To conclude the proof, let us return to (8.80) and write

$$\begin{aligned}0 \le \int_{Q_T} uF \le \int_\Omega u_0 v_0 &= \int_\Omega u_0(v_0 - \overline{v_0}) + u_0\overline{v_0} \\ &\le \|u_0\|_{L^2(\Omega)}\|v_0 - \overline{v_0}\|_{L^2(\Omega)} + \int_\Omega \overline{u_0}v_0 \\ &\le C(\Omega)\|u_0\|_{L^2(\Omega)}\|\nabla v_0\|_{L^2(\Omega;\mathbb{R}^d)} + \overline{u_0}\int_\Omega v_0,\end{aligned}$$

where we have used Hölder's and Poincaré-Wirtinger's[10] inequality, respectively. Recall that $\overline{v} = \dfrac{1}{|\Omega|}\displaystyle\int_\Omega v\,\mathrm{d}x$. The norm of the gradient v_0 can be estimated by (8.81) and the last remaining integral by (8.82) so that we obtain

$$\int_{Q_T} uF \le \left(C(\Omega)\|u_0\|_{L^2(\Omega)} + 2\overline{u_0}\|\sqrt{a}\|_{L^2(Q_T)}\right)\left\|\frac{F}{\sqrt{a}}\right\|_{L^2(Q_T)}, \tag{8.83}$$

which is valid for any $F \in L^2(Q_T)$. Thus, for $F = au$ we can finally write

$$\|\sqrt{a}u\|_{L^2(Q_T)} \le C(\Omega)\|u_0\|_{L^2(\Omega)} + 2\overline{u_0}\|\sqrt{a}\|_{L^2(Q_T)} \tag{8.84}$$

and deduce (8.78) by using the boundedness of a, i.e. $a_1 \le a(t,x) \le a_2$. □

[10] For $1 \le p \le \infty$ and any bounded, open and connected $\Omega \subset \mathbb{R}^d$ with a Lipschitz boundary, there exists a constant $C = C(\Omega, p)$ such that

$$\|v - \overline{v}\|_{L^p(\Omega)} \le C\|\nabla v\|_{L^p(\Omega,\mathbb{R}^d)}$$

holds for all $v \in W^{1,p}(\Omega)$.

Appendix B: Existence of a solution to the EnR RD by the Rothe method

To show the existence of global weak solutions to the reaction-diffusion system (8.20)-(8.22), we can also apply the semi-implicit Rothe method [129, 130]. Roughly speaking, we will consider an approximating system of (8.20)-(8.22) yielding solutions $n_{i,\tau} \in L^2(I; W^{1,2}(\Omega)) \cap L^\infty(I; L^2(\Omega))$, where $\tau > 0$ is a time step used in discretisation of the time derivative. In the limit passage for $\tau \to 0$, which finally shows convergence of the approximations $n_{i,\tau}$ to the weak solutions $n_i \in L^2(Q_T)$ in Q_T for all $T < \infty$, the Aubin-Lions lemma and the continuity of the respective Nemytskiĭ mapping are used. First we state some general results about the Rothe method applied to an abstract parabolic problem from [130]. Then we apply the Rothe method to our specific example of the reaction-diffusion system for the (ir)reversible system. For more complete results on the Rothe method for evolution problems we refer to the book of T. Roubíček [130].

Let us note again that the aforementioned Rothe method provides a constructive proof which can be also used to easily solve the system (8.20)-(8.22) numerically since it decouples the system into separate equations for each species.

Rothe method for an abstract parabolic problem

We say that $u \in \mathscr{W} = W^{1,2,2}(I; V, V^*) = \left\{ u \in L^2(I; V), \dfrac{\mathrm{d}u}{\mathrm{d}t} \in L^2(I; V^*) \right\}$ is a weak solution of an abstract initial-value problem

$$\frac{\mathrm{d}u}{\mathrm{d}t} + A(u(t)) = f(t) \quad \text{for a.a. } t \in I, \quad u(0) = u_0, \tag{8.85}$$

if the first equation in (8.85) holds in V^* and $u(0) = u_0$ in H, where $A : I \times V \to V^*$, I is a fixed bounded time interval, $V = W^{1,2}(\Omega)$ and $H = L^2(\Omega)$. Note that there is no need to restrict ourself to V and H as above, in fact the theory remains valid for any V and H such that they form Gelfand's triple and V is a separable reflexive Banach space embedded continuously and densely into a Hilbert space $H \cong H^*$.

Let $\tau > 0$ be a time step such that T/τ is an integer for simplicity. In some cases it might be necessary to apply a mollifier to f so that we obtain $f_{\varepsilon(\tau)} \in C(I; V^*)$ which is used to approximate values of f at the points $t = k\tau$, $0 \le k \le T/\tau$, i.e. $f_\tau^k = f_{\varepsilon(\tau)}(k\tau)$. Then, we can define $u_\tau^k \in V$ for $k = 1, \dots, T/\tau$ by the following implicit scheme

$$\frac{u_\tau^k - u_\tau^{k-1}}{\tau} + A(u_\tau^k) = f_\tau^k, \quad u_\tau^0 = u_{0,\tau} \tag{8.86}$$

where $u_{0,\tau} \in V$ are approximations of u_0 such that $u_{0,\tau} \to_{\tau \to 0} u_0$ in H and $\|n_{0,\tau}\|_V = \mathscr{O}(1/\sqrt{\tau})$. Note however, that, whenever convenient, the Rothe recursion (8.86) can be started simply from the initial conditions u_0.

A weak solution of (8.85) is then attained in $\mathscr{W}$ by the piecewise affine interpolants $u_\tau \in C(I; V)$—the so-called Rothe functions—defined by

$$u_\tau(t) = \left(\frac{t}{T} - (k-1) \right) u_\tau^k + \left(k - \frac{t}{T} \right) u_\tau^{k-1}, \quad \text{for } (k-1)\tau < t < k\tau, \tag{8.87}$$

with the piecewise constant derivatives $\mathrm{d}u_\tau/\mathrm{d}t \in L^\infty(I; V)$, and the piecewise constant interpolants $\overline{u}_\tau \in L^\infty(I; V)$ defined by

$$\overline{u}_\tau(t) = u_\tau^k, \quad \text{for } (k-1)\tau < t < k\tau,\ k = 0, \dots T/\tau, \tag{8.88}$$

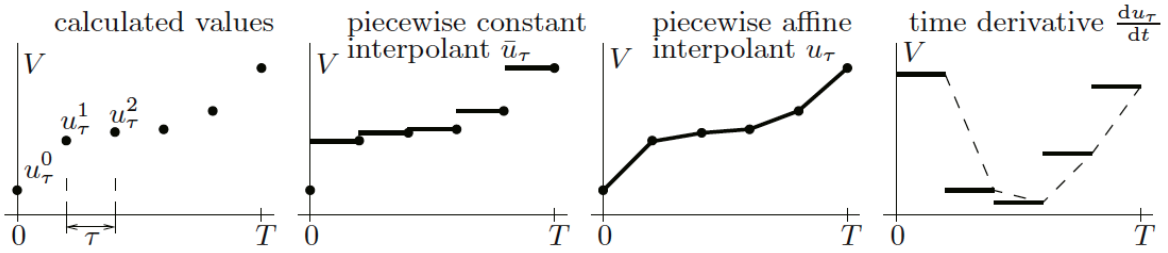

Figure 8.3. Illustration of Rothe's interpolants u_τ and $\overline{u}_\tau$ constructed from a sequence $\{u_\tau^k\}_{k=0}^{T/\tau}$, and the time derivative $\dfrac{\mathrm{d}u_\tau}{\mathrm{d}t}$. The figure is taken from [130], reprinted with kind permission from Springer Science and Business Media.

which have distributional derivatives composed from Dirac masses, Figure 8.3.

Without stating any proofs, let us summarise basic results for the implicit Rothe scheme (8.86), rather less general than in [130].

Lemma 8.19. *i) Let $A : V \to V^*$ be coercive in the sense that $\langle Au, u\rangle \geq c_0\|u\|_V^2$ for all $u \in V$, $f \in L^1(I;V^*)$ and $u_{0,\tau} \in V^*$. Then, for $\tau > 0$, the Rothe solution $u_\tau \in C(I;V^*)$ defined in (8.87) exists.*

ii) Let $A : V \to V^*$ be coercive, $f \in L^2(I;V^*)$, let the mollified approximation f_ε and the corresponding interpolant $\overline{f}_\tau$ (defined as $\overline{u}_\tau$ in (8.88)) satisfy

$$\|f_\varepsilon\|_{C(I;V^*)} \leq \frac{K}{\sqrt{\tau}}, \quad \|\overline{f}_\tau\|_{L^2(I;V^*)} \leq K$$

for some constant $K > 0$ and let $\{u_{0,\tau}\}_{\tau>0}$ be bounded in H. Then for any $0 < \tau \leq \tau_0$ with τ_0 such that $\sqrt{\tau_0}K < 1$, the following a-priori estimates

$$\begin{aligned} \|u_\tau\|_{C(I;H)} &\leq C_1, \quad \|\overline{u}_\tau\|_{L^\infty(I;H)\cap L^2(I;V)} \leq C_1, \\ \|u_\tau|_{[\tau_0,T]}\|_{L^2([\tau_0,T];V)} &\leq C_1, \quad \left\|\frac{\mathrm{d}u_\tau}{\mathrm{d}t}\right\|_{L^2(I;H)} \leq \frac{C_2}{\sqrt{\tau}}, \end{aligned}$$

hold for some constants C_1 and C_2 depending on the given data f and $u_{0,\tau}$. If $u_{0,\tau} \in V$, then

$$\|u_\tau\|_{L^2(I;V)} \leq \left(\tau\|u_{0,\tau}\|_V^2 + \|\overline{u}_\tau\|_{L^2(I;V)}^2\right)^{1/2}. \tag{8.89}$$

If, a superposition mapping $\mathscr{A}$ defined by $[\mathscr{A}(u)](t) := A(u(t))$ satisfies $\mathscr{A} : L^2(I;V) \cap L^\infty(I;H) \to L^2(I;V^*)$, then $\left\|\dfrac{\mathrm{d}u_\tau}{\mathrm{d}t}\right\|_{L^2(I;V^*)} \leq C_3$.

iii) If, in addition to the above assumptions, A satisfies the following growth condition:

$$\exists \mathscr{C} : \mathbb{R} \to \mathbb{R} \text{ increasing } \forall v \in V : \quad \|Av\|_{V^*} \leq \mathscr{C}(\|v\|_H)(1 + \|v\|_V),$$

then

$$\|u_\tau - \overline{u}_\tau\|_{L^2(I;V^*)} = \frac{\tau}{\sqrt{3}}\left\|\frac{\mathrm{d}u_\tau}{\mathrm{d}t}\right\|_{L^2(I;V^*)}, \tag{8.90}$$

by which and by interpolation and (8.89) for $\|u_{0,\tau}\|_V = \mathscr{O}(\tau^{-1/2})$, it follows that

$$\begin{aligned} \|u_\tau - \overline{u}_\tau\|_{L^2(Q_T)} &\leq C\|u_\tau - \overline{u}_\tau\|_{L^2(I;V)}^{1/2}\|u_\tau - \overline{u}_\tau\|_{L^2(I;V^*)}^{1/2} \\ &\leq C\sqrt{\tau}\|u_\tau\|_{L^2(I;V)}^{1/2}\left\|\frac{\mathrm{d}u_\tau}{\mathrm{d}t}\right\|_{L^2(I;V^*)}. \end{aligned} \tag{8.91}$$

iv) Let $A : V \to V^*$ be coercive, $f \in L^2(I;V^*)$ and $u_0 \in H$, then the Cauchy problem (8.85) possesses a weak solution $u \in \mathscr{W}$, which can be attained in $\mathscr{W}$ by a subsequence of Rothe functions $\{u_\tau\}_{\tau>0}$ with $\{u_{0,\tau}\}_{\tau>0} \subset V$ such that $\|u_{0,\tau}\|_V = \mathscr{O}(\tau^{-1/2})$ and $u_{0,\tau} \to u_0$ in H.

Remark 8.20. *Notice that based on the definition of $u_\tau \in C(I;V)$ in (8.87) and $\overline{u}_\tau \in L^\infty(I;V)$ in (8.88), we have, for example,*

$$\|\overline{u}_\tau\|^p_{L^p(I;H)} = \tau \sum_{k=1}^{T/\tau} \|u_\tau^k\|^p_H, \quad \|\overline{u}_\tau\|_{L^\infty(I;H)} = \sup_{k=1,\dots,T/\tau} \|u_\tau^k\|_H,$$

$$\left\| \frac{\mathrm{d}u_\tau}{\mathrm{d}t} \right\|^p_{L^p(I;V^*)} = \tau \sum_{k=1}^{T/\tau} \left\| \frac{u_\tau^k - u_\tau^{k-1}}{\tau} \right\|^p_{V^*}.$$

Remark 8.21. *In some practical applications of the Rothe method, as the one which will be presented below, it is convenient to linearise the nonlinear operator A, e.g., approximate $A(u_\tau^k)$ in (8.86) by $B(u_\tau^{k-1}, u_\tau^k)$, $B(v,\cdot) : V \to V^*$, thus to define* a semi-implicit Rothe scheme. *In the case of a system of equation, such linearisation can decouple effectively the equations, so that the semi-implicit scheme can be advantageously implemented to solve these decoupled problems. The a-priori estimates and convergence analysis, however, have to be made case by case.*

Existence of the global weak solution to (8.20)-(8.22) by the Rothe method

Let $\tau > 0$ as above. Consider the following discretised scheme for the system (8.20)-(8.22) for $k = 1, \dots, T/\tau$:

$$\begin{aligned}
&\frac{n^k_{S,\tau} - n^{k-1}_{S,\tau}}{\tau} - D_S \Delta n^k_{S,\tau} = k_- n^{k-1}_{C,\tau} - k_+ n^k_{S,\tau} n^{k-1}_{E,\tau},\\
&\frac{n^k_{E,\tau} - n^{k-1}_{E,\tau}}{\tau} - D_E \Delta n^k_{E,\tau} = (k_- + k_{p+}) n^{k-1}_{C,\tau} - k_+ n^k_{S,\tau} n^k_{E,\tau} - k_{p-} n^k_{E,\tau} n^{k-1}_{P,\tau},\\
&\frac{n^k_{C,\tau} - n^{k-1}_{C,\tau}}{\tau} - D_C \Delta n^k_{C,\tau} = -(k_- + k_{p+}) n^k_{C,\tau} + k_+ n^k_{S,\tau} n^k_{E,\tau} + k_{p-} n^k_{E,\tau} n^{k-1}_{P,\tau},\\
&\frac{n^k_{P,\tau} - n^{k-1}_{P,\tau}}{\tau} - D_P \Delta n^k_{P,\tau} = k_{p+} n^k_{C,\tau} - k_{p-} n^k_{E,\tau} n^k_{P,\tau}.
\end{aligned} \tag{8.92}$$

For $k = 0$ we consider approximations $n^0_{i,\tau} \in V$ of n^0_i in (8.21) such that $n^0_{i,\tau} \to_{\tau\to 0} n^0_i$ in H and $\|n^0_{i,\tau}\|_V = \mathscr{O}(1/\sqrt{\tau})$, where $H = L^2(\Omega)$ and $V = W^{1,2}(\Omega)$. In addition, let us assume that $n^0_{i,\tau}$ satisfy the conservation laws (8.23) and (8.24), i.e. $\int_\Omega n^0_{E,\tau} + n^0_{C,\tau}\,\mathrm{d}x = M_1$ and $\int_\Omega n^0_{S,\tau} + n^0_{C,\tau} + n^0_{P,\tau}\,\mathrm{d}x = M_2$. Such $\{n^0_{i,\tau}\}_{\tau>0}$ always exists because V is dense in H. The boundary conditions become $\nu \cdot \nabla n^k_{i,\tau} = 0$ and are valid for all $x \in \partial\Omega$, for all $k = 1, \dots, T/\tau$ and for all $i \in \{S, E, C, P\}$.

Remark 8.22. *The system (8.92) is decoupled, so that as soon as we have $n^k_{S,\tau} \in V$, we can proceed with the computation of $n^k_{E,\tau} \in V$, afterwords $n^k_{C,\tau} \in V$ by using the already computed $n^k_{S,\tau}$ and $n^k_{E,\tau}$, and, finally, once we obtain $n^k_{C,\tau}$, we can compute $n^k_{P,\tau} \in V$. Note that the approximation (8.92) is not the only possible discretisation of (8.20), since one can choose a different order of the equations in (8.20) to be discretised.*

For $i \in \{S, E, C, P\}$, let us define the piecewise affine interpolants $n_{i,\tau} \in C(I; V)$ by

$$n_{i,\tau}(t) = \left(\frac{t}{T} - (k-1)\right) n_{i,\tau}^k + \left(k - \frac{t}{T}\right) n_{i,\tau}^{k-1}, \quad \text{for } (k-1)\tau < t < k\tau, \tag{8.93}$$

and the piecewise constant interpolants $\overline{n}_{i,\tau} \in L^\infty(I; V)$ defined by

$$\overline{n}_{i,\tau}(t) = n_{i,\tau}^k, \quad \text{for } (k-1)\tau < t < k\tau,\ k = 0, \dots T/\tau, \tag{8.94}$$

which are used to build up the solutions to the original system (8.20)-(8.22). For illustration see Figure 8.3.

Remark 8.23. *In contrast to the scheme (8.92), let us define a more compact form of (8.92) as*

$$\begin{aligned}
\frac{\partial n_{S,\tau}}{\partial t} - D_S \Delta \overline{n}_{S,\tau} &= k_- \overline{n}_{C,\tau}^R - k_+ \overline{n}_{S,\tau} \overline{n}_{E,\tau}^R, \\
\frac{\partial n_{E,\tau}}{\partial t} - D_E \Delta \overline{n}_{E,\tau} &= (k_- + k_{p+}) \overline{n}_{C,\tau}^R - k_+ \overline{n}_{S,\tau} \overline{n}_{E,\tau} - k_{p-} \overline{n}_{E,\tau} \overline{n}_{P,\tau}^R, \\
\frac{\partial n_{C,\tau}}{\partial t} - D_C \Delta \overline{n}_{C,\tau} &= -(k_- + k_{p+}) \overline{n}_{C,\tau} + k_+ \overline{n}_{S,\tau} \overline{n}_{E,\tau} + k_{p-} \overline{n}_{E,\tau} \overline{n}_{P,\tau}^R, \\
\frac{\partial n_{P,\tau}}{\partial t} - D_P \Delta \overline{n}_{P,\tau} &= k_{p+} \overline{n}_{C,\tau} - k_{p-} \overline{n}_{E,\tau} \overline{n}_{P,\tau},
\end{aligned} \tag{8.95}$$

where $\overline{n}_{i,\tau}^R$ are the "retarded" functions defined by

$$\overline{n}_{i,\tau}^R(t) = \begin{cases} \overline{n}_{i,\tau}(t-\tau), & \text{for } t \in [\tau, T], \\ n_{i,\tau}^0, & \text{for } t \in [0, \tau), \end{cases} \tag{8.96}$$

which satisfy all a-priori estimates (e.g. (8.100) below) as the piecewise constant interpolants $\overline{n}_{i,\tau}$ defined in (8.94). It also holds that $\overline{n}_{i,\tau}^R \to n_i$ whenever $\overline{n}_{i,\tau} \to n_i$ for $\tau \to 0$ (i.e. both $\overline{n}_{i,\tau}^R$ and $\overline{n}_{i,\tau}$ converge to the same limit). For more details on the retarded functions see (8.202) on p. 279 and Exercise 8.92 on p. 288 in [130].

Lemma 8.24. *The elliptic problems (8.92) with the zero-flux boundary conditions posses unique solutions $n_{i,\tau}^k \in V$ which are non-negative ($n_{i,\tau}^k \geq 0$) provided $n_{i,\tau}^0 \geq 0$ for $i \in \{S, E, C, P\}$ and $k = 1, \dots, T/\tau$.*

Proof. (by induction argument) Assume that there exist $n_{i,\tau}^{k-1} \in V$ such that $n_{i,\tau}^{k-1} \geq 0$, $i \in \{S, E, C, P\}$. Then, we see that the linear elliptic problems in (8.92) are, one by one, coercive on V. Indeed, for example, for $i = S$ there is

$$\langle A n_{S,\tau}^k, n_{S,\tau}^k \rangle = \int_\Omega \frac{1}{\tau} (n_{S,\tau}^k)^2 + D_S |\nabla n_{S,\tau}^k|^2 + k_+ n_{E,\tau}^{k-1} (n_{S,\tau}^k)^2 \, \mathrm{d}x \geq c_0 \|n_{S,\tau}^k\|_V^2$$

for $c_0 = \min\left\{\frac{1}{\tau}, D_S\right\}$. Thus, by the Lax-Milgram theorem[11], they possess unique weak solutions $n_{i,\tau}^k \in V$ for each $i \in \{S, E, C, P\}$.

Testing the weak formulation for $n_{S,\tau}^k$, i.e.

$$\int_\Omega \frac{1}{\tau} n_{S,\tau}^k \phi + D_S \nabla n_{S,\tau}^k \cdot \nabla \phi + k_+ n_{E,\tau}^{k-1} n_{S,\tau}^k \phi \, \mathrm{d}x = \int_\Omega \frac{1}{\tau} n_{S,\tau}^{k-1} \phi + k_- n_{C,\tau}^{k-1} \phi \, \mathrm{d}x, \tag{8.97}$$

[11] (Lax-Milgram) Let V be a Hilbert space, $f \in V^*$, $A : V \to V^*$ be a linear continuous operator which is coercive, i.e. there exists $c_0 > 0$ such that $\langle Av, v \rangle \geq c_0 \|v\|_V^2$ holds for all $v \in V$. Then A has a bounded inverse, i.e. there exists a unique $u \in V$ such that $\langle Au, v \rangle = \langle f, v \rangle$ for all $v \in V$.

by $\phi = (n_{S,\tau}^k)^-$ (that is by the negative part of $n_{S,\tau}^k$), we obtain

$$\frac{1}{\tau}\|(n_{S,\tau}^k)^-\|_{L^2(\Omega)}^2 + D_S\|\nabla(n_{S,\tau}^k)^-\|_{L^2(\Omega;\mathbb{R}^d)}^2 \le 0,$$

i.e. $\|(n_{S,\tau}^k)^-\|_V \le 0$, which implies that $(n_{S,\tau}^k)^- = 0$ and so $n_{S,\tau}^k \ge 0$ in V. Analogously we would proceed with the other cases. Thus, we have the existence of unique and non-negative solutions $n_{i,\tau}^k \in V$ to (8.92) for $i \in \{S, E, C, P\}$ and $k = 1, \dots, T/\tau$. □

Lemma 8.25 (A-priori bounds)**.** *For each $i \in \{S, E, C, P\}$ and $\tau < \min\{1/(k_+ + k_{p-}), 1/(k_- + k_{p+})\}$ the following a-priori bounds hold:*

$$\left\|n_{i,\tau}\right\|_{L^2(I;V)} \le C, \tag{8.98}$$

$$\left\|\frac{\partial n_{i,\tau}}{\partial t}\right\|_{L^2(I;V^*)} \le C, \tag{8.99}$$

for the Rothe functions $n_{i,\tau}$ defined in (8.93) and some constant $C > 0$.

Proof. Let us show the estimate (8.98) for $i = S$. Testing the weak formulation (8.97) by $\phi = n_{S,\tau}^k$ gives, by employing Young's inequality and $n_{E,\tau}^{k-1} \ge 0$,

$$\begin{aligned}\frac{1}{\tau}\|n_{S,\tau}^k\|_{L^2(\Omega)}^2 + D_S\|\nabla n_{S,\tau}^k\|_{L^2(\Omega;\mathbb{R}^d)}^2 \le{}& \frac{1}{2\tau}\|n_{S,\tau}^k\|_{L^2(\Omega)}^2 + \frac{1}{2\tau}\|n_{S,\tau}^{k-1}\|_{L^2(\Omega)}^2 \\ &+ \frac{k_-}{2}\|n_{S,\tau}^k\|_{L^2(\Omega)}^2 + \frac{k_-}{2}\|n_{C,\tau}^{k-1}\|_{L^2(\Omega)}^2,\end{aligned}$$

i.e.

$$\frac{1}{2\tau}\|n_{S,\tau}^k\|_{L^2(\Omega)}^2 + D_S\|\nabla n_{S,\tau}^k\|_{L^2(\Omega;\mathbb{R}^d)}^2 \le \frac{1}{2\tau}\|n_{S,\tau}^{k-1}\|_{L^2(\Omega)}^2 + \frac{k_-}{2}\|n_{S,\tau}^k\|_{L^2(\Omega)}^2 + \frac{k_-}{2}\|n_{C,\tau}^{k-1}\|_{L^2(\Omega)}^2.$$

This multiplied by 2τ and summed up for $k = 1, \dots, l$ yields

$$\|n_{S,\tau}^l\|_{L^2(\Omega)}^2 + 2\tau D_S\sum_{k=1}^{l}\|\nabla n_{S,\tau}^k\|_{L^2(\Omega;\mathbb{R}^d)}^2 \le \|n_{S,\tau}^0\|_{L^2(\Omega)}^2 + \tau\sum_{k=1}^{l} k_-\|n_{S,\tau}^k\|_{L^2(\Omega)}^2 + k_-\|n_{C,\tau}^{k-1}\|_{L^2(\Omega)}^2,$$

which is valid for an arbitrary $0 \le l \le T/\tau$. Provided that $\tau < 1/k_-$, discrete Gronwall's inequality[12] gives boundedness of $\|n_{S,\tau}^l\|_{L^2(\Omega)}^2 + \sum_{k=1}^{l}\|\nabla n_{S,\tau}^k\|_{L^2(\Omega;\mathbb{R}^d)}^2$ for all $l = 0, \dots, T/\tau$. As a consequence,

$$\|\overline{n}_{S,\tau}\|_{L^2(I;V)}^2 = \tau\sum_{k=1}^{T/\tau}\|n_{S,\tau}^k\|_V^2 \le C \tag{8.100}$$

i.e. $\overline{n}_{S,\tau} \in L^2(I;V) \cap L^\infty(I;H)$. By recalling the general estimate (8.89) together with the assumption $\|n_{S,\tau}^0\|_V = \mathscr{O}(1/\sqrt{\tau})$, we obtain $\|n_{S,\tau}\|_{L^2(I;V)} \le C$, i.e., $n_{S,\tau} \in L^2(I;V) \cap L^\infty(I;H)$. In both estimates C depends on T linearly.

Analogously we can show (8.98) for the other species $i = E, C$ and P. Note, that Gronwall's inequity for the particular cases requires, respectively, $\tau < 1/(k_- + k_{p+})$, $\tau < 1/(k_+ + k_{p-})$ and $\tau < 1/k_{p+}$.

[12](discrete Gronwall's inequality) If $y_l \le C + \tau\sum_{k=1}^{l}(ay_k + b_k)$ for any $l \ge 0$, then

$$y_l \le \frac{e^{\tau la/(1-a\tau)}}{1-a\tau}\left(C + \tau\sum_{k=1}^{l} b_k\right), \quad \text{for } \tau < \frac{1}{a}.$$

Finally, we can proceed to prove (8.99). Let us show the estimate for $i = S$ since the other cases can be proved analogously. Then, by considering the 'retarded' system (8.95) from Remark 8.23, with the assistance of Hölder's inequality, we can write

$$\begin{aligned}\left\|\frac{\partial n_{S,\tau}}{\partial t}\right\|_{L^2(I;V^*)} &= \sup_{\|v\|_{L^2(I;V)}\le 1}\int_0^T \left\langle \frac{\partial n_{S,\tau}}{\partial t}, v\right\rangle_{V^*\times V} \mathrm{d}t \\ &= \sup_{\|v\|_{L^2(Q_T)}\le 1}\int_{Q_T} k_-\overline{n}^R_{C,\tau}v - k_+\overline{n}_{S,\tau}\overline{n}^R_{E,\tau}v - D_S\nabla\overline{n}_{S,\tau}\cdot\nabla v\,\mathrm{d}x\,\mathrm{d}t \\ &\le k_-\|\overline{n}^R_{C,\tau}\|_{L^2(Q_T)} + k_+\|\overline{n}_{S,\tau}\overline{n}^R_{E,\tau}\|_{L^2(Q_T)} + D_S\|\nabla\overline{n}_{S,\tau}\|_{L^2(Q_T,\mathbb{R}^d)},\end{aligned} \tag{8.101}$$

which bounds $\partial n_{S,\tau}/\partial \mathrm{t}$. □

Remark 8.26. *Notice that $n^k_{i,\tau}$ for $k = 1,\dots,T/\tau$ do not satisfy the conservation laws (8.23). In fact, one can easily check that*

$$\begin{aligned}\int_\Omega n^k_{E,\tau} + n^k_{C,\tau}\,\mathrm{d}x &= \int_\Omega n^{k-1}_{E,\tau} + n^{k-1}_{C,\tau}\,\mathrm{d}x - \tau(k_- + k_{p+})\int_\Omega \left(n^k_{C,\tau} - n^{k-1}_{C,\tau}\right)\mathrm{d}x \\ &= \cdots = \int_\Omega n^0_{E,\tau} + n^0_{C,\tau}\,\mathrm{d}x - \tau(k_- + k_{p+})\int_\Omega \left(n^k_{C,\tau} - n^0_{C,\tau}\right)\mathrm{d}x \\ &= M_1 - \tau(k_- + k_{p+})\int_\Omega \left(n^k_{C,\tau} - n^0_{C,\tau}\right)\mathrm{d}x,\end{aligned} \tag{8.102}$$

nor the conservation (8.24)

$$\begin{aligned}\int_\Omega n^k_{S,\tau} + n^k_{C,\tau} + n^k_{P,\tau}\,\mathrm{d}x = M_2 - \tau\int_\Omega \Bigg[& k_-(n^k_{C,\tau} - n^0_{C,\tau}) - k_+\sum_{j=1}^k n^j_{S,\tau}(n^j_{E,\tau} - n^{j-1}_{E,\tau}) \\ & + k_{p-}\sum_{j=1}^k n^j_{E,\tau}(n^j_{P,\tau} - n^{j-1}_{P,\tau})\Bigg]\,\mathrm{d}x.\end{aligned} \tag{8.103}$$

Proof. (of Theorem 8.3) In the following we prove that the Rothe functions $n_{i,\tau}$ converge weakly to the solutions of the reaction-diffusion system (8.20)-(8.22) in the space $\mathscr{W}^4$ where $\mathscr{W} = W^{1,2,2}(I;V,V^*) = \left\{u \in L^2(I;V), \frac{\mathrm{d}u}{\mathrm{d}t} \in L^2(I;V^*)\right\}$, i.e. $n_{i,\tau} \rightharpoonup n_i$ in $\mathscr{W}$ for $\tau \to 0$ and for each $i \in \{S,E,C,P\}$. In addition, n_i, $i \in \{S,E,C,P\}$, are the unique weak solutions to (8.20)-(8.22) and satisfy the conservation laws (8.23) and (8.24).

Since the sequences $\{n_{i,\tau}\}_\tau$, $i \in \{S,E,C,P\}$, are bounded in $\mathscr{W}$ by (8.98) and (8.99), the Eberlein-Šmuljan theorem[13] implies the existence of weakly convergent subsequences in $\mathscr{W}$, denoted by $\{n_{i,\tau}\}_\tau$. By the Aubin-Lions lemma[14], namely by (8.104), $n_{i,\tau} \to n_i$ in $L^2(Q_T)$.

[13] Actually, $\mathscr{W}$ is the Hilbert space so we do not need such a deep result as the Eberlein-Šmuljan theorem for the existence of weakly convergent subsequence.

[14] (Aubin-Lions) Let $p \in (1,\infty)$, $q \in [1,\infty]$ and X be a Banach space and X_0, X_1 be separable and reflexive Banach spaces such that $X_0 \subset\subset X \subset X_1$, then

$$\left\{u \in L^p(I;X_0), \frac{\mathrm{d}u}{\mathrm{d}t} \in L^q(I;X_1)\right\} \subset\subset L^p(I;X).$$

Thus, for example, for $X = X_0 = V = W^{1,2}(\Omega)$, $X_1 = V^*$ and $H = L^2(\Omega)$ there is

$$W^{1,2,2}(I;V,V^*) \subset\subset L^2(I;V) \subset L^2(I;H) = L^2(Q_T). \tag{8.104}$$

In addition, $\|n_{i,\tau} - \overline{n}_{i,\tau}\|_{L^2(Q_T)} = \mathscr{O}(\sqrt{\tau})$ which follows from (8.91) and the bounds (8.98) and (8.99). Thus, $\overline{n}_{i,\tau} \to n_i$ strongly in $L^2(Q_T)$ for each $i \in \{S, E, C, P\}$.

A limit passage in (8.95) by weak continuity proceeds as follows. Firstly, note that the nonlinearity

$$R_+^7 \to R^4 : (r_1, r_2, r_2', r_3, r_3', r_4, r_4') \mapsto \big(k_- r_3' - k_+ r_1 r_2', (k_- + k_{p+}) r_3' - k_+ r_1 r_2 - k_{p-} r_2 r_4', \\ -(k_- + k_{p+}) r_3 + k_+ r_1 r_2 + k_{p-} r_2 r_4', k_{p+} r_3 - k_{p-} r_2 r_4\big)$$

has at most a quadratic growth so that, by continuity of the respective Nemytskiĭ mapping[15] $L^2(Q_T)^7 \to L^1(Q_T)^4$, the right-hand sides of (8.95) converge strongly in $L^1(Q_T)$ to $k_- n_C - k_+ n_S n_E$, $(k_- + k_{p+}) n_C - k_+ n_S n_E - k_{p-} n_E n_P$, $-(k_- + k_{p+}) n_C + k_+ n_S n_E + k_{p-} n_E n_P$ and $k_{p+} n_C - k_{p-} n_E n_P$, respectively. The left-hand-side terms in (8.95) are linear so that the limit passage is obvious. Note that the mappings $n_i \mapsto n_i(0, \cdot) : \mathscr{W} \to L^2(\Omega)$ is weakly continuous which allows us to pass to the limit in the respective initial conditions.

It is straightforward to verify that n_i satisfy the conservation laws. Indeed, we can notice that $\overline{n}_{i,\tau}$ satisfy (8.102) and (8.103) in Remark 8.26 where we can pass in the limit for $\tau \to 0$. □

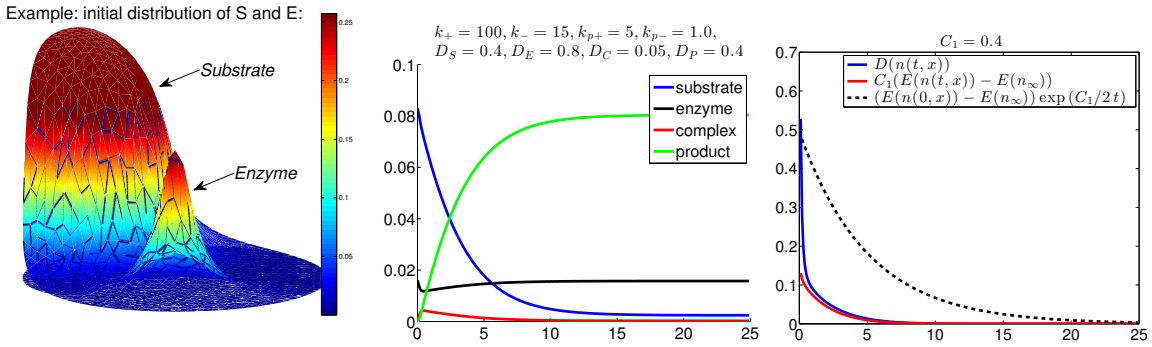

Figure 8.4. An example of 2D FreeFem++ simulation of the reversible enzyme reaction, see also the following section. On the left: initial distribution of the substrate S and the enzyme E. In the middle: evolution of the total concentrations ($\int_\Omega n_i$, $i \in \{S, E, C, P\}$) of the species appearing in the enzyme reaction. On the right: entropy dissipation, relative entropy and an exponential bound appearing in (8.48) and (8.51). The dimensionless parameters are chosen as follows: reaction rates $k_+ = 100$, $k_- = 15$, $k_{p+} = 5$, $k_{p-} = 1$, diffusions $D_S = 0.4$, $D_E = 0.8$, $D_C = 0.05$, $D_P = 0.4$.

Remark 8.27. *Note that the proof of the existence of the solution for the irreversible enzyme reaction-diffusion system by the semi-implicit Rothe method would run exactly in the same way as above. The method can be used to solve numerically PDE systems in 2D and 3D, e.g., in FreeFem++ [62], Figure 8.4. The Rothe method can be even applied to more complicated*

[15] Consider a Carathéodory mapping $a : \Omega \times \mathbb{R}^7 \to \mathbb{R}^4$, that is $a(\cdot; r_1, \dots, r_7) : \Omega \to \mathbb{R}^4$ is measurable for all $(r_1, \dots, r_7) \in \mathbb{R}^7 = \underbrace{\mathbb{R} \times \cdots \times \mathbb{R}}_{7 \text{ times}}$ and $a(x; \cdot) : \mathbb{R}^7 \to \mathbb{R}^4$ is continuous for a.a. $x \in \Omega$. Then the Nemytskiĭ mapping N_a maps functions $u_i : \Omega \to \mathbb{R}$, $i = 1, \dots, 7$, to a function $N_a(u_1, \dots, u_7) : \Omega \to \mathbb{R}^4$ defined by $[N_a(u_1, \dots, u_7)](x) = a(x; u_1(x), \dots, u_7(x))$. If a satisfies the growth condition $|a(x; r_1, \dots, r_7)| \le \gamma(x) + C \sum_{i=1}^7 |r_i|^2$ for some $\gamma \in L^1(\Omega)$ and some constant C, then N_a is bounded continuous mapping $[L^2(\Omega)]^7 = \underbrace{L^2(\Omega) \times \cdots \times L^2(\Omega)}_{7 \text{ times}} \to L^1(\Omega; \mathbb{R}^4) = [L^1(\Omega)]^4$, see [130]. The same is true for $\Omega = Q_T$.

systems such as the 2-compartmental reaction-diffusion systems for the p53 network studied in Chapters 5 and 6.

FreeFem++ code for the reversible EnR system

Let us also print out the full FreeFem++ code for the reversible enzyme reaction, in particular, the implementation of the scheme (8.92). We hope that the code can be easily adapted to the p53 PDE models (the codes for the p53 models are lengthy, thus not shown here; however, they are available upon request). All the computed data are saved to text files which can be then open by other software (e.g., by Matlab). In particular, the concentrations from each time step are saved to "info_concentrations.txt", the entropy, entropy dissipation and relative entropy to "info_entropy.txt" and information about the preserved conservation of masses in "info_mass.txt". The output from the code (with the given parameters and initial data) is shown on Fig. 8.4.

```
// ————————————————————————————————————————————————————————————-
//
// Reversible Enzyme Reaction 2D RD model
// by Ján Eliaš
//
// ————————————————————————————————————————————————————————————-

load "medit"
load "lapack"

// ———————————————— constants & parameters ————————————————————

// technical constants ...
string numb, numb2; int pos; // for a proper data saving
real[int] CameraPositionValue1 = [1.0851,2.77975,1.15398]; // for plots
real[int] CameraFocalPointValue1 = [0,0,0.319209];
real[int] CameraViewUpValue1 = [-0.0979641,-0.25096,0.963028];
real[int] CameraClippingRangeValue1 = [1.4961,5.12329];
real[int] CameraPositionValue = [1.95179,3.32595,2.50164];
real[int] CameraFocalPointValue = [-0.0103131,-0.0187419,0.126953];
real[int] CameraViewUpValue = [-0.254544,-0.456112,0.852742];
real[int] CameraClippingRangeValue = [2.16186,7.62003];

// kinetic rates
real kp1=100.0; // k_{+}
real km1=15.0; // k_{-}
real kp2=5.0; // k_{p+}
real km2=1.0; // k_{p-}

// diffusions
real Ds=0.4, De=0.8, Dc=0.005, Dp=0.4;

// time lag dt, final time T, frequency of saving data
real dt=0.02; real frq = 0.04; real T = 25.01;
```

```
// constants appearing in the iteration process; num. precision is *tol*
real tol=1e-6; int iter; int itermax=10;

real ctotal, etotal, stotal, ptotal; // total concentrations
real cinit, einit, sinit, pinit; // initial concentrations
real sigmas, sigmae, sigmac,sigmap; // σ_i dependent on the kinetic rates
real ceq, eeq, seq, peq; // equilibria
real M1, M2, M1init, M2init; // masses from concervation laws
real err, errM1, errM2; real [int] errM(2);
real entrfun, entrdis, relentr; // entropy functional, entropy dissipation, relative entropy

// Macro for gradient
macro Grad(u) [dx(u),dy(u)] //

// 2D domain Ω, the disc of volume 1
int In=1; //  label of the border ∂Ω
real r = 1.0/sqrt(pi); // radius
border C(t=0,2*pi){ x=r*cos(t); y=r*sin(t); label=In;}
mesh Th=buildmesh(C(100));

// save and plot mesh
savemesh (Th,"mesh.msh");
plot(Th,wait=1);

// space of functions on Th
fespace Vh(Th,P1);

// indices: 0-S, 1-E, 2-C, 3-P
// in the numerical scheme: "uiold" are solutions from the old time step;
// "ui" are newly computed solutions at the current time step;
// "vi" are test functions;
// "uki" are refinements of "ui" at each time step (so that the masses are conserved)
Vh uk0,uk1,uk2,uk3, u0,u1,u2,u3, v0,v1,v2,v3;
Vh u0old,u1old,u2old,u3old;

// initial conditions
func fs=0.4*( (x+0.3)^2+(y+0.3)^2<=0.25^2 );
func fe=2.5*( (x-0.4)^2+y^2<0.05^2 );
func fc=0.0;
func fp=0.0;

uk0=1e-15+fs; uk1=1e-15+fe; uk2=1e-10+fc; uk3=1e-10+fp;
u0old=uk0; u1old=uk1; u2old=uk2; u3old=uk3;

// plot initial data
plot(uk0,value=1,fill=1,wait=1,dim=3,ColorScheme=1,ShowAxes=0);
plot(uk1,value=1,fill=1,wait=1,dim=3,ColorScheme=1,ShowAxes=0);
plot(uk2,value=1,fill=1,wait=1,dim=3,ColorScheme=1,ShowAxes=0);
plot(uk3,value=1,fill=1,wait=1,dim=3,ColorScheme=1,ShowAxes=0);
```

```
// total mass, conservation laws
sinit=int2d(Th)(uk0); einit=int2d(Th)(uk1); //L^1 norm
cinit=int2d(Th)(uk2); pinit=int2d(Th)(uk3); //L^1 norm

M1init=cinit+einit; M2init=sinit+cinit+pinit;

// save information about the conservation of masses into the text file "info_mass.txt"
ofstream ff("info_mass.txt");
ff << "time = 0.0, M1 (M1init) = " << M1init << " (" << M1init << "),
      M2 (M2init) = " << M2init << " (" << M2init << ")" <<endl;

// equilibria (computed analytically): ceq, eeq, seq, peq
real alpha=1.0, beta=km1/kp2;
sigmas=kp1/km1; sigmae=alpha*km1; sigmac=alpha*km1; sigmap=km2/kp2;
real capitalK = ((sigmas+sigmap)*sigmac)/(sigmas*sigmae*sigmap);

ceq = (M1init+M2init+capitalK - sqrt( (M1init+M2init+capitalK)^2 -
4*M1init*M2init) )/2;
eeq = M1init - ceq;
seq = (km1*ceq)/(kp1*eeq);
peq = (kp2*ceq)/(km2*eeq);

// entropy
entrfun=int2d(Th)( uk0*log(sigmas*uk0)-uk0+1.0/sigmas + uk1*log(sigmae*uk1)-
uk1+1.0/sigmae
                 + uk2*log(sigmac*uk2)-uk2+1.0/sigmac + uk3*log(sigmap*uk3)-
uk3+1.0/sigmap );

// entropy dissipation
entrdis=int2d(Th)( Ds*(Grad(uk0)'*Grad(uk0))/uk0
                 + De*(Grad(uk1)'*Grad(uk1))/uk1
                 + Dc*(Grad(uk2)'*Grad(uk2))/uk2
                 + Dp*(Grad(uk3)'*Grad(uk3))/uk3 )
+ int2d(Th)( (kp1*uk0*uk1-km1*uk2)*(log(sigmas*sigmae*uk0*uk1)-log(sigmac*uk2)) )
+ int2d(Th)( (km2*uk1*uk3-kp2*uk2)*(log(sigmae*sigmap*uk1*uk3)-log(sigmac*uk2)) );

// relative entropy
relentr=int2d(Th)( uk0*log(uk0/seq)-(uk0-seq) + uk1*log(uk1/eeq)-(uk1-eeq)
                 + uk2*log(uk2/ceq)-(uk2-ceq) + uk3*log(uk3/peq)-(uk3-peq) );

// save concentrations into the text file "info_concentrations.txt"
ofstream hh("info_concentrations.txt");
hh << "0," << sinit << "," << seq << "," << einit << "," << eeq << ","
          << cinit << "," <<  ceq << "," << pinit << "," << peq << endl;

// save concentrations into the text file "info_entropy.txt"
ofstream en("info_entropy.txt");
en << "0" << "," << entrfun << "," << entrdis << "," << relentr << endl;
```

```
// variational problems for the decoupled equations: Scheme (9.16)
// indices: 0-S, 1-E, 2-C, 3-P
problem PbIRREVs(u0,v0) =
int2d(Th,optimize=0)(Ds*(Grad(u0)'*Grad(v0))
+ u0*v0/dt
+ kp1*u0*uk1*v0
)
- int2d(Th)(u0old*v0/dt
+ km1*uk2*v0
);

problem PbIRREVe(u1,v1) =
int2d(Th,optimize=0)(De*(Grad(u1)'*Grad(v1))
+ u1*v1/dt
+ kp1*u0*u1*v1
+ km2*u1*uk3*v1
)
- int2d(Th)(u1old*v1/dt
+ (km1+kp2)*uk2*v1
);

problem PbIRREVc(u2,v2) =
int2d(Th,optimize=0)(Dc*(Grad(u2)'*Grad(v2))
+ u2*v2/dt
+ (km1+kp2)*u2*v2
)
- int2d(Th)(u2old*v2/dt
+ kp1*u0*u1*v2
+ km2*u1*uk3*v2
);

problem PbIRREVp(u3,v3)=
int2d(Th,optimize=0)(Dp*(Grad(u3)'*Grad(v3))
+ u3*v3/dt
+ km2*u1*u3*v3
)
- int2d(Th)(u3old*v3/dt
+ kp2*u2*v3
);

// Simulations
for(real t=dt;t<=T+dt;t+=dt)
{
iter=0;
errM=100; // Initial error

uk0=u0old;uk1=u1old;uk2=u2old;uk3=u3old;
```

```
while(errM.max¿tol && iter<itermax)
{ // refinement to reach conservation of masses M1 and M2

        // Solving variational problems
        PbIRREVs;
        PbIRREVe;
        PbIRREVc;
        PbIRREVp;

        iter++;

        stotal=int2d(Th)(u0); etotal=int2d(Th)(u1); //L^1 norm
        ctotal=int2d(Th)(u2); ptotal=int2d(Th)(u3);
        M1=ctotal+etotal; M2=stotal+ctotal+ptotal;

        errM1=abs(M1init-M1); errM2=abs(M2init-M2);
        errM[0]=errM1; errM[1]=errM2;

        uk0=u0; uk1=u1; uk2=u2; uk3=u3; // new refinements

}// eof while

if ((iter==itermax) && (errM.min¿tol*10))
{
        cout << "Max. number of allowed iterations reached!" << endl;
        break;
}


// save, print desired data (results) after each "frq" iteration
numb = string(t/frq); pos = numb.find("."); numb2 = numb(pos+1:numb.length);
if ( pos == -1 ? 1 : (numb2=="0" ? 1 : 0)) // save/plot data
{

        numb = string(t);
        pos = numb.find(".");
        numb2 = numb(0:pos+2);

plot(Th,u0,u3,wait=0,value=1,fill=1,dim=3,aspectratio=1,ZScale=0.5,
ColorScheme=1,ShowAxes=0,nbiso=160,NbColorTicks=6,LabelColors=2,
CameraPosition = CameraPositionValue1,CameraFocalPoint-
Value1,
CameraViewUp = CameraViewUpValue1,
CameraViewAngle = 30, CameraClippingRange = CameraClippingRangeValue1,
cmm=t);

stotal=int2d(Th)(u0); etotal=int2d(Th)(u1); //L^1 norm
ctotal=int2d(Th)(u2); ptotal=int2d(Th)(u3);
M1=ctotal+etotal; M2=stotal+ctotal+ptotal;
```

```
hh << t << ",," << stotal << ",," << seq << ",," << etotal << ",," << eeq << ",," << cto-
tal << ",," << ceq
          << ",," << ptotal << ",," << peq << endl;
ff << "time = " << t << ";  M1 (M1init) = " << M1 << " (" << M1init <<
          "), M2 (M2init) = " << M2<< " (" << M2init << ")" <<endl;

entrfun=int2d(Th)(  u0*log(sigmas*u0)-u0+1.0/sigmas  +  u1*log(sigmae*u1)-u1+1.0/
sigmae
          + u2*log(sigmac*u2)-u2+1.0/sigmac + u3*log(sigmap*u3)-u3+1.0/sigmap );
entrdis=int2d(Th)( Ds*(Grad(u0)'*Grad(u0))/u0 + De*(Grad(u1)'*Grad(u1))/u1
          + Dc*(Grad(u2)'*Grad(u2))/u2 + Dp*(Grad(u3)'*Grad(u3))/u3)
         + int2d(Th)( (kp1*u0*u1-km1*u2)*(log(sigmas*sigmae*u0*u1)-log(sigmac*u2)) )
         + int2d(Th)( (km2*u1*u3-kp2*u2)*(log(sigmae*sigmap*u1*u3)-log(sigmac*u2)) );
relentr=int2d(Th)( u0*log(u0/seq)-(u0-seq) + u1*log(u1/eeq)-(u1-eeq)
          + u2*log(u2/ceq)-(u2-ceq) + u3*log(u3/peq)-(u3-peq) );

en << t << ",," << entrfun << ",," << entrdis << ",," << relentr << endl;


}
// save current solution for the next time step
u0old=u0;u1old=u1;u2old=u2;u3old=u3;
}
// ---------------------
```

Bibliography

[1] B. Alberts, A. Johnson, J. Lewis, M. Raff, K. Roberts, and P. Walter. *Molecular Biology of the Cell. Garland Science*. Taylor and Francis Group, fifth edition, 2008.

[2] U. Alon. http://wws.weizmann.ac.il/mcb/UriAlon/.

[3] A. Arnold, J. A. Carrillo, L. Desvillettes, J. Dolbeault, A. Jüngel, C. Lederman, P. A. Markowich, G. Toscani, and C. Villani. Entropies and equilibria of many-particle systems: An essay on recent research. *Monatshefte für Mathematik*, 142(1-2):35–43, 2004.

[4] B. D. Aronson, K. A. Johnson, and J. C. Dunlap. Circadian clock locus frequency: protein encoded by a single open reading frame defines period length and temperature compensation. *Proc. Nat. Acad. Sci. USA*, 91(16):7683–7687, 1994.

[5] M. Ashcroft, R. L. Ludwig, D. B. Woods, T. D. Copeland, H. O. Weber, E. J. MacRae, and K. H. Vousden. Phosphorylation of HDM2 by Akt. *Oncogene*, 21(13):1955–1962, 2002.

[6] T. J. Atkinson and M. S. Halfon. Regulation of gene expression in the genomic context. *Computational and structural biotechnology journal*, 9(13):e201401001, 2014.

[7] C. J. Bakkenist and M. B. Kastan. DNA damage activates ATM through intermolecular autophosphorylation and dimer dissociation through intermolecular autophosphorylation and dimer dissociation. *Nature*, 421(6922):499–506, 01 2003.

[8] A. Ballesta, J. Clairambault, S. Dulong, and F. Lévi. A systems biomedicine approach for chronotherapeutics optimization: Focus on the anticancer drug irinotecan. In A. d'Onofrio, P. Cerrai, and A. Gandolfi, editors, *New Challenges for Cancer Systems Biomedicine*, SIMAI Springer Series, pages 301–327. Springer Milan, 2012.

[9] A. Ballesta, S. Dulong, C. Abbara, B. Cohen, A. Okyar, J. Clairambault, and F. Lévi. A combined experimental and mathematical approach for molecular-based optimization of irinotecan circadian delivery. *PLoS Comput Biol*, 7(9):e1002143, 09 2011.

[10] Y. Barak, E. Gottlieb, T. Juven-Gershon, and M. Oren. Regulation of mdm2 expression by p53: alternative promoters produce transcripts with nonidentical translation potential. *Genes & Development*, 8(15):1739–1749, 1994.

[11] Y. Barak, T. Juven, R. Haffner, and M. Oren. mdm2 expression is induced by wild type p53 activity. *The EMBO Journal*, 12(2):461–468, 02 1993.

[12] J. A. Barboza, T. Iwakuma, T. Terzian, A. K. El-Naggar, and G. Lozano. Mdm2 and mdm4 loss regulates distinct p53 activities. *Molecular Cancer Research*, 6(6):947–954, 2008.

[13] J. Bartkova, C. J. Bakkenist, E. R.-D. Meyts, N. E. Skakkebæk, M. Sehested, J. Lukas, M. B. Kastan, and J. Bartek. ATM activation in normal human tissues and testicular cancer. *Cell Cycle*, 4(6):838–845, 2005.

[14] E. Batchelor, A. Loewer, C. Mock, and G. Lahav. Stimulus-dependent dynamics of p53 in single cells. *Molecular Systems Biology*, 7(1):8 pp, 2011.

[15] E. Batchelor, C. S. Mock, I. Bhan, A. Loewer, and G. Lahav. Recurrent initiation: A mechanism for triggering p53 pulses in response to DNA damage. *Molecular Cell*, 30(3):277–289, 2015/02/16 2008.

[16] S. Ben-Tabou de Leon and E. H. Davidson. Modeling the dynamics of transcriptional gene regulatory networks for animal development. *Developmental biology*, 325(2):317–328, 2009.

[17] M. Bendahmane, T. Lepoutre, A. Marrocco, and B. Perthame. Conservative cross diffusions and pattern formation through relaxation. *Journal de Mathématiques Pures et Appliquées*, 92(6):651–667, 2009.

[18] E. Berkovich, R. J. Monnat, and M. B. Kastan. Roles of ATM and NBS1 in chromatin structure modulation and DNA double-strand break repair. *Nature Cell Biology*, 9(6):683–690, 06 2007.

[19] F. Billy and J. Clairambault. Designing proliferating cell population models with functional targets for control by anti-cancer drugs. *Discrete and Continuous Dynamical Systems - Series B*, 18(4):865–889, 2013.

[20] J. Braga, J. G. McNally, and M. Carmo-Fonseca. A reaction-diffusion model to study RNA motion by quantitative fluorescence recovery after photobleaching. *Biophysical Journal*, 92(8):2694–2703, 2007.

[21] G. E. Briggs and J. B. S. Haldane. A note on the kinetics of enzyme action. *Biochemical Journal*, 19:338–339, 1925.

[22] N. F. Britton. *Reaction-diffusion equations and their applications to biology.* Academic Press, London, 1986.

[23] A. Cangiani and R. Natalini. A spatial model of cellular molecular trafficking including active transport along microtubules. *Journal of theoretical biology*, 267(4):614–625, 2010.

[24] L. C. Cantley and B. G. Neel. New insights into tumor suppression: PTEN suppresses tumor formation by restraining the phosphoinositide 3-kinase/AKT pathway. *Proc. Natl. Acad. Sci. USA*, 96(8):4240–4245, 1999.

[25] C.-J. Chang, D. J. Freeman, and H. Wu. PTEN regulates Mdm2 expression through the P1 promoter. *Journal of Biological Chemistry*, 279(28):29841–29848, 2004.

[26] Y. Chang, Y. Lee, T. Tejima, K. Tanaka, S. Omura, N. Heintz, Y. Mitsui, and J. Magae. mdm2 and bax, downstream mediators of the p53 response, are degraded by the ubiquitin-proteasome pathway. *Cell Growth Differ*, 9(1):79–84, 1998.

[27] C. Y. Chen, J. D. Oliner, Q. Zhan, A. J. Fornace, B. Vogelstein, and M. B. Kastan. Interactions between p53 and MDM2 in a mammalian cell cycle checkpoint pathway. *Proceedings of the National Academy of Sciences of the United States of America*, 91(7):2684–2688, 03 1994.

[28] A. Ciliberto, B. Novák, and J. J. Tyson. Steady states and oscillations in the p53/Mdm2 network. *Cell cycle*, 4(3):488–493, 2005.

[29] J. Clairambault. Modelling physiological and pharmacological control on cell proliferation to optimise cancer treatments. *Mathematical Modelling of Natural Phenomena*, 4:12–67, 1 2009.

[30] J. Clairambault and O. Fercoq. Physiologically structured cell population dynamic models with applications to combined drug delivery optimisation in oncology. In M. Bachar, J. Batzel, and M. Chaplain, editors, *Mathematical modelling of cancer growth and treatment*. Springer, 2013.

[31] D. Claude and J. Clairambault. Period shift induction by intermittent stimulation in a Drosophila model of per protein oscillations. *Chronobiology international*, 17(1):1–14, 2000.

[32] C. N. Cole and J. J. Scarcelli. Transport of messenger RNA from the nucleus to the cytoplasm. *Current opinion in cell biology*, 18(3):299–306, 2006.

[33] T. Deerinck and M. Ellisman. Photograph : Death most beautiful (2008) taken from http://www.cell.com/cell_picture_show-celldeath.

[34] C. DeFranco, M. E. Chicurel, and H. Potter. A general RNA-binding protein complex that includes the cytoskeleton-associated protein MAP 1A. *Molecular biology of the cell*, 9(7):1695–1708, 1998.

[35] D. L. Denault, J. J. Loros, and J. C. Dunlap. WC-2 mediates WC-1–FRQ interaction within the PAS protein-linked circadian feedback loop of Neurospora. *The EMBO journal*, 20(1-2):109–117, 2001.

[36] N. Desilet, T. N. Campbell, and F. Y. Choy. p53-based anti-cancer therapies: an empty promise? *Current issues in molecular biology*, 12(3):143, 2010.

[37] L. Desvillettes and K. Fellner. Exponential decay toward equilibrium via entropy methods for reaction–diffusion equations. *Journal of Mathematical Analysis and Applications*, 319(1):157–176, 2006.

[38] L. Desvillettes and K. Fellner. Duality- and entropy methods for reversible reaction-diffusion equations with degenerate diffusion. Preprint, 2014.

[39] L. Desvillettes and K. Fellner. Exponential convergence to equilibrium for a nonlinear reaction-diffusion systems arising in reversible chemistry. In C. Pötzsche, C. Heuberger, B. Kaltenbacher, and F. Rendl, editors, *System Modeling and Optimization*, volume 443 of *IFIP Advances in Information and Communication Technology*, pages 96–104. Springer Berlin Heidelberg, 2014.

[40] L. Desvillettes, K. Fellner, M. Pierre, and J. Vovelle. About global existence for quadratic systems of reaction-diffusion. *Journal Advanced Nonlinear Studies*, 7:491–511, 2007.

[41] A. Dhooge, W. Govaerts, and Y. A. Kuznetsov. MATCONT: a MATLAB package for numerical bifurcation analysis of ODEs. *ACM Transactions on Mathematical Software (TOMS)*, 29(2):141–164, 2003.

[42] L. Dimitrio. *Modelling nucleocytoplasmic transport with application to the intracellular dynamics of the tumor suppressor protein p53.* PhD thesis, Université Pierre et Marie Curie, Paris, September 2012.

[43] L. Dimitrio, J. Clairambault, and R. Natalini. A spatial physiological model for p53 intracellular dynamics. *Journal of Theoretical Biology*, 316(0):9–24, 2013.

[44] J. C. Dunlap. Molecular bases for circadian clocks. *Cell*, 96(2):271–290, 1999.

[45] J. Eliaš and J. Clairambault. Reaction–diffusion systems for spatio-temporal intracellular protein networks: A beginner's guide with two examples. *Computational and Structural Biotechnology Journal*, 10(16):12–22, 2014.

[46] J. Eliaš, L. Dimitrio, J. Clairambault, and R. Natalini. The dynamics of p53 in single cells: physiologically based ODE and reaction–diffusion PDE models. *Physical Biology*, 11(4):045001, 2014.

[47] J. Eliaš, L. Dimitrio, J. Clairambault, and R. Natalini. The p53 protein and its molecular network: Modelling a missing link between DNA damage and cell fate. *Biochimica et Biophysica Acta (BBA) - Proteins and Proteomics*, 1844(1, Part B):232–247, 2014.

[48] L. C. Evans. *Partial Differential Equations.* Graduate Studies in Mathematics, V. 19. AMS, Providence, second edition, 2010.

[49] S. S. Fakharzadeh, S. P. Trusko, and D. L. George. Tumorigenic potential associated with enhanced expression of a gene that is amplified in a mouse tumor cell line. *The EMBO Journal*, 10(6):1565–1569, 06 1991.

[50] J. Falck, J. Coates, and S. P. Jackson. Conserved modes of recruitment of ATM, ATR and DNA-PKcs to sites of DNA damage. *Nature*, 434(7033):605–611, 03 2005.

[51] K. Fellner. Reaction-diffusion equations. Lecture notes, 2010.

[52] M. Fiscella, H. Zhang, S. Fan, K. Sakaguchi, S. Shen, W. E. Mercer, G. F. Vande Woude, P. M. O'Connor, and E. Appella. Wip1, a novel human protein phosphatase that is induced in response to ionizing radiation in a p53-dependentmanner. *Proceedings of the National Academy of Sciences*, 94(12):6048–6053, 1997.

[53] P. N. Friedman, X. Chen, J. Bargonetti, and C. Prives. The p53 protein is an unusually shaped tetramer that binds directly to DNA. *Proc. Natl. Acad. Sci. USA*, 90(8):3319–3323, 1993.

[54] M. Gajjar, M. M. Candeias, L. Malbert-Colas, A. Mazars, J. Fujita, V. Olivares-Illana, and R. Fåhraeus. The p53 mRNA-Mdm2 interaction controls Mdm2 nuclear trafficking and is required for p53 activation following DNA damage. *Cancer Cell*, 21(1):25–35, 2012.

[55] N. Y. Garceau, Y. Liu, J. J. Loros, and J. C. Dunlap. Alternative initiation of translation and time-specific phosphorylation yield multiple forms of the essential clock protein FREQUENCY. *Cell*, 89(3):469–476, 1997.

[56] N. Geva-Zatorsky, N. Rosenfeld, S. Itzkovitz, R. Milo, A. Sigal, E. Dekel, T. Yarnitzky, Y. Liron, P. Polak, G. Lahav, and U. Alon. Oscillations and variability in the p53 system. *Molecular Systems Biology*, 2(1):1–13, 2006.

[57] B. C. Goodwin. Oscillatory behavior in enzymatic control processes. *Advances in enzyme regulation*, 3:425–438, 1965.

[58] T. M. Gottlieb, J. Leal, R. Seger, Y. Taya, and M. Oren. Cross-talk between Akt, p53 and Mdm2: possible implications for the regulation of apoptosis. *Oncogene*, 21(8):1299–1303, 2002.

[59] D. R. Green and G. Kroemer. Cytoplasmic functions of the tumour suppressor p53. *Nature*, 458(7242):1127–1130, 04 2009.

[60] S. L. Harris and A. J. Levine. The p53 pathway: positive and negative feedback loops. *Oncogene*, 24(17):2899–2908, 2005.

[61] Y. Haupt, R. Maya, A. Kazaz, and M. Oren. Mdm2 promotes the rapid degradation of p53. *Nature*, 387(6630):296–299, 05 1997.

[62] F. Hecht. New development in FreeFem++. *Journal of Numerical Mathematics*, 20(3-4):251–265, 2012.

[63] F. G. Heineken, H. M. Tsuchiya, and R. Aris. On the mathematical status of the pseudo-steady state hypothesis of biochemical kinetics. *Mathematical Biosciences*, 1(1):95–113, 1967.

[64] P. Hinow, C. E. Rogers, C. E. Barbieri, J. A. Pietenpol, A. K. Kenworthy, and E. DiBenedetto. The DNA binding activity of p53 displays reaction-diffusion kinetics. *Biophysical journal*, 91(1):330–342, 2006.

[65] S. Hong, Y.-N. Wang, H. Yamaguchi, H. Sreenivasappa, C.-K. Chou, P.-H. Tsou, M.-C. Hung, and J. Kameoka. Measurement of protein 53 diffusion coefficient in live hela cells using raster image correlation spectroscopy (rics). *Journal of biomaterials and nanobiotechnology*, 1(1):31–36, 2010.

[66] A. C. Joerger and A. R. Fersht. The tumor suppressor p53: from structures to drug discovery. *Cold Spring Harbor Perspectives in Biology*, 2(6):a000919, 2010.

[67] M. B. Kastan and J. Bartek. Cell-cycle checkpoints and cancer. *Nature*, 432(7015):316–323, 11 2004.

[68] J. Keener and J. Sneyd. *Mathematical Physiology I: Cellular Physiology*. Interdisciplinary Applied Mathematics. Springer, second edition, 2009.

[69] J. K. Kim and T. L. Jackson. Mechanisms that enhance sustainability of p53 pulses. *PloS*, 8(6):e65242, 2013.

[70] R. Kitagawa, C. J. Bakkenist, P. J. McKinnon, and M. B. Kastan. Phosphorylation of SMC1 is a critical downstream event in the ATM–NBS1–BRCA1 pathway. *Genes & Development*, 18(12):1423–1438, 2004.

[71] S. V. Kozlov, M. E. Graham, B. Jakob, F. Tobias, A. W. Kijas, M. Tanuji, P. Chen, P. J. Robinson, G. Taucher-Scholz, K. Suzuki, S. So, D. Chen, and M. F. Lavin. Autophosphorylation and ATM activation: additional sites add to the complexity. *Journal of Biological Chemistry*, 286(11):9107–9119, 2011.

[72] S. V. Kozlov, M. E. Graham, C. Peng, P. Chen, P. J. Robinson, and M. F. a. Lavin. Involvement of novel autophosphorylation sites in ATM activation. *The EMBO Journal*, 25(15):3504–3514, 07 2006.

[73] M. Kracikova, G. Akiri, A. George, R. Sachidanandam, and S. A. Aaronson. A threshold mechanism mediates p53 cell fate decision between growth arrest and apoptosis. *Cell Death Differ*, 20(4):576–588, 04 2013.

[74] M. H. G. Kubbutat, S. N. Jones, and K. H. Vousden. Regulation of p53 stability by Mdm2. *Nature*, 387(6630):299–303, 05 1997.

[75] Y. A. Kuznetsov. *Elements of applied bifurcation theory*. Springer-Verlag, New York, third edition, 2004.

[76] O. A. Ladyzhenskaya, V. A. Solonnikov, and N. N. Uraĺtseva. *Linear and quasi-linear equations of parabolic type*, volume 23. American Mathematical Soc., 1968.

[77] G. Lahav, N. Rosenfeld, A. Sigal, N. Geva-Zatorsky, A. J. Levine, M. B. Elowitz, and U. Alon. Dynamics of the p53-Mdm2 feedback loop in individual cells. *Nat Genet*, 36(2):147–150, 02 2004.

[78] Z. Lai, K. V. Ferry, M. A. Diamond, K. E. Wee, Y. B. Kim, J. Ma, T. Yang, P. A. Benfield, R. A. Copeland, and K. R. Auger. Human mdm2 mediates multiple mono-ubiquitination of p53 by a mechanism requiring enzyme isomerization. *Journal of Biological Chemistry*, 276(33):31357–31367, 2001.

[79] S. Lain and D. Lane. Improving cancer therapy by non-genotoxic activation of p53. *European Journal of Cancer*, 39(8):1053–1060, 2003.

[80] J. E. Landers, S. L. Cassel, and D. L. George. Translational enhancement of mdm2 oncogene expression in human tumor cells containing a stabilized wild-type p53 protein. *Cancer Research*, 57(16):3562–3568, 1997.

[81] M. F. Lavin. Ataxia-telangiectasia: from a rare disorder to a paradigm for cell signalling and cancer. *Nat Rev Mol Cell Biol*, 9(12):759–769, 12 2008.

[82] J.-H. Lee and T. T. Paull. ATM activation by DNA double-strand breaks through the Mre11-Rad50-Nbs1 complex. *Science*, 308(5721):551–554, 2005.

[83] Y. Lee, M. J. Chong, and P. J. McKinnon. Ataxia telangiectasia mutated-dependent apoptosis after genotoxic stress in the developing nervous system is determined by cellular differentiation status. *The Journal of Neuroscience*, 21(17):6687–6693, 2001.

[84] J.-C. Leloup and A. Goldbeter. A model for circadian rhythms in Drosophila incorporating the formation of a complex between the PER and TIM proteins. *Journal of biological rhythms*, 13(1):70–87, 1998.

[85] J.-C. Leloup, D. Gonze, and A. Goldbeter. Limit cycle models for circadian rhythms based on transcriptional regulation in Drosophila and Neurospora. *Journal of Biological Rhythms*, 14(6):433–448, 1999.

[86] R. Lev Bar-Or, R. Maya, L. A. Segel, U. Alon, A. J. Levine, and M. Oren. Generation of oscillations by the p53-Mdm2 feedback loop: A theoretical and experimental study. *Proceedings of the National Academy of Sciences*, 97(21):11250–11255, 10 2000.

[87] F. Lévi, A. Okyar, S. Dulong, P. F. Innominato, and J. Clairambault. Circadian timing in cancer treatments. *Annual Review of Pharmacology and Toxicology*, 50(1):377–421, 2010. PMID: 20055686.

[88] A. J. Levine. The paths to death and differentiation. *Cell Death & Differentiation*, 18(9):1391–1392, 2011.

[89] M. Li, C. L. Brooks, F. Wu-Baer, D. Chen, R. Baer, and W. Gu. Mono-versus polyubiquitination: differential control of p53 fate by Mdm2. *Science*, 302(5652):1972–1975, 2003.

[90] D. C. Link, L. G. Schuettpelz, D. Shen, J. Wang, M. J. Walter, S. Kulkarni, J. E. Payton, J. Ivanovich, P. J. Goodfellow, M. Le Beau, et al. Identification of a novel TP53 cancer susceptibility mutation through whole-genome sequencing of a patient with therapy-related AML. *Jama*, 305(15):1568–1576, 2011.

[91] A. Loewer, K. Karanam, C. Mock, and G. Lahav. The p53 response in single cells is linearly correlated to the number of DNA breaks without a distinct threshold. *BMC biology*, 11(114):13, 2013.

[92] X. Lu, T.-A. Nguyen, S.-H. Moon, Y. Darlington, M. Sommer, and L. A. Donehower. The type 2C phosphatase Wip1: An oncogenic regulator of tumor suppressor and DNA damage response pathways. *Cancer Metastasis Reviews*, 27(2):123–135, 2008.

[93] C. Luo, J. J. Loros, and J. C. Dunlap. Nuclear localization is required for function of the essential clock protein FRQ. *The EMBO Journal*, 17(5):1228–1235, 1998.

[94] L. Ma, J. Wagner, J. J. Rice, W. Hu, A. J. Levine, and G. A. Stolovitzky. A plausible model for the digital response of p53 to DNA damage. *Proc. Natl. Acad. Sci. USA*, 102(40):14266–14271, 2005.

[95] L. Macurek, A. Lindqvist, O. Voets, J. Kool, H. R. Vos, and R. H. Medema. Wip1 phosphatase is associated with chromatin and dephosphorylates γH2AX to promote checkpoint inhibition. *Oncogene*, 29(15):2281–2291, 2010.

[96] L. Malbert-Colas, A. Ponnuswamy, V. Olivares-Illana, A.-S. Tournillon, N. Naski, and R. Fåhraeus. HDMX folds the nascent p53 mRNA following activation by the ATM kinase. *Molecular Cell*, 54(3):500–511, 2014.

[97] N. Marchenko, W. Hanel, D. Li, K. Becker, N. Reich, and U. Moll. Stress-mediated nuclear stabilization of p53 is regulated by ubiquitination and importin-α3 binding. *Cell Death & Differentiation*, 17(2):255–267, 2010.

[98] R. Maya, M. Balass, S.-T. Kim, D. Shkedy, J.-F. M. Leal, O. Shifman, M. Moas, T. Buschmann, Z. Ronai, Y. Shiloh, M. B. Kastan, E. Katzir, and M. Oren. ATM-dependent phosphorylation of Mdm2 on serine 395: role in p53 activation by DNA damage. *Genes & Development*, 15(9):1067–1077, 2001.

[99] L. D. Mayo, J. E. Dixon, D. L. Durden, N. K. Tonks, and D. B. Donner. PTEN protects p53 from Mdm2 and sensitizes cancer cells to chemotherapy. *Journal of Biological Chemistry*, 277(7):5484–5489, 2002.

[100] L. D. Mayo and D. B. Donner. A phosphatidylinositol 3-kinase/Akt pathway promotes translocation of Mdm2 from the cytoplasm to the nucleus. *Proceedings of the National Academy of Sciences*, 98(20):11598–11603, 2001.

[101] L. D. Mayo and D. B. Donner. The PTEN, Mdm2, p53 tumor suppressor–oncoprotein network. *Trends in Biochemical Sciences*, 27(9):462–467, 2001.

[102] D. W. Meek. The p53 response to DNA damage. *DNA Repair*, 3(8–9):1049–1056, 2004.

[103] D. W. Meek and U. Knippschild. Posttranslational modification of MDM2. *Molecular Cancer Research*, 1(14):1017–1026, 12 2003.

[104] B. D. Melanson, R. Bose, J. D. Hamill, K. A. Marcellus, E. F. Pan, and B. C. McKay. The role of mRNA decay in p53-induced gene expression. *RNA*, 17(12):2222–2234, 2011.

[105] D. Metzler. *Biochemistry: the chemical reactions of living cells*, volume 2. Elsevier, 2003.

[106] D. Michael and M. Oren. The p53–Mdm2 module and the ubiquitin system. *Seminars in Cancer Biology*, 13(1):49–58, 2003.

[107] L. Michaelis and M. Menten. Die kinetik der invertinwirkung. *Biochem. Z.*, 49:333–369, 1913.

[108] R. Mirzayans, B. Andrais, A. Scott, and D. Murray. New insights into p53 signaling and cancer cell response to dna damage: implications for cancer therapy. *BioMed Research International*, 2012:16 pp, 2012.

[109] J. Momand, G. P. Zambetti, D. C. Olson, D. George, and A. J. Levine. The mdm-2 oncogene product forms a complex with the p53 protein and inhibits p53-mediated transactivation. *Cell*, 69(7):1237–1245, 1992.

[110] J. D. Murray. *Mathematical Biology II: Spatial Models and Biomedical Applications*, volume 17 of *Interdisciplinary Applied Mathematics*. Springer, New York, third edition, 2003.

[111] F. Murray-Zmijewski, E. A. Slee, and X. Lu. A complex barcode underlies the heterogeneous response of p53 to stress. *Nat Rev Mol Cell Biol*, 9(9):702–712, 09 2008.

[112] E. Nagy. *Basic equations of the mass transport through a membrane layer*. Elsevier, first edition, 2012.

[113] Y. Ogawara, S. Kishishita, T. Obata, Y. Isazawa, T. Suzuki, K. Tanaka, N. Masuyama, and Y. Gotoh. Akt enhances Mdm2-mediated ubiquitination and degradation of p53. *Journal of Biological Chemistry*, 277(24):21843–21850, 2002.

[114] J. D. Oliner, K. W. Kinzler, P. S. Meltzer, D. L. George, and B. Vogelstein. Amplification of a gene encoding a p53-associated protein in human sarcomas. *Nature*, 358(6381):80–83, 07 1992.

[115] J. D. Oliner, J. A. Pietenpol, S. Thiagalingam, J. Gyuris, K. W. Kinzler, and B. Vogelstein. Oncoprotein MDM2 conceals the activation domain of tumour suppressor p53. *Nature*, 362(6423):857–860, 04 1993.

[116] D. C. Olson, V. Marechal, J. Momand, J. Chen, C. Romocki, and A. Levine. Identification and characterization of multiple mdm-2 proteins and mdm-2-p53 protein complexes. *Oncogene*, 8(9):2353–2360, 1993.

[117] T. T. Paull and J.-H. Lee. The Mre11/Rad50/Nbs1 complex and its role as a DNA double-strand break sensor for ATM. *Cell Cycle*, 4(6):737–740, 2005.

[118] Y. Peng, L. Chen, C. Li, W. Lu, S. Agrawal, and J. Chen. Stabilization of the MDM2 oncoprotein by mutant p53. *Journal of Biological Chemistry*, 276(9):6874–6878, 2001.

[119] B. Perthame. Growth, reaction, movement and diffusion from biology. Lecture notes, 2012.

[120] M. Pierre. Weak solutions and supersolutions in L^1 for reaction-diffusion systems. In W. Arendt, H. Brézis, and M. Pierre, editors, *Nonlinear Evolution Equations and Related Topics*, pages 153–168. Birkhäuser Basel, 2004.

[121] M. Pierre. Global existence in reaction-diffusion systems with control of mass: a survey. *Milan Journal of Mathematics*, 78(2):417–455, 2010.

[122] M. Pierre and D. Schmitt. Blow-up in reaction diffusion systems with dissipation of mass. *Journal on Mathematical Analysis*, 28(2):259–269, 1997.

[123] J. E. Purvis, K. W. Karhohs, C. Mock, E. Batchelor, A. Loewer, and G. Lahav. p53 dynamics control cell fate. *Science*, 336(6087):1440–1444, 2012.

[124] J. E. Purvis and G. Lahav. Encoding and decoding cellular information through signaling dynamics. *Cell*, 152(5):945–956, 2013.

[125] K. Puszyński, A. Gandolfi, and A. d'Onofrio. The pharmacodynamics of the p53-Mdm2 targeting drug Nutlin: The role of gene-switching noise. *PLoS Comput Biol*, 10(12):e1003991 EP, 2014.

[126] K. Puszyński, B. Hat, and T. Lipniacki. Oscillations and bistability in the stochastic model of p53 regulation. *Journal of Theoretical Biology*, 254(2):452–465, 2008.

[127] K. Ribbeck and D. Görlich. Kinetic analysis of translocation through nuclear pore complexes. *The EMBO journal*, 20(6):1320–1330, 2001.

[128] S. Ries, C. Biederer, D. Woods, O. Shifman, S. Shirasawa, T. Sasazuki, M. McMahon, M. Oren, and F. McCormick. Opposing effects of Ras on p53: Transcriptional activation of mdm2 and induction of p19ARF. *Cell*, 103(2):321–330, 2000.

[129] E. Rothe. Zweidimensionale parabolische randwertaufgaben als grenzfall eindimensionaler randwertaufgaben. *Mathematische Annalen*, 102(1):650–670, 1930.

[130] T. Roubíček. *Nonlinear Partial Differential Equations with Application*, volume 153 of *Intl. Ser. Numer. Math.* Birkhäuser Basel, second edition, 2013.

[131] O. Schon, A. Friedler, M. Bycroft, S. M. Freund, and A. R. Fersht. Molecular mechanism of the interaction between MDM2 and p53. *Journal of Molecular Biology*, 323(3):491–501, 2002.

[132] L. A. Segel. Simplification and scaling. *SIAM review*, 14(4):547–571, 1972.

[133] L. A. Segel and M. Slemrod. The quasi-steady-state assumption: a case study in perturbation. *SIAM Review*, 31(3):446–477, 1989.

[134] A. Serafini. *Mathematical models for intracellular transport phenomena.* PhD thesis, Università degli Studi di Roma "La Sapienza", Rome, Italy, 2007.

[135] Y. Shiloh. ATM and related protein kinases: safeguarding genome integrity. *Nat Rev Cancer*, 3(3):155–168, 2003.

[136] S. Shreeram, O. N. Demidov, W. K. Hee, H. Yamaguchi, N. Onishi, C. Kek, O. N. Timofeev, C. Dudgeon, A. J. Fornace, C. W. Anderson, Y. Minami, E. Appella, and D. V. Bulavin. Wip1 phosphatase modulates ATM-dependent signaling pathways. *Molecular Cell*, 23(5):757–764, 2015/02/16 2006.

[137] S. Shreeram, W. K. Hee, O. N. Demidov, C. Kek, H. Yamaguchi, A. J. Fornace, C. W. Anderson, E. Appella, and D. V. Bulavin. Regulation of ATM/p53-dependent suppression of myc-induced lymphomas by Wip1 phosphatase. *The Journal of Experimental Medicine*, 203(13):2793–2799, 2006.

[138] J. M. Stommel, N. D. Marchenko, G. S. Jimenez, U. M. Moll, T. J. Hope, and G. M. Wahl. A leucine-rich nuclear export signal in the p53 tetramerization domain: regulation of subcellular localization and p53 activity by NES masking. *The EMBO journal*, 18(6):1660–1672, 1999.

[139] J. M. Stommel and G. M. Wahl. Accelerated MDM2 autodegradation induced by DNAdamage kinases is required for p53 activation. *The EMBO Journal*, 23(7):1547–1556, 03 2004.

[140] M. Sturrock, A. Hellander, S. Aldakheel, L. Petzold, and M. A. J. Chaplain. The role of dimerisation and nuclear transport in the Hes1 gene regulatory network. *Bulletin of mathematical biology*, 76(4):766–798, 2014.

[141] M. Sturrock, A. Hellander, A. Matzavinos, and M. A. J. Chaplain. Spatial stochastic modelling of the Hes1 gene regulatory network: intrinsic noise can explain heterogeneity in embryonic stem cell differentiation. *Journal of The Royal Society Interface*, 10(80):20120988, 2013.

[142] M. Sturrock, A. J. Terry, D. P. Xirodimas, A. M. Thompson, and M. A. J. Chaplain. Spatio-temporal modelling of the Hes1 and p53-Mdm2 intracellular signalling pathways. *Journal of Theoretical Biology*, 273(1):15–31, 2011.

[143] M. Sturrock, A. J. Terry, D. P. Xirodimas, A. M. Thompson, and M. A. J. Chaplain. Influence of the nuclear membrane, active transport, and cell shape on the hes1 and p53–Mdm2 pathways: insights from spatio-temporal modelling. *Bulletin of mathematical biology*, 74(7):1531–1579, 2012.

[144] Y. Sun, J. Campisi, C. Higano, T. M. Beer, P. Porter, I. Coleman, L. True, and P. S. Nelson. Treatment-induced damage to the tumor microenvironment promotes prostate cancer therapy resistance through WNT16B. *Nat Med*, 18(9):1359–1368, 09 2012.

[145] Y. Sun, Y. Xu, K. Roy, and B. D. Price. DNA damage-induced acetylation of lysine 3016 of ATM activates ATM kinase activity. *Molecular and Cellular Biology*, 27(24):8502–8509, 2007.

[146] D. Y. Vargas, A. Raj, S. A. Marras, F. R. Kramer, and S. Tyagi. Mechanism of mRNA transport in the nucleus. *Proc. Natl. Acad. Sci. USA*, 102(47):17008–17013, 2005.

[147] B. Vogelstein, D. Lane, and A. J. Levine. Surfing the p53 network. *Nature*, 408(6810):307–310, 11 2000.

[148] T. von der Haar. Mathematical and computational modelling of ribosomal movement and protein synthesis: an overview. *Computational and structural biotechnology journal*, 1(1):e201204002, 2012.

[149] K. H. Vousden and D. P. Lane. p53 in health and disease. *Nature reviews Molecular cell biology*, 8(4):275–283, 2007.

[150] K. H. Vousden and C. Prives. Blinded by the light: the growing complexity of p53. *Cell*, 137(3):413–431, 2009.

[151] J. Wagner, L. Ma, J. Rice, W. Hu, A. Levine, and G. Stolovitzky. p53–Mdm2 loop controlled by a balance of its feedback strength and effective dampening using ATM and delayed feedback. *IEE Proceedings-Systems Biology*, 152(3):109–118, 2005.

[152] R. L. Weinberg, D. B. Veprintsev, and A. R. Fersht. Cooperative binding of tetrameric p53 to DNA. *Journal of Molecular Biology*, 341(5):1145–1159, 2004.

[153] J. Wenus, H. Düssmann, P. Paul, D. Kalamatianos, M. Rehm, P. E. Wellstead, J. H. Prehn, and H. J. Huber. ALISSA: an automated live-cell imaging system for signal transduction analyses. *Biotechniques*, 47(6):1033–1040, 2009.

[154] X. Wu, J. H. Bayle, D. Olson, and A. J. Levine. The p53-mdm-2 autoregulatory feedback loop. *Genes & Development*, 7(7a):1126–1132, 1993.

[155] H. Yamaguchi, S. R. Durell, D. K. Chatterjee, C. W. Anderson, and E. Appella. The Wip1 phosphatase PPM1D dephosphorylates SQ/TQ motifs in checkpoint substrates phosphorylated by PI3K-like kinases. *Biochemistry*, 46(44):12594–12603, 2007.

[156] H.-Y. Yang, Y.-Y. Wen, Y.-l. Lin, L. Pham, C.-H. Su, H. Yang, J. Chen, and M.-H. Lee. Roles for negative cell regulator 14-3-3σ in control of MDM2 activities. *Oncogene*, 26(52):7355–7362, 06 2007.

[157] Y. Yang, P. Cheng, and Y. Liu. Regulation of the Neurospora circadian clock by casein kinase ii. *Genes & Development*, 16(8):994–1006, 2002.

[158] Y. Yin, C. W. Stephen, M. G. Luciani, and R. Fahraeus. p53 stability and activity is regulated by Mdm2-mediated induction of alternative p53 translation products. *Nat Cell Biol*, 4(6):462–467, 06 2002.

[159] D. B. Young, J. Jonnalagadda, M. Gatei, D. A. Jans, S. Meyn, and K. K. Khanna. Identification of domains of ataxia-telangiectasia mutated required for nuclear localization and chromatin association. *Journal of Biological Chemistry*, 280(30):27587–27594, 2005.

[160] T. Zhang, P. Brazhnik, and J. J. Tyson. Exploring mechanisms of the DNA-damage response: p53 pulses and their possible relevance to apoptosis. *Cell cycle*, 6(1):85–94, 2007.

[161] X.-P. Zhang, F. Liu, and W. Wang. Two-phase dynamics of p53 in the DNA damage response. *Proc. Natl. Acad. Sci. USA*, 108(22):8990–8995, 2011.

[162] Z. Zhao, J. Zuber, E. Diaz-Flores, L. Lintault, S. C. Kogan, K. Shannon, and S. W. Lowe. p53 loss promotes acute myeloid leukemia by enabling aberrant self-renewal. *Genes & Development*, 24(13):1389–1402, 2010.

[163] B. P. Zhou, Y. Liao, W. Xia, Y. Zou, B. Spohn, and M.-C. Hung. HER-2/neu induces p53 ubiquitination via Akt-mediated MDM2 phosphorylation. *Nature cell biology*, 3(11):973–982, 2001.